universiteit hasselt

2013 | Faculteit Wetenschappen

DOCTORAATSPROEFSCHRIFT

From dosimetry to damage: Unravelling the biological effects of environmental radioactivity in Arabidopsis thaliana.

Proefschrift voorgelegd tot het behalen van de graad van doctor
in de wetenschappen, biologie, te verdedigen door

Geert Biermans

Promotor: prof. dr. Ann Cuypers
Copromotoren: prof. dr. Nele Horemans en prof. dr. Jaco Vangrondsveld

D/2013/2451/51

PhD Thesis presented on the 26th of September 2013 at Hasselt University

Members of the jury

Prof. Dr. Karin Coninx, UHasselt, Diepenbeek, BELGIUM, Chair
Prof. Dr. A. Cuypers, UHasselt, Diepenbeek, BELGIUM, Promotor
Prof. Dr. J. Vangronsveld, UHasselt, Diepenbeek, BELGIUM, co-promotor
Prof. Dr. N. Horemans, Studiecentrum voor Kernenergie, Mol, BELGIUM, co-promotor
Prof. Dr. J. Colpaert, UHasselt, Diepenbeek, BELGIUM
Prof. Dr. R. Blust, Universiteit Antwerpen, Antwerpen, BELGIUM
Dr. C. Adam-Guillermin, IRSN, St-Paul-lez-Durance, FRANCE
Prof. Dr. J. Vives i Batlle, Studiecentrum voor Kernenergie, Mol, BELGIUM
Prof. Dr. L. Hernandez, Universidad Autónoma de Madrid, Madrid, SPAIN

Put off your imagination, as you put off your overcoat, when you enter the laboratory. Put it on again, as you put on your overcoat, when you leave.

Claude Bernard
(1813-1878)
the father of physiology

ACKNOWLEDGEMENTS

A wise man once said that a PhD is a lonely business. A task which, much like quests in Arthurian tales or in fairy tales, has to be performed alone to prove one's worth. To slay a dragon, save the damsel, and publish five papers about it. A task which, once completed, opens the castle gates and wins eternal grants and glory.

But that's not entirely accurate..

A PhD, dear readers, is a Wagner opera. Sometimes tedious, sometimes eventful, but above all a long and exciting journey past trolls, through caverns, swamps and mythical lands to find enchanted rings and swords. But like in any quest, the hero of the PhD drama does not have to be alone. A team of people and institutions has accompanied me throughout my travels through science. This chapter, this prelude to the Ride of Valkyries that follows, is for them.

Above all I wish to thank my supervisors Nele and Ann. I could not have wished for two better supervisors than my own. For four years, they have followed me, kept up with all the sudden plot twists, developments and changes to the libretto. Their experience and advice has been of most precious value to me. While other projects and quests crossed their path, they have always taken their time to steer me back onto the right path of research. With all my heart, thank you.

I'd like to thank Nathalie, Jaco, Hildegarde and Hans for their counselling and input into my work throughout these four years. In this respect, I also wish to thank the members of the jury, Prof. Dr. Jan Colpaert, Prof. Dr. Ronny Blust, Dr. Christelle Adam-Guillermin, Prof. Dr. Jordi Vives i Batlle and Prof. Dr. Luis Hernandez, for their critical evaluation and comments which have made this thesis a stronger and more robust work of science.

Furthermore, such a long and perilous journey could not have been completed without the financial, administrative support of the Research Foundation Flanders (FWO), the Belgian Nuclear Research Centre (SCK•CEN) and the University of Hasselt. In particular I wish to express my gratitude to the Molecular and Cellular Biology group (SCK•CEN) for the use of their infrastructure. To the Dosimetry and Calibration unit (SCK•CEN) for the use of the radiation facility and valuable theoretical and technical assistance. To the Low-level Radioactivity Measurements unit for the gamma spectrometry measurements and assistance. To Michèle Coeck and Griet Vanderperren for the support of the Academy. And finally to Els van Musscher, Betty Vandingelen and Kristine Leysen for their administrative (and motivational) support.

Every good opera has a strong supporting cast to accompany the dramatic moments. To share in the joy of successful experiments, to peer for hours and hours over small eppendorf tubes to place miniscule *Arabidopsis* seeds on agar (why oh why didn't I choose beans as a model plant?). To freeze thousands of little seedlings to an icy death. To spend hours in darkened rooms to watch amputated leaves photosynthesise. To provide coffee, chocolate, cake and support. My most profound thanks to all the people (past and present) of the Biosphere Impact Studies Unit…and to May, Jean and Robin in particular for all the lab assistance. Thank you for these four wonderful years of my life. You have been like family.

There has to be a special mention for my train colleagues (and train VITO'ers) here: Wim, Patrick, Karen, Peter and ex-/future colleague Geert. Sharing two hours each day in a confined space on wheels creates a bond. Especially when that space is usually late or subject to the mysteries of railway operations. Their good humour has on many occasions saved my mood of the day to come.

Between the days of eppendorf labelling and failed PCR's, there were always the moments of relaxation and comfort among friends. Some had their own quest, and exchanged hints on how to tackle the dragons and save the treasure. Some did not have a clue what I was raving on about (Plants? Mutants?), but nodded

quietly and smiled. Some were lost along the way and some arrived late on the scene. But all were part of this thesis. All contributed in their way to make this voyage through research bearable. This is as much their work as mine.

A tous mes amis français qui m'ont suivi lors de mon voyage scientifique… à tous mes amis périgourdins qui m'accompagnent depuis tout ce temps (certains depuis plus de 20 ans)…cette thèse est la votre aussi. Une grande partie de cet ouvrage a été écrit dans mon pays d'adoption, cette terre d'accueil qui s'appelle le Périgord. A travers ces pages vous verrez, je l'espère, le canard, les noix et le Monbazillac qui ont accompagné ces moments d'écriture et les promenades dans la Bessède, peut-être même les moments de repos au bord de la Dordogne. Ecoutez, les gascons, c'est la Gascogne !

And finally, but most importantly, I could not have done any of this this without my family. Without both the moral and financial support my parents have given me throughout all these years of study and research. Without the support only a brother and sisters can give to their 'little brother'. And perhaps most of all, this PhD thesis is my parents'. I could not have done this without the assurance and advice of my father, or without my mother, who sadly cannot be here today to see the result of all the support and love she has given me. I hope I would have made her proud.

For you, dear reader, who is about to relive this journey, this four year quest, through my eyes. Don't let the technicalities of the libretto, the formulas and the strange world of radiation discourage you.

There will be music.

ABBREVIATIONS

AO	Ascorbate oxidase
APX	Ascorate Peroxidase
AsA	Ascorbic acid
BER	Base Excision Repair
Bq	Becquerel
CI	Confidence Interval
CR	Concentration ratio
DCC	Dose Conversion Coefficient
DHA	Dehydroascorbate
DHAR	Dehydroascorbate Reductase
DSB	Double Strand break
DTNB	5,5'-Dithio-Bis (2-Nitrobenzoic Acid)
DTT	Dithiothreitol
DW	Dry weight
EDTA	Ethylenediaminetetraacetic acid
ETR	Electron transfer rate
eV	Electron Volt
GA	Genetic Algorithm
GR	Glutathione reductase
GSSG	Glutathione disulfide
GSH	Glutathione
Gy	Gray
HR	Homologous Recombination
IC	Induction Curve
IR	Ionising Radiation
LET	Linear Energy Transfer
NADP	Nicotinamide adenosine diphosphate
NER	Nucleotide Excision Repair
NHEJ	Non-homologous end-joining
NORM	Naturally Occuring Radioactive Materials

NPQ	Non-photochemical quenching
PAR	Photosynthetically Active Radiation
PCD	Programmed Cell Death
PCR	Polymerase Chain Reaction
RBE	Relative Biological Effectiveness
RLC	Rapid Light Curve
ROS	Reactive Oxygen Species
SSB	Single strand break
TF	Transfer factor
UV	Ultraviolet

SUMMARY

Increased human activity has led to a rise in the amount of radioactive elements in the environment. In addition to radionuclides from controlled and accidental releases by nuclear power facilities and medical activity, a significant amount of radionuclides is annually released from the earth's crust by the so-called NORM industries (Naturally Occurring Radioactive Material; e.g. phosphate industry, mining,…). The presence of these radionuclides and their decay products in the biosphere pose an increased risk of exposure to external as well as internal ionising radiation for biota. Though significant scientific efforts have been made in the past to understand the effects of ionising radiation in non-human biota, there is still a considerable knowledge gap as to how organisms respond on the molecular and physiological level and how this response ties in to effects on morphology and growth. For plants in particular, the dose-dependent effects of radiation are poorly understood. Studies on acute γ-irradiation suggest DNA repair and the anti-oxidative response play an important role at the cellular level, though very little is know about the long-term response to chronic radiation by radionuclides in the environment. Nor are there clear indications on how the response differs or overlaps between the different types of radiation.

The aim of this study was to unravel the biological effects of chronic α, β, and γ-radiation on seedlings of the widely used model plant *Arabidopsis thaliana* (Columbia ecotype) at the morphological, physiological and molecular level.

The current environmental radiation dosimetry tools are not adapted to accurately estimate doses for exposure scenarios in small, fast-growing organisms such as *Arabidopsis* seedlings. In **Chapter 3** and **Chapter 4**, we describe the creation of a dynamic dosimetry model for *Arabidopsis thaliana* roots and shoots based upon easily obtainable growth parameters such as leaf area and root length. We applied the model to an exposure scenario with α- (^{241}Am), β- (^{90}Sr) or γ-radiation (^{133}Ba) and compared the behaviour of absorbed dose over time in both organs for a 96h exposure. The results show that root dosimetry does not depend on root length and only on radionuclide

uptake. In the shoots, the timing of the exposure has a considerable effect on the total dose, especially for β-radiation delivered by ^{90}Sr. Finally, our results suggest shows that by including growth and radionuclide dynamics into the model, a more accurate dose estimate is obtained compared to conventional static dosimetry models.

Previous studies have shown that effects of radiation differ between plants in different growth stages. In **Chapter 5**, we investigate whether *Arabidopsis thaliana* shows age-dependency in its response to ionising radiation. 7-, 10- and 14-day-*old Arabidopsis thaliana* seedlings were exposed to 96 h and 168 h of 100 mGy h^{-1} chronic γ-radiation in a hydroponic setup. The response of growth, photosynthesis and transcription of genes involved in DNA repair, cell cycle and signalling were measured. After the exposure, growth recovery capacity was determined. The results show that there is a difference in growth response and recovery capacity between plants of different ages, and decreasing radiosensitivity with increasing seedling age. This is linked to differences in regulation of DNA repair and cell cycle control at the transcriptional level.

In **Chapter 6** and **Chapter 7**, we look at the dose-dependent biological effects of β-radiation (delivered by ^{90}Sr) and α-radiation (delivered by ^{241}Am). We exposed 14-day old *Arabidopsis thaliana* seedlings for 4 and 7 days to a range of one of the radionuclides (0 – 250,000 Bq L^{-1} for ^{90}Sr, 0 – 50,000 Bq L^{-1} for ^{241}Am) in a hydroponical setup. Besides uptake and distribution of the radionuclides, we sampled growth, biomass and leaf area to look at the overall effect on morphology. At the physiological level, we measured photosynthesis performance. Finally, we analysed the effects at the molecular level, measuring expression of genes involved in cell cycle control, DNA damage repair and oxidative stress and the anti-oxidative defense pathways. These results were linked to measurements of DNA damage (base modification) and the redox status of ascorbate and glutathione.

Our results show that ^{90}Sr accumulates primarily in the shoot tissue of *Arabidopsis thaliana* seedlings, resulting in high internal shoot β-dose rates. We

observed a transcriptional response in the shoots on ROS scavenging, DNA repair and cell cycle regulation starting in the mGy h^{-1} order of magnitude and above. The timing of this response was earlier for higher dose rates. Despite these responses to ionising radiation exposure, we observed an increase in DNA damage and loss of redox balance, suggesting that the plants are unable to counterbalance chronic β-exposure. In the roots, dose rates were found to be much lower. At the transcriptional level most genes showed early down-regulation at all dose rates, while late transcription was characterised by up-regulation of ROS scavenging and DNA repair only at the highest dose rates.

Our results show that ^{241}Am has high transfer to the roots but low translocation to the shoots, resulting in α-dose rates up to 35 mGy h^{-1} in the roots. In the roots, we observed a transcriptional response of ROS scavenging and DNA repair pathways. At the physiological and morphological level this resulted in a response which evolves from redox balance control and stable biomass at low dose rates to growth reduction, reduced transfer and redox balance decline at higher dose rates. This situation was also reflected in the shoots where, despite the absence of a transcriptional response, the control of photosynthesis performance and redox balance were maintained then declined with increasing dose rate. Our results further suggest that the effects of α-radiation were initiated in the roots, where the highest dose rates occurred, ultimately affecting photosynthesis performance, transport and carbon assimilation.

While these results show that *Arabidopsis thaliana* seedlings have a shared molecular response to the three types of radiation used in this study, our data also show that the physico-chemical characteristics of the radionuclide play a major role in the overall response of the plant to ionising radiation. The interplay of macro- and microlocalisation of the element, radiation type and internal distribution between organs seem to be a determining factor in the global response of the individual to radionuclide exposure. This begs the question whether a toxicological framework where radiation is seen as a single stressor rather than an integral part of the mode of action of an element is a viable route to take.

SAMENVATTING

Een gestage toename in menselijke activiteit zorgt voor steeds groeiende concentraties aan radioactive elementen in het leefmilieu. Naast de gecontroleerde en accidentele lozingen door medische en nucleaire installaties wordt jaarlijks een aanzienlijke hoeveelheid radionucliden vanuit de aardkorst vrijgesteld in het leefmilieu door zogenaamde NORM-industrieën. De aanwezigheid van deze radionucliden en hun dochters in het leefmilieu zorgt voor een verhoogd risico op blootstelling van biota aan zowel externe als interne ioniserende straling. Ondanks de belangrijke wetenschappelijke inspanningen in de voorbije jaren zijn er nog steeds belangrijke hiaten in onze kennis over de fysiologische en moleculaire effecten van ioniserende straling in non-human biota, en hoe deze verband houden met de effecten op groei en morfologie. Voor planten in het bijzonder zijn de dosisafhankelijke effecten van straling slecht begrepen. Studies met acute gammastraling lijken aan te tonen dat DNA-herstel en de anti-oxidatieve respons een rol spelen op het cellulair niveau, maar er is weinig gekend over de effecten van chronische straling afkomstig van radionucliden in het leefmilieu. Bovendien zijn er geen duidelijke aanwijzingen wat de overlap of verschillen in respons zijn tussen de verschillende types straling. Het doel van deze studie was het ophelderen van de morfologische, fysiologische en moleculaire biologische effecten van chronische α-, β- en γ-straling op zaailingen van de modelplant Arabidopsis thaliana (Columbia ecotype).

De dosimetrietools die momenteel beschikbaar zijn op internationaal niveau om risk assessment van straling in het leefmilieu uit te voeren zijn niet aangepast om dosissen en dosistempo's te bepalen voor blootstellingen in kleine, snelgroeiende organismen zoals zaailingen van *Arabidopsis*. In **Hoofdstuk 3** en **Hoofdstuk 4** beschrijven we het opstellen van een dynamische dosimetriemodel voor *Arabidopsis thaliana*-zaailingen. Dit model is gebaseerd op eenvoudig meetbare parameters zoals wortellengte en bladoppervlakte. We pasten dit model toe op een 96u blootstellingsscenario voor α- (^{241}Am), β- (^{90}Sr) en γ-straling (^{133}Ba), en vergeleken hoe de dosisabsorptie verloopt voor elk type

straling doorheen de tijd in beide organen. Onze resultaten tonen dat de timing van de blootstelling een sterke invloed heeft op de totale dosis in de bladeren, vooral voor ^{90}Sr. Bovendien tonen we aan dat door groei en radionuclidetransport op te nemen in het model een meer accurate schatting bekomen wordt van dosissen en dosistempo's vergeleken met conventionele, statische dosimetriemodellen.

Eerdere studies hebben aangetoond dat effecten van straling verschillen tussen planten in verschillende groeistadia. In **Hoofdstuk 5** onderzoeken we leeftijdsafhankelijke stralingseffecten in *Arabidopsis thaliana*. 7-, 10- en 14-dagen oude zaailingen werden 96u of 168u blootgesteld aan 100 mGy h^{-1} chronische γ-straling onder hydroponie. De effecten op groei, herstelcapaciteit, fotosynthese en transcriptie van genen in DNA-herstel, celcycluscontrole en signaaltransductie werden gemeten. Onze resultaten tonen aan dat *Arabidopsis*-zaailingen een leeftijdsafhankelijk verschil tonen in groeirespons en herstelcapaciteit, alsook een lagere radiosensitiviteit bij oudere zaailingen. Op moleculair niveau is dit gelinkt aan verschillen in DNA-herstel en celcycluscontrole.

In **Hoofdstuk 6** en **Hoofdstuk 7** onderzoeken we de dosisafhankelijke effecten van β- (^{90}Sr) en α-straling (^{241}Am). 14-dagen oude zaailingen werden hydroponisch blootgesteld voor 4 en 7 dagen aan een reeks radionuclideconcentraties (0 – 250000 Bq L^{-1} ^{90}Sr of 0 – 50000 Bq L^{-1} ^{241}Am). Naast opname en transport van radionucliden werden groei, biomassa en fotosynthese bestudeerd. Om de onderliggende mechanismen te begrijpen analyseerden we expressie van genen betrokken in DNA-herstel, celcycluscontrole, oxidatieve stress en anti-oxidatieve beschermingsmechanismen. Bovendien werden DNA-schade (basemodificatie) en de redoxstatus van ascorbaat en glutathion gemonitored.

^{90}Sr accumuleert voornamelijk in de blaadjes, wat leidt tot een hoog β-dosistempo. ROS scavenging, DNA-herstel en celcycluscontrole in dit orgaan waren duidelijk opgereguleerd bij dosistempo's boven de orde mGy h^{-1}, hoewel

de timing van de respons afhankelijk lijkt van het dosis-tempo. Ondanks deze duidelijke transcriptionele respons van de plant op ioniserende straling tonen de dosisafhankelijke afname in redoxstatus en toename in DNA-schade aan dat de bladeren niet in staat zijn om bij hoge dosissen β-straling cellulaire balans te behouden. In de wortels waren de dosistempo's veel lager, en was de respons gekarakteriseerd door vroege suppressie van de meeste genen en late verhoogde expressie van ROS-scavenging en DNA-herstel bij de hoogste dosis.

Americium-241 toont een volledig ander beeld, met lage transfer naar de blaadjes, maar hoge transfer naar de wortels waar dit resulteerde dit in α-dosistempo's tot 35 mGy h^{-1}. De wortels vertoonden, naast verhoogde genexpressie in ROS scavenging en DNA herstel, een dosisafhankelijke respons met stabiele redoxstatus en biomass onder loge dosistempo's, en verminderde groei en transport en een verlies van de redoxbalans bij hoge dosistempo's. Deze situatie was ook aanwezig in de blaadjes waar, ondanks het ontbreken van een transcriptionele respons, er een duidelijke regulatie van fotosynthese en redoxbalans optrad bij lage dosistempo's, en een verlies aan controle bij hoge tempo's. Dit lijkt er op te wijzen dat de effecten van α-straling door ^{241}Am geinitieerd worden in de wortels en uiteindelijk leiden tot een verminderde fotosynthese, transport en koolstofassimilatie.

Deze resultaten tonen aan dat zaailingen van *Arabidopsis thaliana* een overlappende respons vertonen op chronische blootstelling aan α-, β- en γ-straling. Desalniettemin tonen de verschillen in stralingsgevoeligheid tussen wortels en blaadjes en tussen de effecten van de verschillende stralingstypes aan dat fysico-chemische factoren een grote rol spelen. Het samenspel van macro- en microlocalisatie van de radionucliden, het stralingstype en de interne verdeling tussen de organen lijkt een bepalende rol te spelen in het globale effectbeeld van een radionuclide op de plant. Gebaseerd op deze bevindingen kan men zich afvragen of een toxicologisch model waarbij straling als een single stressor wordt gezien in plaats van een integraal deel van de mode of action van een radioactief chemisch element een leefbare optie is in toekomstig onderzoek.

TABLE OF CONTENTS

Chapter 1:

Introduction

1.1 Ionising Radiation

1.1.1 Sources and types of ionising radiation

Radioactivity occurs when an atom becomes unstable due to an imbalance in its nucleus between the number of protons and neutrons. Any element is determined by its number of protons but can contain a variable amount of neutrons, which leads to a number of different isotopes for that element. If the ratio between neutrons and protons is too high or too low, the nucleus will attempt to reach a more stable configuration by changing the constitution of the nucleus, thereby emitting energy and ionising particles. This can occur either by α-decay (emission of 2 protons + 2 neutrons) or β-decay (switch between a proton and neutron in the nucleus with the emission of an electron or positron and γ-rays) or by nuclear fission into two more stable products. The result of this process is a new element, the daughter nuclide, which can either be stable or can decay in turn to a third configuration (and so on). When a series of these transformations occur, this is called a decay chain (ASTDR, 1999).

Several of these long decay chains occur in nature, each starting with a radioactive isotope of uranium or thorium and ending with a stable lead isotope after several decay steps and intermediate elements. These so-called primordial radionuclides, ^{238}U, ^{235}U and ^{232}Th, have an extremely long half-life (millions of years) and were already present at Earth's formation. They are therefore present in nature in minerals, rocks and sediments, where they and their progeny nuclides in the chain constitute an important part of environmental radioactivity (ASTDR, 1999). A second group of primordial radionuclides is formed of elements such as ^{40}K and ^{87}Rb, which are also present in the earth's crust and have a long half-life but are also easily transferred in biological systems. There, they constitute an important source of radioactivity inside the organism (Van der Stricht & Kirchmann, 2001). Finally, a third group of radionuclides is constantly being formed in the atmosphere by bombardment of

gases with cosmic radiation. Important radionuclides such as ^{3}H and ^{14}C, mostly β- and γ-emitters, have their origin there (ASTDR, 1999).
It has to be noted that, while these are naturally occurring radioactive materials (NORM), their abundance in the environment can locally be increased by anthropogenic action such as mineral mining (Vandenhove, 2002).

In addition to the naturally occurring radionuclides, there are considerable amounts of anthropogenic radionuclides in the environment. These are mainly the result of nuclear fission processes in the operation of nuclear power plants, produced during the fission of fissile uranium (^{235}U) or plutonium (^{239}Pu). Most of these fission products are β- and γ-emitters (ASTDR, 1999), of which ^{131}I, ^{137}Cs and ^{90}Sr (see section 1.1.3) are especially of radiological concern. Under normal circumstances, radionuclides produced as a result of fission are only released in minimal quantities by atmospheric or liquid discharge (EU, 2010). However, a large amount of radioactive material can be released into the environment during accidental releases or nuclear weapons testing.

1.1.2 Alpha radiation

1.1.2.1 Properties of alpha radiation

Alpha (α) radiation consists of the emission of a ^{4}He nucleus (2 protons + 2 neutrons, the alpha particle) from the nucleus of a parent radionuclide (ASTDR, 1999). This type of decay occurs in heavy nuclei where the proton:neutron ratio is high, and where α-decay consequently results in a more stable daughter nuclide through emission of a highly stable He-nucleus. This escape of the α-particle from the parent nucleus is in essence a quantum tunnelling event. The decay can be written as equation 1:

$$^{A}_{Z}N \rightarrow {}^{A-4}_{Z-2}N' + {}^{4}_{2}He \qquad (1)$$

The kinetic energy of the α-particle depends, by conservation of momentum, on the mass of the resulting daughter nucleus. However, as the daughter nuclide is usually much larger in mass than the α-particle, most of the energy resulting from the change in binding energy will be in the emitted particle. Therefore, most α-particles are emitted at 4 to 5 MeV, with very little spread around the average emission energy.

As α-particles are naked He nuclei, they have a charge of 2^+. As a result, the particles interact heavily with electrons of atoms along their path, adding excitation energy or removing them from their orbits altogether. With each interaction, the α-particle loses an amount of kinetic energy and slows down, until it comes to a halt and finally acquires two electrons to form helium.

1.1.2.2 Properties of americium-241

Americium (Am) is an artificial actinide element with atomic number 95. It was discovered as a new element in 1944 by Glenn Seaborg at the University of California, Berkeley during research related to the Manhattan project. Americium is only produced as a result of nuclear fission by neutron bombardment of ^{238}U or ^{238}Pu. The Pu isotopes formed by this process decay to americium by β-emission (ASTDR, 2004a). It is a soft, silver-white metal, which can occur under a range of oxidation states from II through VII. Under environmental conditions, the trivalent $Am(III)^{3+}$ state is dominant (Moulin et al., 1988), leading to predominant americium carbonates ($Am(CO_3)_3$) and americium hydroxide (AmH_3O_3) species in an aquatic environment. Americium also has a high affinity for organic compounds (IRSN, 2004a).

	^{241}Am
Half-life	432 years
Specific Activity	1,27 x 10^{11} Bq g^{-1}
Decay	
α	5486 keV (85%)
	5443 keV (13%)
γ	61 keV (13%)

Table 1.1 Radioactive properties of ^{241}Am (IRSN, 2005a). ^{241}Am predominantly decays by α-mode, with complementary emission of a γ-ray.

Though several isotopes of americium exist, only ^{241}Am, with a 432 year half-life, occurs in relatively large quantities (Table 1.1). ^{243}Am, which has a much longer half-life (7370 years), is formed in much smaller quantities. ^{241}Am is formed by β-decay of ^{241}Pu with a half-life of 14.4 years. It decays by α-mode to Neptunium-237 (^{237}Np), which in turn is an α-emitter with a half-life of 2 million years. ^{237}Np is at the start of a long decay chain (the Neptunium series), which ultimately ends with stable thallium (^{205}Tl) (equation 2):

$$^{241}_{95}Am \rightarrow \ ^{237}_{93}Np \rightarrow Neptunium\ Series \rightarrow \ ^{205}_{81}Tl \qquad (2)$$

During the α-decay, emission of low-energy γ-rays occurs which allows for detection of ^{241}Am by gamma spectrometry.

1.1.2.3 Sources of ^{241}Am in the environment

There are three main sources of ^{241}Am in the environment: atomic bomb tests, discharges from nuclear installations and accidents. It must be noted however that the current environmental levels of ^{241}Am are in part also the result of the release of ^{241}Pu, which subsequently decays into ^{241}Am. The levels of ^{241}Am have not yet reached their maximum, as the production from Pu decay is still higher than the decay to Np (IRSN, 2005a).

80% of the transuranic elements in the environment are the result of the nuclear weapons tests' fall-out. An estimated 55 x 10^{14} Bq of ^{241}Am have been released in the atmosphere since 1945, and have primarily been deposited in the Northern hemisphere (IRSN, 2005a). Secondly, the discharges from nuclear installations do not originate from nuclear power stations, but rather from reprocessing plants such as Le Hague (France) and Sellafield (UK). The ^{241}Am releases into the marine environment from these installations are of the order of 10^{9} to 10^{10} Bq per year (EU, 2010). Finally, a large amount of ^{241}Am has been released into the environment as a result of accidents. Apart from incidents in nuclear power installations such as Chernobyl (Ukraine) or Windscale (UK), localised contaminations also exist at two crash sites of B52 planes in Palomares (Spain) and Thulé (Greenland). The amount of ^{241}Am in the Chernobyl exclusion zone is estimated at 5.9 x 10^{13} Bq (IRSN, 2004b).

Environmental concentrations of ^{241}Am in freshwater are generally low, between 1 and 3 µBq L^{-1} (Coughtrey & Thorne, 1983), while soil concentrations are in the range of 10 Bq kg^{-1} dry weight (Pourcelot et al., 2003). Evidently, the ^{241}Am levels can locally reach much higher values at accident sites (Mboulou et al., 1998).

1.1.3 Beta Radiation / Strontium-90

1.1.3.1 Properties of β-radiation

Beta (β) decay occurs when an atomic nucleus of an element emits an electron (β- decay) or a positron (β+ decay) (ASTDR, 1999). The reason for this disintegration lies in the ratio between neutrons and protons in the nucleus. When the N/P-ratio is too high, a neutron changes into a proton, with emission of an electron (e^-) and an antineutrino (v^e) to conserve the total mass, energy and charge. In a similar way, a positron and a neutrino are emitted as a neutron changes into a proton when the N/P-ratio is too low. Therefore, β^- and β^+-decay of a nucleus N to N' can be written as equation 3 and 4, respectively:

$$^{A}_{Z}N \rightarrow {}_{Z+1}^{A}N' + e^{-} + v_e \qquad (\beta^-) \qquad (3)$$

$$^{A}_{Z}N \rightarrow {}_{Z-1}^{A}N' + e^{+} + v_e \qquad (\beta^+) \qquad (4)$$

Because of the transformation inside the nucleus between neutron and proton, the atomic number Z of the nucleus decreases (in the case of β^+ decay) or increases (in the case of β^- decay) with 1. Because the mass of a proton and that of a neutron are identical, the atomic mass A of the nucleus remains the same in the process. The potential and kinetic energy of the emitted particle depend on the change in binding energy involved, which is distributed into the recoil of the nucleus and the potential and kinetic energy of both the neutrino and the electron. Consequently, the energy of the electrons or positrons in a particular type of β emission is not a discrete value but distributed in a continuous spectrum around an average decay energy.

A third type of β-decay occurs when an orbital electron (usually from the K shell) reacts with a nuclear proton to form a neutron. The net result for the nucleus is identical to that of β^- decay, though sometimes it is associated with emission of γ-rays, such as in the case of Barium-133 (^{133}Ba) (Section 1.1.4.2).

1.1.3.2 Properties of strontium-90

Strontium (Sr) is a naturally occurring alkaline earth metal with atomic number 38, which mostly occurs in oxidation state +2 (ASTDR, 2004b; IRSN, 2005b). In its pure form it is a hard, silver-white coloured metal, though it almost never occurs as such in nature, but rather under its mineral form as celestite ($SrSO_4$) or strontianite ($SrCO_3$). The element makes up 0.02 to 0.03% of the earth's crust, with concentrations in carbonated rocks ranging up to 400 ppm. Physically and chemically, it is similar in behaviour to its closest neighbours in the periodic table of elements, barium and calcium.

Natural strontium occurs as fours stable isotopes: ^{84}Sr (0.56%), ^{86}Sr (9.86%), ^{87}Sr (7.0%) and ^{88}Sr (82.58%). It is mostly used in glass and ceramics, e.g. in cathode-ray tubes of television sets (ASTDR, 2004b). However, all radioactive isotopes of strontium are the result of anthropogenic activity. Though there are many unstable isotopes of strontium, only ^{89}Sr and ^{90}Sr are of major concern (Table 1.2). Both are produced during nuclear fission, either as fission product or by neutron activation, and are therefore present in spent fuel rods. Both are β-emitters, which makes them of use in medical applications.

	^{89}Sr	**^{90}Sr**
Half-life	50.5 days	29.14 years
Specific Activity	1.08 x 10^{15} Bq g^{-1}	5.05 x 10^{12} Bq g^{-1}
Decay		
β	1492 keV (100%) ($β^+$)	546 keV (100%) ($β^-$)

Table 1.2: Radioactive properties of ^{89}Sr and ^{90}Sr (IRSN, 2005b). Both are pure β-emitters, though ^{89}Sr emits positrons, whereas ^{90}Sr emits electrons.

^{90}Sr, also known as radiostrontium, has a half-life of 29.14 years and is a pure $β^-$-emitter (546 keV). It decays to its daughter nuclide yttrium-90 (^{90}Y), which decays in turn with a short half-life of 64 h by $β^-$-decay (2.48 MeV) to stable zirconium-90 (equation 5):

$$^{90}_{38}Sr \rightarrow {}^{90}_{39}Y \rightarrow {}^{90}_{40}Zr \qquad (5)$$

1.1.3.3 Sources of ^{90}Sr in the environment

Stable strontium is mainly present in the environment due to rock erosion and soil transport. Surface water usually contains less than 1 mg L^{-1}, but this may depend on the geological characteristics of the area. Atmospheric deposition

represents only a minor dispersal pathway (IRSN, 2005b). Strontium-90 however is only produced artificially in nuclear fission reactors, and the amounts of ^{90}Sr in the environment are therefore all the result of anthropogenic emissions, either voluntary or accidental. Three major sources of ^{90}Sr in the environment can be distinguished: nuclear weapons, nuclear power plant and reprocessing facility discharges and accidents.

Between 1945 and 1980, an estimated 622 PBq amount of ^{90}Sr has been released into the atmosphere as a result of nuclear weapons testing. In the northern hemisphere alone, the total deposited amount is estimated at 470 PBq (UNSCEAR, 2000). Secondly, nuclear installations release radionuclides into the environment through airborne or liquid emission. Whereas controlled ^{90}Sr emission from nuclear power plants is generally low (EU, 2010), fuel reprocessing plants such as those of La Hague and Sellafield have considerable annual amounts of ^{90}Sr in liquid discharge (169 Gbq and 1.7 Tbq in 2008 respectively; EU, 2010). Finally, large accidental releases of radiostrontium have occurred several times in history, notably 74 GBq during the Windscale/Sellafield (UK) accident in 1957 (Galle, 1997), 58 PBq in Mayak (Russia) in the same year (leading to formation of the East Ural Radioactive Trail; Kryshev et al., 1998) and 8000 Tbq as a result of the Chernobyl accident in 1986.

Current levels of ^{90}Sr in surface, ground and drinking water and in soils vary depending on the location, but measurements in Europe indicate levels between 0.2 and 10 Bq kg^{-1} dry soil (IRSN, 2005b) and lower than 10 mBq L^{-1} in surface waters (Pujol & Sanchez-Cabeza, 2000). Most of this ^{90}Sr originates from the atomic bomb tests.

1.1.4 Gamma Radiation

1.1.4.1 Properties of gamma radiation

Gamma (γ) radiation is the emission of an electromagnetic radiation by a nucleus when it returns to a ground state. This usually occurs as a by-product of either α- or β-decay, when the daughter nucleus is left in an excited state. The energy of the emitted photon is therefore dependent on the energy difference between the excited and ground states of the nucleus (ASTDR, 1999). As γ-rays are photons, they have no mass and a high velocity, which allows them to pass through matter without much interaction and thereby can reach large distances. Because of its wave-like properties, the intensity decreases with the square of the distance to the source.

As γ-rays pass through matter, they can interact in several ways. The photoelectric effects occur when all of the photon energy is transferred to an electron, which is thereby ejected from its atom. Compton scattering is a similar mechanism, though in this case not all of the energy is transferred and the remaining energy is emitted as a new photon in a direction away from that of the parent photon. Finally, pair production can occur when a γ-ray with an energy higher than 1.022 MeV interacts with an atomic nucleus and transforms into an electron-positron pair, emitted in opposite directions. The contribution of each interaction pathway to the total absorption inside the material depends on the energy of the γ-rays involved.

γ-radiation is a form of indirect ionising radiation, as most of the ionising reactions occur by proxy of the excited electrons or by the emitted positrons and electrons in pair production.

1.1.4.2 Barium-133

Though the penetrative properties of γ-radiation allow for the use of external sources in e.g. effects studies, γ-emitting radionuclides can be of interest in

cases where they accumulate inside the organism. However, as noted in the previous section, γ-decay seldom occurs without the presence of other types of radiation. Nevertheless, some pure γ-emitters exist such as ^{133}Ba.

Barium is an alkaline earth metal with atomic number 56. Its chemical properties are quite similar to those of strontium, calcium and magnesium, and it also has an oxidation state +2. Barium is a very common element in the earth's crust, where it occurs in the form of minerals such as barite ($BaSO_4$) (IRSN, 2002). Whereas several radioactive isotopes of barium exist, barium-133 is only formed during nuclear fission as a result of proton or neutron capture and is therefore an artificial radionuclide. Although the net decay of ^{133}Ba is the emission of a γ-ray (356 keV (62%); 81 keV (34%) with a half-life 10.5 years), it is in fact the result of electron capture (equation 6).

$$^{133}_{56}Ba \rightarrow {}^{133}_{55}Cs + \gamma \qquad (6)$$

Very little data are available on ^{133}Ba activity in soil and surface water. Although the behaviour of barium in plants and animals is not well known, it seems to correspond to that of strontium (IRSN, 2002).

1.1.5 Effects of ionising radiation in living organisms

1.1.5.1 Interaction of ionising radiation with living matter

An important concept in understanding the effects of ionising radiation in matter is linear energy transfer (LET), which describes the way in which particles lose energy when they travel through matter (ICRU, 1970). Alpha particles have high-LET because of the 2+ charge and low velocity, which ensures a high number of ionising interactions along their path. Because of these high interactions, they slow down very quickly and travel only very short distances in matter along a straight track. Furthermore, the number of interactions increases

as the particle slows down. Beta particles however, can be considered high-LET or low-LET, depending on their kinetic energy, though both interact readily with matter due to their +1 or -1 charge. High energy β-particles interact less often with matter along their path, while low-energy β-particles are slower and have more interactions. The concept of LET does in principle not apply to photons, due to their dual particle-wave nature. However, their behaviour in matter can be described as low-LET (ASTDR, 1999).

A second distinction should be made between direct and indirect damage. Direct damage occurs when particles directly ionise biomolecules along their track. However, most living organisms predominantly consist of water. When ionising particles pass through water, they provoke water radiolysis and give rise to a number of radicals (ASTDR, 1999). Ionising radiation excites an electron in a water molecule from its orbit (equation 7), forming ionised water (H_2O^-). The electron can then interact with another water molecule to ultimately form hydroxyl (OH^-) and a hydrogen radical ($H^\bullet$) (equation 8). The ionised water molecule dissociates into a hydroxyl radical ($^\bullet OH$) and a proton (equation 9).

$$H_2O + IR \rightarrow H_2O^+ + e^- \quad (7)$$

$$e^- + H_2O \rightarrow H_2O^- \rightarrow OH^- + H^\bullet \quad (8)$$

$$H_2O^+ \rightarrow {}^\bullet OH + H^+ \quad (9)$$

These radicals can interact with biomolecules or quickly further combine to hydrogen peroxide (H_2O_2) and (in the presence of oxygen) superoxide ($O_2^\bullet$), which can also cause cellular damage. These radicals add to the pool of cellular reactive oxygen species (ROS) (See section 1.2)

Direct and indirect ionising radiation can cause extensive modifications of biomolecules in the cell, such as bond breaking and crosslink formation in lipids, proteins and carbohydrates. These modifications lead to structural as well as

functional damage. However, the most critical biomolecule is DNA, as it carries the information necessary to build and maintain cellular and organismal stability. Any modification or reshuffling that results from DNA damage is therefore a possible threat to integrity of the genetic information (UNSCEAR, 2008). Most organisms have a range of repair mechanisms, which aim to limit the damage to the genome (see section 1.3).

1.1.5.2 Effects of ionising radiation in humans and other animals

To assess the effects of radiation on humans, a framework has been created to calculate the doses absorbed by the body and the different organs in case of an exposure (UNSCEAR, 2008; ICRP, 2007). The standard unit for absorbed dose is the Gray (Gy), which described the energy (in J) absorbed per kg of tissue. As each type of radiation interacts differently with matter, the value for absorbed dose has to be amended by means of a radiation weighting factor (w_R) (Table 1.3), based on the relative biological effectiveness (RBE) of each type of radiation.

Radiation type	**w_R**
Alpha	20
Beta	1
Protons	2
Photons	1

Table 1.3: Radiation weighting factors (w_R) (ICRP, 2007). Each value represents the relative biological effectiveness (RBE) of its radiation type, by which absorbed doses can be multiplied to obtain an effective dose.

However, the sensitivity of each organ to radiation might differ, as this is dependent on the type of cells and the rate at which they divide. Fast-dividing tissues, such as bone marrow, are more sensitive to radioactive exposure than

slow-dividing tissues. Each tissue therefore has to be given a tissue weighting factor (w_T). By taking into account the type of radiation and the tissue type, a so-called "effective dose" can be calculated, expressed in Sievert (Sv). For example, an absorbed dose of 1 mGy by α-particles to the lungs (w_T = 0.12; ICRP, 2007) would result in an effective dose of 1 x 20 x 0.12 = 2.4 mSv. It has to be noted that this framework is only applicable to humans. The doses in non-human animal species can only be assessed in Gray, not in Sievert.

The deterministic effects of acute irradiation on humans are relatively well described as the so-called "Acute Radiation syndrome" (ARS) (Finch, 1987; Fliedner et al. 2001). Acute full-body doses above 1 Gy result in damage to fast-dividing tissues such as lymphocytes and platelets, which in turn decreases the immune response and causes anaemia. Above 5 Gy, the intestinal function and central nervous system start to be disrupted.

Apart from these deterministic effects, stochastic effects such as cancer induction and mutations are likely to occur as a result of irradiation. The current model (Linear No-Threshold) used in radiation protection is based on a linear relation between dose and stochastic effect probability, without a lower threshold boundary. There are however indications that this model does not hold at doses below 1 Gy (UNSCEAR, 2008).

1.1.5.3 Effects of ionising radiation in plants

As in humans, the main interaction of radiation with plants occurs by hydrolysis and direct damage to structural and functional biomolecules in the cells.

Until recently, the effects of ionising radiation on plants were mainly studied at the level of growth, morphology, reproduction and genotoxicity. These studies were mostly performed either under lab conditions using acute γ-radiation (mostly on crops), or in field studies at contaminated sites such as Chernobyl. These studies have shown a variety of responses, from growth and yield reduction to chromosomal instability (reviewed in Holst & Nagel, 1997).

Furthermore, they have revealed a broad spectrum of interspecies variation in radiosensitivity, partly based upon genome size (Sparrow & Miksche, 1961). In some cases, positive effects on growth and physiology have been observed at low doses. While these responses have been labelled as "hormesis", their functional role or underlying mechanism are currently not known (Calabrese & Baldwin, 2001). Recently, there has been an interest in studies at the molecular level, which have revealed the importance of DNA repair pathways, cell cycle regulation and oxidative stress in the response to ionising radiation (Esnault et al., 2010). These results are discussed in more detail at the end of sections 1.2 and 1.3.

At an international level, current screening values are based upon species sensitivity distributions (SSD), which are constructed from effects data gathered in databases such as FREDERICA (Copplestone et al., 2008). Within the ERICA approach (Brown et al., 2008), a risk assessment approach based upon species sensitivity distributions of benchmark values, 10 μGy h^{-1} has been derived as a no-effect screening value. Similarly the PROTECT project, which has used a similar approach for each group of organisms, has derived 70 μGy h^{-1} as a specific screening value for plants (PROTECT, 2008). As most of the studies in FREDERICA were performed using growth or genotoxicity endpoints, a better characterisation of molecular and physiological endpoints is needed to confirm or alter these derived benchmarks for plants. The United Nations Scientific Committee on the Effects of Atomic Radiation (UNSCEAR) concluded that dose rates up to 400 μGy h-1 to a small proportion of individuals in aquatic populations would not have a detrimental effect at the population level (UNSCEAR, 1996). The International Commission on Radiological Protection (ICRP) has proposed a 'derived consideration reference level' (DCRL) of 4-40 μGy h-1 for the most sensitive reference animals and plants (ICRP, 2008)

1.2 Oxidative Stress

1.2.1 Introduction

Historically, the presence of reactive oxygen species (ROS) in plant cells during unstressed conditions has been regarded as an undesired by-product of metabolism, which leads to oxidative damage to cellular components such as proteins, lipids and DNA (Mittler et al., 2002).

However, this is a logical result of the emergence of photosynthetic processes during the course of evolution, which have led to an increase in the cellular concentrations of the highly reactive molecule O_2 (Halliwell, 2006). The discovery that plants use ROS as a way to detect and signal abiotic and biotic stress and as a control mechanism in essential developmental processes (Dat et al., 2000) has led to a shift in the way we see cellular ROS (Foyer & Noctor, 2005a). Instead of a negative association to damage and cell death, the observation that oxidative stress and signalling are a heavily regulated and complex process shows that ROS are an essential part of the perception, transmission and response to environmental changes (Foyer & Noctor 2005b).

1.2.2 ROS Production

The presence of molecular oxygen (O_2) inside the cell enables ROS to be formed as a by-product of normal metabolism (Battachjree et al., 2005; Gill & Tuteja, 2010; Vranova et al., 2002). Such sites can evidently be found in the mitochondria and the chloroplasts, respective locations of the respiration and photosynthesis chains, both of which are prone to ROS formation.

The inability to dissipate energy at the light harvesting complexes (LHC) can produce highly reactive singlet oxygen ($^1O_2$), which is an important source of photo-oxidative stress in the chloroplast (Tryantaphylides et al., 2008).

Nevertheless, most of the ROS produced by the photosynthetic electron transport chain (ETC) or the respiration chain are $O_2^{\bullet-}$, formed after transfer of 1 electron to O_2 (Figure 1.1). Electron leakage by P_{450} is an additional source of $O_2^{\bullet-}$ in the cytoplasm and the endoplasmatic reticulum (Urban et al., 1997; Vranova et al., 2002). Superoxide has a short half-life (2-4 µs) and cannot pass lipid membranes. However, its protonated form $HO_2^{\bullet}$ (Figure 1.1) can migrate into lipid layers and induces auto-oxidation of poly-unsaturated fatty acids (PUFA) (Bielski et al., 1983). Another source of $O_2^{\bullet-}$ can be found in the peroxisomes, where it is generated in purine catabolism by xanthine oxidase (Del Rio et al., 2006).

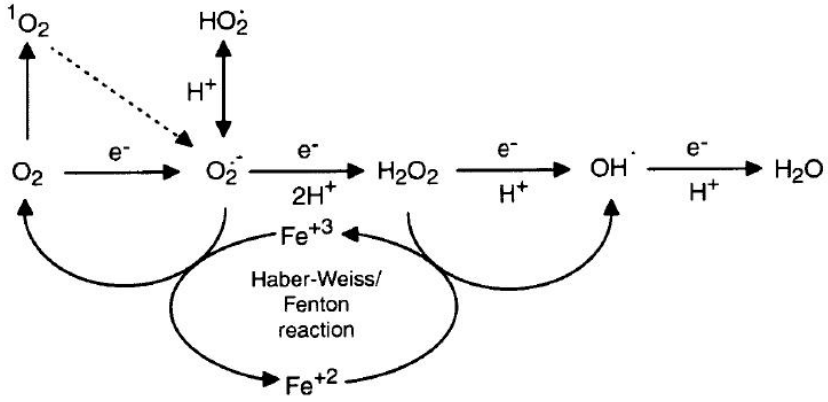

Figure 1.1: Main reactive oxygen species and reactions. Singlet oxygen ($^1O2$) formed in the chloroplast, while superoxide ($O_2^{\bullet-}$) is formed at various locations in the cell (Endoplasmatic reticulum, chloroplast, peroxisomes, cell wall). Hydrogen peroxide (H_2O_2) is predominantly formed in the cell wall and the peroxisomes Superoxide dismutates to H_2O_2. Both can, through the Haber-Weiss/Fenton reaction, form the hydroxyl radical ($^{\bullet}OH$). (Vranova et al., 2002).

Superoxide can be reduced to hydrogen peroxide (H_2O_2) (Figure 1.1), a molecule with a much longer half-life (order of ms), either spontaneously or by

superoxide dismutases (SODs). Because H_2O_2 is uncharged and long-lived, it can readily diffuse through membranes and travel a considerable distance inside the cell (Vranova et al., 2002). This makes it an ideal candidate as a signalling molecule and a large amount of research has indeed shown that H_2O_2 can function as a second messenger in a broad range of physiological processes such as photosynthesis, cell cycle and development (Gill & Tuteja, 2010) and more importantly in a large number of stress responses, pathogenic as well as abiotic, where it can also induce programmed cell death (PCD) (Vranova et al., 2002). It can also influence the functioning of proteins by oxidising their thiol groups (Bowler et al., 1994). Apart from the dismutation of $O_2^{\bullet-}$, which co-locates it at the sites where $O_2^{\bullet-}$ is present, H_2O_2 is also formed *de novo* by cell wall peroxidases in the biotic stress response (see section 1.3.4) (Bolwell & Wojtaszek, 1997) and in the peroxisome during purine catabolism. A final reduction can occur when $O_2^{\bullet-}$ or H_2O_2 are reduced to the hydroxyl radical ($^{\bullet}OH$), an extremely reactive compound which can react with nearly any component of the cell and is able to induce PCD (Halliwell & Gutteridge, 1998). This reduction takes places in the presence of a metal catalyst in the Haber-Weiss and Fenton reactions (Figure 1.1).

Finally, an important site of ROS production is the plasma membrane, where NADPH oxidases produce $O_2^{\bullet-}$ and play an important role in the oxidative burst, together with cell wall peroxidases, in the response to biotic stress (Vranova et al.,2002). NADPH oxidases are homologs to the respiratory burst oxidases (RBO; hence the plant homolog genes are designated as RBOH) in mammalian neutrophils. They are triggered upon detection of a pathogen attack or abiotic stress, creating $O2^{\bullet-}$ by NADPH-mediated reduction of O_2 (Sagi & Fluhr, 2006).

1.2.3 Oxidative Burst

In response to environmental stress, pathogen attack or wounding, plants exhibit a response, described as 'oxidative burst', in which they actively produce

ROS (Mittler, 2002; O'Brien et al., 2012). The early nature of this response, and the picture of a complex downstream signalling network which starts to emerge from recent studies (Knight & Knight, 2001; Miller et al., 2010; Mittler et al., 2010; Vranova et al., 2002), suggests that plants use ROS as a signal to respond appropriately to different types of abiotic or biotic stress.

The initial production of ROS occurs at the level of the cell wall and the plasma membrane. In the plasma membrane, NADPH-oxidases (RBOH's) produce apoplastic $O_2^{\bullet-}$, which are subsequently transformed to H_2O_2 by SODs (see section 1.2.4). NADPH-oxidases have been identified as the homologs of mammalian respiratory burst oxidases (RBOs), which perform multiple roles in animal cells. The RBOH family in plants has several members, all of which have been implicated to a different extent in pathogen response, abiotic stress response and developmental processes (Torres & Dangl, 2005). In addition to these membrane-bound enzymes, apoplastic peroxidases can directly produce H_2O_2 (Bolwell et al., 2002). While both systems are believed to be active in the oxidative burst, the relative importance of both depends on the species and the pathogen or stress encountered (O'Brien et al., 2012).

Hydrogen peroxide can readily diffuse through the cell membrane and enter the cell, where it adds onto the ROS produced by cellular metabolism (section 1.2.2). The burst of ROS triggers downstream signalling, which ultimately activates either an appropriate gene expression response or PCD, depending on the concentration of H_2O_2 (Vranova et al., 2002). The downstream signalling network responsible for initiating an appropriate response is not independent, but forms a part of a much wider integrated network which links to other signal transduction pathways such as those involved in e.g DNA damage, the cellular redox status and the cell cycle (Mittler et al., 2010).

1.2.4 Anti-oxidative defence

The cellular ROS concentrations are kept under control by a series of mechanisms, which consist of both protein and metabolite scavenger components (Noctor & Foyer, 1998). The reason for this strict control is twofold. On the one hand, the balance between ROS formation and ROS detoxification in the cell has to be controlled to avoid an increase of oxidative damage to the cellular components such as lipids, proteins and DNA. On the other hand, correct signalling relies on a modulation and control of ROS concentrations to obtain a transient signal (Miller et al., 2010; Mittler, 2002).

Superoxide dismutases convert $O_2^{\bullet-}$ to H_2O_2 by disproportionation. As $O_2^{\bullet-}$ cannot pass lipid membranes, it has to be transformed at its site of production (Alscher et al., 2002; Gill & Tuteja, 2010). Therefore nearly every compartment where $O_2^{\bullet-}$ is likely to be formed, including the apoplast, contains SODs (Elstner, 1991). Plant cells contain several groups of SODs, determined by their metal co-factor: iron-SODs (FeSOD), manganese-SODs (MnSOD) and copper/zinc-SODs (CuZnSOD). FeSODs, can mainly be found in the chloroplast, a localisation linked to their ancestral presence in cyanobacteria. MnSODs have been localised in the mitochondria and peroxisomes. The third group, the CuZnSODs, is unique to eukaryotes (with a few exceptions), and is present in the cytosol, chloroplasts, mitochondria, peroxisomes and the apoplast (Alscher et al., 2002). Several types of biotic and abiotic stresses have been shown to induce differential expression of SOD isoforms (Gill & Tuteja, 2010).

The hydrogen peroxide produced by SOD activity can cross membranes and function as a signal molecule. Additional amounts of this mobile ROS are directly formed in several cellular compartments, of which the peroxisomes are the most important. Because of the important signalling function, keeping the H_2O_2 levels inside the cell under control is a heavily regulated process. Several pathways scavenge H_2O_2, of which the catalases (CAT) and the ascorbate-glutathione cycle are the two major representatives.

Catalases, which can mainly be found in the peroxisomes and glyoxysomes, catalyse the conversion of H_2O_2 to water without the need for a reductant (Mittler, 2002; Willekens et al., 1995). The active site of catalase has two hydrogen peroxide binding sites and, while the turnover rate is very high, the affinity for the substrate is low, scavenging only in the mM range (Mittler, 2002).

A second hydrogen peroxide scavenging mechanism, the ascorbate-glutathione pathway (Figure 1.2), consists of a series of enzymes and metabolites (Noctor and Foyer, 1998) starting with the reduction of H_2O_2 by ascorbate peroxidase (APX). Contrary to catalases, APX needs a reductant, ascorbate (AsA). The rest of the cycle is required to restore the reductive capacity by regenerating AsA, ultimately drawing reductive capacity from the NADPH pool (see Figure 1.2 for the detailed description).

The affinity of APX for hydrogen peroxide is much higher than that of catalase, in the µM range. Furthermore, the cycle is present in nearly every cellular compartment, underlining its importance in ROS control (Mittler, 2002). Ascorbate and glutathione have important roles outside of the ascorbate-glutathione cycle as well (Foyer & Noctor, 1998). Ascorbate, present in nearly every compartment to a certain extent, is able to directly scavenge hydroxyl, $O2^{\bullet-}$ and $^1O_2$ radicals. Glutathione has an important role in redox signalling and the sulphur metabolism (Jozefczak et al. 2012).

Ultimately, stress signalling and the subsequent response are the result of a complex interplay between the different enzymes and metabolites involved in each step of ROS detoxification. For example, the balance between SODs on the one hand and APX and catalase pathways on the other is crucial in the flow and release of the hydrogen peroxide signal and in oxidative damage control (Mittler, 2002). Furthermore, the response to stress relies on a selective control of the scavenger isozymes located in the different compartments of the cell and in the extracellular matrix.

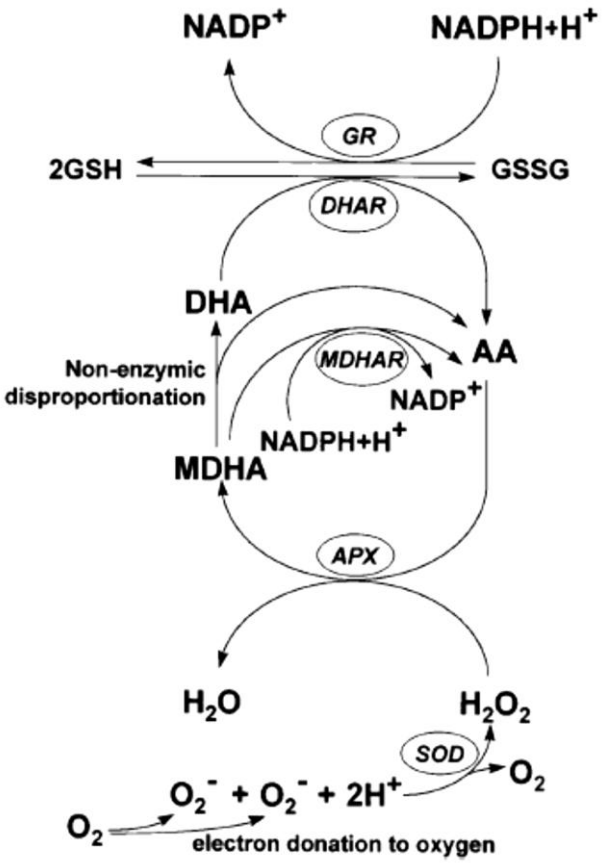

Figure 1.2: The Ascorbate-Glutathione Cycle. Hydrogen peroxide is reduced to water by ascorbate peroxide (APX), using two molecules of ascorbate (AsA) as a reductant with the production of Monodehydroascorbate (MDHA). MDHA in its turn either spontaneously disproportionates to AA and dehydroascorbate (DHA), or is reduced to ascorbate by Monodehydroascorbate reductase (depending on the compartment). DHA is reduced to AA by dehydroascorbate reductase (DHAR), using 2 molecules of glutathione (GSH) as reductans, with the production of GSSG. The pool of reduced glutathione is restored by the action of glutathione reductase (GR), drawing reductive power from the NADPH pool. (Noctor & Foyer, 1998)

1.2.5 Anti-oxidative defence in response to ionising radiation

Ionising radiation increases the cellular levels of most ROS (Lee et al., 2009), and increases in $^{\bullet}OH$, $O2^{\bullet-}$ and H_2O_2 have all been demonstrated after acute irradiation with γ-radiation (Esnault et al., 2010). Kim et al. (2011) has shown that APX, SODs and CAT are all up-regulated in response to low dose (2-8 Gy) acute irradiation in peppers, while Sahr et al. (2005) found that most genes involved in the stress response and anti-oxidative and cell defence were induced in *Arabidopsis* after exposure to chronic exposure to radioactive caesium. Similarly, 3 days of chronic low-dose rate γ-radiation induced effects in 18-day old *A.thaliana* seedlings (Vanhoudt et al., 2010). This was confirmed by transcriptomics studies by Kovalchuk et al. (2007) and Kim et al. (2007), although both studies used different life stages of *Arabidopsis thaliana* and therefore showed differences in the timing and intensity of the response. In summary, the involvement of CATs, SODs and the ascorbate-glutathione scavenging cycle have all been observed, though the exact details of their role and interplay in the response to chronic low-dose radiation remains to be determined (Esnault et al., 2010).

1.3 DNA Damage and the Cell Cycle

1.3.1 Introduction

DNA damage occurs both in healthy plants, as a result of normal functioning of the cell, and in plants exposed to biotic or abiotic stress, due to increased oxidative, chemical or physical interference with the structure of the double helix (Britt, 1996). The nature of the interference will determine the type and extent of the damage inflicted. Direct interaction of high-LET ionising radiation (IR) with the DNA may result in a break of both DNA strands, while low-LET ionising radiation or indirect oxidative damage by reactive oxygen species (ROS; Section

1.2) will more likely cause single strand breaks (SSB) or base modifications (Neary et al. 1972). Prokaryotes as well as eukaryotes have a certain number of detection and repair mechanisms for each type of DNA damage, which ensure that the integrity of the genome and the genetic information is maintained. This is especially of concern during mitosis and meiosis, when DNA is replicated before cell division. The cell cycle contains several DNA-integrity checkpoints, is therefore intrinsically linked to DNA repair.

1.3.2 Double Strand Breaks

Double strand breaks (DSB) are created when lesions occur in both strands at a single location, generating two loose ends and disrupting the continuity of the genetic information. DSB are a threat to the integrity of the genome, as they form a break in the continuity of the genetic information (Britt, 1996). At least two separate repair pathways are present in plant cells (Figure 1.3; Waterworth et al. 2011). Homologous recombination (HR) is a conservative mechanism, which repairs the break by recombining the damaged region with an identical template within the cell (Figure 1.3). The damaged ends are stripped to single stranded DNA and form a complex with recombinases, after which the DNA-protein complex is led to a homologous DNA sequence where recombination can occur (Baumann et al. 1996). The most important of these recombinases is RAD51 (Doutriaux et al.,1998), a homolog to the prokaryotic RecA. RAD51 leads the damaged DNA sequence to a homologous sequence, whereupon recombination can occur.

Non-homologous end-joining (NHEJ) is not conservative, contrary to homologous recombination, as the loose ends of several double strand breaks are joined in a random way (Figure 1.3). As a result, the genetic information can be reshuffled or deleted which may lead to accumulation of damage to the genetic information and ultimately disrupt the functioning of the cell. The NHEJ pathway is highly conserved in eukaryotes, and contains two main protein complexes: NHEJ is initiated when a heterodimer DNA dependent protein kinase,

which consists of the KU70 and KU80 subunits, detects, binds and protects the double strand break ends from degradation (Bleuyard et al., 2006; Boulton & Jackson, 1996). After preparation of the ends for ligation, a second complex formed by XRCC4 and DNA ligase IV (LIG4) performs ATP-dependent ligation of the strands (West et al. 2000).

How DSB are detected within the plant cell, is not yet fully understood, though likely candidates are the proteins of the Ku70-Ku80 complex and the Mre11-Rad50-Nbs1 (MRN) complex, the latter of which is involved in both NHEJ and HR, and recruits ataxia telangiectasia mutated (ATM), a protein kinase, to the location of the DSB (Waterworth et al., 2011). Through its kinase activity, ATM is involved in downstream signalling, which links DNA damage to cell cycle progression, and intiates a transcriptional response (Amiard et al., 2010). While both pathways, NHEJ and HR, are both active in most plants the choice between both pathways seems to be in favour or NHEJ, however this is dependent on the developmental stage (Britt, 1996; Waterworth et al., 2011). Boyko et al. (2006b) have shown that *A. thaliana* seedlings gradually switch with age from a HR induction upon irradiation to induction of NHEJ.

A specific type of DSB repair occurs in plastids and mitochondria, organelles which contain their own genetic information. Mori et al. (2005) has characterized two PolI-like polymerases, encoded by AtPolIA and AtPolIB, that are both present in plastids and involved in organelle DNA replication. More recent work by Parent et al. (2011) has shown that both polymerases are present in mitochondria as well, highlighting their homology to prokaryote DNA polymerases. Their study also showed that AtPolIB, present in the TAIR database as POLG1, is involved in DSB repair in organelle DNA. *Arabidopsis* mutants impaired in AtPolIB were unable to repair DSB in organelle DNA and were shown to be more sensitive to DSB-inducing chemicals. This suggests that the protein is required for correct repair of strand breaks under abiotic stress.

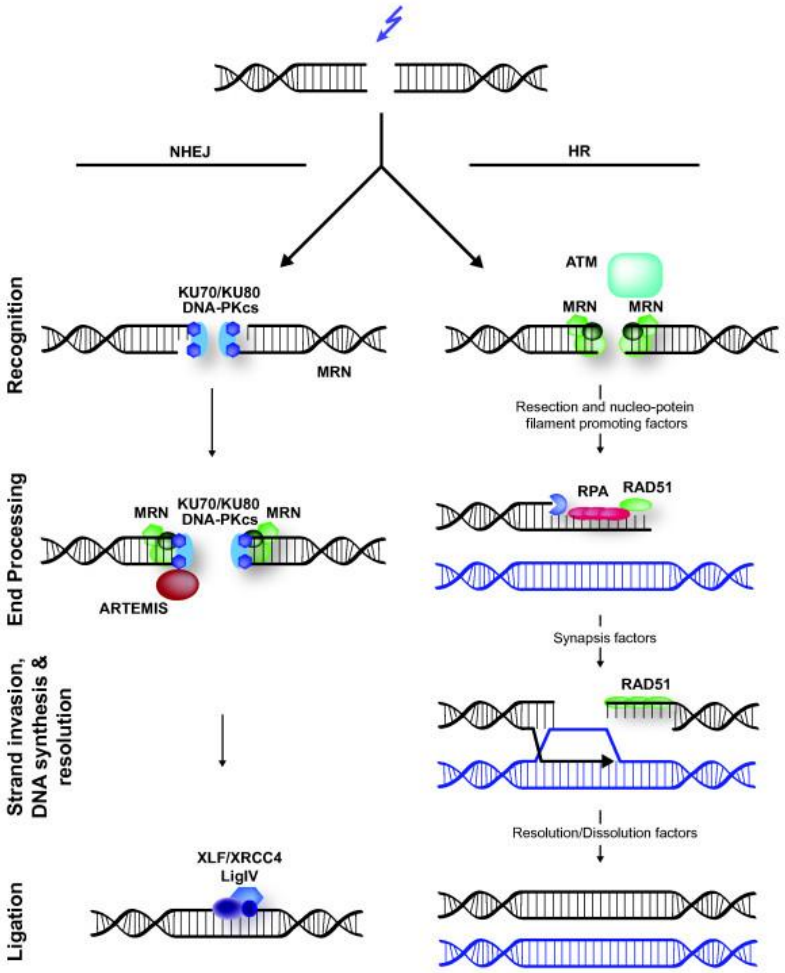

Figure 1.3: Comparison of NHEJ and HR DSB repair pathways (Lans et al., 2012). In the NHEI pathway (left), Ku70/80 binds the loose ends and recruits the MRN and Artemis complexes, which stabilise and process the ends and recruits DNA Ligase IV. In the HR pathway (right), MRN and ATM detect and bind the DSB loose ends and recruit RAD51 and RPA, which process the ends and lead the strands to a homologous sequence, where recombination occurs.

1.3.3 Single Strand Breaks and Base Modification

As single strand breaks (SSB) occur in only one strand at a time at a given location, the second, undamaged strand can be used as a template to reconstruct the genetic information. SSB damage does not only occur due to physical strand breaking by chemical agents or ionising radiation. More commonly, the breaks are created by repair mechanisms aimed at removing mismatched or modified bases which occur in the DNA through oxidative damage or inclusion of chemical analogues into the DNA molecule. Several mechanisms, such as base excision repair (BER) and nucleotide excision repair (NER), are present in plant cells to detect and repair single strand damage (extensively reviewed in Britt, 1996; Holst & Nagel, 1997). Both produce, through their action, single-strand lesions, which can then be detected and repaired.

Poly(ADP-Ribosyl)-polymerases (PARPs) are nuclear proteins, only present in eukaryotes, which perform post-translational modification of specific target proteins by adding Poly(ADP-ribose) chains to their lysine residues (Chen et al 1994), an action which can enhance or alter the behaviour and dynamics of those targets. The targets of PARP activity are proteins involved in cellular processes such as chromatin structure, DNA repair and gene transcription. Due to its consumption of NAD^+ to form Poly(ADP-Ribose) chains, PARP activity is directly linked to the redox status of the cell and, therefore, to the cellular response to biotic and abiotic stress and cell death. Several studies have shown that inhibition or reduced expression of PARPs modifies the response of plants to abiotic and biotic stress conditions by increasing the available NAD^+ pool (Adams-Philips et al. 2010; Schulz et al. 2012). Schulz et al. (2012) found an increased performance of photosynthesis in *A.thaliana* after inhibition of PARP activity. Three PARPs, PARP1, PARP2 and more recently PARP3, have been identified in Arabidopsis. Of these, PARP1 and PARP2 have been linked to DNA damage, more specifically to SSB damage induced after exposure to ionising radiation. Doucet-Chabeaud et al. (2001) reported increased transcription of

both PARP genes after induction of strand breaks by IR, whereas only PARP2 showed up-regulation after cadmium stress. Its involvement in abiotic stresses other than radiation indicates that PARP2 is likely to play a role in oxidative stress signalling as well, linking ROS-induced damage to the . The role of PARP1 is more complex, as its ability to recognize DNA damage, its link to the anti-oxidative system and its protein-modifying function put it in a controlling position in the cell during the response to plant stress.

1.3.4 Cell Cycle and Signalling

The progression of the cell cycle is a heavily regulated process, especially the transition points from G1 to S-phase and from G2-phase to mitosis. Transition through these two checkpoints can only happen if DNA repair has occurred, thereby ensuring correct transmission of the genetic information to the two daughter cells. Cell cycle regulation is performed by a combination of cyclins and their association to a series of cyclin-dependent kinases (CDKs) to form complexes (reviewed in De Veylder & Inzé 2007). These Cyclin-CDK complexes in their turn regulate the processes necessary for the progression through the cycle's phases.

Abiotic and biotic stresses alter progression of the cell cycle by inducing DNA damage, which requires repair. Until the DNA is repaired, the cycle remains blocked in G2-phase (De Veylder & Inzé, 2007). Signalling proteins, such as those of the ATR/ATM pathway, detect and report DNA strand breaks and eventually leads to a downstream point that affects Cyclin-CDK dynamics (Garcia et al., 2003; Culligan et al., 2006).

Several classes of proteins that modulate the behaviour of Cyclin-CDK complexes by direct inhibition or activation or by altering their inhibition or activation have been identified in plants. KRP2 is a Kip-related protein (De Veylder 2001a) which inhibits CDKA;1 and has been identified as an important factor in the transition from mitosis to endoreduplication in differentiating leaf

cells (Verkest et al., 2005). Overexpression of *KRP2* inhibits mitosis, and steers the cell cycle towards endoreduplication. CKS1 is a modulator of cyclin-CDK inhibition and activation. De Veylder et al (2001b) have shown that overexpression of AtCKS1 results in reduced root growth and meristem size and smaller leaves by altering the timing of G1 and G2 phase.

1.3.5 DNA Repair and Cell cycle control in the response to ionising radiation

After acute γ-irradiation of *A.thaliana*, 17% of all the differentially expressed genes were shown to have a role in DNA metabolism, control of the cell cycle and transcription control, such as PARP1, PARP2 and genes involved in both DSB repair mechanisms (Culligan et al., 2006). This was later confirmed by Kovalchuk et al. (2007). The transcriptional response on cell cycle control factors and DNA repair proteins seems to be under the control of ATM (Cools & De Veylder, 2009; Culligan et al., 2006). ATM-mediated regulation of the cell cycle arrest, which allows cells to repair DNA damage before mitosis is signalled in *Arabidopsis* through WEE1, a protein kinase (Amiard et al., 2010; De Schutter et al., 2007; Preuss & Britt, 2003).

In summary, it is clear from previous studies that *A.thaliana* regulates DNA repair, cell cycle control, oxidative stress and anti-oxidative defence in response to IR. However, as previously mentioned, these studies have mostly been performed with external acute radiation or high-dose rate chronic radiation, leaving a large amount of uncertainty as to the involvement and regulation of these pathways under low-dose rate radiation delivered by radionuclides.

Chapter 2:

Scope and Objectives

Increased human activity has led to a rise in the amount of radioactive elements in the environment. In addition to radionuclides from controlled and accidental releases by nuclear power facilities and medical activity, a significant amount of radionuclides is annually released from the earth's crust by the so-called NORM industries (Naturally Occurring Radioactive Material; e.g. phosphate industry, mining,…).

The presence of these radionuclides and their decay products in the biosphere pose an increased risk for exposure of biota to external as well as internal ionising radiation. Although significant scientific efforts have been made in the past to understand the effects of ionising radiation in non-human biota, there is still a considerable knowledge gap concerning how organisms respond on the molecular and physiological level and how this response ties in to effects on morphology and growth. For plants in particular, the dose-dependent effects of radiation are poorly understood. Studies on acute γ-irradiation suggest that DNA repair and the anti-oxidative response play an important role at the cellular level, though very little is known about the long-term responses to chronic radiation by radionuclides in the environment. Nor are there clear indications on how the responses differ or overlap between the different types of radiation.

In the first part of this study, we aimed to establish a dosimetry model for radionuclide exposure experiments on the model plant *Arabidopsis thaliana* seedlings grown under hydroponic conditions. We first described a static model for roots and shoots separately, and applied this to uptake and translocation data for three radionuclides: ^{241}Am, ^{90}Sr and ^{133}Ba (α-, β- and γ-emitters respectively) (**Chapter 3)**. We then expanded this model mathematically by including the seedlings' uptake, growth and geometry dynamics to investigate the effect of growth on dosimetry and to obtain a more precise estimation of dose rates and dose during radionuclide exposure (**Chapter 4**).

As other authors already mentioned differences in responses between plants in different growth stages, our next objective was to investigate whether

Arabidopsis thaliana seedlings display age-dependent effects to ionising radiation. In the second part of our research, we therefore exposed seedlings of different ages to high dose rates of external γ-radiation (**Chapter 5**) and analysed growth, photosynthesis, DNA damage and the transcriptional response of DNA repair. From this study, we selected the most appropriate stage for use in further radionuclide experiments.

In the third part of this study, our objective was to unravel the biological effects of chronic α- and β-radiation by exposing *Arabidopsis thaliana* seedlings for 7 days to a wide range of activity concentrations of ^{90}Sr (**Chapter 6**) and ^{241}Am (**Chapter 7**) respectively. We determined the uptake and distribution of each element between roots and leaves to obtain a detailed dosimetry, and measured growth, biomass and photosynthesis at several time points during exposure. To understand the effects at the morphological and physiological level, we measured the levels of pigments, DNA damage and anti-oxidative metabolites and characterised the transcriptional response of DNA repair and key enzymes in oxidative stress and ROS scavenging. In addition to understanding the way ionising radiation affects plants, we aimed to compare the mode of action of both radiation types and to try to fit them in a common framework.

Chapter 3:

An organ-based approach to dose calculation in the assessment of dose-dependent biological effects of ionizing radiation in *Arabidopsis thaliana*

Biermans, G., Horemans, N., Vanhoudt, N., Vandenhove, H., Saenen, E., Van Hees, M., Wannijn, J., Vives i Batlle, J., Cuypers, A., 2013. An organ-based approach to dose calculation in the assessment of dose-dependent biological effects of ionizing radiation in Arabidopsis thaliana. J. Environ. Radioactiv.

Published online: http://dx.doi.org/10.1016/j.jenvrad.2013.03.011.

Abstract

There is a need for a better understanding of biological effects of radiation exposure in non-human biota. Correct description of these effects requires a more detailed model of dosimetry than that available in current risk assessment tools, particularly for plants. In this paper, we propose a simple model for dose calculations in roots and shoots of *Arabidopsis thaliana* seedlings exposed to radionuclides in a hydroponic exposure setup. This model is used to compare absorbed doses for three radionuclides, ^{241}Am (α-radiation), ^{90}Sr (β-radiation) and ^{133}Ba (γ radiation). Using established dosimetric calculation methods, dose conversion coefficient values were determined for each organ separately based on uptake data from the different plant organs. These calculations were then compared to the DCC values obtained with the ERICA tool under equivalent geometry assumptions. When comparing with our new method, the ERICA tool appears to overestimate internal doses and underestimate external doses in the roots for all three radionuclides, though each to a different extent. These observations might help to refine dose-response relationships. The DCC values for ^{90}Sr in roots are shown to deviate the most. A dose-effect curve for ^{90}Sr β-radiation has been established on biomass and photosynthesis endpoints, but no significant dose-dependent effects are observed. This indicates the need for use of endpoints at the molecular and physiological scale.

3.1 Introduction

The recent events in Fukushima and the subsequent release of radioactive material to the environment have again underlined the need for a robust system that enables assessment of risks and protection of non-human biota from the adverse environmental effects of radioactive substances. There has been a considerable international effort on a regulatory and scientific level to develop an international system of radiological protection for the environment (ICRP, 2007; IUR, 2002; Copplestone et al., 2004). However, any such approach for risk assessment relies necessarily on benchmark values that indicate safe levels of environmental radiation and contamination for the organism or group of organisms involved, enabling a comparison of assessments with protection goals. These benchmark levels are not well defined for most organisms (Andersson et al., 2009) and the approach therefore currently adopted in environmental risk assessment tools is mainly based on reference animals and plants (ICRP 2009), such as those within the ERICA tool (Brown et al, 2008). Garnier-Laplace et al. (2004) have highlighted that there are considerable data gaps in the knowledge and understanding of low-dose radiation effects on all levels of biological organisation. Furthermore, there the extrapolation methods used to fill these gaps are not fool-proof, which leads to increased uncertainties and generalisations in environmental risk assessment.

In order to reduce uncertainties in the risk estimates, there is need for a better understanding of the way non-human biota react to different types of radiation received at with low doses. It is, in particular, essential to know which underlying biological mechanisms are involved in the response of organisms to radioactive exposure on all levels of biological organisation and whether they differ between α, β and γ radiation. Such necessity has recently been highlighted by the European Radioecological Alliance as an objective in the draft version of a Strategic Research Agenda for radioecology (Hinton et al., 2013). To attain this

objective, dose-effect relations have to be established for biological endpoints on the morphological as well as on the physiological and molecular scale for the different types of radiation. Dose-effect curves relate the observed effect on the endpoint to an absorbed dose or dose rate and therefore rely on accurate dosimetric calculations of the organism under the assessed internal and/or external exposure conditions. However, if a correct description of the biological mechanisms is to be made, these calculations must be performed on a more detailed scale than before, as uptake of radionuclides and sensitivity to radiation is likely to vary in cases where a heterogeneous distribution between organs exists. For humans, such a model is well established (ICRP 1996), but for most non-human biota it is non-existent (Garnier-Laplace et al., 2004).

Plants form an interesting model as they can roughly be described as two distinct parts, roots and shoots, that are spatially separate and functionally different. Roots provide uptake of nutrients from the environment, whereas shoots provide energy from sunlight through photosynthesis and in most species produce the offspring through sexual reproduction. Moreover, with the two compartments located in two different environments: roots in an aquatic or soil medium and shoots in the open air, the external dose they receive will differ. A dosimetric plant model should therefore incorporate these basic properties, and link them to the uptake and distribution of radionuclides in the plant organs. Very few such models are available and most have a limited range of application (ICRP 2009).

Arabidopsis thaliana (Mouse-ear cress) is a small terrestrial plant from the Brassicaceae family that has become popular as a model organism for flowering plants in cellular and molecular plant biology during the past decades. It is small and can easily be grown under controlled conditions on soil or hydroponic medium (Smeets et al., 2008), has a short lifecycle of six weeks and can produce a considerable amount of offspring, all of which reasons make it a convenient organism for lab studies. Moreover, its entire genome has been

sequenced and annotated (Poole, 2007) and its complete development and lifecycle have been described in detail (Boyes et al., 2001). A rosette of basal leaves is formed around a inflorescence stem which emerges after approximately 4 weeks of growth. Until the emergence of the inflorescence, the seedling shoots consist only of the rosette, of which the shape can be simplified to a single flat circular ellipsoid. The length and branching of the *Arabidopsis* root system can vary between experimental conditions, but the diameter of the individual roots is consistent at 100-150 µm.

The aim of this study is to establish a simple dosimetric model for *Arabidopsis thaliana* seedlings that can be used in radionuclide exposure scenarios to calculate absorbed doses and dose rates in roots and shoots from measured medium and organ activity concentrations, and use it to compare the behaviour of three radionuclides representing α, β and γ decay respectively.

3.2 Methods

3.2.1 Plant culture

Prior to sowing, *Arabidopsis thaliana* (Columbia ecotype) were spread-out on moist filter paper and vernalized for three days at 4 °C to synchronize germination. The seeds were subsequently sown on plugs from 1.5 mL eppendorf tubes filled with 0.6% agar in Hoagland solution. The plugs were mounted on a PVC cover, capable of holding 36 plugs, after which each cover was placed on a container filled with 1.35 L modified Hoagland solution (1mM KNO_3, 0.3 mm $Ca(NO_3)_2$, 0.2 mM $MgSO_4$, 0.1 mM $NH_4H_2PO_4$, 1.62 µM FeSO4, 0.78 µM Na_2EDTA, 4.6 µM H_3BO_3, 0.9 µM $MnCl_2$, 0.032 µM $CuSO_4$, 0.055 µM H_2MoO_4, 0.077 µM $ZnSO_4.7H_2O$).

Plants were grown in a growth chamber (Microclima 1000E, Snijders Scientific B.V.) under a 16/8 day/night photoperiod with 22°C/16°C day/night temperatures and 65% relative humidity. Photosynthetic photon flux density was 100 µmol m^{-2} s^{-1} at the leaf level (Sylvania BriteGro F36WT8/2084 and F36WT8/2023 lamps). The nutrient medium was aerated with a peristaltic pump from 7 days after sowing onwards.

3.2.2 Experimental Setup

In a first experiment, the uptake of three radionuclides, each representative of a specific type of ionising radiation, was measured. In our choice of elements, environmental relevance of the isotopes as well as ease of use and measurement were both taken into account. ^{241}Am and ^{90}Sr were used as α- and β-emitters respectively. Both are fission products, and of environmental concern in the Chernobyl fall-out (Kashparov et al., 2003) as well as on nuclear test sites. ^{133}Ba was chosen as γ-emitter because this element is known to be readily taken-up by plants (IRSN, 2002) and can as such be used as a source of internal γ exposure.

18-day old seedlings were exposed to an activity concentration between 1.5 and 2.5 kBq/L of one of the above radionuclides, using two duplicate trays per radionuclide. The radionuclides were added to the growth medium as a carrier-free $AmCl_3$ (in 1M HCl), $SrCl_2$ and $BaCl_2$ solution (both in 0.1M HCl) respectively. The pH of the liquid medium was adjusted to that of the control treatment with NaOH. This was done before exposure of the plants, and the resulting pH was typically 5.5 ± 0.1. After 3 days (72 h), roots and shoots were harvested separately for activity measurements.

After dose rate calculations (see 2.4), the radionuclide with the highest total dose (summed over the plant organs) was then selected from the uptake

experiment and used in a second experiment to establish a broad range dose-response curve with biomass and photosynthesis parameters as endpoints.

18 day-old seedlings were exposed to 0, 23, 230, 2330 and 22400 Bq/L activity concentrations of ^{90}Sr for 4 days (96 h), with three trays per radionuclide. After exposure, roots and shoots were sampled separately and weighed for fresh weight determination. The rest of the plants were snap-frozen in liquid nitrogen, shoots and roots separately, and stored at -80°C for pigment analysis.

3.2.3 Transfer

Half of the plants were collected for dry weight and uptake determination. The roots were rinsed immediately (twice 10 min. in 1 mM $Pb(NO_3)_2$, and once for 10 min. in dH_2O; at 4°C). It was observed in preliminary tests that $Pb(NO_3)_2$ removes most of the external contamination (data not shown). Plant organs were subsequently dried for 7 days at 60°C, after which dry weight could be determined (9 plants per biological replicate). Dried samples were all ashed in a muffle oven for 48 h at 550°C.

Samples for ^{90}Sr determination were dissolved in 1M HCl, diluted ten times with dH_2O and subsequently diluted four times with scintillation cocktail (Optiphase Hisafe 3, PerkinElmer). ^{90}Sr activity was measured with a β- liquid scintillation counter (Packard 1600TR Tri-Carb, Canberra,,Zellik, Belgium) for 60 minutes. The counting efficiency was determined using a dilution series of ^{90}Sr with known activities between 0 and 5000 Bq.

^{241}Am and ^{133}Ba activities were measured through HPGe Gamma spectrometry. Although ^{241}Am is primarily an α-emitter, it can easily be detected through its γ-emission spectrum. Samples for ^{241}Am or ^{133}Ba determination were dissolved in 1M HCl, and further diluted ten times with dH_2O. Samples were measured with a HPGe Gamma spectrometer (Canberra, Zellik, Belgium) calibrated for ^{241}Am and ^{133}Ba with a known source of identical geometry.

The organ activity concentrations of each radionuclide were calculated on a fresh and dry mass basis by dividing the measured activity by the respective fresh and dry masses. Transfer factors and concentration ratios were determined by dividing organ activity concentration by the activity concentration of the hydroponic medium.

3.2.4 Dose calculations

The method applied to calculate dose conversion coefficients (DCCs, defined as the dose rate per unit activity concentration in μGy h^{-1} / Bq kg^{-1}) was based on a previous Monte Carlo approach (Vives I Batlle et al., 2004) which uses point-specific absorbed fractions for γ rays (Berger, 1968). For β particles, Berger's tabulated values of r_p (the radius r of a sphere within which p% of the energy is absorbed from a point β source located at the centre) are used (Berger, 1971). These values are transformed to values of fractional absorption from a point β emitter within a sphere of radius equal to r/r90 around the source, which makes the fractional absorption relatively independent of energy. The method is fully described elsewhere (Copplestone et al., 2001). The absorbed fractions (number of iterations = 5000) were used to calculate the internal and external exposure DCCs (unweighted by radiation quality) for the individual radionuclides.

Internal shoot DCC were calculated based on the rosette area of 22-day old *Arabidopsis thaliana* seedlings after 4 days of control treatment. The total leaf area of an individual rosette was determined using the image software ImageJ (Leister et al., 1999; Schneider et al., 2012). This area was defined by means of a circle of which the diameter delivers two of the ellipsoidal axes. From these calculations, the geometrical assumptions for the leaves of 1 cm x 1 cm x 0.015 cm were derived. Individual *Arabidopsis thaliana* roots have a diameter of approximately 100 µm and, (under our growth conditions) a length of 10 cm at 22 days of growth. The root mass spreads uniformly when submerged, and each

individual root is surrounded by liquid medium. We therefore made the assumption of a 10 cm x 0.01 cm x 0.01 cm geometry in our calculations. To compare with the ERICA tool's in-built dose calculator, we entered three new geometries as three separate new organisms in the software: the geometries for root and shoot described above, and a third geometry that comprises the entire root mass as one single ellipsoid with a 10 cm x 0.138 cm x 0.138 cm geometry. We then calculated the internal and external DCC.

Assuming a linear increase of fresh weight based organ activity concentrations with time during the experiment, this leads to the following expressions for cumulative dose:

$dose_{internal} = (DCC_{internal} * activity\ concentration_{organ} * t) / 2$

$dose_{external} = (DCC_{external} * activity\ concentration_{medium} * t)$

3.2.5 Photosynthesis

Immediately after harvest, four plants from each treatment were chosen at random. These were selected from the plants destined for activity and dry weight measurements. Their 4^{th} leaf was then removed, and stored on wet paper in a closed petri dish in the dark.

The leaves were pre-adapted to dark conditions for at least 15 minutes and the induction curve (IC) for photosystem II (P680) was then measured using PAM Fluorometry (Dual PAM-1000; Waltz, Germany) (Schreiber et al., 2004). From these data, values for photosynthetic efficiency (φPSII), non-photochemical quenching (NPQ) and photosynthetic capacity (Fv/Fm) could be calculated.
The induction curve measurement was immediately followed by a rapid light curve (RLC) measurement. These data were then fitted to the continuous model of Platt without photoinhibition as used in Ralph and Gademan (2005) using a Marquardt-Levenberg curve fitting algorithm in statistical software package R.

3.2.6 Pigment analysis

Pigments were extracted from frozen shoots by incubation in 100% N,N-dimethylformamide (DMF) overnight at 4°C under dark conditions. The pigment absorbance was measured spectrophotometrically at 480, 647 and 664 nm and pigment concentrations for chlorophyll a, chlorophyll b and carotenoids were calculated from these-absorbance values using the appropriate equations for DMF according to Wellburn (1994).

3.2.7 Statistical Analysis

All biological endpoints were evaluated statistically using one-way analysis of variance (ANOVA) and Tukey multiple comparison testing. Analyses were carried out with the freeware software package GNU R (version 2.13.0).

3.3 Results and Discussion

3.3.1 Transfer of ^{241}Am, ^{90}Sr and ^{133}Ba

Measured activity concentrations in the growth medium and transfer parameters to the plant organs are presented in Table 3.1. The medium activities of all radionuclides were well within the desired range of 1.5 to 2.5 kBq/L.
Americium showed a very low transfer to both roots and shoots, and the activity was primarily present in the roots, yielding a low shoot:root ratio. Duffa et al. (2002) found a ratio of 0.025 in rice on dry weight base, and our findings (0.0181 ± 0.0021) are consistent with their findings. The transfer factor is high compared to that from soil to plant (Sokolik et al., 2004), but Americium quickly binds to organic matter in an aquatic medium, which facilitates adsorption by the plant tissues (Bondareva et al., 2010).

^{90}Sr accumulated in high levels (Table 3.1) and showed a high transfer from root to shoot. Most of the ^{90}Sr was located in the shoots of the seedlings. Strontium is known to be mobile and accumulate at high concentrations in plants, due to the high chemical resemblance to calcium (Moyen & Roblin, 2010; Seregin & Kozhevnikova, 2004). Vanhoudt et al. (2011) found a high shoot:root ratio for both calcium and magnesium in *Arabidopsis thaliana* under a growth setup identical to ours, which suggests that ^{90}Sr accumulation is indeed linked to their pattern of uptake and transport in the growing seedlings.

Table 3.1: Transfer parameters of ^{241}Am, ^{90}Sr and ^{133}Ba in *Arabidopsis thaliana* roots and shoots after 72 hours of exposure to the measured medium activity concentrations. Activity concentrations are mean ± SE with 3 replicates. All transfer parameter values are mean ± SE with at least 4 biological replicates.

		^{241}Am α	^{90}Sr β	^{133}Ba γ
Activity Concentration Medium [Bq L^{-1}]		2230 ± 300	1500 ± 200	1450 ± 170
Transfer Factor	*Root*	715 ± 80	606 ± 17	1660 ± 90
[Bq kg DW^{-1} / Bq L^{-1}]	*Shoot*	13.5 ± 0.6	2920 ± 80	1900 ± 50
Concentration Ratio	*Root*	12 ± 1	17 ± 3	28 ± 5
[Bq kg FW^{-1} / Bq L^{-1}]	*Shoot*	1.48 ± 0.09	328 ± 13	214 ± 3

This likely also accounts for the distribution pattern of ^{133}Ba (Table 3.1), which showed high uptake in roots and shoots and a shoot:root ratio greater than 1. Very few transfer data are available on this element. However, the few available studies on ^{133}Ba and its stable isotope reveal a behaviour close to that of strontium and calcium (IRSN, 2002), which is confirmed in our findings.

3.3.2 Dose calculations

The accumulated absorbed doses calculated for each plant organ are presented in Table 3.2. They clearly reflect the overall spatial distribution of each radionuclide within the plant. Whilst the transfer parameters are the main determining factor in the observed dose pattern, they cannot entirely account for the differences observed between the radionuclides.

Table 3.2: Calculated absorbed doses in *Arabidopsis thaliana* organs after 72 hours of exposure to ^{241}Am, ^{90}Sr and ^{133}Ba. All doses presented are (mean ± SE) with at least 3 biological replicates

		^{241}Am	^{90}Sr	^{133}Ba
Absorbed Dose [µGy]		α	β	γ
Internal	*Root*	2960 ± 260	13 ± 1,2	25 ± 5
	Shoot	360 ± 20	4670 ± 200	312 ± 5
External	*Root*	4 ± 0,4[b]	67 ± 9	25 ± 4
Total		***3324 ± 260***	***4780 ± 200***	***403 ± 7***

[b]the external dose from ^{241}Am is non-zero due to the low amount of γ-radiation it emits aside from its α-decay.

In our experimental setup, ^{90}Sr and ^{241}Am have comparable values for root concentration ratios (Table 3.1), but the internal doses delivered to the roots are very dissimilar (Table 3.2). This is a result of the difference in behaviour between the types of ionising particles involved, as well as their energies and decay pathways, all of which impinges on the dose conversion coefficients. The energy of the ^{241}Am α-particles is deposited entirely within the organ, whereas β particles emitted by ^{90}Sr (which have higher range in matter than α-particles) can travel longer distances and escape the plant, as can the photons emitted by

^{133}Ba. Therefore, ^{241}Am has a higher DCC, and a higher dose is absorbed by the organ at equality of activity concentration.

An additional difference in behaviour between radiation types becomes apparent if we compare the internal doses from ^{90}Sr and ^{133}Ba in each organ. In the roots, both have similar DCCs and concentration ratios (Table 3.1) and consequently have similar resulting doses (Table 3.2). Conversely, in the shoots, the concentration ratios of both radionuclides also lie within the same order of magnitude, but there the resulting dose for ^{90}Sr is ten times higher than that caused by ^{133}Ba. This difference arises from the DCC calculations, which yield an internal DCC of 3.0×10^{-5} µGy h^{-1} / Bq kg FW^{-1} for ^{133}Ba and 2.8×10^{-4} µGy h^{-1} / Bq kg FW^{-1} for ^{90}Sr. Logically, this is directly influenced by the various geometrical assumptions. For the roots, we assumed a diameter of 100 µm, a length below the range of both high-energy β- and γ-radiation (which therefore seem to behave similarly). In the shoots, which have a 1-cm diameter and a thickness of 1.5 mm, the proportions are very different and the difference in dose deposition between β- and γ-radiations comes into play.

3.3.3 Comparison with the ERICA tool dosimetry

The observed effects of radionuclide distribution and geometry on the absorbed dose underline the need for a plant dosimetry that takes into account all plant organs separately. Roots and shoots have very different functions in the organism. To understand the dose-dependent effects of each type of radioactive decay on the plant and the biological mechanisms that lead to these effects, it is essential that a correct estimation of dose is made for each functional unit. In using a single ellipsoid to represent the entire organism (as is the case for the methodology used for reference animals and plants within the ERICA tool - Brown et al., 2008), a conservative dose estimate is obtained. This is desirable for environmental protection purposes, but has the opposite effect when establishing dose-effect curves. Overestimation of the absorbed doses shifts the

dose-effect curve to the right of the dose scale and makes the dose response appear more conservative than it really should be, thus overestimating the dose needed to elicit the observed effect.

The only way to calculate DCC for root and shoot separately in the ERICA tool is to enter them into the software as two new organisms in the Tier 2 assessment. When we performed this exercise as a comparison with the values obtained in our study, the DCC values for ^{241}Am, ^{90}Sr and ^{133}Ba for the shoots were found to be almost identical to those in our model (data not shown). This was not the case in the roots, where we found an overestimation by ERICA of the internal DCC compared to our model for all three radionuclides (Fig.3.1A). This is a direct consequence of the mass limitations of ERICA, which dictates a minimum of 10^{-6} kg for aquatic species, a factor 10 above the mass of our model's geometry (10^{-7} kg). In ERICA, one must then resort to accept this minimum value if the mass of the organism is below it. The magnitude of this difference in internal DCC between the two calculations depends on the radiation type. While the internal DCC values for ^{241}Am and ^{133}Ba show only a minor increase compared to our *Arabidopsis* model (0.001 and 1.33-fold respectively), the DCC for ^{90}Sr increases 4-fold in the ERICA calculation. When we tried to overcome the mass limitation problem by modelling the entire root mass in one single ellipsoid the overestimation increased even more due to the change in geometry, which has a larger effect on β-decay as previously reported. In this total root mass model, the internal DCC was overestimated 12-fold compared to our *Arabidopsis* model (Fig. 3.1A), while those for ^{241}Am and ^{133}Ba remained within the limits of a 2-fold overestimation. The external DCC values were underestimated by the ERICA models by approximately 20% for ^{241}Am and ^{90}Sr, while the DCC for ^{133}Ba remained constant. It should be noted, however, that the external DCC value for ^{241}Am is negligible (1.8×10^{-5} to 2.5×10^{-5} μGy h^{-1} / Bq kg^{-1}) compared to the internal DCC, as only a small percentage of α particles emitted by ^{241}Am is taken into account in the external dose calculations.

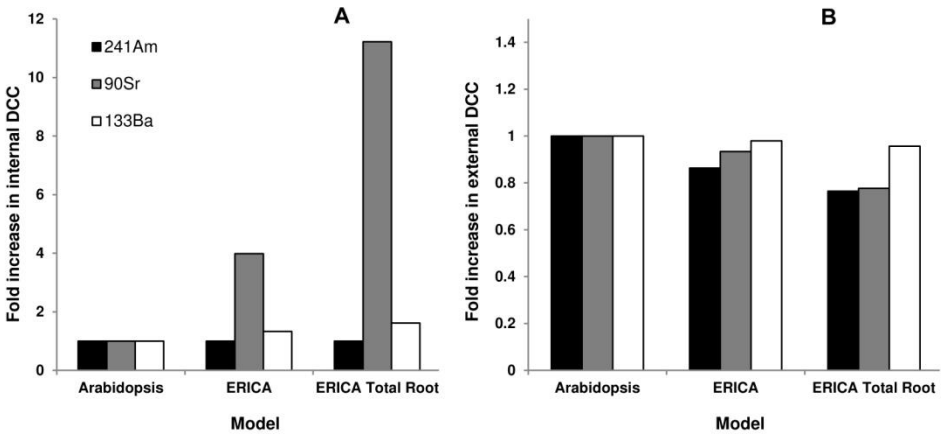

Figure 3.1: Comparison of internal (A) and external (B) DCCs for ^{241}Am, ^{90}Sr and ^{133}Ba between two ERICA simulations for single root (10 cm x 0.01 cm x 0.01 cm) and total root mass (10 cm x 0.138 cm x 0.138 cm) and the model presented for Arabidopsis thaliana in our study. Data for each radionuclide are presented relative to values from our model.

3.3.4 Evaluation of the dosimetry model

While our method can be taken as a step forward in dose calculation of plants in a hydroponic setup, it still has several conceptual limitations. By representing the *Arabidopsis* rosette and the separate leaves by a single ellipsoid, the DCCs for internal doses delivered by β- and γ-radiation are more conservative than those in a model with separate leaves. However, our method has the advantage that total leaf area of *Arabidopsis* seedlings can easily be measured and is well related to seedling growth (Leister et al., 1999). For the roots, we favoured the modelling of a single root over that of the root mass as a whole. The disadvantage of this concept is that it does not take into account the behaviour of the root network as one single organ, with close proximity of the separate root strands to each other. Therefore, this method underestimates somewhat the external dose for β and γ radiation in the roots.

While our model is not directly compatible with the current tools available for environmental risk assessment such as ERICA, it does integrate key aspects of the standard methodology used to calculate absorbed fractions (e.g. using ellipsoids to approximate plant shape). However, it improves the accuracy of dose calculations by representing the plant as an organism with a heterogeneous body plan. We propose that the accuracy of the dosimetry could be increased further by including the data available on *Arabidopsis thaliana* growth and by mathematically linking the time-dependent changes in root and shoot geometry to changes in DCC. By collecting detailed activity concentration data for the different organs and the surrounding aquatic medium for different time points over time, it ought in theory 'to be possible to model dose and dose rates during the complete growth of *Arabidopsis* seedlings.

3.3.5 Dose-response curve of ^{90}Sr

Based on the summed doses over root and shoot, similar medium concentrations of ^{90}Sr and ^{241}Am give doses within the same order of magnitude if summed over the entire plant (Table 3.2). In choosing the radiation type to establish a dose-effect curve, we therefore took into account the nature of the endpoints used. Photosynthesis only takes place in the shoots, and so ^{90}Sr was favoured over ^{241}Am in our assessment.

The calculated absorbed doses for each treatment after 4 days are reported in Table 3.3. These values show that in our setup, a 10-fold increase in environmental activity concentration results in a 10-fold increase in accumulated dose in both root and shoot, with a maximum of 84.4 ± 2.5 mGy in the shoots and approximately 2 mGy in the roots at exposure to a 22000 Bq L^{-1} medium activity concentration. This linear relationship between medium concentration and organ activity concentration indicates that the transfer and translocation of

^{90}Sr is not affected by an increase in β-radiation dose (and dose rate) within the range tested in our study.

Table 3.3: Calculated absorbed doses in *Arabidopsis thaliana* roots and shoots after 96 hours of exposure to ^{90}Sr.

	Absorbed Dose [µGy]		
	Shoots	Roots	
	Internal	*Internal*	*External*
Treatment [Bq*L^{-1}]			
Control	1 ± 1	0,07 ± 0,1	0,04 ± 0,12
22 ± 3	84 ± 4	0,56 ± 0,03	1,35 ± 0,17
230 ± 11	830 ± 15	6,5 ± 0,3	14,1 ± 0,6
2330 ± 50	8000 ± 500	54 ± 6	142,6 ± 2,5
22400 ± 700	84400 ± 2500	556 ± 24	1370 ± 30

No dose-dependent effects could be observed on fresh weight or dry weight in the roots or shoots of the seedlings (data not shown). At the level of photosynthesis, we observed a significant decrease in saturated electron transport rate (ETR_{max}) at the lowest ^{90}Sr concentration (Fig. 3.2) with the values returning to that of the control treatment with increasing dose. ETR_{max} reflects the maximum electron transport rate through the photosynthesis chain obtained under high light flux conditions (Ralph & Gademan, 2005). At low flux rates, we found no differences in ETR between treatments. This decrease in ETR_{max} at the lowest dose appears to be accompanied by a decrease in quantum photosynthetic efficiency of Photosystem II Φ_{PSII} (Fig. 3.3A) and an increase in non-photochemical quenching (NPQ) (Fig. 3.3B). Neither Φ_{PSII} (ANOVA, $F_{4,14}$=2.32, p=0.108) or NPQ (ANOVA, $F_{4,13}$=2.64, p=0.084) showed significant differences between treatments, but the trend of a high difference with the control at low dose and a return to control values with increasing dose was present in both parameter measurements.

A decrease in Φ_{PSII} indicates that a smaller fraction of the incoming energy is fed into the photosynthesis chain through Photosystem II and the increased value for NPQ indicates that the excess of the light absorbed energy is quenched as heat to avoid damage.

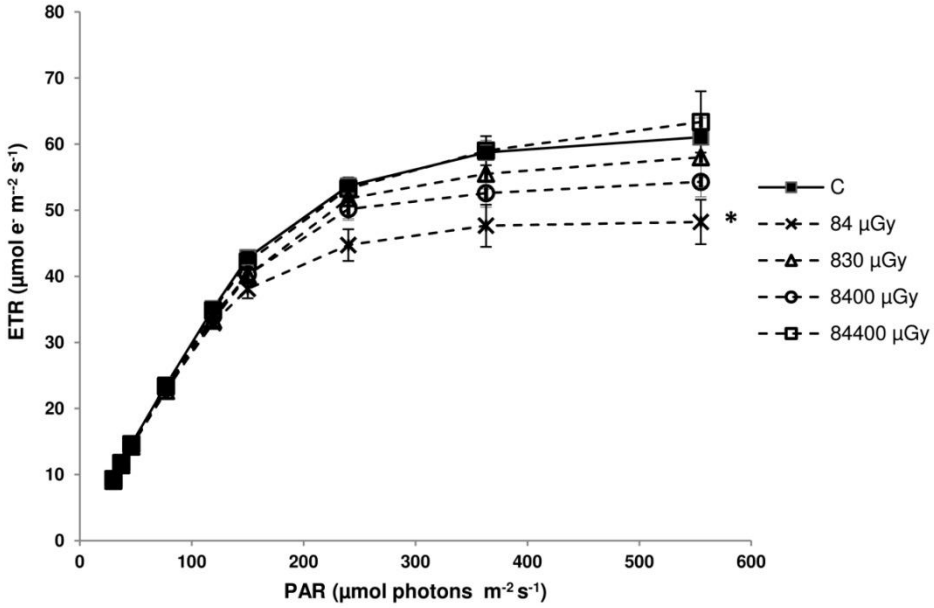

Figure 3.2: Light curve measurements on leaves of Arabidopsis thaliana after 4 days of exposure to ^{90}Sr. Values are expressed as Mean ± SE. Significance levels are indicated for values at 555 µmol photons $m^{-2}s^{-1}$ (* $p<0.05$).

We observed no dose-dependent effect on maximum variable fluorescence after dark-adaptation (Fv/Fm) or the chlorophyll ratio (Fig.3.3C and D), indicating that there is no alteration to the light harvesting capacities of the plant. While none of the trends observed appear significant, it is interesting to note that our observations are contrary to the effects Moon et al. (2008) observed after irradiation of *Arabidopsis* leaves with high doses of acute external γ-radiation.

Their study observed a decrease in carotenoids, a group of pigments necessary in the build-up of non-photochemical quenching after 4 hours of exposure to 50 Gy h^{-1}. Low dose rates of irradiation such as those found in our study are likely to induce effects on physiology different to those in acute high radiation exposures (Kovalchuk et al., 2007).

Our data have shown that, within the range of medium activity concentrations tested, no conclusive effect of β-radiation could be found on the endpoints measured after a 4-day exposure of 18-day old *Arabidopsis thaliana* seedlings. This indicates that to find biological endpoints sensitive to radiation in *Arabidopsis thaliana*, we need to look at the changes at the physiological and molecular scale. However, in unravelling the biological mechanisms of the plant response to radiation exposure we need to see how these underlying mechanisms affect growth and development on a morphological scale, both in root and shoot tissues. While photosynthesis gives an indication of the overall energetic health of the plant, the differential uptake and dosimetry of the different tissues highlight that the use of endpoints which can be compared between tissues, such as DNA damage or gene expression. Further research will also have to assess whether a more sensitive stage in the development of *Arabidopsis* seedlings can be found.

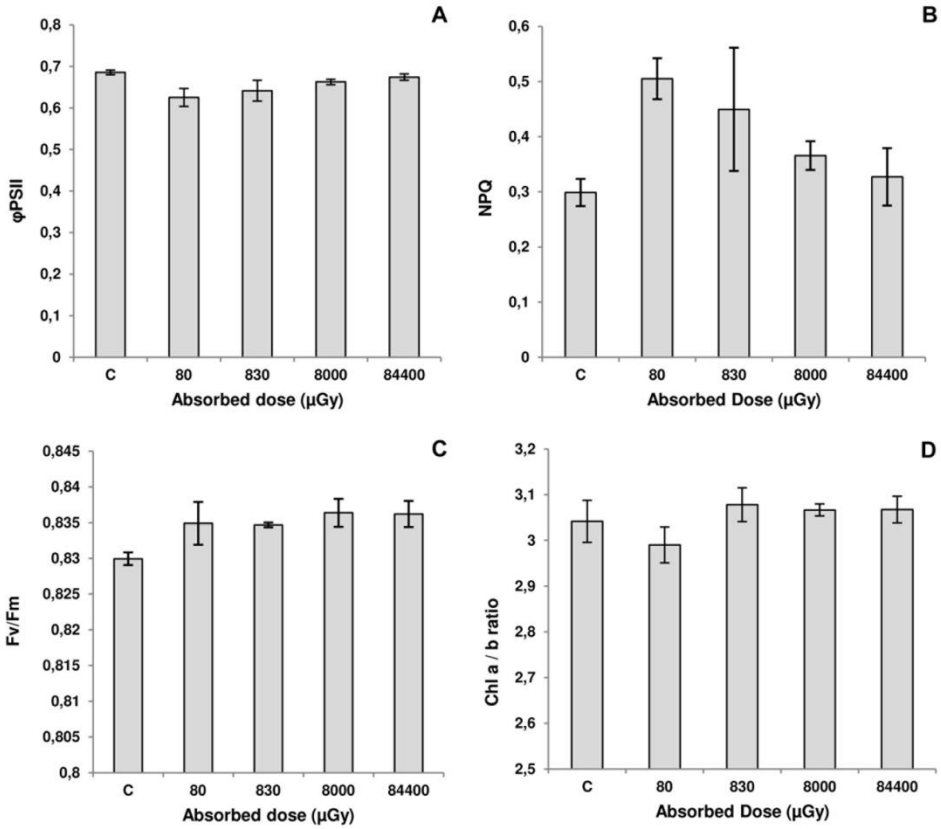

Figure 3.3: Photosynthesis parameters (A-C) and Chlorophyll ratio (D) determined during induction measurement in dark-adapted Arabidopsis thaliana leaves after 4 days of exposure to ^{90}Sr. The data presented are expressed as (Mean ± SE) with N = 4.

Chapter 4:

A dynamic dosimetry model for radioactive exposure scenarios in *Arabidopsis thaliana*.

Biermans, G., Horemans, N., Hens, N., Vives i Batlle, J., Vandenhove, H., Cuypers, A., 2013. A dynamic dosimetry model for radioactive exposure scenarios in Arabidopsis thaliana.

Submitted to Journal of Theoretical Biology

ABSTRACT

To obtain a better understanding on how non-human biota are affected by exposure to environmental radioactivity, it is essential to link observed effects to a correct estimate of absorbed ionising radiation dose. Current wildlife dose rate and risk assessment tools are not set up to assess changes in dose rate during organism development. This paper presents a dosimetry model for assessing dose rate and absorbed dose during seedling development of the model plant Arabidopsis thaliana. We included growth and radionuclide absorption dynamics into the dose calculations. This model was subsequently used to compare the dose and dose rate calculations for three radionuclides, ^{241}Am (α-radiation), ^{90}Sr (β-radiation) and ^{133}Ba (γ-radiation), in a standard exposure scenario. We show that growth influences dose and dose rate and that this influence depends on the radionuclide and the organ involved. The use of dynamic dosimetry models greatly improves the dose calculations for effect studies.

4.1 Introduction

Anthropogenic levels of radioactivity in the environment are ever increasing, either as routine releases by nuclear power plants and the NORM industries, or by accidental releases such as that of the recent Fukushima accident. Evaluating the risks associated with the presence of radioactive material in the environment not only necessitates a description of the interaction and transport of radionuclides with and within the biosphere, but also requires a good understanding of the delivered dose and the adverse effects it may cause in biota. International effort has therefore been made, both by regulatory bodies and by the scientific community, to build a radiological environmental protection system. Environmental protection benchmarks have been derived by different organisations (Andersson et al., 2009; Garnier-Laplace et al., 2006; ICRP, 2009) and protection may be rather at the ecosystem level (Garnier-Laplace et al., 2006) or rather at the organism group level or individual level (ICRP, 2009). Comparison of the dose rate assessment results with the benchmark values allows to make a judgement in how far the contamination or exposure to radioactivity affects the wildlife or is of no environmental concern. Gaps in our present understanding of radionuclide transfer to biota and low-dose radiation effects and the subsequent extrapolations and uncertainty in the dosimetric calculations over an organism life span, contributes to a considerable amount of uncertainty in risk assessment for non-human biota (Garnier-Laplace et al., 2005).

Hitherto, the dosimetric approach used within environmental risk assessment software tools such as ERICA (Brown et al., 2008) has been based upon absorbed energy fractions of radioactive decay within a given geometry. In all models commonly used for calculating dose to non-human biota (including the present one), the reference organism is reduced to a single ellipsoid, which is defined by its three axes. A stochastic method is used to calculate the fraction of energy absorbed within the body as a function of decay energy. This approach

allows for the calculation of a dose conversion coefficient (DCC, μGy h^{-1} / Bq kg^{-1} or Bq kg^{-1}) for each radionuclide whose decay pathways and quantum yield are known (Copplestone et al., 2001). This DCC value reflects how much of the decay energy is absorbed inside the organism per unit contamination in the environmental media (external exposure) or in the body (internal exposure). It is specific to the defined geometry of organism and exposure medium (and homogeneous/inhomogeneous distribution of the radioactivity in media and body) and converts a known or calculated radionuclide activity concentration into a dose rate, which can then be used to integrate the absorbed dose over exposure time. When we want to understand the effects of radiation exposure, we need a robust estimation of the dose rate and absorbed doses delivered to the exposed organisms (Copplestone et al., 2001; Hinton et al., 2013). In a foregoing study, we described a simple dose rate assessment approach for the model plant *Arabidopsis thaliana* based on the geometries for root and shoot organs and radionuclide incorporation at the end of the hydroponic growth experiment. We compared the exposure for three types of radiation (α, β and γ) (Biermans et al., 2013). Our study showed that dose assessment can be improved by providing a more detailed description of the biota geometry, i.e. by describing each organ separately (i.e. root and shoot) and by considering the radionuclide distributions between the organs. We also showed that internal DCC values for some of the radionuclides were quite sensitive to changes in geometry. This means that the rapid changes in shoot and root size during growth of Arabidopsis thaliana seedlings are likely to affect the dose during radionuclide exposure. By including growth dynamics in the dosimetric calculations, we can therefore obtain an improved estimation of dose rates and doses delivered during the time of exposure.

Our aim in this study is to develop an improved dosimetric model for Arabidopsis thaliana seedlings under hydroponic growth, based upon the dosimetric principles described above, and further taking into account the rapid changes in geometry of the organs during early growth and changes in radionuclide uptake. We then use this model to calculate the dose rates and absorbed doses delivered

to roots and shoots in an exposure scenario of different radiation quality (α-, β-, and γ-radiation). Finally, we compared our dose predictions with those obtained for a non-dynamic dose assessment.

4.2 Methods

4.2.1 Experimental Setup

To introduce growth dynamics into the dosimetry model, we needed to measure the changes in geometry during growth for the roots and shoots of *Arabidopsis thaliana* seedlings, and calculate the resulting changes in DCC. ^{241}Am, ^{90}Sr and ^{133}Ba were chosen as representative radionuclides for α-, β-, and γ-radiation, respectively, to allow for comparison with the data from our previous study (Biermans et al., 2013). We selected the time interval between 96 and 504 hours or 21 days after seeding, as this is a period of rapid plant growth and the preferred growth period for exposure experiments on *Arabidopsis* seedlings.

4.2.2 Plant culture

Prior to sowing, *Arabidopsis thaliana* (Columbia ecotype) were spread-out on moist filter paper and vernalized for three days at 4 °C to synchronize germination. The seeds were subsequently sown on plugs from 1.5 mL eppendorf tubes filled with 0.6% agar in modified Hoagland solution (1mM KNO_3, 0.3 mM $Ca(NO_3)2$, 0.2 mM $MgSO_4$, 0.1 mM $NH_4H_2PO_4$, 1.62 µM $FeSO_4$, 0.78 µM Na_2EDTA, 4.6 µM H_3BO_3, 0.9 µM $MnCl_2$, 0.032 µM $CuSO_4$, 0.055 µM H_2MoO_4, 0.077 µM $ZnSO_4.7H_2O$). The plugs were mounted on a PVC cover, capable of holding 36 plugs, after which each cover was placed on a container filled with 1.35 L modified Hoagland solution.

Plants were grown in a growth chamber (Microclima 1000E, Snijders Scientific B.V.) under a 16/8 day/night photoperiod with 22°C/16°C day/night temperatures and 65% relative humidity. Photosynthetic photon flux density was 100 µmol m^{-2} s^{-1} at the leaf level (Sylvania BriteGro F36WT8/2084 and F36WT8/2023 lamps). The nutrient medium was aerated with a peristaltic pump from 7 days after sowing onwards and was replaced every 3 days.

4.2.3 Biometry

Plant growth was monitored between 4 and 21 days after sowing. The rosette area was measured with imageJ software on pictures taken at several time points within the growth interval (Leister et al., 1999; Schneider et al., 2012). Root length was determined after 7, 10 and 21 days.

4.2.4 DCC calculations

To determine the DCC for each plant age, we used an improved version of the Monte Carlo method described in detail by Vives i Batlle et al. (2004) and Copplestone et al. (2001), which calculate the DCC value for a given ellipsoid geometry and a given radionuclide. This method is based on an iterative calculation of the probability of absorption of a radioactive particle across a large number of possible trajectories within the geometry, defined randomly.

4.2.4.1 Defining ellipsoid geometries

The leaf geometries for each time point were derived from the rosette area values measured in Section 4.2.3. This total leaf area was then defined as a circle of which the diameter D delivers two of the ellipsoidal axes. The third axis, which defines the leaf thickness, was kept identical for all time points at 0.15 cm as a simplifying assumption to facilitate calculations. Ellipsoid geometry was therefore defined as D x D x 0.15 cm with density 1 g cm^3. Root ellipsoid

geometries for each time point were defined as using a constant root diameter of 100 µm for two of the ellipsoid axes. The third axis was defined as the root length determined under Section 2.3.

4.2.4.2 Calculation of absorbed energy fractions

These geometries were then used as input for the Monte Carlo calculation method for absorbed fractions as a function of decay energy. This method uses point-specific absorbed fractions (AF) for γ-rays (Berger, 1968). For β particles, Berger's tabulated values of r_p (the radius r of a sphere within which p% of the energy is absorbed from a point β source located at the centre) were used (Berger et al., 1971). These values were transformed to values of fractional absorption from a point β emitter within a sphere of radius equal to r/r_{90} around the source, which makes the fractional absorption relatively independent of energy. For α-particles, the absorbed fraction was defined as being 1 for all geometries used, due to the short range of the particles in living tissue. Absorbed fractions as a function of decay energy E_d for γ- and β-particles were respectively fitted to the functions (1) and (2) (Vives i Batlle et al., 2004):

$$F\gamma(E_d) = \exp\ -\ \frac{E}{2\sigma}^{\ n}\ + a \cdot exp\ -\lambda E^m \quad (1)$$

$$F_\beta\ E_d\ = \frac{1}{1+bE^q} \quad (2)$$

with σ, n, a, λ and m as fitted parameters for $F_\gamma(E_d)$ and b and q for $F_\beta(E_d)$.

We adapted the original Excel VBA code used for the absorbed fraction calculation into the programming language for the statistical software R (R Development Core Team, 2011). This enabled us to perform the calcuations much faster and automate them for a large series of geometries operating in a batch mode. Absorbed fractions for each geometry at 18 energy values (0.015 – 3 MeV) were calculated with 50,000 iterations, sufficient for the values to

converge enough to keep the uncertainty at ≤2% (2σ) for the β-values and ≤10% (2σ) for the γ-values.

To fit the AF values to equations (1) and (2), the original VBA tool relied on manual estimation of the starting parameters σ, n, a, λ and m or b and q. Then, the Excel solver add-on was used to minimize the sum of squared deviations (χ^2). While we used this method for $F_\beta(E)$, estimation of the parameters for $F_\gamma(E)$ proved more difficult due to the convergence to local minima, especially for small geometries. To fit $F_\gamma(E)$ we therefore used a combination of an elitist genetic algorithm (GA) based upon Gulsen et al. (1995) and the Levenberg-Marquardt fit algorithm (Marquardt, 1963) included in the *minpack.lm* package for R (Elzhov et al., 2010).

The GA for $F_\gamma(E)$ was run on a large initial population with size N of parameter combinations, with each parameter randomly drawn from a uniform distribution devoid of lower or upper boundaries. During every iteration, the data were first fitted to the $F_\gamma(E)$ function formed by each parameter set, recording χ^2 as a value for fitness. 50% of the individuals with the highest fitness (i.e. the lowest value for χ^2) were then retained and defined as the *parent population*, of which one half was subsequently crossed-over with the second half in random pairs, forming 'offspring' with randomly shuffled values for each parameter compared with their parent pair. This was defined as the *crossover population*. A second offspring population was created by randomly sampling half of the parent population and multiplying the parameter values by the range of the parameter values in this subpopulation and a mutation factor. This mutation factor was drawn randomly for each parameter during each iteration from a uniform distribution with lower and upper limits ($-K$, K). The resulting *mutated population* was then reunited with the *parent population* and the *crossover population* into a single population which was then used in the next iteration.

We ran the algorithm with N=10,000, K=5 and 15 iterations, whereupon the values from the parameter set with the highest fitness value were used as the

starting parameters in the Levenberg-Marquardt algorithm. This combination of GA and Levenberg-Marquardt was run a 100 times, after which the parameter set with the best fit was selected for DCC calculation. Previous tests of this combined algorithm showed that this gives a 99% probability to obtain stable resultant parameter values.

4.2.4.3 Calculation of DCC values

The resulting parameter sets for $F_{\beta}(E)$ and $F_{\gamma}(E)$ for each geometry were used to calculate the internal DCC values (unweighted by radiation quality) for ^{241}Am, ^{90}Sr and ^{133}Ba. DCC's (in μGy h^{-1} / Bq kg^{-1}) for each radionuclide are obtained by summation of the decay pathways of the radionuclide in question and those of its chain of daughter radionuclides, each multiplied by (a) the associated AF at that energy (as derived from equations (1) and (2)) and (b) a conversion factor of 5.77 x 10^{-4} between MeV s^{-1} and μJ h^{-1}. Where relevant, the tool included daughters in equilibrium with parent radionuclides, as judged to occur in the environment. External DCC values are obtained in the same way, but by substituting AF by (1-AF) in the calculations. The method is given in detail in (Vives i Batlle et al., 2011).

4.3 Exposure Model

The aim of our model is to be able to predict dose rates and total absorbed doses during development of *Arabidopsis thaliana* seedlings exposed to different types of radiation by uptake of radionuclides from a liquid medium.

4.3.1 General Model

The DCC value converts activity concentration (AC), the measure of radioactivity in the tissue or surrounding water (in Bq kg^{-1} or Bq L^{-1}), into a dose rate, which

describes the amount of energy deposed into the living tissue per kg per unit of time (here in µGy h^{-1}). Therefore, at any given moment in the exposure, the dose rate can be calculated by multiplying the AC and DCC at that time point. Though calculation of the DCC value is only dependent on geometry in our method, values for AC can be obtained in several ways. An important point here is that the biota respond dynamically to the medium activity concentration. This will be further discussed in more detail below.

4.3.1.1 External exposure

The external dose rate is delivered by the surrounding medium, which activity concentration is measured during the course of an experiment and for which sampling is usually not limited. For an experiment where the external media concentration remains constant during the exposure, the external dose rate can be described as in equation (3) and is time-independent.

$$DR_{ext}\ t\ = AC_{ext}\ \cdot DCC_{ext}(t) \tag{3}$$

with AC_{ext} the activity concentration in the hydroponic medium, DCC_{ext} the external DCC value at time t and DR_{ext} the resulting external dose rate at that time point. The total dose delivered between the start of the exposure, S and for the duration of the exposure, E , equals the integral of equation 4 between time points S and $S+E$.

$$Dose_{ext}(S,E) = AC_{ext} \cdot \int_{S}^{S+E} DCC_{ext}\ t\ \ dt \tag{4}$$

4.3.1.2 Internal exposure

Internal dose rate depends on the internal activity concentration of the radionuclide in the tissue or organ and the homogeneity by which activity is distributed within the organism. This can either be calculated based on values

for medium-to-tissue concentration ratios available in literature for a number of radionuclides (IAEA, 2010), or measured directly by analysing the tissue.

Both methods have their specific advantages and disadvantages. While concentration ratios do not require measurement of internal biota concentrations, they are prone to high variability and are dependent on environmental conditions and species resulting in a 'compound parameter' that can span several orders of magnitude. For elements and species for which no transfer parameters are available, the values are interpolated based upon rules such as chemical or species similarity (Beresford et al., 2009). This makes it preferable to work with measured activity concentrations where possible, even if it relies on destructive measurements, which use material that might otherwise be available for analysis of biological endpoints. Radioecological risk assessment tools such as ERICA can handle both types of input, but use measured activity concentrations when available.

We therefore chose to base our dose (rate) assessment model on the concept of an experimentally determined AC at the end of the exposure period. Risk assessment tools such as ERICA and RESRAD-BIOTA (DOE, 2011) assume instantaneous equilibrium between environment and living tissue, which means that the AC measured at the end of the experiment is assumed to be constant from the start of the exposure. This is unlikely a valid assumption since biological and environmental processes are dynamic Pasatalki et al., 2013; Vives i Batlle et al., 2011) and for more accurate dose assessment a growth stage dependent uptake was considered.

Based on earlier experiments (Biermans et al., 2013), we showed that that the accumulation of the radionuclides considered inside a plant organ is linear in time for exposure lengths up to 7 days (168 h). We here assume that the accumulation rate (α, Bq kg^{-1} h^{-1}) remains constant for seedlings exposed between 96 to 504 h after seeding. Under this assumption, the radionuclide-specific accumulation rate for a given tissue can be calculated by dividing the AC

of the radionuclide of interest measured at the end of exposure, by the exposure duration of the experiment.

$$\alpha = \frac{AC_{end}}{E_{experiment}} \quad (5)$$

The change of AC with exposure time can then be described by equation 6, which calculates the radionuclide accumulation from the start of the exposure.

$$AC\ t\ = \alpha(t - S) \qquad \text{so that AC} \geq 0 \text{ for } t \geq S \quad (6)$$

The internal dose rate at time *S* + *E* can then be described by adapting equation 3 into an equation with AC dependent on time (equation 7)

$$DR_{int}\ t\ = \alpha(t - S) \cdot DCC_{int}(t) \quad (7)$$

$$DR_{int}\ S, E\ = \alpha E \cdot DCC_{int}(S + E)$$

Similarly, total internal dose then becomes

$$Dose_{int}(S, E) = \int_{S}^{S+E} \alpha(t - S) \cdot DCC_{int}\ t\ dt \quad (8)$$

Combining each of the equations (3), (4), (7) and (8) with the obtained data for *DCC(t)*, we can make the dosimetric model for each plant organ account for growth.

4.3.2 Shoot Dosimetry

In aquatic hydroponic exposure experiments, the shoot is only exposed internally to radionuclides transported to the shoot tissue from the roots. The external dose can be neglected. The internal DCC values for the different growth stages of *Arabidopsis thaliana* seedlings were obtained by defining the geometry

for each stage, based on the rosette area (section 4.2.4). Table 4.1 lists the measured area values and the derived diameter D for the Monte Carlo calculations.

To define the internal $DCC_{shoot}(t)$ for each radionuclide, we fitted the values to a logarithmic function of the form $b + c\ ln(t)$. This function most accurately described DCC as a function of time for all three radionuclides and for the time interval studied. Figure 4.1A-C shows the calculated DCC values and the fitted $DCC(t)$ curve for each radionuclide. Table 4.2 lists the fitted values for parameters b and c for each fit, the adjusted r^2 and sigma, *i.e.* the standard deviation of the random error. The results show that the function is able to accurately predict the DCC for all three elements for t = [96,504] days.

Time (h)	Rosette Area (cm²)	D (cm)
96	0.01	0.11
120	0.02	0.16
168	0.04	0.23
240	0.08	0.32
264	0.13	0.41
288	0.19	0.49
312	0.25	0.57
336	0.34	0.66
408	0.83	1.03
432	1.07	1.17
456	1.41	1.34
480	1.78	1.51
504	2.18	1.67

Table 4.1: Rosette area and derived D values for each time point used in the Monte Carlo DCC calculations on ellipsoid geometry (0.15 cm x D x D). Standard error on rosette area is <2% for all time points with N>30.

By introducing $DCC_{shoot}(t)$ into equation (7), the internal shoot dose rate after exposure length E (at $t=S+E$) equals

$$DR_{shoot,int}(S,E) = \alpha E \cdot (b + c \ln(S+E)) \quad (9)$$

Similarly, total dose for a given starting point S and exposure length E, by expansion of equation (8) and by solving the integral, becomes

$$Dose_{shoot,int}(S,E) = \alpha \int_{S}^{S+E} (t-S) \cdot (b + c \ln(t))\, dt \quad (10)$$

$$= \frac{\alpha}{2} bE^2 + c S^2(\ln S - \ln(S+E)) + \frac{E^2(2\ln(S+E) - 1)}{2} + ES$$

Transects for a specific value of S give the evolution of accumulated dose during exposure. Conversely, transects for a given exposure length E represent the dose at the end of the exposure as a function of the starting point during the seedlings' growth.

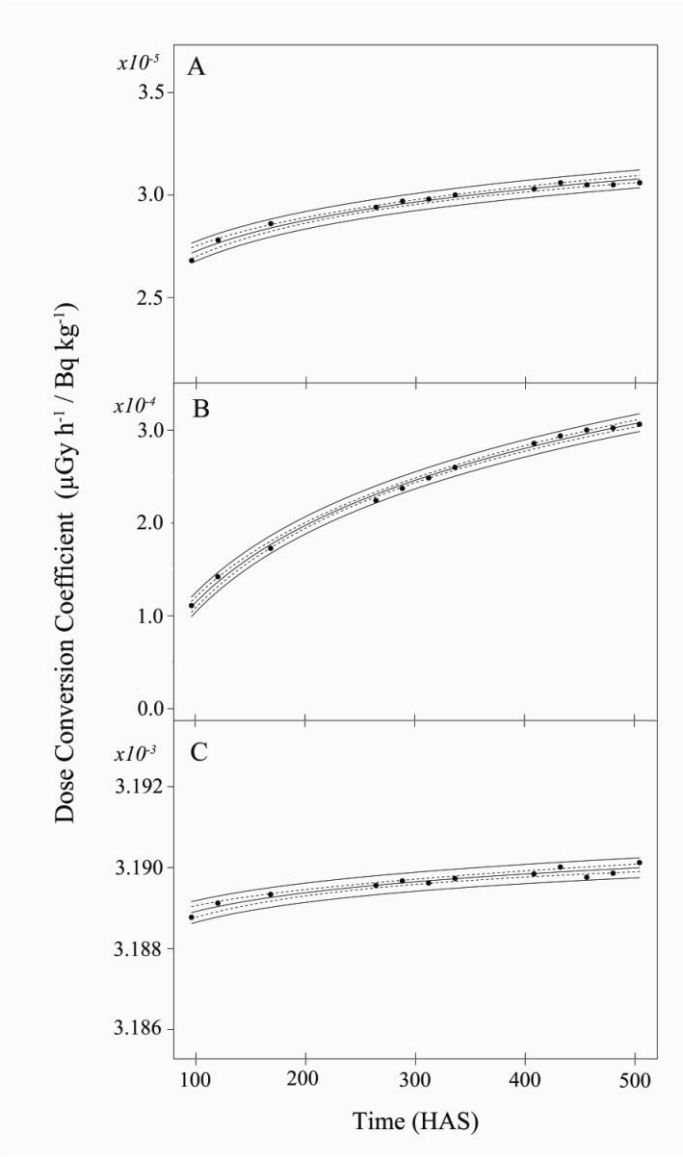

Figure 4.1: Internal Shoot Dose conversion coefficients (DCC). Values are presented as a function of time for ^{133}Ba (A), ^{90}Sr (B) and ^{241}Am (C). Confidence (dashed line) and prediction bands (solid line) for the fitted model $DCC(t) = b + c\ ln(t)$ are shown.

			b	95% CI	c	95% CI	r²	sigma
γ	**^{133}Ba**	*Fig. 1A*	1.720 x 10^{-5}	*[1.595 - 1.845] x 10^{-5}*	2.184 x 10^{-6}	*[1.964 - 2.404] x 10^{-6}*	0.978	1.811 x 10^{-7}
β	**^{90}Sr**	*Fig. 1B*	-4.360 x 10^{-4}	*[-4.633 - -4.087] x 10^{-4}*	1.196 x 10^{-4}	*[1.148 - 1.244] x 10^{-4}*	0.996	3.964 x 10^{-6}
α	**^{241}Am**	*Fig. 1C*	3.186 x 10^{-3}	*[3.185 - 3.187] x 10^{-3}*	6.673 x 10^{-7}	*[5.447 - 7.899] x 10^{-7}*	0.930	1.011 x 10^{-7}

Table 4.2: Fitted *DCC(t)* parameters for internal shoot dosimetry for ^{133}Ba. ^{90}Sr and ^{241}Am. The function DCC(t) = b + c ln(t) was fitted to the calculated DCC values for each radionuclide. For each radionuclide. both parameters and their 95% confidence interval are given. as well as the adjusted r² value for goodness-of-fit and the standard deviation of random error sigma.

Time (h)	**Root length (cm)**	**External DCC** [µGy h^{-1} / Bq L^{-1}]			**Internal DCC** [µGy h^{-1} / Bq L^{-1}]		
		^{133}Ba	***^{90}Sr***	***^{241}Am***	***^{133}Ba***	***^{90}Sr***	***^{241}Am***
96	2.1	2.429E-04	6.315E-04	2.313E-05	1.953E-05	2.081E-05	3.185E-03
168	3.3	2.430E-04	6.315E-04	2.314E-05	1.950E-05	2.078E-05	3.185E-03
240	4.8	2.429E-04	6.315E-04	2.313E-05	1.953E-05	2.076E-05	3.185E-03
504	10.2	2.429E-04	6.315E-04	2.313E-05	1.953E-05	2.076E-05	3.185E-03

Table 4.3: Root length and calculated external and internal root DCC values for for ^{133}Ba. ^{90}Sr and ^{241}Am. Ellipsoid geometry for DCC calculation at each time point was (0.01 cm x 0.01 cm x root length). Standard error on root length is <3% with N>20.

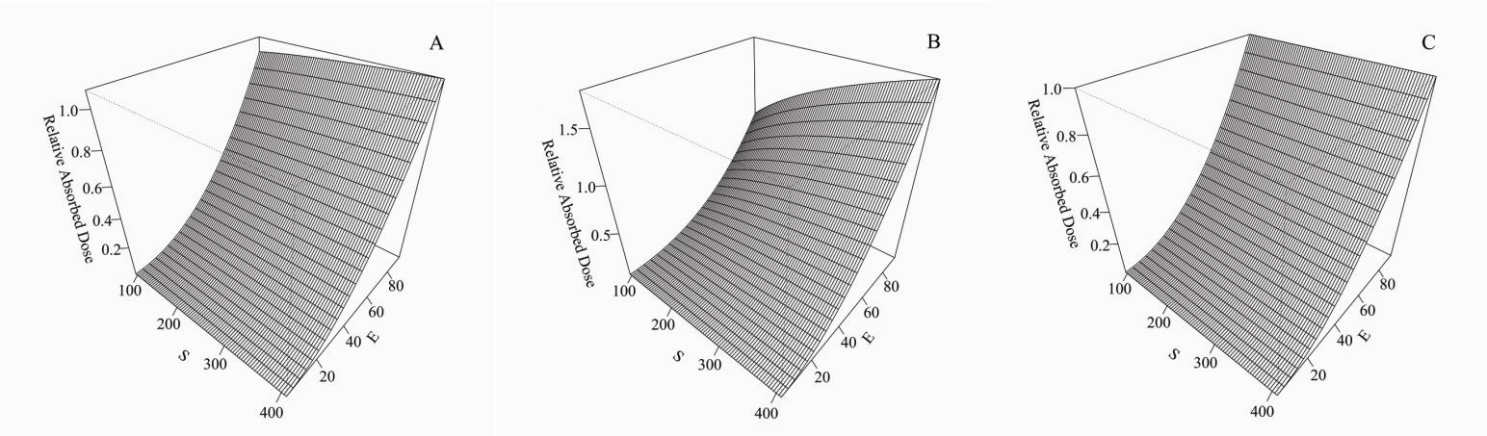

Figure 4.2: Shoot dosimetry models for 133Ba (A), 90Sr (B) and 241Am (C). Calculations are shown for exposure of seedlings between 96 and 408 h after seeding with exposure length from 0 to 96 h. Doses are expressed as a ratio to the dose at S=96 h, E=0 h.

Figure 4.2A-C shows the absorbed dose for each radionuclide for an exposure with *S* from 96 to 408 hours after seeding and a maximum exposure length of 96 hours. The absorbed dose is expressed relative to the dose value for *S* = 96 h and *E* = 96 h. As α is constant and therefore outside of the integral in equation (10), the relative difference between two points on the surface is independent of α.

A relative 95% confidence interval (CI) was constructed for each point of the surface using the parametric bootstrap method (Davison et al., 1997), drawing random newly predicted DCC values from a normal distribution with standard deviation σ (Table 4.2). The number of bootstraps equalled 5000 for each data point. The average relative 95% CI was 2.00% for ^{133}Ba, 5.9% for ^{90}Sr and 0.01% for ^{241}Am.

4.3.3 Root Dosimetry

Roots receive external exposure from the radionuclides in the surrounding hydroponic medium as well as internally from the radionuclides absorbed into the tissue. Root lengths and the derived external and internal DCC's are shown in Table 4.3. These data show that external and internal root DCC did not increase or decrease more than 1% for either of the radionuclides studied between the first measurement at 96 h and the last time point at 504 h after seeding. This is in contrast with the shoots, where changes in geometry during growth has much larger influence on DCC, except for ^{241}Am. For the roots, we can therefore assume that *DCC(t)* is a constant within the interval t = [96,504] for the three radionuclides. The external dose rate (equation 11) and internal dose (equation 12), derived from equations (3) and (4), can then be derived for the root-specific form

$$DR_{root,ext}\ S,E\ = AC_{ext}\ \cdot DCC_{root,ext} \tag{11}$$

$$Dose_{root,ext}(S,E) = AC_{ext}\ \cdot\ DCC_{root,ext}\ \int_{S}^{S+E} dt \tag{12}$$

$$=\ AC_{ext}\ \cdot DCC_{root,ext}\ \cdot E$$

We can conclude from the foregoing that the dose rate delivered to the roots by the medium is constant, and that the total absorbed dose after exposure length E is independent of the exposure starting point.

The internal root dose rate (equation 13) and dose (equation 14) can be derived from equations (7) and (8) in a similar way. Again, both equations are independent of the timing of the exposure.

$$DR_{root,int}\ S,E\ = DCC_{root,int}\ \cdot \alpha E \tag{13}$$

$$Dose_{root,int}(S,E) = \alpha \cdot DCC_{root,int}\ \cdot\ \int_{S}^{S+E}(t-S)\,dt \tag{14}$$

$$= DCC_{root,int}\ \cdot \frac{\alpha E^2}{2}$$

4.4 Results and Discussion

The main aim of this study was to develop a plant dosimetry model that integrates growth and variations in radionuclide uptake into the calculations. The

backbone of the model is the calculation of the DCC values for the three representative radionuclides, ^{241}Am (α), ^{90}Sr (β) and ^{133}Ba (γ), as a function of time (seedling development).

It is clear from the internal DCC values for the leaves (Figure 4.1A-C) that shoot growth influences the evolution of the DCC values over time, but not to the same extent for every radiation type. Whereas the DCC for β-emitter ^{90}Sr increased nearly 3-fold between 96 h and 504 h after seeding, that of γ-emitter ^{133}Ba increased by only 14% and that of ^{241}Am remained virtually constant (0.04% increase). Although ^{241}Am is an α-emitter and would therefore have a constant internal DCC it also has a low-energy γ-decay, which can explain the small change in DCC over time. The ultimate reason for the observed difference between elements is the way different types of particles interact with matter (Turner, 2005). The β-particles (electrons or positrons) emitted by ^{90}Sr penetrate less far into living matter than the γ-particles (photons) emitted by ^{133}Ba, while the energy of heavy α-particles inside the organism (He nuclei) is fully contained within the tissue due to the very low travel length of α-radiation in living matter (a few tens of microns). If we look at the shoot dosimetry model itself (Figure 2A-C), it is immediately clear that these differences in DCC lead to similar differences in dose rate and dose. For ^{90}Sr, for example (Figure 4.2B), we can deduce that if we were to expose seedlings for 4 days starting at 17 days (408 h) of growth, they would accumulate 78% more dose in their shoots than in an 4-day exposure period that starts 96 h after seeding. For shoots exposed to ^{133}Ba (Figure 4.2A) this reduces to 8.5% and for ^{241}Am (Figure 4.2C) the dose difference between both 4-days' exposure periods is only 0.023%. These surface plots also show that dose does not accumulate in a linear way as would be the case under assumptions of instant equilibrium, but instead follows the dominating bE^2 term in equation 10. Similar calculations can be made for dose rate.

Contrary to the shoots, the root dosimetry does not depend on the timing of the exposure, which simplifies the calculations. However, this also means that the

ratio between shoot and root dose (and hence dose rate) changes with timing, which might be of importance in understanding the effects of radioactive exposure on the functioning of the plant as a whole. The conclusion arising from these findings is that shoot dosimetry in *Arabidopsis thaliana* seedlings is very dependent on the timing of the exposure, especially for β and γ-radiation. It is therefore essential to take into account the growth and uptake parameters in effects studies, even more so when comparing effects between life stages.

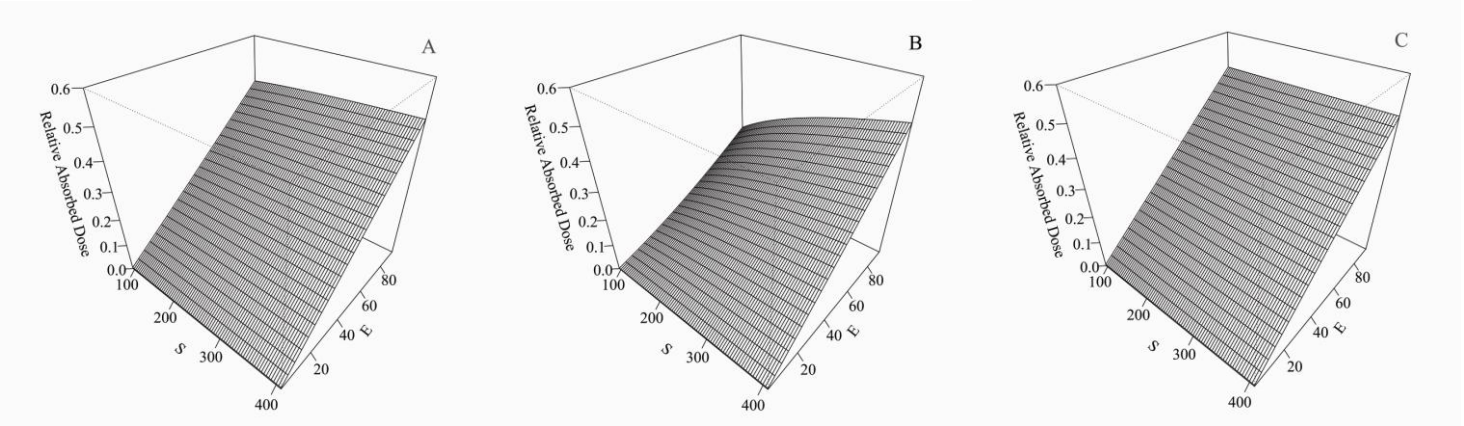

Figure 4.3: Comparison of our shoot dose calculations for ^{133}Ba (A), ^{90}Sr (B) and ^{241}Am (C) to calculations under static assumptions. Data from our dynamic model are shown relative to calculations under the classic model for S = [96 h, 408 h] and E = [0 h, 96 h].

We next compare the dose and dose rates obtained using the dynamic dose rate modelling approach with the results from a dose calculation method based on end-of experiment geometry and activity concentration, we compared our internal absorbed dose calculations to those of a model that operates under the assumptions of ERICA, namely, (1) instant equilibrium of tissue activity concentration and (2) constant DCC.

$$Dose\ static = AC_{end} \cdot DCC_{end} \cdot E \quad (15)$$

with AC_{end} obtained from the measured tissue activity concentration at the end of exposure. In the above equation, DCC_{end} is defined as the DCC obtained for the geometry at t = 504. The surface plots in Figure 4.3A-C give the ratio of the dose obtained with the dynamic dose estimate model divided by the dose calculated according to Eq. 15 and this for the full exposure duration. The relative differences between the radiation types are evidently still present, but it is clear that for any radionuclide the 'static' approach would overestimate the shoot dose at least twofold. The growth effect is again evident if we compare young and old seedlings exposed to ^{90}Sr. The 'static' dose model overestimates doses more (5-fold) at early growth stages (96 h old seedlings exposed for 96 h) that at later growth stages (2-fold, for 408 h old seedlings expose for 96 h). The comparison for ^{241}Am, which has a near constant DCC, shows that the observed minimum of twofold overestimation results from the assumption of instant equilibrium, an overestimation which therefore increases in a linear way with decreasing exposure length. This effect of uptake on the difference between both models becomes more manifest when carrying out the comparison for internal root dosimetry, which by definition assumes a constant DCC (equation (14)). We can calculate the ratio between both models as

$$\frac{Dose\ dynamic\ model}{Dose\ static\ model} = \frac{0.5\ DCC_{root,int}\ \alpha E^2}{AC_{end} \cdot DCC_{end} \cdot E} \quad (16)$$

For root dosimetry $DCC_{end} = DCC_{root,int}$ and $AC_{end} = \alpha E_{max}$, which simplifies equation (16) to

$$\frac{Dose\ growth\ model}{Dose\ static\ model} = \frac{0.5\ DCC_{root,int}\ \alpha E^2}{\alpha E_{max} DCC_{root,int}\ E} = \frac{0.5\ E}{E_{max}}$$

For $E = E_{max}$, the ratio between the two models equals 0.5, a twofold overestimation by the static model. Equation (16) only describes the difference in internal root dose caused by inclusion of radionuclide uptake over time.

The above comparison shows that the doses (and dose rates) calculated by the 'dynamic' model are lower than doses calculated by the static dose calculation approach. Dose rate and risk assessment tools such as ERICA or RESRAD are not developed to estimate doses and dose rates during biota development and will give a 'static' dose (rate) (or semi-static – if different geometries and related uptake assessed in a consecutive manner). It would in principle be possible, at least for the shoots, to enter each growth stage's geometry manually in these models and, in this way, obtain DCC values which would be identical to those found in our calculations. While this would undoubtedly remove the growth-related bias on the dose estimates, it requires the manual input of each growth stage as a separate organism into the software and furthermore would not remove the overestimation due to the assumption of instant equilibrium. This makes for a very time-consuming approach, as these tools were not designed for such a purpose. The modifications made to the original VBA calculator designed by Vives i Batlle et al. (2004) allow for a fast way to calculate DCC values for a nearly unlimited amount of geometries in batch and therefore constitute a practical improvement for use in situations outside the normal range of application of these tools, where batch calculations are required.

Though our model represents a considerable improvement due to its organ-based approach and the inclusion of seedling growth, several conceptual limits remain that future research will have to address. We have used the

radionuclide-specific yet time-constant uptake rate α to describe the accumulation in a tissue when calculating internal dose. Our previous experiments suggested that this rate indeed remains constant throughout the time interval for a given environmental activity concentration. These assumptions have to be addressed more thoroughly if we were to extend the dosimetric model to the entire lifecycle, to other plant models or to other radionuclides. The assumption of linear accumulation not only provides the advantage that just a single measurement of activity concentration is needed, but also allows for dosimetry calculations in field situations where generally only one measurement can be obtained. However, if we were to observe experimentally a different pattern of accumulation than the linear pattern used in this study, the new relationship for *AC(t)* could easily be inserted into the equations. The only remaining mathematical difficulty would be to solve the integration of the dose rate over the exposure.

Our dosimetry model relies on describing a *DCC(t)* relationship, which for the shoots was fitted quite well by a logarithmic function (Figure 4.1; Table 4.2). Even for ^{241}Am, which has a near constant DCC, this function allowed to describe the small change in DCC caused by the small contribution of γ-decay to the dose. Theoretically, the DCC value should converge to a maximum value with increasing rosette diameter, as the fraction of energy absorbed within the geometry approaches unity. The rosette diameter itself is dependent on the typical logistic plant growth curve, and reaches a maximum before flowering (Boyes et al., 2001). Finally, preliminary attempts to expand the model to a longer list of radionuclides (data not shown) have taught us that for many elements the logarithmic relation does not hold true within the whole interval. Hence, while the logarithmic function is a good fit within the studied interval and for the three selected radionuclides, it does not correctly reflect the theoretical physical and biological background.

Our model dispenses with a direct description of growth by calculating the DCC for intermediate time points and fitting a curve to the evolution of DCC over

time. Therefore it still requires the input from a plant culture for which the geometries have been experimentally determined over time, and for which a new set of Monte Carlo calculations has to be carried out if the experimental growth conditions are changed. Ideally, the basis of the model would be a theoretical description of DCC as a function of diameter, *DCC=f(D)*, for which the DCC calculations have to be performed only once. Any experiment-specific growth function for *Arabidopsis thaliana* which describes dose as a function of time can then be nested into the diameter-dependent function for DCC to produce *DCC(t),* making the resultant function directly dependent on the plant growth parameters, and retaining the theoretical physical background enclosed in the relation of DCC to D.

Though establishing such a theoretical framework goes beyond the scope of this paper, we believe that it would greatly improve the flexibility of our plant dosimetry model. This is true not only with respect to other plant species, but also regarding application to scenarios outside laboratory conditions, where growth can be significantly altered by environmental factors other than radioactive exposure. Several authors have previously stressed the importance of dynamic models in calculating time-integrated doses for release or exposure scenarios (Lepicard et al., 2004; Vives i Batlle et al., 2008). To our knowledge, our study marks the first time that such an approach is proposed for plants with inclusion of growth. Whilst this adumbrates a more general, theoretically underpinned plant dosimetry model, we believe that the concepts put forward in this study can equally be of use in additional organisms where fast growth rate and small geometry might induce rapidly evolving DCC values.

We conclude that our model sheds light on how radionuclide doses delivered to *Arabidopsis thaliana* shoots are highly dependent on the life stage at which the plant is contaminated. Further, the extent of the growth effect depends on the physical properties of the radionuclide. Finally, we have validated our study hypothesis that the absorbed doses (and dose rates) obtained are resulting in more robust dose (rate) predictions, required for establishing more reliable

dose-effect relationships and hence finally leading to more realistic assessments in radiological environmental protection and derivation of more robust protection benchmarks.

Chapter 5:

Arabidopsis thaliana seedlings show an age-dependent response on growth and DNA repair after exposure to chronic γ-radiation.

Biermans, G., Horemans, N., Vanhoudt, N., Vandenhove, H., Saenen, E., Van Hees, M., Wannijn, J., Vangronsveld, J., Cuypers, A., 2013. *Arabidopsis thaliana* seedlings show an age-dependent response on growth and DNA repair after exposure to chronic γ-radiation.

In preparation for Experimental and Environmental Botany

ABSTRACT

The biosphere is constantly exposed to ionising radiation, due to cosmic radiation and the presence of natural and anthropogenic radionuclides in the environment. The biological effects of the resulting radiation exposure are currently poorly understood in plants, due to a large influence of parameters such as species, cultivar, experimental setup and plant age on the response. In this study, 7-, 10- and 14-day-*old Arabidopsis thaliana* seedlings were exposed to 96 h and 168 h of 100 mGy h^{-1} chronic γ-radiation in a hydroponic setup. The response of growth, photosynthesis and transcription of genes involved in DNA repair, cell cycle and signalling were measured. After the exposure, growth recovery capacity was determined. The results show that there is a difference in growth response and recovery capacity between plants of different ages, and decreasing radiosensitivity with increasing seedling age. This is linked to differences in regulation of DNA repair and cell cycle control at the transcriptional level.

5.1 Introduction

Living organisms are constantly exposed to ionising radiation (IR), either from natural sources such as cosmic radiation or naturally occurring radionuclides, or from controlled or accidental anthropogenic releases. Plants, through their inability to move or hide from radiation sources and by their dependence on light energy, are a particular case. Most studies on plants have investigated the effects of UV and gamma irradiation, as both consist of photons that can penetrate deep into the plant tissues.

Studies on γ-irradiation treatment of plants have shown a wide range of effects on growth, morphology, physiology and reproductive capacity (Daly & Thompson, 1975; Kovalchuk et al., 1999; Zaka et al., 2004; Wi et al., 2007). While only a few general patterns have emerged from these studies, the effects and the response of plants range from hormesis to growth inhibition, and depend on additional factors such age, species or chronic versus acute irradiation (Kovalchuk et al., 2007; Esnault et al., 2010). Previous studies indicate that *Arabidopsis thaliana* is a rather radioresistant species due to its small genome (Sax, 1954; Sparrow & Miksche, 1961). While recent work on *Arabidopsis thaliana* has shown that seedlings of different ages show a differential growth response to acute γ-irradiation on growth (Kurimoto et al., 2010), little is known whether this holds true under chronic conditions, where plants are exposed for more than 24 hours at dose rates in the μGy h^{-1} or the mGy h^{-1} range.

The interaction of IR with living organisms starts by energy deposition in the cells. This can happen either by direct interaction of the ionizing particle with biomolecules or by hydrolysis of water in the cell, leading to the formation of reactive oxygen species (ROS) such as hydroxyl (•OH), hydrogen peroxide (H_2O_2) and to a lower extent superoxide ($O_2^{\bullet-}$) (Lee et al., 2009). These ROS not only damage cellular components, but are also added unto the existing pool of

ROS inside the cell which are produced during normal metabolism (Koyama et al., 1998; Wi et al., 2007; Kim et al., 2011).

Direct interaction of IR with DNA may result in double strand breaks (DSB), while indirect oxidative damage by ROS will more likely cause single strand breaks (SSB) or base modifications (Neary et al., 1972; Holst & Nagel, 1997; Roldàn-Arjona & Ariza 2009). At least two separate DSB repair pathways are present in plants. Homologous recombination (HR) is a conservative repair mechanism which recombines the damaged region with an identical template within the cell, whereas non-homologous end-joining (NHEJ) joins the loose ends of double strand breaks in a random way (Waterworth et al., 2011). As a result, NHEJ may reshuffle the genetic information, which may lead to accumulation of damage and ultimately disrupt the functioning of the cell. While both repair mechanisms are active in the cell, most DSBs in plants are repaired through the NHEJ pathway (Britt, 1996). The balance between both pathways might be an important factor in acclimation and adaptation to ionizing radiation (Kovalchuk et al., 2000).

Single strand breaks occur in only one strand at a time at a given location, and the second, undamaged strand can therefore be used as a template to repair the damage. In eukaryotes, pathways such as base excision repair (BER) and nucleotide excision repair (NER) detect and repair single strand damage (Britt, 1996). Single-strand lesions in DNA are detected by Poly(ADP-Ribosyl)-polymerases (PARPs), nuclear proteins which enhance or alter the behaviour and dynamics of specific target proteins by adding Poly(ADP-ribose) chains to their lysine residues, consuming NAD+ in the process (Chen et al., 1994). PARP targets are proteins involved in cellular processes such as chromatin structure, DNA repair and gene transcription. By PARP-mediated modification, they become targeted for ubiquitination and subsequent breakdown, or change conformation, modifying the accessibility of their binding site. Inhibition or down-regulation of PARPs can modify the response of plants to stress conditions by increasing the

available NAD+ pool for the anti-oxidative system (Adams-Philips et al., 2010; Schulz et al., 2012). One author has reported increased transcription of *PARP* genes after induction of strand breaks by IR, indicating that this might not be a general mechanism involved in all types of stress (Doucet-Chabeaud et al., 2001).

DNA damage causes instability and errors in the genetic material, and it is therefore of importance for the cell to repair the damage before it goes into mitosis. Cells ensure the correct transmission of genetic information to their daughter cells by controlling the progression of the cell cycle based on the status of the DNA. Cell cycle regulation is performed by a combination of cyclins and their association to a series of cyclin-dependent kinases (CDKs) to form cyclin-CDK complexes (De Veylder et al., 2007). These Cyclin-CDK complexes regulate in turn the processes necessary for the progression through the cycle. The progression of the cell cycle is a heavily regulated process, especially the transition points from G1 to S-phase and from G2-phase to mitosis. Transition through the latter can only happen if DNA repair has occurred, thereby ensuring correct transmission of the genetic information to the two daughter cells. When DNA damage occurs due to abiotic or biotic stress, the cycle remains blocked in G2-phase until DNA repair has occurred (De Veylder et al., 2007). Signalling proteins such as those of the ATR/ATM pathway detect and report DNA strand breaks by physically binding the lesion and recruiting protein complexes involved in repair and signalling. Eventually, this leads to a downstream point that affects Cyclin-CDK dynamics (Garcia et al., 2003; Culligan et al., 2006).

In this study we investigate whether seedlings of *Arabidopsis thaliana* show an age-dependent response to chronic gamma radiation exposure and a difference in radiosensitivity. We analysed the effects on growth, recovery, photosynthesis and DNA damage in 7, 10 and 14 days old seedlings, and measured the expression of genes involved in DNA repair, signalling and the cell cycle.

5.2 Materials and Methods

5.2.1 Plant growth

Prior to sowing, *Arabidopsis thaliana* (Columbia ecotype) seeds were spread-out on moist filter paper and vernalized for three days at 4°C to synchronize germination. The seeds were subsequently sown on plugs from 1.5 mL microcentrifuge tubes filled with 0.6% agar in a modified Hoagland solution (1mM KNO_3, 0.3 mm $Ca(NO_3)_2$, 0.2 mM $MgSO_4$, 0.1 mM $NH_4H_2PO_4$, 1.62 µM $FeSO_4$, 0.78 µM Na_2EDTA, 4.6 µM H_3BO_3, 0.9 µM $MnCl_2$, 0.032 µM $CuSO_4$, 0.055 µM H_2MoO_4, 0.077 µM $ZnSO_4.7H_2O$). The plugs were mounted on a PVC cover, capable of holding 36 plugs, after which each cover was placed on a container filled with 1.35 L modified Hoagland solution

Plants were grown in a growth chamber (Microclima 1000E, Snijders Scientific B.V.) under a 16/8 day/night photoperiod with 22°C/16°C day/night temperatures and 65% relative humidity. Photosynthetic photon flux density was 150 µmol m^{-2} s^{-1} at the leaf level (Sylvania BriteGro F36WT8/2084 and F36WT8/2023 lamps). The nutrient medium was aerated with a peristaltic pump from 7 days after sowing onwards, and replaced every 4 days.

5.2.2 Gamma Irradiation

Seedlings were grown until 7, 10 or 14 days after sowing and subsequently transferred to the irradiation facility at SCK•CEN, where they were kept under conditions similar to those in the growth chamber.

Each seedling age group was divided into four groups: The first group was exposed to γ-radiation from a ^{137}Cs source for 96 hours under an average dose rate of 113 mGy h^{-1}, receiving a total dose of approximately 10.9 Gy. A second

group was exposed for 168 hours under identical conditions, receiving a total dose of approximately 18.4 Gy. The two remaining groups were used as unexposed controls for the two irradiated groups, and were kept in a separate room of the facility, shielded from the irradiation, but under identical environmental conditions.

5.2.3 Plant Sampling and Biomass measurement

Immediately after the irradiation period, control and irradiated plants were returned to the growth chamber, and each divided into two groups. One half was immediately harvested. The second half was allowed to recover for 7 days in the growth cabinet, after which the remaining plants were harvested as in the first group.

Shoot tissue for gene expression, pigment and DNA damage analysis was pooled to ±100 mg samples in eppendorf tubes and snap frozen in liquid nitrogen for storage at -80°C. For biomass measurements, leaf fresh weight was determined for at least 15 biological replicates from each age/treatment combination.

5.2.4 Photosynthesis and pigments

Immediately after harvest, four plants from each treatment were selected from the plants destined for physiological measurements. Their 4th leaf was then removed, and stored on wet paper in a closed petri dish in the dark. The leaves were pre-adapted to dark conditions for at least 15 minutes and the induction curve (IC) for photosystem II (P680) was then measured using PAM Fluorometry (Dual PAM-1000; Waltz, Germany) (Schreiber et al., 2004) until stabilisation of the quenching parameters. From these data, values for photosynthetic efficiency (φPSII), non-photochemical quenching (NPQ) and photosynthetic capacity (Fv/Fm) could be calculated. The induction curve measurement was immediately

followed by a rapid light curve (RLC) measurement at 6 light intensities between 0 and 800 µE with a 30 second interval. These data were then fitted to the continuous model of Platt without photoinhibition as used in Ralph & Gademan (2005) using a Marquardt-Levenberg curve fitting algorithm in statistical software package R, from which the values for maximum electron transfer rate (ETRmax) could be derived.

5.2.5 Gene expression analysis

Gene expression of selected marker genes involved in DNA repair and cell cycle was measured on shoot tissue exposed for 96 h. Frozen shoot tissue (max.100 mg) was shredded (Retsch MM400, Retsch, Haan, Germany) with beads (specs) at -80 °C for 2 minutes at 30 Hz. The RNA was then extracted using the DNeasy Plant Mini Kit according to the manufacturer's instructions (Qiagen). RNA quality was determined by gel electrophoresis (Bioanalyzer, Agilent Technologies) and the quantity checked spectrophotometrically at 260 nm (Nanodrop 2000, Isogen Life Sciences). Genomic DNA was removed from the samples with the Turbo DNA-free Kit (Ambion) for 30 minutes at 37°C.

From these RNA samples, cDNA production was perfomed with High-Capacity cDNA Reverse Transcription Kit (Applied Biosystems) according to the manufacturer's instructions, using 1 µg of RNA for each sample. Quantitative Real-Time PCR reactions were then performed using SYBR Green chemistry in a 10 µL volume (0.3 µL forward primer, 0.3 µL reverse primer, 5 µL Fast SYBR Green Master Mix, 2.9 µL RNase-free H_2O) on the 7500 Fast Real-Time PCR system (Applied Biosystems). Primers used for gene expression analysis are given in Table 5.1. Efficiency of each primer pair was checked on beforehand.

Gene expression was normalized against multiple reference genes (*ACT2,TIP41-like,UBC, UBQ10*) using the method described by Remans et al. (2008) and the geNorm algorithm (Vandesompele et al., 2002).

5.2.6 Base Modification

Frozen shoot tissue (75-100 mg), harvested from plants irradiated for 168 h, was mechanically shredded with beads (Retsch MM400, Retsch, Haan, Germany), and the DNA extracted from the samples using DNeasy Plant Mini Kit (Qiagen). DNA concentrations were measured spectrophotometrically (Nanodrop 2000, Isogen Life Sciences).

The DNA samples were then digested as described in Debiane et al. (2009). 38 µL of DNA extract was incubated for 2 minutes at 100°C, and subsequently digested with Nuclease P1 (2µL 5U/µL; Sigma) in the presence of 3 µL 250 mM potassium acetate buffer (pH 5.4) and 3 µL 10 mM zinc sulphate. Digestion was performed at 37°C overnight. Subsequently, the digests were treated for 2 hours at 37°C with 2 µL alkaline phosphatase (0.3 U/µL; Sigma) in the presence of 6 µL 0.5 M Tris-HCl buffer (pH 8.3). Base modification (8-OHdG) was determined by competitive ELISA (New 8-OHdG Check kit, Japan Institute of Aging) according to the manufacturer's instructions. The assay is based on spectrophotometric detection at 415 nm.

5.2.7 Statistical analysis

For the biometry, photosynthesis, pigment and gene expression datasets, differences between control and exposed plants were analysed by student-t-test for each time point and seedling age class separately after testing of normality and homoscedasticity assumptions. Base modification was analysed by two-way ANOVA after testing of normality and homoscedasticity assumptions, followed by the Tukey Honest Significant Difference post-hoc test for two-by-two comparisons.

Gene Name	Accession	Forward Primer Sequence	Reverse Primer Sequence
Reference Genes			
ACT2	AT3G18780	CTTGCACCAAGCAGCATGAA	CCGATCCAGACACTGTACTTCCTT
EF-1α	AT5G60390	TGAGCACGCTCTTCTTGCTTTCA	GGTGGTGGCATCCATCTTGTTACA
TIP41-like	AT4G34270	GTGAAAACTGTTGGAGAGAAGCAA	TCAACTGGATACCCTTTCGCA
UBC	AT5G25760	CTGCGACTCAGGGAATCTTCTAA	TTGTGCCATTGAATTGAACCC
Cell cycle regulation			
CKS1	AT2G27960	CACGTCGTTCTTCCTCCTGAAG	TCCTATCGCTCGCCATTCG
GAR1	AT3G52115	CTAAGATGGTTGGTGATGCAAGAGA	CGCTAAGCTCATCCAAACCCTT
KRP2	AT3G50630	GGAATAAGTTGTTGGAATGTTCTATGAAGT	AACCCACTCGTATCTTCCTCCAC
NHEJ			
KU80	AT1G48050	CTTCTTCCAGCACAACTCCTCAA	CTACGCATCGCAGGACCTACAT
LIG4	AT5G57160	TGATGTATCGGATATCAAGGGCA	GAATGGGACCGAGGCACG
HR			
DMC1	AT3G22880	ATGAAGACGAAGATCTATTTGAGATGATT	CTTGTAGCTTTTTCACATCTCCTGC
RAD51	AT5G20850	GTCCAACAACAAGACGATGAAGAA	AACAGAAGCAATACCTGCTGCC
Other DSB repair			
MND1	AT4G29170	GAACGAGATGGTACAATTTGCTGA	CCGACTGGTGAGCAACTTCAAT
POLG1	AT3G20540	GAAACTGGACGCTTATCGGCTAG	CTGACGGATTTTGTACCGATCTTT
SSB repair			
PARP1	AT2G31320	TGCATTGGGAGAAATACATGAGC	CCGAGCCCTTTGGTCGAG
Signalling			
LPP1	AT2G01180	TCACTTTCTGATGACAATAGGGTCG	CCTCTCTGCGCCTCCTGG
PARP2	AT4G02390	ATCGGAGGTGATTGATCGGTATG	AAATCATGAGGTATCACTGTGTAGAACTCT

Table 5.1: Selected genes and their primers for gene expression analysis

5.3 Results

5.3.1 Biometry

After 96 h of γ-irradiation, shoot fresh weight of 7- and 14-day-old seedlings had significantly increased as compared to non-irradiated control plants (Figure 5.1). After the recovery period of one week, the shoot fresh weight of these two age classes was still significantly higher than the control plants, though the difference had slightly decreased. No effects on shoot biomass were observed for the 10-day-old seedlings at this exposure time.

7-day-old seedlings exposed for 168 h still showed significantly increased shoot biomass (Figure 5.1) relative to the control plants, however the fold difference with control plants had decreased as compared to the fold change after 96 h of exposure. It had decreased even further after the recovery period. 10- and 14-day-old seedlings irradiated for 168 h had a significantly lower shoot fresh weight than control plants. Both classes retained this difference after the recovery period, though not significant for 10-day-old plants ($t30 = 2{,}0422$, $p = 0.25$).

5.3.2 Photosynthesis and pigments

In general, γ-radiation did not affect non-photochemical quenching (NPQ), photosynthetic efficiency (φPSII) or electron transfer rate (ETR) in 10- and 14-day-old seedlings (data not shown). No measurements could be performed on the 7-day age class seedlings due to the small leaf size and the limitations on minimum amount of tissue needed for other analyses.

Photosynthetic capacity (Fv/Fm) was significantly increased after the recovery period in 10-day-old seedlings exposed during 96 h (Table 5.2). A similar increase was found after recovery in seedlings from the same

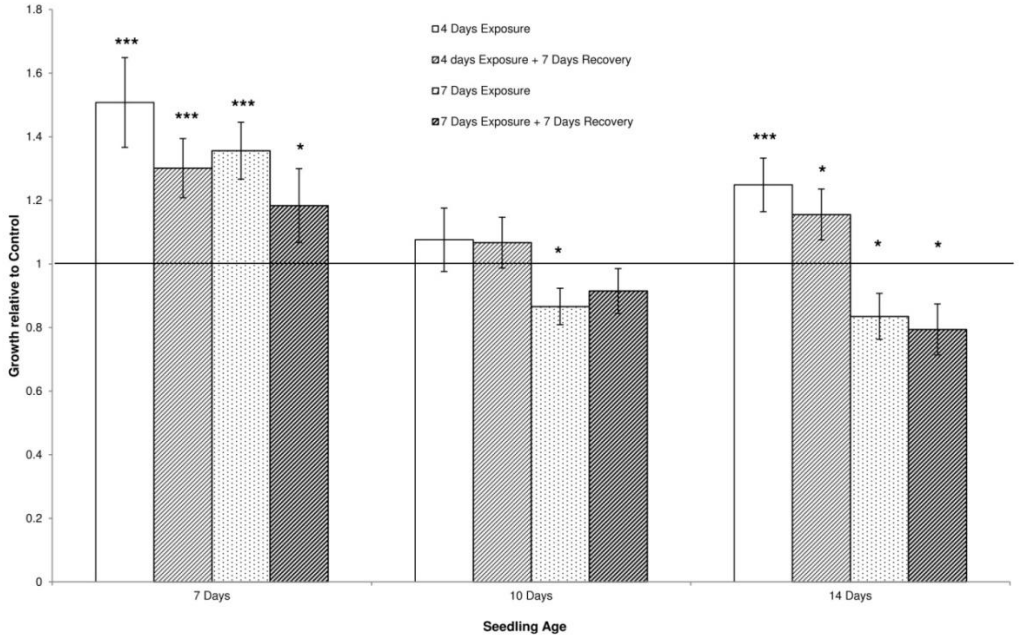

Figure 5.1: Relative fresh weight of *Arabidopsis thaliana* shoot tissue after exposure and recovery. Fresh weight increase or decrease relative to control treatment is shown for each seedling age and treatment. Data are represented as mean ± SE, with n>15. significanceevels between exposed plants and control (represented as a horizontal line) are shown as * $p<0.05$, ** $p<0.01$, *** $p<0.001$ (Student-t-test) for each treatment.

age class exposed for 168 h, though this was not statistically significant (t_4 = 2.7764, p = 0.33). In 14-day-old seedlings, Fv/Fm was significantly reduced after recovery in plants exposed for 168 h (Table 5.2).

10-Day-old Seedlings	**Control**	**SE**	**Exposed**	**SE**	
96 h Exposure	0,807	0,004	0,808	0,004	
96 h Exposure + Recovery	0,732	0,009	0,765	0,006	*
168 h Exposure	0,782	0,007	0,784	0,002	
168 h Exposure + Recovery	0,762	0,022	0,790	0,005	

14-Day-old Seedlings	**Control**	**SE**	**Exposed**	**SE**	
96 h Exposure	0,800	0,016	0,795	0,019	
96 h Exposure + Recovery	0,750	0,009	0,758	0,004	
168 h Exposure	0,790	0,009	0,788	0,004	
168 h Exposure + Recovery	0,795	0,002	0,737	0,007	**

Table 5.2: Fv/Fm values. Fv/Fm data obtained by PAM fluorometry after 15 minutes of dark adaptation for 10- and 14- day-old seedlings immediately after treatment and after 7 days of recovery. Values are the mean ± SE of at least 3 biological replicates. Significance levels between treatment and control are shown * $p<0.05$, ** $p<0.01$ (Student-t-test).

5.3.3 Gene expression analysis

To better understand the differences in effects on growth between the different seedling ages, we examined gene expression of several genes involved in DNA repair and regulation or modulation of the cell cycle. For reasons of limited sampling of plant material, we chose to measure gene expression for all three age classes at 96 h of exposure.

For genes involved in the NHEJ pathway (*KU80; LIG4*), only *LIG4* was differentially expressed as compared to control plants, showing up-regulation, though not significantly, in 7-day-old seedlings and significant down-regulation in 14-day-old plants (Figure 5.2A and B). A similar pattern was observed for the mitochondrial DNA polymerase gene polymerase gamma 1 (*POLG1*; Figure 5.2D). RAD51 homolog 1 (*RAD51*), involved in the homologous recombination pathway, was only significantly up-regulated in 10-day-old seedlings (Figure 5.2C). *MND1* and *DMC1* are genes known to be involved in HR in somatic tissues, but did not show differences in expression. The two PARPs, involved in sensing, signalling and repair of SSB, showed very different expression patterns. *PARP1* expression showed a decreasing trend with increasing seedling age in the exposed plants (Figure 5.2E), with up-regulation in 7- and 10-day-old seedlings, and down-regulation in 14-day-old seedlings. *PARP2,* however, was strongly up-regulated in all age classes (Figure 5.2F).

Expression of genes involved in the cell cycle (*CKS1; KRP2*) and stress signalling (*LPP1*) also showed age-dependent expression patterns. *CKS1* was up-regulated in 7- and 10-day-old seedlings exposed to gamma-radiation (Figure 5.3A), while both *KRP2* and *LPP1*, were significantly down-regulated in the 14-day age class (Figure 5.3B and C). Expression of both genes increased with age in the control plants.

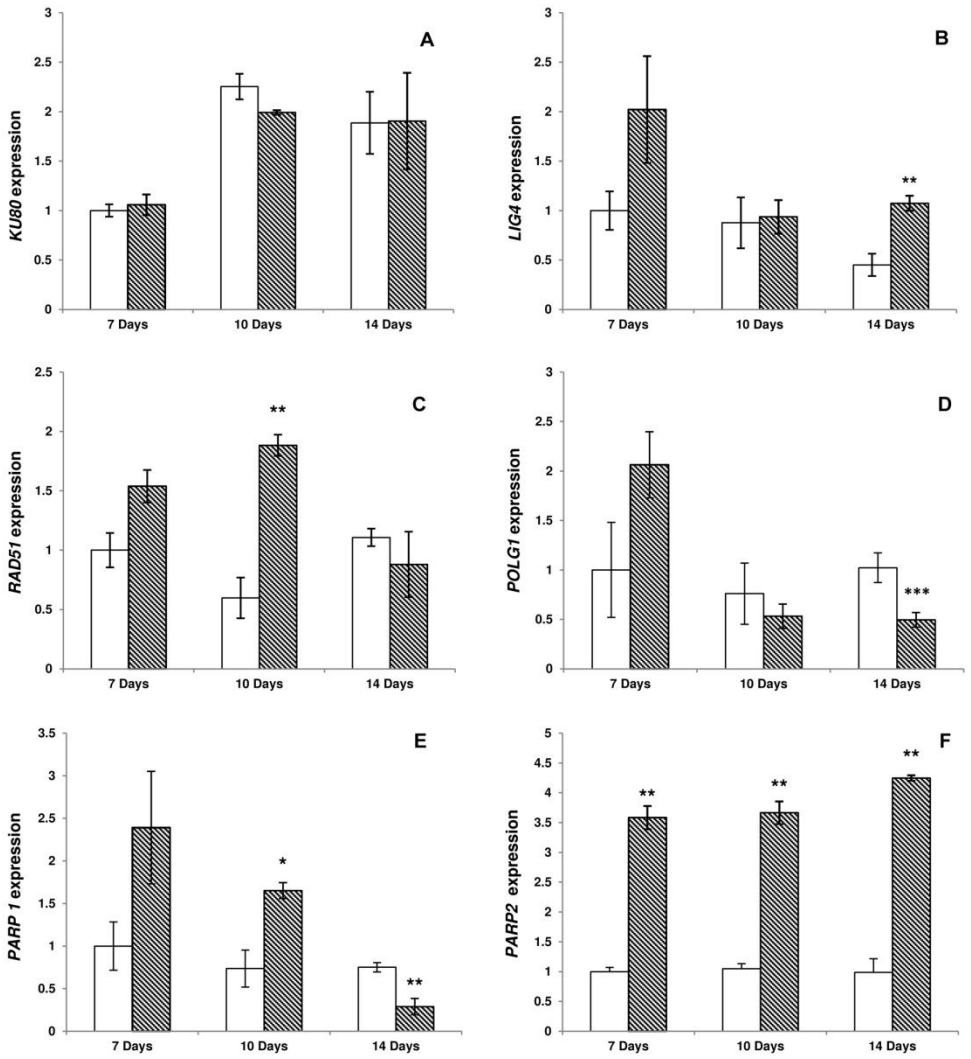

Figure 5.2: Expression of genes involved in DNA damage repair and signalling in shoot tissue of *Arabidopsis thaliana* seedlings of different ages after 96 h of γ-exposure. Data are represented as mean ± SE of control (white bars) and treated plants (grey bars) with n≥3, and expressed relative to the expression levels of 7-day-old control seedlings. Significance levels between treatment and control are shown * $p<0.05$, ** $p<0.01$ (Student-t-test).

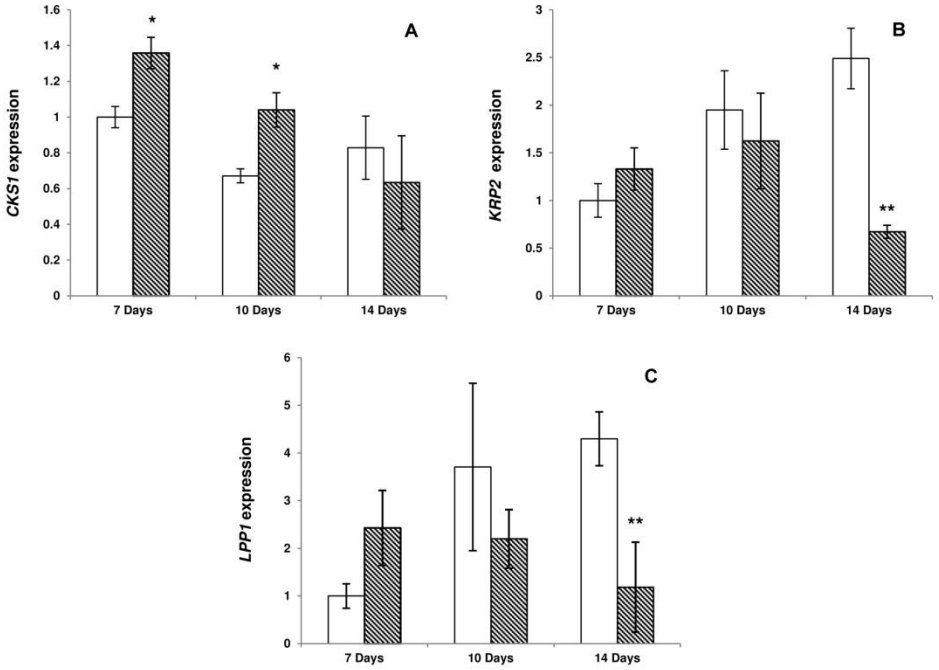

Figure 5.3: Expression of genes involved in the cell cycle and lipid signalling in shoot tissue of *Arabidopsis thaliana* seedlings of different ages after 96 h of γ-exposure. Data are represented as mean ± SE of control (white bars) and treated plants (grey bars) with n≥3, and expressed relative to the expression levels in 7 day-old control seedlings. Significance levels between treatment and control are shown * $p<0.05$, ** $p<0.01$ (Student-t-test).

5.3.4 Base modification

Modified bases such as 8-OHdG, which indicate the level of oxidative damage to genomic DNA, were measured at the end of the exposure. After 168 h of irradiation, 8-OHdG levels were elevated as compared to control plants in shoots of 7- and 10-day-old plants, whereas plants from the 14-day age class showed significantly reduced modified base levels as compared to non-irradiated plants.

Control levels did not vary between the age classes, showing that a constitutive level of base modification (and oxidative damage) in the control treatment remained constant throughout the age interval studied.

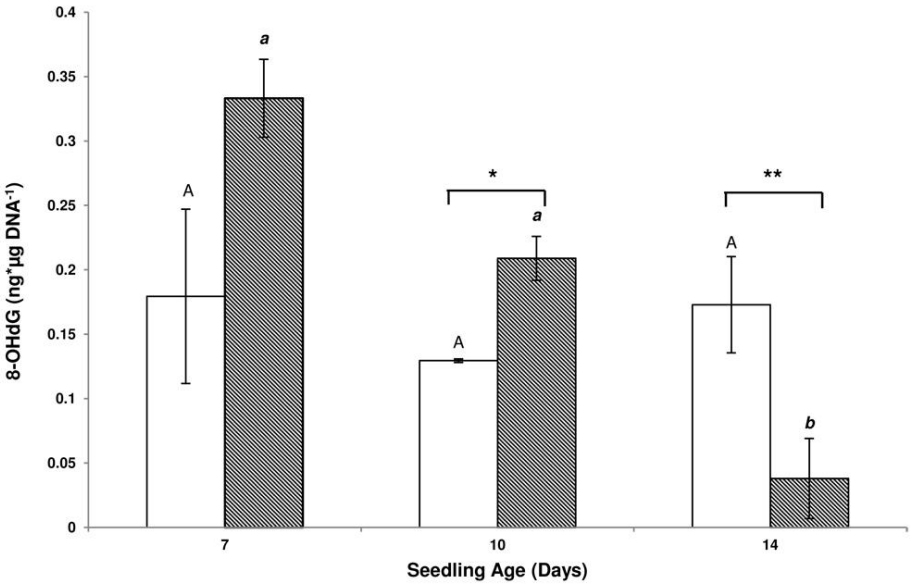

Figure 5.4: 8-OHdG concentration in shoots of *Arabidopsis thaliana* seedlings of different ages after 168 h of exposure as measured by ELISA assay. Differences in 8-OHdG concentration between age classes within control (white bars) and exposed (grey bars) treatments are shown as differences in uppercase letters and lowercase letters respectively. Significance levels between treatment and control are shown * $p<0.05$, ** $p<0.01$ (Student-t-test). Data are presented as mean ± SE with $n\geq3$

5.4 Discussion

The aim of this study was to examine whether *Arabidopsis thaliana* seedlings show age-dependent differences in the response to γ-radiation. We therefore examined the biological effects of exposure to IR at the morphological, physiological and molecular level and compared them for the different age classes tested.

Our biomass measurements (Figure 5.2) show that chronic exposure to 100 mGy h^{-1} γ-radiation influenced fresh weight and growth of *Arabidopsis thaliana* seedlings in an age-dependent way. Plants in our study initially increased in biomass as a result of exposure to high dose rates of γ-radiation. In 7-day-old plants, the positive difference in fresh weight between control and plants γ-exposed during 96 h was considerably higher than that in the older plants. Nevertheless, the decline of this fresh weight difference between 96 h and 168 h of irradiation in all treatments indicates that the positive effect on plant growth is transient, irrespective of plant age. The effects of recovery are less clear. While the relative fresh weight of the youngest seedlings after the recovery period was lower than that at the onset for both exposure lengths, the 10- and 14-day age classes retained their relative difference in fresh weight to the control. So, while the relative increase in biomass in younger seedlings was more pronounced, their relative growth rate declined during the 7-day recovery after treatment. The stability of relative fresh weight in the older life stages indicates that their relative growth rate returned to values near those of the control plants and that they are capable of recovering from this treatment.

Several previous studies on plants have reported an influence of the developmental stage on the effects of IR, both under acute and chronic irradiation conditions. Early studies were mostly done for agricultural purposes on economically relevant crops. Kawai & Inoshita (1965) and Killion & Constantin (1975) both observed growth stage dependent effects of γ-radiation,

in rice and soy bean respectively, but the effects were very dependent on the lifecycle and on the plant species used. Studies with the specific aim of studying age-dependent response to IR in *Arabidopsis thaliana* are scarce, though Kovalchuk et al. (2000) reported an increased frequency of homologous recombination in 10-day-old *Arabidopsis* seedlings exposed to low doses of acute γ-radiation compared to plants exposed at the seed stage. Kurimoto et al. (2010) performed an acute exposure study with a broad dose range on *Arabidopsis thaliana* seedlings at time points between 15 and 25 days after germination. Measuring leaf biomass at the end of the life cycle, they found a reduction at doses as low as 0.5 Gy in seedlings irradiated at 15 days after germination, but not in older seedlings. Their study also did not observe effects on photosynthesis or respiration, which is in correspondence with our measurements and recent observations by Kim et al. (2011) that the photosynthesis chain can tolerate up to 200 Gy. The implications of the small effects on photosynthetic capacity we observed are not clear, as we have no data on the youngest seedlings' photosynthesis.

An additional difficulty in comparing the data with earlier studies comes from the observation that equal doses of radiation can induce non-overlapping responses on the transcriptome level when applied at two radically different dose rates (Kovalchuk et al., 2007). Previous chronic exposure studies on *Arabidopsis thaliana,* between 2 days to full life cycle exposure, have shown little effect of γ-radiation on growth. Vanhoudt et al. (2010) observed no effect on biomass after a 3 days of 36 mGy h^{-1} exposure (a total of 3.5 Gy) of 18-day-old seedlings, whereas a comparable dose administered over the entire life-cycle at approximately 2 mGy h^{-1} induced a 30% reduction in biomass, though only when measured at the end of the growth cycle (Vandenhove et al., 2010). Comparison between these studies and our results are difficult, due to the differences in both dose rate and plant age.

Differences in growth response to stress conditions between developmental stages are likely to be a result of underlying age-dependent differences in regulation of molecular and physiological processes. One of these processes crucial to development is DNA damage repair. DNA damage occurs in all cells as part of the normal functioning of the cell, as a result of oxidative damage by metabolic ROS or due to errors during DNA replication (Britt, 1996). Double-strand breaks, where a lesion occurs in both strands at a single site in the DNA, are the most important threat to integrity of the genome. Eukaryotes have several competing pathways to repair DSB, of which HR and NHEJ are considered the most important (Waterworth et al., 2011). The HR pathway repairs breaks by recombination of the damaged region with a homologous template sequence and through mediating action of recombinases such as RAD51 (Baumann et al., 1996; Doutriaux et al.,1998). The NHEJ pathway, which joins DNA ends at random, is highly conserved in eukaryotes, and contains two main protein complexes. The binding of a DNA dependent protein kinase, which consists of Ku70 and Ku80 subunits, initiates the pathway and a second complex formed by XRCC4 and DNA ligase IV (LIG4) performs ATP-dependent ligation of the strands (West et al., 2000; Bleuyard et al., 2006). The rise in constitutive expression of the Ku subunit with age observed (Figure 5.2A) has been reported before in non-irradiated control *Arabidopsis* seedlings over a similar developmental time span (Boyko et al., 2006b) and is linked to the replacement of HR by NHEJ as the dominant repair system with aging of plants.

Ionising radiation can induce DNA lesions either by direct interaction with the molecule, or through indirect action by water hydrolysis and the creation of ROS. In addition to the IR-induced reactive species, plants can also produce ROS as part of the oxidative stress response, (Foyer & Noctor, 2005), leading to possible oxidative damage to biomolecules and structural components. RAD51 has been shown to be strongly up-regulated in response to acute γ-irradiation (Culligan et al., 2006). In our experiment, younger shoot tissue showed up-regulation whereas the oldest age class did not, indicating that activation of the HR

pathway declines with increasing age of the plants. This is similar to the previous observations on UVB-irradiation by Boyko et al. (2006a) that HR frequency upon γ-radiation exposure declines with age in *Arabidopsis thaliana* shoots in favour of NHEJ. However, this general trend of HR replacement by NHEJ with age cannot explain the *LIG4* expression pattern we observed in the exposed shoots, where expression is up-regulated in young shoots, and down-regulated in old shoots. An expression pattern similar to that of *RAD51* and *LIG4* was also observed for *PARP1*, involved in detection, signalling and repair of SSBs. *PARP1, RAD51 and LIG4* have all been shown to be under regulatory control by the Ataxia-telangiectasia mutated (ATM) protein (Garcia et al., 2003; Culligan et al., 2006). ATM detects and binds DNA lesions (preferably DSB), and through its kinase activity it recruits repair proteins and initiates downstream signalling that leads to modifications in cell cycle dynamics and altered expression of DNA repair pathways. Therefore the similar expression pattern we observe for these DNA repair genes upon irradiation is very likely to be a common result of the upstream regulation by ATM, and thus the result of a reduction in DNA damage with increasing age class. Indeed, though we have no data at 96 h of exposure, the decreasing pattern of oxidative DNA damage we observed under the form of base modifications (Figure 5.4) at the end of the exposure period seems to confirm this view. Additional evidence in favour of this hypothesis comes from the expression of *POLG1*, a DNA polymerase in mitochondria and chloroplasts, also involved in DNA repair (Mori et al. 2005, Parent et al., 2011). ROS production increases in organelles during stress-induced damage to the respiration and photosynthesis chains (Boesch et al., 2011), and the observation that the *POLG1* expression pattern echoes that of the nuclear DNA repair genes points towards a decline in oxidative damage in organelles with age. In summary, the decline of DNA repair as well as DNA damage with age indicates that *Arabidopsis thaliana* seedlings seem to shift from a strategy of increased DNA repair towards one that limits DNA damage through prevention of damage by ROS.

At the level of the cell cycle, this translates into modified cycle dynamics. Several classes of proteins modulate the behaviour and turnover of Cyclin-CDK complexes. We also analysed expression of *CKS1At*, which is a modulator of cyclin-CDK inhibition and activation. De Veylder et al. (2001a) have shown that overexpression of *AtCKS1* results in reduced root growth and meristem size and smaller leaves by altering the timing of G1 and G2 phase. Indeed, the up-regulation of *CKS1* in shoots of 7- and 10-day-old seedlings irradiated for 96 h might account for the subsequent decline in relative growth rate observed between 96 h and 168 h of treatment. A second protein, KRP2 (Kip-related protein), has been identified as an important factor in the transition from mitosis to endoreduplication in differentiating leaf cells (De Veylder et al., 2001b; Verkest et al., 2005). Overexpression of *AtKRP2* inhibits mitosis, and steers the cell cycle towards endoreduplication. We therefore believe that the strong down-regulation we observed in the shoots of the oldest plants exposed to γ-radiation (Figure 5.3B) points towards an inhibition of the endocycle in favour of mitosis. An additional clue on how 14-day-old plants maintain low DNA damage comes from the expression pattern of LPP1 (Figure 5.3C). *AtLPP1* is a lipid phosphate phosphatase, which has previously been shown to be transiently up-regulated in roots and shoots after exposure of *Arabidopsis* to IR (Pierrugues et al., 2001). LPP1 has a preference to cleave diaglycerol pyrophosphate (DGPP) and to a lesser extent phosphatidate (PA), which both can act as second messengers and are involved upstream in the abscisic acid-mediated response to environmental stress (van Schooten et al.; 2006; Nakamura & Ohta, 2010). The action of LPP1 attenuates this signal, which means that the observed down-regulation of LPP1 in the shoots of the oldest plants in our experiment leads to increased stress signalling and possibly an amplified response compared to that of the younger age classes. However, the up-regulation of *LPP1* and *KRP2* cannot explain the reduction in relative biomass in the 14-day-old seedlings between 96 h and 168 h of exposure.

If we compare the transcriptional response of 7-day-old seedlings at 96 h of exposure with that of the 14-day stage (Figure 5.5), two contrasting situations emerge. Young exposed seedlings showed high up-regulation of DNA repair pathways and proteins involved in cell cycle slowdown. As a result, the relative growth rate during subsequent recovery was reduced. Older plants showed down-regulated DNA repair as well as supressed cell cycle arrest at 96 h of exposure, which might explain how their relative growth rate was able to recover after irradiation. Our data do not provide clues as to which mechanisms are involved in the observed late decline in DNA damage at 168 h, but it is likely that increased action of the ROS scavenging pathways and the antioxidant response play a role in the response to IR, limiting the ROS-induced damage to biomolecules in the 14-day age class. One indication for involvement of oxidative stress signalling in the IR response is the strong up-regulation of the PARP2 protein at 96 h. The protein has previously been shown to be part of oxidative stress signalling in cadmium stress (Doucet-Chabeaud et al., 2001).

In conclusion, our data show that plant age is a determining factor in the response of *Arabidopsis* thaliana seedlings to chronic IR stress. All age classes except 10-day-old-seedlings showed a transient increase in relative fresh weight after 96 h of irradiation at 100 mGy h^{-1}, while the relative fresh weight decreased in all age classes between 96 and 168 h of exposure. When allowed to recover for a week after the exposure, 7-day-old seedlings showed a further reduction in relative fresh weight, whilst 14-day-old seedlings were able to maintain their relative growth. At the transcript level, we found important differences in the expression of cell cycle control and DNA damage pathways between both plant ages, suggesting that younger plants are more sensitive to IR and have a lower capacity for recovery, due to a higher reliance on DNA repair and cell cycle arrest. Older plants showed high capacity for recovery and lower oxidative DNA damage levels, suggesting a role for ROS scavenging in the long-term response to chronic IR.

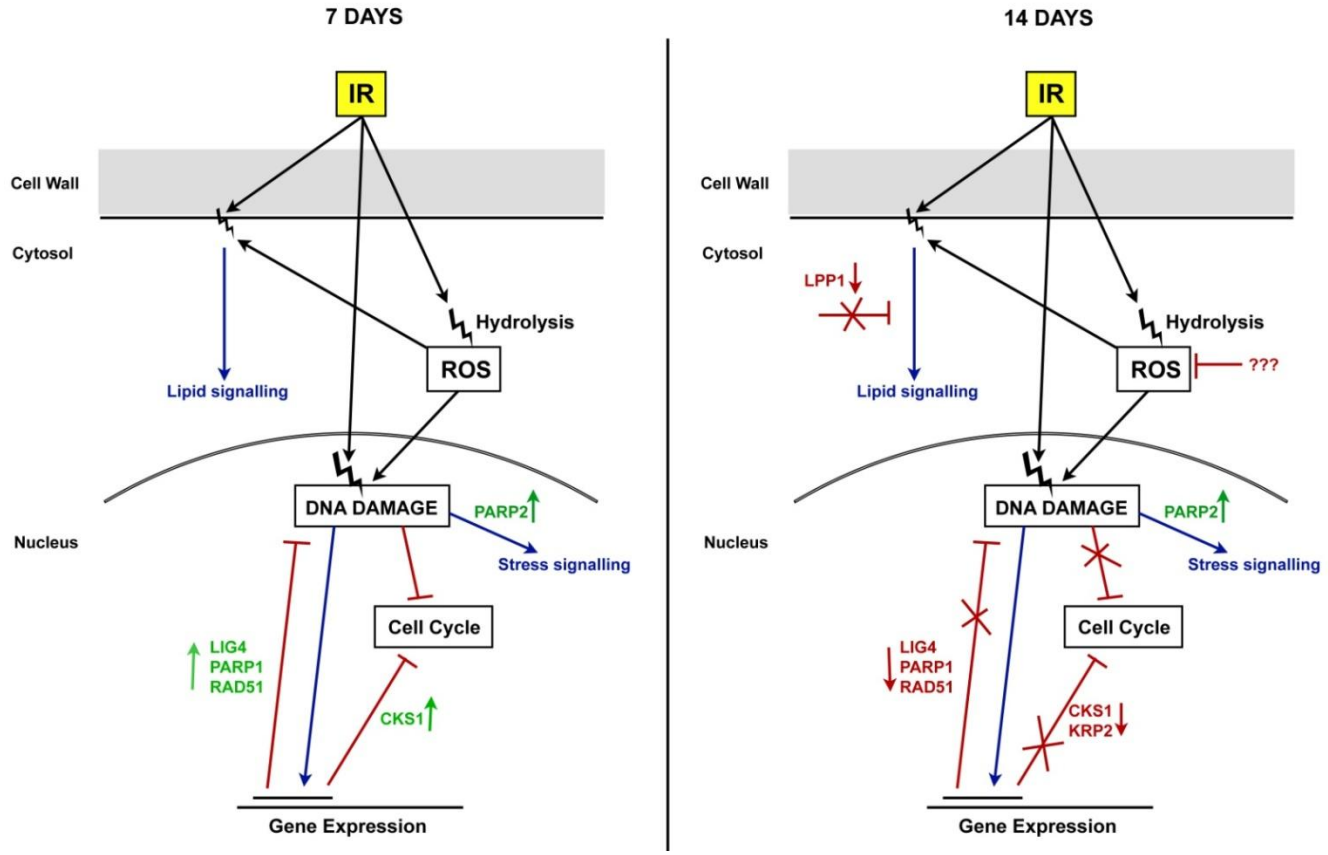
7 DAYS
IR
Cell Wall
Cytosol
Hydrolysis
ROS
Lipid signalling
DNA DAMAGE
PARP2
Stress signalling
Nucleus
Cell Cycle
LIG4
PARP1
RAD51
CKS1
Gene Expression
14 DAYS
IR
Cell Wall
Cytosol
LPP1
Hydrolysis
ROS
???
Lipid signalling
DNA DAMAGE
PARP2
Stress signalling
Nucleus
Cell Cycle
LIG4
PARP1
RAD51
CKS1
KRP2
Gene Expression

Figure 5.5: Transcriptional response mechanisms in 7-day-old (left) and 14-day-old (right) Arabidopsis thaliana leaves exposed to 100 mGy h^{-1} γ-radiation for 96 h. Ionising radiation induces indirect and direct DNA damage through ROS production and direct hits respectively. This DNA damage negatively influences cell cycle progression, and induces a transcriptional response which is targeted both at DNA repair (LIG4/PARP1/RAD51) and cell cycle arrest (CKS1/KRP2). The link between DNA damage and oxidative stress is made by PARP2. In addition to the response to DNA damage, action of ROS and IR create damage-induced lipid stress signalling, which is negatively influenced by LPP1-mediated cleavage. In 7-day-old seedlings (left), DNA repair pathways and cell cycle slowdown were both up-regulated, leading to reduced relative growth during recovery. In 14-day-old seedlings (right), DNA repair and negative cell cycle control were suppressed, resulting in maintained growth capacity and potential for recovery. In this age class, LPP1 expression was supressed, which potentially led to increased lipid signalling. At both age classes, PARP2 was up-regulated, providing a link to the oxidative stress response. However, though there is reason to believe it is implicated in the observed reduction in DNA damage at 168 h of exposure, the role of ROS scavenging is not clear from our data.

Chapter 6:

Biological effects of β-radiation exposure by ^{90}Sr in *Arabidopsis thaliana* seedlings

Biermans, G., Horemans, N., Vanhoudt, N., Vandenhove, H., Saenen, E., Nauts, R., Van Hees, M., Wannijn, J., Vangronsveld, J., Cuypers, A., 2013. *Biological effects of β-radiation exposure by ^{90}Sr in* Arabidopsis thaliana *seedlings*.

In draft

ABSTRACT

The β-emitter ^{90}Sr is of major concern in environmental radiological exposure scenarios. However, little is known about the dose-dependent biological effects of β-radiation on non-human biota, and plants in particular. In this study, we exposed 14 day-old seedlings of *Arabidopsis thaliana* to a wide range of ^{90}Sr activity concentrations for 4 and 7 days. We monitored biomass, growth, photosynthesis, DNA damage, redox balance and the transcription of ley genes involved in DNA repair, cell cycle and the oxidative stress response. Our results show that ^{90}Sr accumulates primarily in the shoot tissue of *Arabidopsis thaliana* seedlings, resulting in high internal shoot dose rates. We observed a transcriptional response in the shoots on ROS scavenging, DNA repair and cell cycle regulation starting in the mGy h^{-1} order of magnitude and above. The timing of this response was earlier for higher dose rates. Despite these responses to ionising radiation exposure, we observed an increase in DNA damage and loss of redox balance, suggesting that the plants are unable to counterbalance chronic exposure. In the roots, dose rates were found to be much lower. At the transcriptional level most genes showed early down-regulation at all dose rates, while late transcription was characterised by up-regulation of ROS scavenging and DNA repair only at the highest dose rates.

6.1 Introduction

In a recent proposal for a strategic research agenda for radioecology by the European Radioecological Alliance (Hinton et al., 2013), a strong call has been made for integration of ecotoxicological models in radioecological research. Radionuclide release is nearly always associated with multiple contaminants, either in a mixture of radionuclides and chemotoxic heavy metals (Vanhoudt et al., 2012) or in a mixture of several types of ionising radiation. Assessment of the effects of a complex mixture that includes radiation emitting compounds therefore requires a thorough understanding of dose-dependent effects for individual types of ionising radiation, at different levels of biological organisation. For plants in particular, the current understanding of low-dose effects remains inadequate for most radiation types except γ-radiation, where considerable progress has been made on estimating/understanding effects on the morphological, physiological and molecular level (Esnault et al., 2010).

In contrast to γ-radiation (photons), which has a high penetration capacity in living tissue and can therefore easily be applied by means of an external source such as ^{60}Co or ^{137}Cs, the limited penetration distance of β-radiation (electrons or positrons) precludes any experimental setup using external exposure. The dose has therefore to be administered by proxy of a β-emitting radionuclide. Radiostrontium (^{90}Sr) decays by β-emission (0.546 MeV, 28.8 year half-life) to Yttrium (^{90}Y), which in turn also decays by β-emission (2.28 MeV, 64 h half-life) to stable zirconium. It is known to have a high mobility in plants due to its chemical resemblance to calcium (Moyen & Roblin, 2008; Queen et al., 1964; Rediske & Selders, 1953; Seregin & Kozhevnikova, 2004; Von Fircks et al., 2002; Wang et al., 1998) and at least one study describes uptake in *Arabidopsis thaliana* (Kanter et al., 2010). In addition to its potential use in delivering β-radiation, ^{90}Sr is a product of nuclear fission and therefore of major concern in environmental radionuclide release, especially at sites of accidental release such

as Chernobyl (Kashparov et al., 2003) or the East Ural Radioactive Trail (EURT) (Kryshev et al., 1998; Nikipelov et al., 1989).

Ionising radiation can induce damage to the major components of the cell by direct energy transfer to macromolecules such as proteins, lipids or DNA. Indirect damage occurs through water radiolysis, which produces reactive oxygen species (ROS), such as superoxide ($O2^{\bullet -}$) and hydrogen peroxide (H_2O_2) (Lee et al., 2009). Besides the damage they can inflict on cellular components, these radicals add to the existing pool of ROS, which are produced as a result of normal metabolic processes and play an important role in signalling and oxidative stress responses (Foyer & Noctor 2005; Mittler et al., 2002). The plant response to oxidative stress consists of several antioxidative pathways which scavenge the ROS in order to maintain redox balance in the cell and avoid oxidative damage. These scavenging pathways consist either of metabolites, such as ascorbate and glutathione (Noctor & Foyer, 1998), or enzymatic reactions in which several classes of proteins such as superoxide dismutases (SOD) and catalases (CAT) remove $O2^{\bullet -}$ and H_2O_2 respectively (Mittler et al., 2004). The DNA damage induced by direct or indirect interaction is repaired by several competing pathways. Double-stranded breaks (DSB) in plants are repaired either conservatively by homologous recombination (HR) or non-conservatively by non-homologous end-joining (NHEJ) (Britt, 1996; Waterworth et al., 2011; West et al., 2000). Single-stranded breaks (SSB) and base modifications such as 8-OHdG are signalled by proteins such as PARPs (Adams-Philips et al., 2010; Schulz et al., 2012). DNA damage ultimately feeds back to the cell cycle, which cannot progress through the control checkpoints before DNA repair has occurred (De Veylder et al., 2007)

Though there are several studies in literature on the chemical effects of stable strontium in plants (Chen et al., 2012; Su et al., 2007), very few studies look at β-radiation as single stressor (Biermans et al., 2013; Killian and Constantin, 1974; Chapter 3). Nevertheless, from their similarity in energy levels and relative biological effectiveness (RBE) (ICRP 2003), we can expect that the

effects of high-energy β-radiation (such as that of ^{90}Sr-^{90}Y) and γ-radiation would be similar. While γ-radiation has been shown to induce a wide range of effects on growth, development and reproductive capacity (Holst & Nagel, 1997), the overall trend in plant response is difficult to characterise, as responses vary from hormesis to inhibition depending factors such as exposure type (acute or chronic) and species (Esnault et al., 2010) and show an overall decrease with plant age (Chapter 5). Finally, previous work has shown that 18-day old *Arabidopsis thaliana* seedlings do not show effects on growth or photosynthesis when exposed to high doses by ^{90}Sr (Biermans et al., 2013) and that younger plants might be more sensitive to radiation (Chapter 5).

In this study, we wanted to unravel the response of *Arabidopsis thaliana* to chronic β-radiation, by exposing 14-day old seedlings for 7 days to a wide environmental range of ^{90}Sr in a hydroponic setup. First we aimed to characterise uptake and dose of ^{90}Sr in roots and shoots under a hydroponic setup, and analysed the response on classical endpoints such as growth and photosynthesis. Secondly, we wanted to link these morphological and physiological effects to the underlying response at the molecular level. To this end, we measured DNA damage and the concentrations of scavenging metabolites, as well as transcriptional levels of genes involved in DNA repair, cell cycle, signalling and the anti-oxidative response.

6.2 Methods

6.2.1 Plant culture and Strontium exposure

Before sowing, *Arabidopsis thaliana* (Columbia ecotype) were spread out on moist filter paper and vernalized for three days at 4°C to synchronize germination. Subsequently, the seeds were sown on plugs from 1.5 mL eppendorf tubes filled with 0.6% agar. The plugs were placed in a PVC cover, capable of holding 36 plugs, after which each cover was placed on a container

filled with 1.35 L modified Hoagland solution (1mM KNO_3, 0.3 mm $Ca(NO_3)_2$, 0.2 mM $MgSO_4$, 0.1 mM $NH_4H_2PO_4$, 1.62 µM $FeSO_4$, 0.78 µM Na_2EDTA, 4.6 µM H_3BO_3, 0.9 µM $MnCl_2$, 0.032 µM $CuSO_4$, 0.055 µM H_2MoO_4, 0.077 µM $ZnSO_4.7H_2O$).

Plants were grown in a growth chamber (Binder) under a 16/8 day/night photoperiod and 22°C/16°C day/night temperatures and 65% relative humidity. Photosynthetic photon flux density was 120 µE at the leaf level (Sylvania BriteGro F36WT8/2084 and F36WT8/2023 lamps). Plants were aerated with a peristaltic pump from 7 days after sowing onwards.

After 14 days, seedlings were exposed for 4 or 7 days to 0, 250, 2500, 25000 and 250000 Bq/L ^{90}Sr, added as $SrCl_2$. The pH of the liquid medium was adjusted to that of the 0 Bq/L treatment prior to exposure of the plants.

6.2.2 Plant sampling and biomass

Roots and shoots were sampled after 4 and 7 days, and fresh weight determined for minimum 18 biological replicates. Half of the tissues from each treatment were snap frozen in liquid nitrogen for RNA and DNA extractions (as 50 to 100 mg samples in eppendorf tubes) and stored at -80°C until processing.

The other half was collected for ^{90}Sr concentration and dry weight determination and dried for 7 days at 80°C. The roots were first rinced (at 4°C) with 2x10 min. in 1 mM $Pb(NO_3)_2$, then 1x10 min. in dH_2O to remove external strontium.

6.2.3 Leaf Area

Leaf area was determined at regular intervals during exposure using a compact CCD digital camera (Canon). Images were analysed using ImageJ (US National Institutes of Health, Bethesda, Maryland, US), and calibrated using centrifuge

tube width as a constant scaling parameter in each image. By isolating the correct range of green values in each image, the plants could then be isolated from the background and their individual surfaces measured after transformation to a binary image.

6.2.4 Transfer and Dosimetry

Samples for transfer measurements were dry-ashed in a muffle furnace, and subsequently digested in 0.1 M HCl. Digested samples were then diluted 10x in dH_2O, vortexed and diluted again 4x in scintillation cocktail (Optiphase Hisafe 3, PerkinElmer). Medium samples (5 mL) were also taken from each tray and brought to 20 mL with scintillation cocktail. After careful mixing of sample and scintillation fluid, the ^{90}Sr activity was measured for 60 minutes by beta scintillation counting (Packard 1600TR Tri-Carb, Canberra,,Zellik, Belgium). The counting efficiency was determined using a dilution series of ^{90}Sr with known activities between 0 and 5000 Bq. Transfer factors were calculated as activity (in Bq) per kg dry weight. Concentration ratios were calculated as activity (in Bq) per kg fresh weight.

Internal and external root dose rates and internal shoot dose rates at each harvest point, and the corresponding absorbed doses over the exposure period, were determined by the plant dosimetry method described in Biermans et al. (2013), which uses separate dosimetry models for *Arabidopsis* root and shoot, and is based on the measured activity concentrations in the organs. Shoot dose conversion coefficient (DCC) values for each harvest point were determined by taking into account the leaf area measurements (Section 2.4). Doses were calculated under assumption of linear increase in tissue activity concentration during the exposure.

6.2.5 Photosynthesis measurement and pigment analysis

At harvest, four plants from each treatment were chosen at random. These were selected from the plants destined for activity and dry weight measurements. Their 4th leaf was then removed, and stored on wet paper in a closed petri dish in the dark.

The leaves were pre-adapted to dark conditions for at least 15 minutes and the induction curve (IC) for photosystem II (P680) was then measured using PAM Fluorometry (Dual PAM-1000; Waltz, Germany) (Schreiber et al., 2004). From these data, values for photosynthetic efficiency (φPSII), non-photochemical quenching (NPQ) and photosynthetic capacity (Fv/Fm) could be calculated. The induction curve measurement was immediately followed by a rapid light curve (RLC) measurement between 0 and 800 µE. These data were then fitted to the continuous model of Platt without photoinhibition as used in Ralph and Gademan (2005) using a Marquardt-Levenberg curve fitting algorithm in statistical software package R (R Development Core Team, 2011).

Pigments were extracted from frozen shoots by incubation in 100% N,N-dimethylformamide (DMF) overnight at 4°C under dark conditions. The pigment absorbance was measured spectrophotometrically at 480, 647 and 664 nm and pigment concentrations for chlorophyll a, chlorophyll b and carotenoids were calculated from these-absorbance values using the appropriate equations for DMF according to Wellburn (1994).

6.2.6 Base modification (8-OHdG formation)

Frozen shoot tissue (75-100 mg), harvested from plants irradiated for 7 days, was mechanically shredded with beads (MM400, Retsch, Germany; -80 °C, 2.5 min. at 30 Hz), and the DNA extracted from the samples using DNeasy Plant Mini Kit (Qiagen). DNA concentrations were measured spectrophotometrically (Nanodrop 2000, Isogen Life Sciences).

The DNA samples were then digested as described in Debiane et al. (2009). 38 µL of DNA extract was incubated for 2 minutes at 100°C, and subsequently digested with Nuclease P1 (2µL 5U/µL; Sigma) in the presence of 3 µL 250 mM potassium acetate buffer (pH 5.4) and 3 µL 10 mM zinc sulphate. Digestion was performed at 37°C overnight, after the digests were treated for 2 hours at 37°C with 2 µL alkaline phosphatase (0.3 U/µL; Sigma) in the presence of 6 µL 0.5 M Tris-HCl buffer (pH 8.3). Base modification (8-OHdG) was determined by competitive ELISA (New 8-OHdG Check kit, Japan Institute of Aging) according to the manufacturer's instructions. The assay is based on spectrophotometric detection at 415 nm.

6.2.7 Gene Expression analysis

Frozen root and shoot tissue (50-100 mg) was homogenized in a tissue shredder (MM400, Retsch, Germany; -80 °C, 2.5 min. at 30 Hz) prior to RNA extraction. RNA from shoot tissue was extracted using Ambion RNaqueous Kit (Invitrogen), and root RNA with RNeasy Plant Mini Kit (Qiagen, Venlo, Netherlands). RNA quality was checked through electrophoresis on Bioanalyzer (Agilent Technologies) and its quantity was determined with spectrophotometry at 260 nm on Nanodrop (Isogen Life Science). Genomic DNA was removed from the samples with TURBO DNA-free™ Kit (Invitrogen) according to the manufacturer's instructions. RNA was then transformed to cDNA with the High-Capacity cDNA Reverse Transcription Kit (Applied Biosystems), using equal amounts of starting material (1 µg).

Quantitative realtime-PCR was performed using SYBR Green fluorescence on a 7500 Fast Real-Time PCR system (Applied Biosystems) in a 10µL volume, containing 2.5 µL cDNA sample, 5 µL of Fast SYBR Green Master Mix (Applied Biosystems), 0.3 µL forward primer, 0.3 µL reverse primer and 1.9 µL RNase-free water. Primers used are shown in Table 6.1 Primer efficiency was determined by standard curve. Gene expression data was normalized to

housekeeping genes (ACT2, EF-1α, TIP41-like, UBC) using GeNorm software according to Vandesompele et al. (2002) and presented relative to control (gene expression at 0 Bq/L) of the respective harvest point.

6.2.8 Metabolites

Ascorbate and glutathione levels were determined in the leaves of *Arabidopsis thaliana* seedlings exposed for 7 days to ^{90}Sr using a spectrophotometric assay as described by Queval & Noctor (2007) This method enables measurement of both oxidised and reduced forms for both components of the ascorbate-glutathione cycle.

Frozen shoot tissue (50-100 mg) was homogenized in a tissue shredder (MM400, Retsch, Germany; -80 °C, 2.5 min. at 30 Hz) and extracted by addition of 800 µL 0.1M HCl. The entire procedure was performed on ice. Measurements were performed at room temperature.

Total glutathione concentrations (reduced form GSH + oxidised form GSSG) were measured by the reduction of 5,5-dithiobis(2-nitro-benzoic acid) (DTNB), in the presence of glutathione reductase (GR). Reactions were performed in the presence of 100 µl phosphate buffer (200 mM NaH2PO4, 10 mM EDTA (pH 7.5)), 60 µl dH2O, 10 µl 10 mM NADPH and 10 µl 12 mM DTNB. After addition of 10 µL GR, 10 µL of extract was added, after which DTNB reduction was monitored spectrophotometrically as an increase in A_{415}. To measure only the oxidised GSSG fraction, a similar measurement was performed (using 20 µL of sample) after blocking the GSH present in the sample with 2-vinylpyridine.

Total ascorbate (the sum of the oxidised (dehydroascorbate; DHA) and reduced (AsA) forms) was determined by converting the DHA present in the sample to AsA by incubation with 25 mM Dithiothreitol (DTT) and 125 mM NaH_2PO_4 (pH 7.5) for at least 15 minutes. After adjustment of the pH to 5.5 with HCl, AsA and total ascorbate measurements were performed with 40 µL of extract, in the

presence of 100 µl 200 mM NaH_2PO_4 (pH 5.6) and 55 µl dH_2O, by determining absorbance of AsA at 265 nm. After addition of 5 µL Ascorbate oxidase (AO), the change in A_{265} was measured until stable values were obtained.

6.2.9 Statistical Analysis

Datasets from transfer, biomass, photosynthesis, pigments, base modification and gene expression were analysed using statistical software package R (R Development Core Team, 2011).

All datasets, except those for transfer, leaf area and pigments, were analysed for each time point and tissue separately, comparing means between treatments. Assumptions of normality of the model residuals and consistency of variance were tested using a Shapiro test and a Bartlett test respectively, after which a one way-ANOVA and pairwise comparisons between means were performed using the Tukey correction. If necessary, when assumptions were not met, appropriate transformation of the data was performed using a Box Cox transformation. The assumptions were then checked again. If none of the assumptions were met, a non-parametrical Kruskal-Wallis test was performed and pairwise comparisons using the Bonferoni correction.

Transfer and leaf area datasets were analysed by time point and treatment using a two-way ANOVA and pairwise comparisons with the Tukey method. Pigment data were analysed by two-way ANOVA as described in the results (Section 6.3.6).

Gene Name	Forward Primer Sequence	Reverse Primer Sequence
ACT2	*CTTGCACCAAGCAGCATGAA*	*CCGATCCAGACACTGTACTTCCTT*
EF-1α	*TGAGCACGCTCTTCTTGCTTTCA*	*GGTGGTGGCATCCATCTTGTTACA*
TIP41-like	*GTGAAAACTGTTGGAGAGAAGCAA*	*TCAACTGGATACCCTTTCGCA*
UBC	*CTGCGACTCAGGGAATCTTCTAA*	*TTGTGCCATTGAATTGAACCC*
CKS1	CACGTCGTTCTTCCTCCTGAAG	TCCTATCGCTCGCCATTCG
DMC1	ATGAAGACGAAGATCTATTTGAGATGATT	CTTGTAGCTTTTTCACATCTCCTGC
GAR1	CTAAGATGGTTGGTGATGCAAGAGA	CGCTAAGCTCATCCAAACCCTT
KU80	CTTCTTCCAGCACAACTCCTCAA	CTACGCATCGCAGGACCTACAT
LIG4	TGATGTATCGGATATCAAGGGCA	GAATGGGACCGAGGCACG
LPP1	TCACTTTCTGATGACAATAGGGTCG	CCTCTCTGCGCCTCCTGG
MND1	GAACGAGATGGTACAATTTGCTGA	CCGACTGGTGAGCAACTTCAAT
PARP1	TGCATTGGGAGAAATACATGAGC	CCGAGCCCTTTGGTCGAG
PARP2	ATCGGAGGTGATTGATCGGTATG	AAATCATGAGGTATCACTGTGTAGAACTCT
POLG1	GAAACTGGACGCTTATCGGCTAG	CTGACGGATTTTGTACCGATCTTT
RAD51	GTCCAACAACAAGACGATGAAGAA	AACAGAAGCAATACCTGCTGCC
APX1	TGCCACAAGGATAGGTCTGG	CCTTCCTTCTCTCCGCTCAA
CAT1	AAGTGCTTCATCGGGAAGGA	CTTCAACAAAACGCTTCACGA
CAT2	AACTCCTCCATGACCGTTGGA	TCCGTTCCCTGTCGAAATTG
CAT3	TCTCCAACAACATCTCTTCCCTCA	GTGAAATTAGCAACCTTCTCGATCA
CSD1	TCCATGCAGACCCTGATGAC	CCTGGAGACCAATGATGCC
CSD2	GAGCCTTTGTGGTTCACGAG	CACACCACATGCCAATCTCC
CSD3	GTTGTTGTGCATGCGGATCC	CACATCCAACTCTCGAGCCTG
FSD1	CTCCCAATGCTGTGAATCCC	TGGTCTTCGGTTCTGGAAGTC
FSD2	TTGGAAAGGTTCAAGTCGGCT	CATTTGCAACGTCAAGTCTATTCG
FSD3	AACGGGAATCCTTTACCCGA	TGTCTCCACCACCAGGTTGC
GR1	CTCAAGTGTGGAGCAACCAAAG	ATGCGTCTGGTCACACTGC
LOX1	TTGGCTAAGGCTTTTGTCGG	GTGGCAATCACAAACGGTTC
LOX2	TTTGCTCGCCAGACACTTG	GGGATCACCATAAACGGCC
RBOHA	CATTTCGCTAGGCCAAACTG	TTCACTAACCCAGCTGCTCCA
RBOHC	TCACCAGAGACTGGCACAATAAA	GATGCTCGACCTGAATGCTC
RBOHE	GTGATGCAAGATCAACCCTGA	GCCTTGCAAAATGTGTTCTCA

Table 6.1: Primers for gene expression analysis

6.3 Results

6.3.1 Activity concentrations of the medium

Measured activity concentrations corresponded well to the order of magnitude of the desired nominal activity concentrations in the medium (Table 6.2), though they were slightly lower than expected. This difference was most likely due to the adsorption of ^{90}Sr to the glass source vessel wall and/or the exposure tray. At a nominal activity concentration of 250,000 Bq L^{-1}, the chemical concentration of ^{90}Sr is approximately equal to 0.5 nM.

Table 6.2: nominal and measured activity concentrations for each treatment. Values presented are mean ± SE of 4 replicates.

Activity Concentration [Bq L^{-1}]	
Nominal	Measured
0	0 ± 0.001
250	212 ± 5
2500	2050 ± 190
25 000	22 293 ± 26
250 000	220 600 ± 900

6.3.2 Transfer

Dry weight transfer factors to the plant tissues for ^{90}Sr are shown in Table 6.3. For medium-to-shoot transfer, the values were slightly higher at 7 days compared to those at 4 days, and in general the effect of harvest time was significant (ANOVA; $F_{1,3}=29.13$, $p= 2.36 \times 10^{-5}$). However, no significant

differences were detected between treatments by pairwise comparison. Similarly, no individual differences were found for the medium-to-root transfer factors, though the effect of harvest time was significant there as well (ANOVA $F_{1,3}$= 6.87, p= 0.016).

Table 6.3: Transfer factors for *Arabidopsis thaliana* seedlings exposed for 4 and 7 days to ^{90}Sr. Results present mean ± S.E. of at least 3 biological replicates. Analysis was done separately for each tissue type. Differences in lower case letters indicate significant differences in dose rate between treatments on the same harvest day (p<0.05). Differences in upper case letters indicate significant differences in dose rate between harvest points for a specific treatment (p<0.05).

		^{90}Sr Transfer Factor [Bq kg^{-1} DW / Bq L^{-1}]	
		ROOTS	SHOOTS
4 DAYS	*212 Bq L^{-1}*	^{A} 273.1 ± 135.22 ^{a}	^{A} 1255.05 ± 233.31 ^{a}
	2050 Bq L^{-1}	^{A} 297.45 ± 110.52 ^{a}	^{A} 1905.39 ± 647.85 ^{a}
	22293 Bq L^{-1}	^{A} 315.67 ± 14.02 ^{a}	^{A} 2027.56 ± 607.27 ^{a}
	220600 Bq L^{-1}	^{A} 416.93 ± 82.95 ^{a}	^{A} 1388.7 ± 96.71 ^{a}
7 DAYS	*212 Bq L^{-1}*	^{A} 478.21 ± 16.47 ^{a}	^{B} 2471.02 ± 161.64 ^{a}
	2050 Bq L^{-1}	^{A} 405.97 ± 27.8 ^{a}	^{A} 2146.58 ± 44.34 ^{a}
	22293 Bq L^{-1}	^{A} 386.49 ± 31.69 ^{a}	^{A} 2233.34 ± 40.74 ^{a}
	220600 Bq L^{-1}	^{A} 551.64 ± 28.07 ^{a}	^{A} 2026.11 ± 42.86 ^{a}

Concentration ratios (CR) for the roots did not show dose- or time-dependent differences (Table 6.4), CR values for the shoots increased in the 212 and 220,600 Bq L^{-1} treatment between 4 and 7 days of exposure, indicating an increase in root-to-shoot transfer for these treatments. Overall, CR values show

a high variability, which seems to be a result of high individual variation in uptake, as the relative error in exposure concentration (Table 6.2) between biological replicates (trays) is much lower than that of the transfer values.

Table 6.4: Concentration Ratios for *Arabidopsis thaliana* seedlings exposed for 4 and 7 days to ^{90}Sr. Results present mean ± S.E. of at least 3 biological replicates. Analysis was done separately for each tissue type. Differences in lower case letters indicate significant differences in dose rate between treatments on the same harvest day ($p<0.05$). Differences in upper case letters indicate significant differences in dose rate between harvest points for a specific treatment ($p<0.05$).

		^{90}Sr Concentration Ratio [Bq kg^{-1} FW / Bq L^{-1}]		
		ROOTS	SHOOTS	TOTAL PLANT
4 DAYS	*212 Bq L^{-1}*	^{A} 22.91 ± 16.22 ^{a}	^{A} 111.65 ± 25.34 ^{a}	^{A} 54.63 ± 27.53 ^{a}
	2050 Bq L^{-1}	^{A} 18.21 ± 12.72 ^{a}	^{A} 192.7 ± 84.29 ^{a}	^{A} 155.62 ± 69.15 ^{a}
	22293 Bq L^{-1}	^{A} 13.42 ± 0.28 ^{a}	^{A} 181.82 ± 62.82 ^{a}	^{A} 95.72 ± 6.58 ^{a}
	220600 Bq L^{-1}	^{A} 16.17 ± 3.25 ^{a}	^{A} 110.69 ± 14.06 ^{a}	^{A} 86.62 ± 7.88 ^{a}
7 DAYS	*212 Bq L^{-1}*	^{A} 29.83 ± 3.64 ^{a}	^{B} 210.55 ± 16.6 ^{a}	^{A} 180.07 ± 14.03 ^{a}
	2050 Bq L^{-1}	^{A} 12.53 ± 2.26 ^{a}	^{A} 197.18 ± 8.9 ^{a}	^{A} 133.91 ± 11.34 ^{a}
	22293 Bq L^{-1}	^{A} 20.34 ± 1.46 ^{a}	^{A} 214.75 ± 4.88 ^{a}	^{A} 162.94 ± 2.21 ^{a}
	220600 Bq L^{-1}	^{A} 28.21 ± 3.15 ^{a}	^{B} 186.91 ± 7.22 ^{a}	^{A} 150.91 ± 3.93 ^{a}

6.3.3 Dosimetry

The calculated internal dose rates at 4 and 7 days of exposure to ^{90}Sr increased roughly 10-fold for every 10-fold increase in exposure activity concentration

(Table 6.5A), both in the roots and the shoots. This could be expected from the concentration ratios (Table 6.4), which all lie within the same order of magnitude.

In the roots, the external dose rate delivered by the surrounding contaminated medium exceeded the internal dose rate in all treatments. Between 4 and 7 days of exposure, the internal dose rate had increased for nearly all treatments and in both root and shoot, indicating that no saturation of strontium occured in the tissues within the time interval of the exposure. At least for the shoots the internal dose rate increased linear with exposure time. When adding the assumption that the dose rate was zero at the start of the exposure, the r^2 for the linear relation between shoot dose rate and exposure time was found to be between 0.85 to 0.99 in all treatments.

Absorbed doses accumulated to a maximum of 16 mGy in the roots and 340 mGy in the shoots after 4 days of exposure to 220,600 Bq $L^{-1.}$ At 7 days of exposure, the total doses had increased to 31 mGy in the roots and approximately 1 Gy in the shoots (Table 6.5B).

6.3.4 Leaf area

We monitored the leaf area at several time points during exposure using image analysis. Leaf area was significantly increased in the 2050, 22,293 and 220,600 Bq L^{-1} treatments relative to the control (Figure 6.1). The maximum, a 30 to 40% increase compared to the control plants' leaf area, was reached at 96 h after the onset of exposure, with a subsequent decline of 20-30% at 168 h compared to the values at 96 h. By the end of the ^{90}Sr treatment, only the plants exposed to 22,239 and 220,600 Bq L^{-1} had retained a significantly larger leaf area. The response was not dose-dependent, as all significantly responding treatments showed a similar increase in area.

Table 6.5 Dose rates (**A**) and Total absorbed doses (**B**) for *Arabidopsis thaliana* seedlings exposed for 4 and 7 days to ^{90}Sr. Results present mean ± S.E. of at least 3 biological replicates. Analysis was done separately for each tissue type. Significant differences in dose rate between harvest days are shown as * p<0.05; **p<0.01; ***p<0.001

A

		^{90}Sr Dose rates [µGy/h]		
		ROOTS - INTERNAL	ROOTS - EXTERNAL	SHOOTS
4 DAYS	*0 Bq L^{-1}*	0 ± 0.001	0 ± 0.001	0 ± 0.001
	212 Bq L^{-1}	0.07 ± 0.04	0.135 ± 0.003	6.8 ± 1.7
	2050 Bq L^{-1}	0.5 ± 0.4	1.31 ± 0.12	90 ± 23
	22293 Bq L^{-1}	4.2 ± 0.1	14.231 ± 0.017	770 ± 80
	220600 Bq L^{-1}	50 ± 10	140.8 ± 0.6	7000 ± 900
7 DAYS	*0 Bq L^{-1}*	0 ± 0.001	0 ± 0.01	0 ± 0.004
	212 Bq L^{-1}	0.09 ± 0.013	0.135 ± 0.003	*13.3 ± 0.9
	2050 Bq L^{-1}	0.36 ± 0.08	1.31 ± 0.12	120 ± 10
	22293 Bq L^{-1}	*6.3 ± 0.5	14.231 ± 0.017	***1440 ± 30
	220600 Bq L^{-1}	**87 ± 10	140.8 ± 0.6	***12400 ± 500

B

		^{90}Sr Dose [mGy]		
		ROOTS - INTERNAL	ROOTS - EXTERNAL	SHOOTS
4 DAYS	*0 Bq L^{-1}*	0 ± 0.0001	0 ± 0.01	0 ± 0.001
	212 Bq L^{-1}	0.0033 ± 0.0024	0.01296 ± 0.00029	0.33 ± 0.08
	2050 Bq L^{-1}	0.03 ± 0.02	0.128 ± 0.012	4.5 ± 1.1
	22293 Bq L^{-1}	0.2 ± 0.005	1.3662 ± 0.0016	37 ± 4
	220600 Bq L^{-1}	2.4 ± 0.5	13.52 ± 0.06	340 ± 40
7 DAYS	*0 Bq L^{-1}*	0 ± 0.00016	0 ± 0.01	0 ± 0.0003
	212 Bq L^{-1}	0.0075 ± 0.0011	0.0227 ± 0.0005	1.12 ± 0.07
	2050 Bq L^{-1}	0.03 ± 0.006	0.22 ± 0.02	10.1 ± 0.9
	22293 Bq L^{-1}	0.53 ± 0.04	2.3908 ± 0.0029	120.6 ± 2.8
	220600 Bq L^{-1}	7.3 ± 0.8	23.65 ± 0.1	1050 ± 40

Figure 6.1: Relative leaf area for each treatment at different time points after the start of exposure to 212, 2050, 22,393 and 220,600 Bq L^{-1} (grey to black bars), relative to the control treatment (0 Bq L^{-1}, white bars) at each time point. Values are presented as mean ± SE of at least 15 biological replicates. Statistical analysis was performed on each time point separately. Differences in capital letters between treatments within each time point reflect significant differences in leaf area between treatments ($p<0.05$)

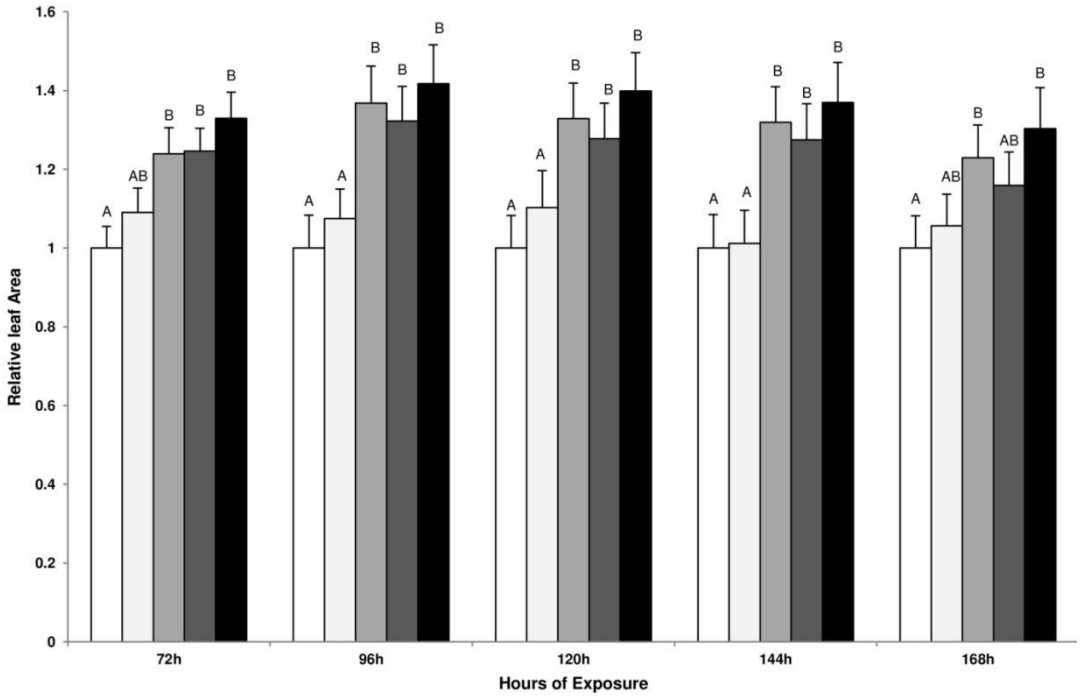

6.3.5 Biomass

At 4 days of exposure, the root fresh weight showed an increasing trend with increasing dose rate (Table 6.6). At the highest dose rate at 4 days of exposure, the roots were 2.4-fold increased in fresh weight compared to untreated plants. The dry weight percentage of the roots at 4 days showed a decreasing trend (ANOVA, $F_{4,12}$ = 1.586, p = 0.24), indicating an increased water content of the tissue. At 7 days of exposure, only the 2050 Bq L^{-1} treatment showed an effect on biomass, as root dry weight percentage was only (46 ± 18)% of that of the untreated plants (Table 6.6). At the higher dose rates, the effects on root fresh weight and dry weight percentage had returned to the control values.
In the leaves, there were no observed effects of ^{90}Sr exposure on biomass at either of the time points (Table 6.6).

Table 6.6: Fresh weight and dry weight percentage of roots and shoots at 4 and 7 days of exposure to ^{90}Sr. Fresh weight values are the mean ± S.E. of at least 18 biological replicates. Dry weight percentages are the mean ± SE of 4 biological replicates. Significance levels * p<0.05. For associated doses and dose rates, see Table 6.5A and B.

		Fresh Weight [mg]		**% Dry Weight [%]**	
		SHOOTS	ROOTS	SHOOTS	ROOTS
4 DAYS	*0 Bq L^{-1}*	14.1 ± 0.4	2 ± 0.06	6.8 + 1.1	6.7 + 0.5
	212 Bq L^{-1}	15.1 ± 0.6	2.9 ± 0.7	8.5 + 0.7	6.6 + 2.1
	2050 Bq L^{-1}	14.8 ± 0.5	3.1 ± 1	7.9 + 0.4	5.8 + 1.2
	22293 Bq L^{-1}	16.1 ± 0.7	*4.1 ± 0.7	8.7 + 0.7	4.4 + 0.2
	220600 Bq L^{-1}	15.6 ± 0.6	*4.8 ± 0.8	7.9 + 0.5	3.9 + 0.5
7 DAYS	*0 Bq L^{-1}*	32.4 ± 1.4	10 ± 1.1	9 + 0.5	6.6 + 0.9
	212 Bq L^{-1}	36.1 ± 1.6	9.2 ± 0.6	8.5 + 0.4	6.2 + 0.6
	2050 Bq L^{-1}	31.9 ± 1.4	8.3 ± 0.6	9.2 + 0.3	*3.0 + 0.4
	22293 Bq L^{-1}	36.3 ± 1.5	9 ± 0.7	9.6 + 0.1	5.3 + 0.1
	220600 Bq L^{-1}	34.7 ± 1.3	9.3 ± 0.8	9.2 + 0.3	5.1 + 0.5

6.3.6 Photosynthesis

At each harvest point, values for maximum photosynthetic efficiency (Fv/Fm), Photosystem II quantum yield (Φ_{PSII}) and the yield of non-photochemical quenching (Y_{NPQ}) were derived from induction curves. Electron transfer rate (ETR) was derived from rapid light curve measurements. After 4 days of exposure to ^{90}Sr, maximum photosynthetic Fv/Fm showed an increasing trend with increasing internal shoot dose rate, indicating a rise in available open Photosystem II reaction centres (Figure 6.2). At 7 days of exposure no such trend was evident, though the values at 13.3 µGy h^{-1} were significantly reduced. The control levels were within the expected range at both harvest points (Maxwell & Johnson, 2000).

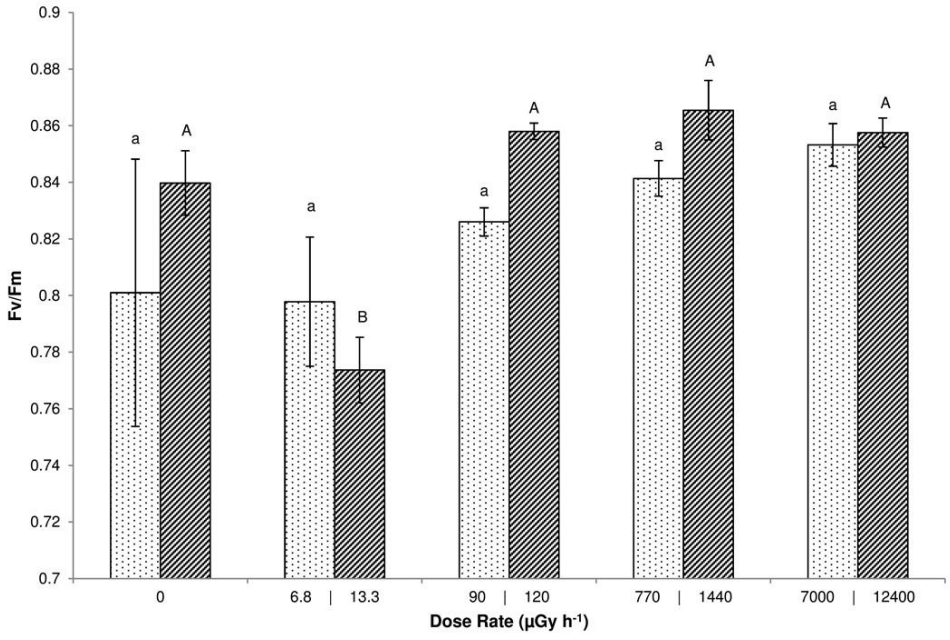

Figure 6.2: Fv/Fm in *Arabidopsis thaliana* shoots after 4 days (light bars) and 7 days (dark bars) of exposure to ^{90}Sr. Data are presented as mean ± SE (n>3) Differences in

lower case letters between treatments reflect significant differences between dose rates at 4 days ($p<0.05$). Differences in capital letters between dose rates reflect significant differences at 7 days ($p<0.05$).

The dose-dependent increase in photosynthesis performance after 4 days exposure was also evident from the measurements of Φ_{PSII}. After 4 days, there was a clear increasing trend in Φ_{PSII} (ANOVA, $F_{4,10} = 3.346$, $p = 0.055$), reaching an increase in quantum yield of nearly 8% compared to control at 7000 µGy h^{-1} (Figure 6.3). After 7 days, quantum yield had increased in all treatments, including the control, compared to the values at 4 days. Nevertheless, the increasing trend observed at 4 days was no longer present (ANOVA, $F_{4,14} = 0.757$, $p = 0.75$). Figure 6.4 shows that the increase in photosynthetic yield at 4 days was accompanied by a trend of reduction of non-photochemical quenching with increasing dose rates (ANOVA, $F_{4,11} = 2.361$, $p = 0.11$). At 7 days, NPQ yield was near identical at all dose rate at a level of 3% of the incoming light energy. No effects on ETR were observed for either dose rate or harvest point (data not shown).

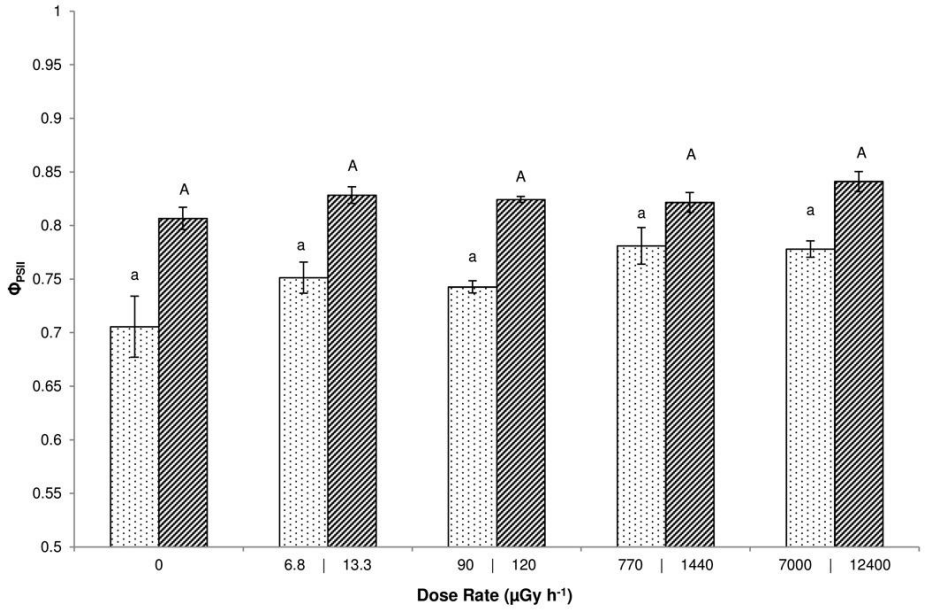

Figure 6.3: ΦPSII in *Arabidopsis thaliana* shoots after 4 days (light bars) and 7 days (dark bars) of exposure to ^{90}Sr. Data are presented as mean ± SE (n>3) Differences in lower case letters between treatments reflect significant differences between dose rates at 4 days ($p<0.05$). Differences in capital letters between dose rates reflect significant differences at 7 days ($p<0.05$).

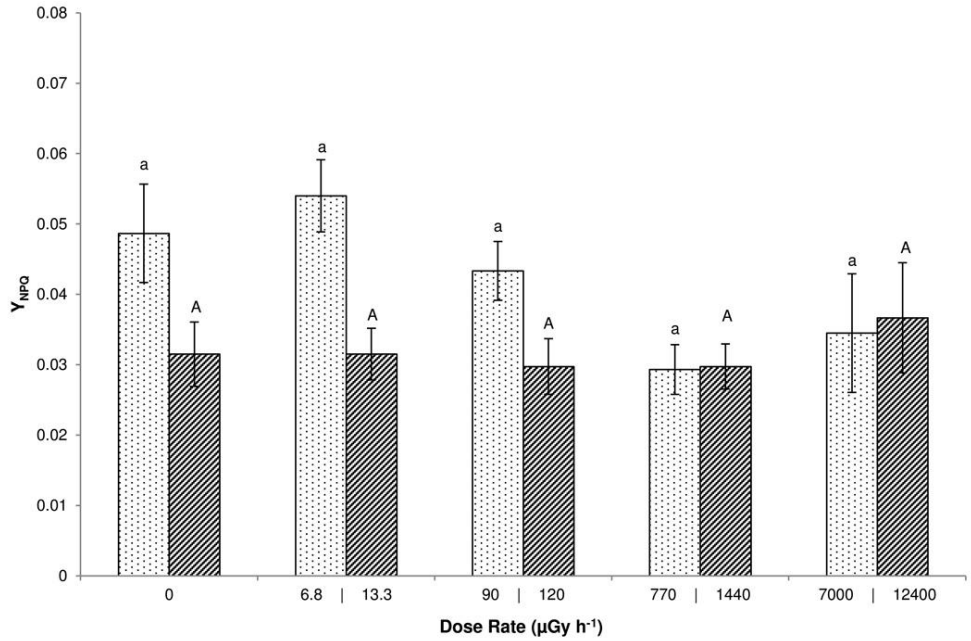

Figure 6.4: Y_{NPQ} in *Arabidopsis thaliana* shoots after 4 days (light bars) and 7 days (dark bars) of exposure to ^{90}Sr. Data are presented as mean ± SE (n>3) Differences in lower case letters between treatments reflect significant differences between dose rates at 4 days ($p<0.05$). Differences in capital letters between dose rates reflect significant differences at 7 days ($p<0.05$).

6.3.7 Pigments

Pigment levels were measured by extraction with DMF after 7 days of exposure. Chlorophyll a, b and the carotenoids all show a very similar dose-dependent pattern in concentration (Table 6.7), reaching an approximately 12-14%

reduction in pigment concentration at 120 µGy h^{-1} and rising again towards control levels at higher dose rates.

To compare the dose-dependent pattern between pigments, we divided the concentrations of each pigment by the mean of their respective control treatment. This allowed us to compare the relative dose-dependent effects between pigments in a two-way ANOVA with pigment type and dose rate as factors. The effect of pigment (ANOVA, $F_{2,44}$ = 1.038, p = 0.36) as well as the interaction effect (ANOVA, $F_{4,44}$= 0.905, p = 0.47) were not significant, indicating that the relative effects of dose rate on pigment concentration did not differ between pigment types. The effect of dose-rate, however, was highly significant (ANOVA, $F_{4,44}$ = 6.43, p = 0.003). Pair-wise comparison with the Tukey method showed that the effects on pigment concentration were significant at 13.3 µGy h^{-1} (p = 0.04), 120 (p = 0.001) and 1440 µGy h^{-1} (p = 0.03), but not at 12400 µGy h^{-1} (p = 0.23).

The chlorophyll a to b ratio and the ratio of chlorophyll to the carotenoids both increased (Table 6.7) with increasing dose rate, though neither of these trends was significant (one-way ANOVA, $F_{4,12}$ = 1.903 p = 0.17 for the chlorophyll a/b ratio; $F_{4,12}$ = 1.875 p = 0.18 for the chlorophylls to carotenoid ratio).

Table 6.7: Pigment concentrations and ratios at 7 days of exposure to ^{90}Sr. Values are the mean ± S.E. of at least 3 biological replicates. For statistical analysis, see text (section 3.7)

Dose rate [µGy h^{-1}]	**Chl a**	**Chl b** [µg g FW^{-1}]	**Carotenoids**
0	0.993 ± 0.011	0.324 ± 0.007	0.244 ± 0.005
13.3	0.925 ± 0.007	0.294 ± 0.005	0.2235 ± 0.0025
120	0.88 ± 0.05	0.279 ± 0.018	0.212 ± 0.012
1440	0.944 ± 0.029	0.292 ± 0.007	0.222 ± 0.006
12400	0.96 ± 0.04	0.303 ± 0.009	0.225 ± 0.007

Dose rate [µGy h^{-1}]	**Ratio a/b**	**Ratio (a+b)/carotenoids**
0	3.06 ± 0.05	5.41 ± 0.04
13.3	3.144 ± 0.025	5.455 ± 0.008
120	3.16 ± 0.05	5.48 ± 0.05
1440	3.23 ± 0.04	5.56 ± 0.06
12400	3.16 ± 0.04	5.6 ± 0.08

6.3.8 DNA Damage

6.3.8.1 Base modification

At 4 days of exposure, concentrations of the modified base 8-OHdG in the shoots increased linear with increasing dose rate (Figure 6.4), with a significant increase compared to control at 7000 µGy h^{-1}. At 7 days of exposure, a significant peak concentration of modified base levels was observed at 1440 µGy h^{-1}, declining again at the highest dose rate of 12,400 µGy h^{-1}.

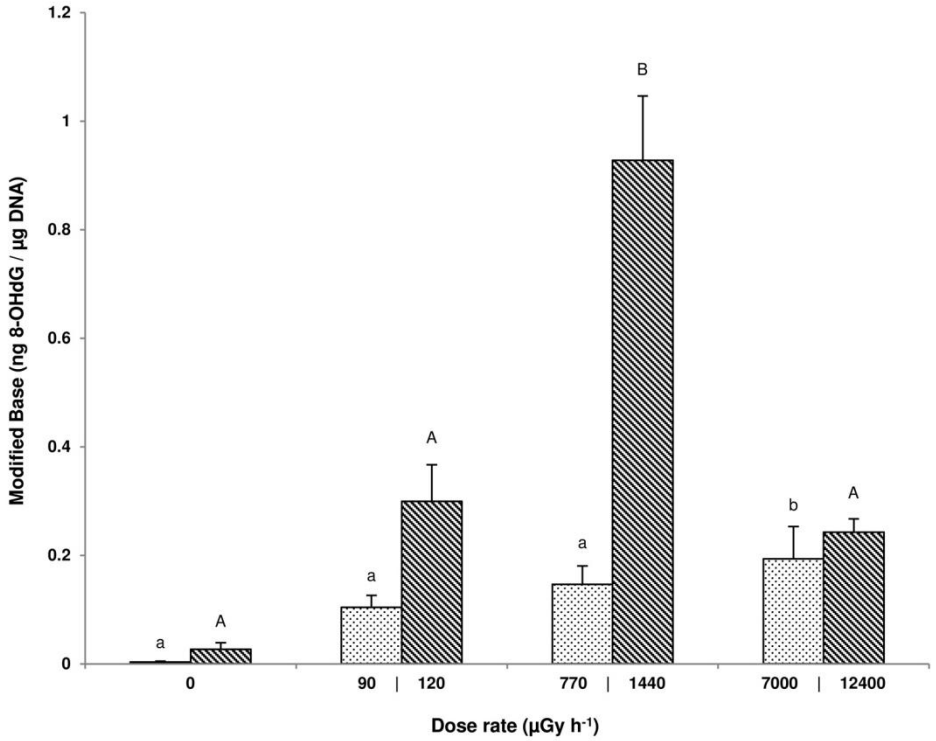

Figure 6.4: Concentration of modified base in leaves of *Arabidopsis thaliana* exposed for 4 days (light bars) and 7 days (dark bars) to ^{90}Sr. All values are the mean of at least 3 biological replicates. Differences in lower case letters reflect significant differences between treatments at day 4 ($p<0.05$). Differences in capital letters reflect significant differences between treatments at day 7 ($p<0.05$).

6.3.8.2 Gene expression

To analyse at the response on a molecular level, we measured transcript levels of proteins involved in DNA repair and the cell cycle by realtime-PCR. Gene expression, normalised to household genes and presented relative to the expression of the control treatment at 4 days, is presented for shoots (Table 6.8) and roots (Table 6.9).

In the shoots (Table 6.8), the expression levels of genes involved in the NHEJ repair pathway were significantly altered for *KU80* after 4 days at 7000 µG h^{-1} but not at 7 days. After 7 days of ^{90}Sr exposure, the expression levels of *LIG4* (DNA ligase IV) were significantly up-regulated compared to control at 1440 µGy h^{-1}. Both genes involved in the HR repair pathway (*RAD51* and *DMC1*) showed a shoot expression pattern at 7 days similar to that of *LIG4*, with significant increase in transcripts at 1440 µGy h^{-1} and a decline at higher dose rates (Table 6.8). The shoot transcript levels of genes involved in single-strand break repair (*PARP1* and *PARP2*) or organelle DNA repair (*POLG1*) were not significantly altered by exposure to ionising radiation at either time point. Nor were those of LPP1, a protein involved in lipid signalling control and of *GAR1*, involved in blocking mitosis upon irradiation. Only *CKS1*, a cell cycle regulator, was significantly up-regulated after 4 days, at 1440 and 12400 µGy h^{-1}.

In the roots (Table 6.9), *LIG4* was significantly down-regulated starting at 1.8 µGy h^{-1} at 4 days, while its expression levels were increased compared to control at 7 days for 28 to 228 µGy h^{-1}. The expression of Polymerase gamma I (*POLG1*) followed a similar pattern. Except for down-regulation of *RAD51* between 0.2 and 1.7 µGy h^{-1} at 7 days, no other alterations were observed on HR genes (Table 6.9). Transcript levels for PARP1, which detects single-stranded DNA breaks, were down-regulated at 4 days for all treatments. For PARP2, involved in DNA damage signalling, a similar decrease in transcripts was observed, though only significant at 190 µGy h^{-1}. After 7 days of exposure, PARP1 expression did not deviate from the control levels, while *PARP2* was up-regulated at nearly all dose rates. LPP1 only showed down-regulated transcript levels at 1.7 µGy h^{-1} at 7 days, while GAR1 transcript levels were down-regulated for all dose-rates at 7 days.

6.3.9 Anti-oxidative response

6.3.9.1 Antioxidant Metabolites

To measure the state of the ascorbate-glutathione scavenging pathway at the end of the exposure in the leaves, we measured the oxidised and reduced forms of the metabolites glutathione and ascorbate in a spectrophotometric assay on shoot samples harvested after 7 days. From these measurements, the reduction state of each metabolite could also be derived. Because root material was limited and exposed to much lower dose rates, antioxidant metabolites were not measured in the roots.

Total glutathione levels in the shoots (GSH + GSSG) were significantly higher than those in the control treatment in shoots exposed to 12400 µGy h^{-1}, indicating an increased biosynthesis of glutathione (Figure 6.5A; left). At this dose rate, we also observed a significant increase in the levels of the oxidised form GSSG, and an significant decrease in the reduced glutathione percentage present in the tissue by 2% (Figure 6.5A). At 120 µGy h^{-1}, there was a small but significant reduction in GSSG.

Total ascorbate levels in the shoots (AsA + DHA) did not show dose rate-dependent differences (Figure 6.5B; left). However, we observed a gradual increase in DHA, which was significant at 1440 and 12400 µGy h^{-1}. The increase in DHA at steady total levels created a significant decrease in reduction status to 53% at 12400 µGy h^{-1} (Figure 6.5B).

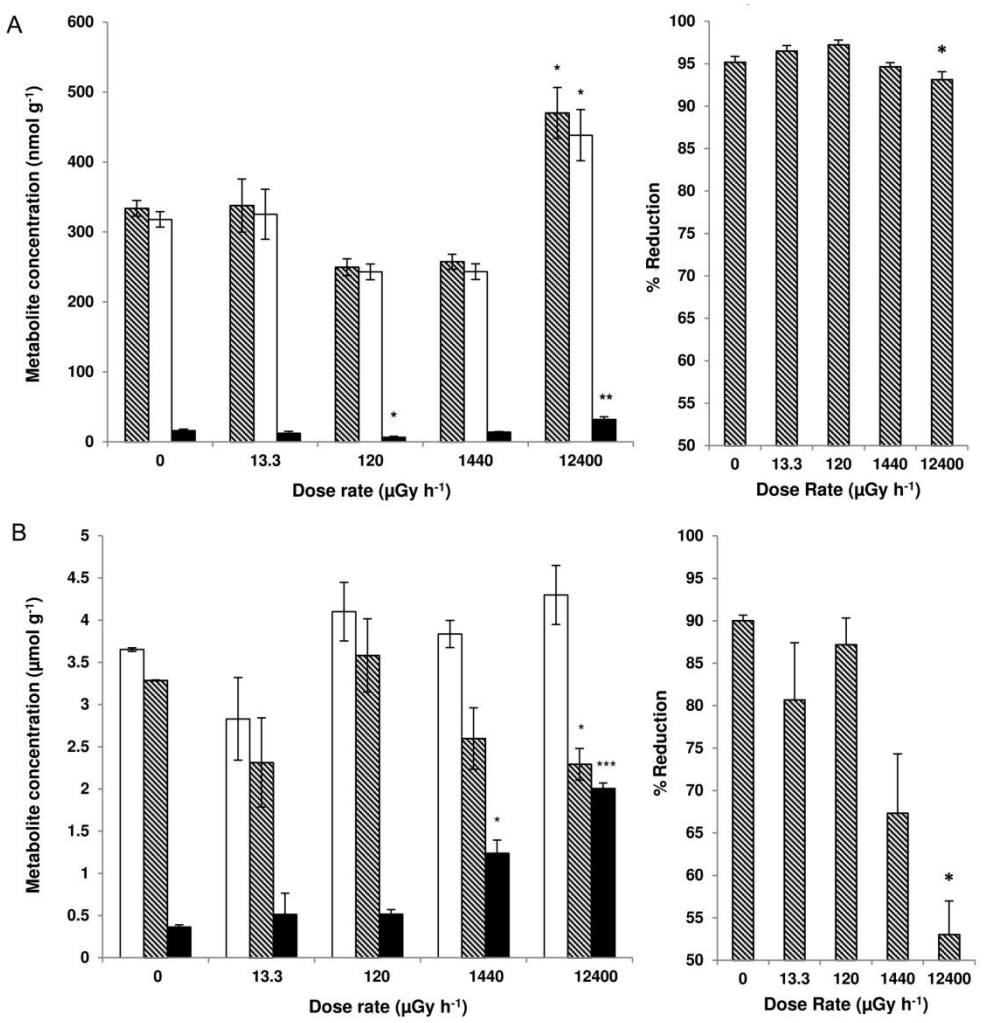

Figure 6.5: Antioxidant metabolite concentrations in *Arabidopsis* shoots exposed to ^{90}Sr for 7 days. **A.** Concentrations of total glutathione (GSH + GSSG; grey bars), GSH (white bars) , GSSG (black bars) and the degree of reduction (right graph). **B.** concentrations of total ascrobate (AsA + DHA; white bars), reduced ascorbate (grey bars), dehyroascorbate (DHA; black bars) and the reduction status (right graph). Significance levels are * $p<0.05$, ** $p<0.01$. Values are mean and SE of at least 3 biological replicates.

6.3.9.2 Gene expression

The anti-oxidative response was further analysed at a transcript level by measuring gene expression of ROS producing enzymes such as NADPH oxidases (*RBOHA/C/E*) and lipoxygenases (*LOX1/2*), as well as enzymes involved in the ascorbate-glutathione scavenging pathway (glutathione reductase *GR1*; ascorbate peroxidase *APX1*) and multiple isoforms of CuZnSODs (CSD1/2/3), FeSODs (FSD1/2/3) and catalases (CAT1/2/3). Gene expression is presented for shoots (table 6.10) and roots (Table 6.11).

In the shoots (Table 6.10) we observed no alterations in the transcript levels of the ROS producing NADPH oxidases (*RBOHA/C/E*). The expression levels of *LOX2* had strongly increased after 4 days of ^{90}Sr exposure, at 770 and 7000 µGy h^{-1}. The cytosolic (*CSD1*) and plastidic (*CSD2*) isoforms of CuZnSODs were both up-regulated at 7000 µGy h^{-1} at 4 days and at 1440 µGy h^{-1} after 7 days though not at higher dose rates. However, transcript levels of the peroxisomal isoform (*CSD3*) were not altered (Table 6.10). The plastidic FeSOD (*FSD1*) was significantly down-regulated at 4 days at 90 µGy h^{-1} and higher dose rates but remained at control levels at 7 days of exposure. The expression levels of the other FeSOD isoforms remained unaltered upon exposure. No significant dose-dependent differences in expression were observed for any of the hydrogen peroxidase scavenging catalases (*CAT1/2/3*) or for *APX1*. Glutathione reductase (GR1) was significantly up-regulated after 4 days at 90, 770 and 7000 µGy h^{-1}, though remained unaltered at all dose rates after 7 days (Table 6.10).

In the roots (Table 6.11), expression levels of all three analysed NADPH oxidases were altered by exposure to ^{90}Sr, though the alterations depended on the isozyme and the time point. *RBOHA*, *RBOHC* and *RBOHE* were all strongly down-regulated at 4 days compared to control, starting at 1.8 µGy h^{-1}. After 7 days of exposure, *RBOHA* returned to control levels, while *RBOHC* transcripts at 21 and 228 µGy h^{-1} were 4- and 7-fold those of the control respectively. CuZnSOD transcription was altered in all isoforms, though not all to the same extent. At 4 days, *CSD1* and *CSD3* expression remained constant, while *CSD2*

expression was significantly reduced at dose rates above 1.8 µGy h^{-1}. After 7 days, Both *CSD1* and *CSD2* were up-regulated 2- to 3-fold at 21 and 228 µGy h^{-1} (Table 6.11), but *CSD3* transcript levels remained stable except for down-regulation at the lowest dose rate (0.2 µGy h^{-1}). Overall, FeSOD expression was found to be down-regulated at all time points and dose rates, except for *FSD3*, which remained at control levels for all dose rates at 7 days. Catalase expression remained generally unaltered, except for *CAT3*, which was only up-regulated after 7 days at 21 and 228 µGy h^{-1}. A pattern identical to that of *CAT3* was observed for *GR1* (Table 6.11), while APX1 transcript levels remained unchanged.

[Bq L^{-1}]		**0**	**250**	**2500**	**25 000**	**250 000**
	4 d	*0 µGy h^{-1}*	*6.8 µGy h^{-1}*	*90 µGy h^{-1}*	*770 µGy h^{-1}*	*7000 µGy h^{-1}*
	7 d	*0 µGy h^{-1}*	*13.3 µGy h^{-1}*	*120 µGy h^{-1}*	*1440 µGy h^{-1}*	*12400 µGy h^{-1}*
KU80	*4 d*	1.00 ± 0.24	3.29 ± 1.42	2.38 ± 0.75	3.69 ± 1.41	4.61 ± 1.46
	7 d	2.83 ± 0.72	3.22 ± 0.48	4.01 ± 1.00	4.63 ± 0.11	3.86 ± 0.21
LIG4	*4 d*	1.00 ± 0.62	1.43 ± 0.71	0.17 ± 0.06	0.69 ± 0.21	1.02 ± 0.18
	7 d	0.59 ± 0.23	0.62 ± 0.10	1.01 ± 0.15	3.69 ± 0.17	2.66 ± 0.27
RAD51	*4 d*	1.00 ± 0.33	0.82 ± 0.21	0.38 ± 0.20	0.63 ± 0.45	0.39 ± 0.01
	7 d	1.17 ± 0.34	0.46 ± 0.09	0.85 ± 0.14	1.91 ± 0.07	0.82 ± 0.05
DMC1	*4 d*	1.00 ± 0.46	0.90 ± 0.41	0.24 ± 0.11	0.24 ± 0.20	0.24 ± 0.04
	7 d	0.46 ± 0.06	0.52 ± 0.17	1.04 ± 0.43	2.17 ± 0.83	0.99 ± 0.23
PARP1	*4 d*	1.00 ± 0.47	0.58 ± 0.24	0.30 ± 0.11	0.81 ± 0.43	0.67 ± 0.07
	7 d	1.10 ± 0.07	0.54 ± 0.09	1.05 ± 0.29	1.00 ± 0.04	0.73 ± 0.09
PARP2	*4 d*	1.00 ± 0.26	1.18 ± 0.22	1.09 ± 0.19	1.54 ± 0.39	1.75 ± 0.35
	7 d	2.23 ± 1.30	0.63 ± 0.04	1.49 ± 0.27	1.70 ± 0.37	1.00 ± 0.16
LPP1	*4 d*	1.00 ± 0.31	1.23 ± 0.24	0.75 ± 0.13	0.70 ± 0.18	1.22 ± 0.16
	7 d	0.99 ± 0.33	0.86 ± 0.16	2.10 ± 0.65	1.62 ± 0.18	0.93 ± 0.11
POLG1	*4 d*	1.00 ± 0.43	1.13 ± 0.22	0.33 ± 0.11	0.39 ± 0.12	0.59 ± 0.08
	7 d	0.39 ± 0.17	0.32 ± 0.07	0.86 ± 0.16	1.14 ± 0.28	0.59 ± 0.09
CKS1	*4 d*	1.00 ± 0.46	0.87 ± 0.16	0.47 ± 0.19	0.35 ± 0.08	0.52 ± 0.06
	7 d	0.44 ± 0.14	0.34 ± 0.06	0.63 ± 0.10	1.53 ± 0.46	1.36 ± 0.10
GAR1	*4 d*	1.00 ± 0.15	1.40 ± 0.48	2.08 ± 0.45	2.24 ± 0.59	1.19 ± 0.25
	7 d	1.73 ± 0.91	1.97 ± 1.30	2.22 ± 0.93	4.77 ± 3.15	1.24 ± 0.18

Table 6.8: Gene expression of genes involved in DNA repair and the cell cycle in the shoots of *Arabidopsis thaliana* after exposure to ^{90}Sr for 4 and 7 days. Data are presented relative to 0 Bq L^{-1}. Dark grey shading indicate significant up-regulation ($p<0.05$) compared to the control at that time point. Light grey shading indicates significant down-regulation ($p<0.05$).

	[Bq L^{-1}]	**0**	**250**	**2500**	**25 000**	**250 000**
	4 d	*0 µGy h^{-1}*	*0.21 µGy h^{-1}*	*1.8 µGy h^{-1}*	*18 µGy h^{-1}*	*190 µGy h^{-1}*
	7 d	*0 µGy h^{-1}*	*0.23 µGy h^{-1}*	*1.7 µGy h^{-1}*	*21 µGy h^{-1}*	*228 µGy h^{-1}*
KU80	*4 d*	1.00 ± 0.56	0.02 ± 0.01	1.58 ± 0.27	1.45 ± 0.36	0.75 ± 0.22
	7 d	1.22 ± 0.34	1.22 ± 0.35	0.60 ± 0.11	1.73 ± 0.10	1.67 ± 0.02
LIG4	*4 d*	1.00 ± 0.24	0.89 ± 0.1	0.18 ± 0.04	0.09 ± 0.03	0.25 ± 0.09
	7 d	0.19 ± 0.04	0.38 ± 0.1	0.21 ± 0.06	0.7 ± 0.1	0.60 ± 0.04
RAD51	*4 d*	1.00 ± 0.02	1.29 ± 0.37	0.19 ± 0.05	0.32 ± 0.07	1.64 ± 0.24
	7 d	1.68 ± 0.57	0.31 ± 0.05	0.37 ± 0.06	1.31 ± 0.19	1.5 ± 0.12
DMC1	*4 d*	1.00 ± 0.58	1.27 ± 0.33	0.06 ± 0.01	0.17 ± 0.05	0.13 ± 0.06
	7 d	0.15 ± 0.07	0.07 ± 0.03	0.08 ± 0.02	0.13 ± 0.01	0.11 ± 0.01
PARP1	*4 d*	1.00 ± 0.11	0.01 ± 0.01	0.25 ± 0.07	0.21 ± 0.07	0.29 ± 0.1
	7 d	0.25 ± 0.07	0.15 ± 0.04	0.13 ± 0.02	0.37 ± 0.02	0.36 ± 0.04
PARP2	*4 d*	1.00 ± 0.33	0.81 ± 0.07	0.53 ± 0.06	0.54 ± 0.08	0.29 ± 0.07
	7 d	0.26 ± 0.05	0.52 ± 0.04	0.26 ± 0.04	0.70 ± 0.07	0.63 ± 0.06
LPP1	*4 d*	1.00 ± 0.52	0.73 ± 0.20	0.52 ± 0.06	0.47 ± 0.06	0.3 ± 0.07
	7 d	0.45 ± 0.08	0.38 ± 0.06	0.2 ± 0.04	0.48 ± 0.03	0.47 ± 0.04
POLG1	*4 d*	1.00 ± 0.32	0.74 ± 0.1	0.12 ± 0.04	0.2 ± 0.07	0.21 ± 0.08
	7 d	0.29 ± 0.08	0.31 ± 0	0.25 ± 0.02	0.57 ± 0.05	0.58 ± 0.05
CKS1	*4 d*	1.00 ± 0.91	0.86 ± 0.41	0.38 ± 0.26	0.07 ± 0.05	0.35 ± 0.12
	7 d	0.33 ± 0.07	1.22 ± 0.73	0.49 ± 0.18	0.56 ± 0.1	0.58 ± 0.04
GAR1z	*4 d*	1.00 ± 0.4	0.84 ± 0.08	0.5 ± 0.12	0.68 ± 0.12	0.35 ± 0.03
	7 d	0.39 ± 0.02	0.15 ± 0.06	0.10 ± 0.10	0.17 ± 0.02	0.15 ± 0.01

Table 6.9: Gene expression of genes involved in DNA repair and the cell cycle in the roots of *Arabidopsis thaliana* after exposure to ^{90}Sr for 4 and 7 days. Data are presented relative to 0 Bq L^{-1}. Dark grey shading indicate significant up-regulation ($p<0.05$) compared to the control at that time point. Light grey shading indicates significant down-regulation ($p<0.05$).

[Bq L^{-1}]		**0**	**250**	**2500**	**25 000**	**250 000**
	4 d	*0 µGy h^{-1}*	*6.8 µGy h^{-1}*	*90 µGy h^{-1}*	*770 µGy h^{-1}*	*7000 µGy h^{-1}*
	7 d	*0 µGy h^{-1}*	*13.3 µGy h^{-1}*	*120 µGy h^{-1}*	*1440 µGy h^{-1}*	*12400 µGy h^{-1}*
RBOHA	*4 d*	1,00 ± 0.18	1.74 ± 1.15	2.97 ± 1.58	0.58 ± 0.31	0.22 ± 0.20
	7 d	0.76 ± 0.60	0.33 ± 0.26	0.50 ± 0.07	0.24 ± 0.21	0.03 ± 0.02
RBOHC	*4 d*	1.00 ± 0.76	0.22 ± 0.14	0.91 ± 0.02	2.73 ± 1.95	1.78 ± 0.98
	7 d	4.19 ± 2.95	1.5 ± 0.30	1.44 ± 0.68	6.51 ± 2.84	1.92 ± 0.32
RBOHE	*4 d*	1.00 ± 0.76	0.22 ± 0.14	0.91 ± 0.02	2.73 ± 1.95	1.78 ± 0.98
	7 d	4.19 ± 2.95	1.5 ± 0.30	1.44 ± 0.68	6.51 ± 2.84	1.92 ± 0.32
LOX2	*4 d*	1.00 ± 0.83	0.03 ± 0.03	2.41 ± 1.00	67.2 ± 24.5	38.7 ± 27.1
	7 d	38.6 ± 36.1	16.4 ± 10.8	28.4 ± 20.8	14.1 ± 5.75	5.54 ± 0.70
CSD1	*4 d*	1.00 ± 0.29	2.06 ± 0.38	1.53 ± 0.38	0.98 ± 0.28	3.73 ± 1.55
	7 d	2.95 ± 0.16	3.46 ± 0.22	2.87 ± 0.62	9.53 ± 2.26	5.57 ± 1.11
CSD2	*4 d*	1.00 ± 0.25	1.78 ± 0.29	2.04 ± 0.53	0.81 ± 0.26	5.46 ± 0.99
	7 d	2.12 ± 0.47	5.17 ± 0.97	2.91 ± 0.60	8.19 ± 0.83	4.72 ± 0.75
CSD3	*4 d*	1.00 ± 0.42	1.29 ± 0.4	5.71 ± 2.78	3.02 ± 1.80	2.69 ± 0.24
	7 d	1.08 ± 0.43	2.00 ± 1.21	3.53 ± 2.33	1.56 ± 0.32	0.54 ± 0.27
FSD1	*4 d*	1.00 ± 0.11	0.79 ± 0.16	0.40 ± 0.10	0.49 ± 0.04	0.37 ± 0.05
	7 d	0.65 ± 0.17	0.16 ± 0.04	0.36 ± 0.18	0.60 ± 0.24	1.09 ± 0.06
FSD2	*4 d*	1.00 ± 0.35	0.54 ± 0.21	0.22 ± 0.08	0.25 ± 0.07	0.62 ± 0.09
	7 d	1.12 ± 0.45	0.41 ± 0.10	0.48 ± 0.16	0.43 ± 0.08	0.72 ± 0.14
FSD3	*4 d*	1.00 ± 0.29	1.47 ± 0.53	0.27 ± 0.02	0.47 ± 0.28	0.51 ± 0.19
	7 d	1.31 ± 0.16	0.17 ± 0.04	0.25 ± 0.06	1.42 ± 1.20	0.5 ± 0.19
CAT1	*4 d*	1.00 ± 7.40	25.00 ± 4.32	17.0 ± 4.54	27.3 ± 4.55	25.5 ± 3.5
	7 d	26.8 ± 9.67	17.9 ± 10.1	35.8 ± 11.6	41.7 ± 25.7	23.7 ± 1.9
CAT2	*4 d*	1.00 ± 39.8	48.8 ± 6.66	14.0 ± 5.3	13.3 ± 0.88	11.2 ± 1.34
	7 d	31.9 ± 13.0	34.6 ± 7.44	37.38 ± 7.41	71.6 ± 33.1	22.7 ± 4.52
CAT3	*4 d*	1.00 ± 2.64	39.6 ± 21.0	67.0 ± 4.91	71.4 ± 53.3	20.9 ± 6.40
	7 d	16.8 ± 0.66	14.74 ± 5.13	27.8 ± 13.6	29.5 ± 8.6	12.8 ± 6.11
GR1	*4 d*	1.00 ± 0.34	0.81 ± 0.44	0.11 ± 0.05	0.08 ± 0.02	0.06 ± 0.02
	7 d	0.14 ± 0.05	0.19 ± 0.06	0.30 ± 0.12	0.97 ± 0.68	0.60 ± 0.50
APX1	*4 d*	1.00 ± 0.61	1.41 ± 0.59	0.54 ± 0.18	0.72 ± 0.12	0.37 ± 0.01
	7 d	1.10 ± 0.26	1.16 ± 0.38	0.84 ± 0.08	0.68 ± 0.68	1.38 ± 0.15

Table 6.10: Gene expression of genes involved in oxidative stress in the shoots of *Arabidopsis thaliana* after exposure to ^{90}Sr for 4 and 7 days. Data are presented relative to 0 Bq L^{-1}. Dark grey shading indicate significant up-regulation ($p<0.05$) compared to the control at that time point. Light grey shading indicates significant down-regulation ($p<0.05$).

[Bq L^{-1}]		**0**	**250**	**2500**	**25 000**	**250 000**
	4 d	*0 µGy h^{-1}*	*0.21 µGy h^{-1}*	*1.8 µGy h^{-1}*	*18 µGy h^{-1}*	*190 µGy h^{-1}*
	7 d	*0 µGy h^{-1}*	*0.23 µGy h^{-1}*	*1.7 µGy h^{-1}*	*21 µGy h^{-1}*	*228 µGy h^{-1}*
RBOHA	*4 d*	1.00 ± 0.26	0.62 ± 0.23	0.15 ± 0.02	0.23 ± 0.05	0.11 ± 0.03
	7 d	0.24 ± 0.07	0.44 ± 0.10	0.47 ± 0.08	0.37 ± 0.09	0.38 ± 0.05
RBOHC	*4 d*	1.00 ± 0.29	0.85 ± 0.15	0.24 ± 0.02	0.31 ± 0.07	0.21 ± 0.06
	7 d	0.43 ± 0.10	0.64 ± 0.14	0.25 ± 0.06	1.92 ± 0.01	3.01 ± 0.10
RBOHE	*4 d*	1.00 ± 0.01	0.69 ± 0.23	0.15 ± 0.03	0.17 ± 0.05	0.37 ± 0.14
	7 d	0.55 ± 0.13	0.18 ± 0.07	0.10 ± 0.02	0.42 ± 0.06	0.30 ± 0.04
LOX2	*4 d*	1.00 ± 0.16	1.48 ± 0.38	0.12 ± 0.02	0.32 ± 0.14	0.24 ± 0.11
	7 d	1.29 ± 0.50	0.24 ± 0.04	0.20 ± 0.04	0.78 ± 0.05	0.82 ± 0.12
CSD1	*4 d*	1.00 ± 0.28	0.95 ± 0.09	0.89 ± 0.11	0.84 ± 0.12	0.44 ± 0.01
	7 d	0.45 ± 0.05	0.95 ± 0.24	0.69 ± 0.13	1.16 ± 0.12	1.25 ± 0.07
CSD2	*4 d*	1.00 ± 0.17	0.78 ± 0.10	0.40 ± 0.05	0.43 ± 0.07	0.34 ± 0.08
	7 d	0.46 ± 0.05	0.55 ± 0.17	0.40 ± 0.06	0.79 ± 0.01	1.76 ± 0.01
CSD3	*4 d*	1.00 ± 0.34	0.67 ± 0.04	0.81 ± 0.15	0.91 ± 0.22	0.43 ± 0.10
	7 d	0.56 ± 0.03	0.21 ± 0.02	0.54 ± 0.13	0.24 ± 0.04	0.33 ± 0.07
FSD1	*4 d*	1.00 ± 0.33	0.26 ± 0.05	0.12 ± 0.01	0.20 ± 0.05	0.03 ± 0.01
	7 d	0.20 ± 0.02	0.03 ± 0.01	0.09 ± 0.01	0.10 ± 0.02	0.12 ± 0.03
FSD2	*4 d*	1.00 ± 0.13	0.34 ± 0.07	0.18 ± 0.01	0.28 ± 0.01	0.13 ± 0.03
	7 d	0.18 ± 0.02	0.09 ± 0.01	0.13 ± 0.03	0.06 ± 0.01	0.04 ± 0.01
FSD3	*4 d*	1.00 ± 0.02	0.57 ± 0.22	0.11 ± 0.02	0.21 ± 0.05	0.12 ± 0.06
	7 d	0.12 ± 0.04	0.06 ± 0.02	0.12 ± 0.01	0.10 ± 0.02	0.12 ± 0.02
CAT1	*4 d*	1.00 ± 0.45	1.20 ± 0.27	0.32 ± 0.07	0.28 ± 0.09	0.20 ± 0.08
	7 d	0.15 ± 0.04	0.18 ± 0.04	0.29 ± 0.06	0.21 ± 0.02	0.35 ± 0.09
CAT2	*4 d*	1.00 ± 0.50	0.85 ± 0.10	0.20 ± 0.02	0.23 ± 0.07	0.20 ± 0.20
	7 d	0.35 ± 0.04	0.36 ± 0.01	0.25 ± 0.05	0.36 ± 0.06	0.56 ± 0.13
CAT3	*4 d*	1.00 ± 0.42	1.28 ± 0.11	0.19 ± 0.02	0.32 ± 0.09	0.42 ± 0.14
	7 d	1.11 ± 0.12	0.13 ± 0.02	0.26 ± 0.07	0.89 ± 0.25	0.73 ± 0.18
GR1	*4 d*	1.00 ± 0.73	1.15 ± 0.29	0.18 ± 0.02	0.23 ± 0.10	0.14 ± 0.06
	7 d	0.16 ± 0.06	0.37 ± 0.20	0.17 ± 0.02	0.39 ± 0.05	0.48 ± 0.12
APX1	*4 d*	1.00 ± 0.34	0.59 ± 0.13	0.35 ± 0.04	0.71 ± 0.23	1.50 ± 0.42
	7 d	1.12 ± 0.23	0.44 ± 0.08	0.26 ± 0.06	2.40 ± 0.06	1.18 ± 0.08

Table 6.11: Gene expression of genes involved in oxidative stress in the roots of *Arabidopsis thaliana* after exposure to ^{90}Sr for 4 and 7 days. Data are presented relative to 0 Bq L^{-1}. Dark grey shading indicate significant up-regulation ($p<0.05$) compared to the control at that time point. Light grey shading indicates significant down-regulation ($p<0.05$).

6.4 Discussion

In this study, we aimed to investigate the biological effects of β-radiation in *Arabidopsis thaliana* through chronic exposure to ^{90}Sr. Therefore we measured the effects of exposure on several morphological, physiological and molecular endpoints, with the aim to link the effects on growth and photosynthetic performance to the underlying molecular response.

Previous studies on a wide range of plant species have shown that strontium has a high mobility in plants. Rediske & Selders (1953) noted a higher transfer to the shoots compared to the roots in *Phaseolus vulgaris*, with nearly no redistribution within the leaves during exposure. They also noted that strontium concentrations in the organs remained proportional to the exposure concentration, even at high chemical concentrations. Several studies have since confirmed these observations for other plant species, both for soil and aquatic exposure conditions (Luksiene et al., 2013; Singh et al., 2008; Soudek et al.,2006; Wang et al., 1998), though Moyen & Roblin (2010) have noted that strontium accumulation seems to be biphasic in maize roots. Our data (Table 6.3 and 6.4), which show high strontium uptake and a high root-to-shoot transfer independent of the environmental activity concentration, agree with the previous observations and with our previous results on 18-day old seedlings (Chapter 3). Nevertheless, due to high individual variation in our data, it is not clear whether the transfer to the shoots changes during ^{90}Sr exposure. The distribution pattern we observed is very similar to that of calcium, which is known to accumulate in the leaves of seedlings (Ericsson, 1994), and also agrees well with that of calcium in *Arabidopsis thaliana* seedlings under identical growth and exposure conditions (Vanhoudt et al., 2011). Strontium and calcium are closely resembling alkaline earth metals and therefore are known to behave in a nearly identical way (Muyttenaere & Masset, 1971; Queen et al., 1963; Von Fircks et al., 2002). However, at least one study has shown that some accessions of *Arabidopsis thaliana* can discriminate between Ca^{2+} and Sr^{2+}, but only at very

low total concentrations of bivalent cations (Kanter et al., 2010). Calcium is transported within the plant by symplastic and apoplastic routes (White, 2001), which might give an indication of the transport routes accessible to ^{90}Sr. Several authors have indeed shown that strontium crosses the Casparian band through the symplast, and then travels primarily to the apoplast of the vascular bundles in the shoots (Coughtrey & Thorne, 1983; Seregin & Kozhevnikova, 2004).

Despite the high dose rates (Table 6.5), there was a notable absence of effects on shoot biomass (Table 6.6) or conclusive effects on photosynthesis. At 4 days of exposure there seemed to be a trend of increasing photosynthetic performance with increasing dose rate, (Figure 6.3) mostly due to a reduction of non-photochemical quenching (Figure 6.4), but these trends have disappeared at day 7. These results are comparable to those of an identical exposure experiment on older (and less sensitive) seedlings of *Arabidopsis thaliana* (Chapter 3). However, while there were no apparent effects on biomass, the observed increase in leaf area is remarkable (Figure 6.1) as we previously observed no such effect at even higher dose rates (100 mGy h^{-1}) of external γ-radiation (Chapter 5). Leaf expansion is a complex process, which ultimately depends on the temporary asymmetric loosening of the cell wall and action of turgor pressure. It is modulated by hormonal action and can be impaired during abiotic stress (Volkenburgh, 1999). Furthermore, it has been shown that the plant cell wall is weakened after treatment with high acute doses of UV or γ-radiation by modification of the pectin crosslink fraction (Kovacs & Keresztes, 2002). While we have at present no evidence for such a mechanism in our study, the preferential presence of ^{90}Sr in the apoplast might provide a clue towards a passive (interference of ionising radiation or ROS with cell expansion) or active mechanism (by hormonal or signalling action) for leaf expansion under ^{90}Sr exposure.

In general, very few effects were found at the transcriptional level in the leaves. The shoot response at 4 days seemed to be confined to the 7000 µGy h^{-1} dose rate, with up-regulation of *KU80* (Table 6.8), part of a heterodimer protein

kinase (Ku70-Ku80) which binds the loose ends of double-strand breaks, and recruits proteins involved in the NHEJ pathway (Waterworth et al., 2011; West et al., 2004). A similar up-regulation was observed for the CuZnSOD isoforms CSD1 and CSD2 (Table 6.10), which transform superoxide ($O2^{\bullet -}$) to hydrogen peroxide (H_2O_2) in the cytoplasmatic and plastidic compartments, respectively (Mittler et al., 2004). At 7 days, most effects are seen at a lower dose rate namely 1440 µGy h^{-1}, where the transcription of *CSD1* and *CSD2* as well as that of genes involved in both NHEJ (*LIG4*) and HR double-strand break repair (*RAD51/DMC1*) pathways reached a peak. Though this peak is absent in our data at 4 days, it can be expected that it occurs at higher dose rates, and shifts towards lower dose rates with exposure duration. These data confirm earlier observations that both DSB repair pathways work simultaneously (Britt, 1999; Waterworth et al., 2011) and more specifically under ionising radiation (Kovalchuk et al., 2000). Interestingly, 7 days at 12,400 µGy h^{-1} the gene expression had declined again to control transcript levels for all up-regulated genes. This seems to suggest that in the shoots the timing of a (transient) response to ionising radiation at the expression level is dependent on the dose rate, with an earlier response at higher dose rates.

At the level of scavenging, there was a dose-dependent increase in oxidation at the end of the exposure for both ascorbate and glutathione (Figure 6.5A and B). For ascorbate, the shift towards DHA was very clear for 1440 and 12400 µGy h^{-1}, dose rates at which we also saw a clear response on the transcriptional level. As maintaining the AsA levels is needed for the efficient reduction of H_2O_2 (Blokhina et al., 2003), the shift towards ascorbate pool oxidation indicates that, despite the absence of effects on photosynthesis or biomass and upregulation of ROS scavenging, the plants have great difficulty in maintaining redox balance in the shoots. This is similar to the situation under metal stress (Drazkiewicz et al., 2003; Eline Saenen, personal communication) Previous authors have noted that plants compensate for ascorbate oxidation under stress by increasing the levels of GSH (Jozefczak et al., 2012; Noctor et al., 2002), thereby promoting the reconstruction of AsA by increased reduction of DHA. The increased levels of

GSH at 12400 µGy h^{-1} indeed point towards such a mechanism, though the redox state of the GSH/GSSG is also significantly reduced at that dose rate. The redox state of GSH is not only important in the ascorbate-glutathione pathway, but also has a signalling function towards ROS defense genes and systemic acquired resistance (Ball et al., 2003; Mou et al., 2003; Noctor et al., 2012). The down-regulation of GR1 (glutathione reductase), which catalyses the oxidation of GSSG to GSH, after 4 days of exposure (Table 6.10) might therefore also be of importance in a stress response, though metabolite measurements at earlier time points are needed to further investigate the role of the ascorbate-glutathione cycle in this respect. A final indication that an oxidative stress response occurs is the strong up-regulation of LOX2 (lipoxygenase) at 1440 and 12400 µGy h^{-1}, a protein involved in lipid peroxidase signalling during the oxidative burst (Porta & Rocha-Sosa, 2002). LOX signalling is involved in the oxidative response to abiotic stressors such as cadmium (Smeets et al., 2008).

A clue on how the shoots integrate the response to IR might lie in the measurements of oxidative DNA damage, measured as modified base 8-OHdG (Figure 6.4). At both harvesting days, there was a dose-dependent increase in damage. The rate of increase with increasing dose rate was higher at 7 days, but dropped sharply at 12,400 µGy h^{-1}. If we assume that under normal metabolic functioning DNA repair can keep up with the rate at which damage occurs, the amount of damage we observe must be the net result of damage by ROS and direct radiation damage on one hand, and ROS scavenging and DNA repair mechanisms on the other. DNA repair mechanisms were found to be up-regulated at 4 days and not at 7 days, which might suggest that early transient up-regulation ensures more efficient repair mechanisms in the longer term. At the level of ROS scavenging, the increased GSH concentration indeed points toward a regulation of the metabolite scavenging mechanism. Nevertheless, the increased oxidation of both ascorbate and glutathione pools in the shoots indicates that the plants pay a price for this balance in the available reductive capacity. We can also refute the hypothesis that the decrease in DNA damage

could be an effect of decreased ROS, as this would be reflected in an improvement in the antioxidant metabolite reduction state.

An alternative explanation to increased ROS scavenging or DNA repair for the decreased damage at 12,400 µGy h^{-1} in the shoots could be that, rather than a true decrease in total damage, it is a result of an increase in genetic material by a shift of the cell cycle towards endoreduplication, a mechanism which is known to occur under abiotic stress (Skirycz & Inzé, 2010). Cell cycle progression is heavily regulated, in particular the transition points from G1 to S-phase and from G2-phase to mitosis (De Veylder et al., 2007) Transition through these checkpoints can only occur if DNA repair is completed, thereby ensuring correct transmission of the genetic information to the two daughter cells. Progression is controlled by a large number of cyclin-dependent kinases (CDKs) and associated cyclins, and the modulation or inhibition thereof (De Veylder et al., 2001a). One of these modulators is CKS1, which is known to slow down cell cycle progression in *Arabidopsis thaliana* leaves when up-regulated (De Veylder et al., 2001b). The up-regulation of *CKS1* in the shoots after 7 days starting at 1440 µGy h^{-1} might be an indication that there is a response at the level of cell cycle control. DNA damage is signalled to the cell cycle by pathways downstream of the protein kinase ataxia telangiectasia mutated (ATM) (Culligan et al., 2006; Garcia et al., 2003) that is normally recruited by the complexes involved in DNA damage detection and repair. If endoreduplication indeed occurred, this would be able to explain the observed decreased levels of oxidative damage per µg of DNA (Figure 6.4). Although not done at present time, it should in principle be possible to test this hypothesis by flow cytometry analysis.

In the roots, the anti-oxidative response was repressed at 4 days, as most of the genes involved in ROS production or ROS scavenging were down-regulated at that time in nearly all treatments (Table 6.11). This is in striking contrast with the transcriptional response in the shoots. A similar observation can be made for DNA repair and the cell cycle, where transcript levels were significantly reduced in roots exposed to ^{90}Sr at 4 days compared to control. At 7 days, the pattern

was constrained mostly to the 25,000 and 250,000 Bq L^{-1} treatments (at 21 and 228 µGy h^{-1}) with up-regulation of LIG4, PARP2 and POLG1 transcripts (Table 6.9) except for GAR1, which was clearly down-regulated at all dose rates. GAR1 is known to be involved in the suppression of mitosis and promotion of the endocycle (Deveaux et al., 2000). Combined with increased repair by the NHEJ pathway (*LIG4*), its down-regulation might show a priority for fast, inaccurate DNA repair rather than growth reduction by cell cycle stalling. *PARP2* codes for a poly(ADP-ribose) polymerase which has previously been shown to accumulate under ionising radiation induced DNA damage (Doucet-Chabeaud et al., 2001) with a putative function in oxidative stress signalling. However *PARP1*, which normally has a similar expression pattern, was not up-regulated under our exposure conditions, which indicates that PARP2 has a role here as a signalling protein. POLG1 (Polymerase Gamma 1) is involved in organelle strand break repair, indicating that oxidative damage in mitochondria likely occurs under ^{90}Sr exposure. As in the shoots, *CSD1* and *CSD2* up-regulation in the roots indicates the involvement of superoxide in the oxidative response (Table 6.11). Contrary to the shoots however, there is clear involvement of GR1 and APX1 (ascorbate peroxidase) up-regulation to maintain the ascorbate-glutathione scavenging pathway at these dose rates. The involvement of the superoxide generating enzyme NADPH-oxidase (located in the plasma membrane) points towards a role for oxidative burst in the response to ionising radiation. The reversal from general response suppression at 4 days to more refined up-regulation of genes at 7 days echoes the observations on morphology and might explain the disappearance of a dose-dependent response on root biomass between 4 and 7 days.

Whilst no effects were observed in the shoots between 0 and 120 µGy h^{-1}, significant alterations of *CSD, FSD, RBOH* and DNA repair pathway transcript levels could be found in the shoots starting at dose rates as low as 0.2 µGy h^{-1}. Though this discrepancy seems to point towards a difference in sensitivity to ionising radiation between both organs, a complementary explanation might be found in the way ^{90}Sr deposits energy in both organs and how it is therefore

perceived by the plant. Delivery of root dose is primarily external, whereas ^{90}Sr in the shoots migrates from xylem transport to the vascular cell wall, generating internal dose that emanates primarily from the apoplast, and might be partially contained there by the higher density of the cell wall structure. There is most definitely an active oxidative stress response to β-radiation in both organs, indicated by the up-regulation of LOX and RBOHC. Both are involved in the oxidative burst (Bhattacharjee, 2005), though it is not clear from our data whether their respective up-regulation in shoot and root reflects a difference in stress perception and defence strategy between both organs rather than a temporal shift in the stress response.

Further research is needed to investigate how plants maintain stable biomass and growth when faced with high β-dose rates. Furthermore, though this study provides evidence for the involvement of a transcriptional response on ROS scavenging and DNA repair in the response to β-radiation delivered by ^{90}Sr, more detailed study is needed to uncover the mechanism behind the apparent decline in DNA damage at high dose rates, and behind the transient increase in leaf area. Finally, as ROS scavenging and DNA repair seem to be insufficient to counterbalance ROS-induced damage and maintain redox balance, it is still unclear how these elements fit together in a dose rate- and time-dependent framework.

Chapter 7:

Biological effects of α-radiation exposure by ^{241}Am in *Arabidopsis thaliana*

Biermans, G., Horemans, N., Vanhoudt, N., Vandenhove, H., Saenen, E., Nauts, R., Van Hees, M., Wannijn, J., Vangronsveld, J., Cuypers, A., 2013. *Arabidopsis thaliana* shows a dose-dependent response in damage and repair after exposure to α-radiation by ^{241}Am.

In draft

ABSTRACT

Anthropogenic activity has led to an increasing amount of radionuclides in the environment and subsequently to an increased risk of exposure of the biosphere to ionising radiation. Due to their high linear energy transfer, α-emitters in particular form a threat to biota when absorbed or integrated in living tissue. Among these, ^{241}Am is of major concern due to high affinity for organic matter and high specific activity. This study examines the dose-dependent biological effects of α-radiation delivered by ^{241}Am at the morphological, physiological and molecular level in 14-day old seedlings of *Arabidopsis thaliana* after hydroponic exposure for 4 or 7 days. Our results show that ^{241}Am has high transfer to the roots but low translocation to the shoots. In the roots, we observed a transcriptional response of ROS scavenging and DNA repair pathways. At the physiological and morphological level this resulted in a response which evolves from redox balance control and stable biomass at low dose rates to growth reduction, reduced transfer and redox balance decline at higher dose rates. This situation was also reflected in the shoots where, despite the absence of a transcriptional response, the control of photosynthesis performance and redox balance were maintained then declined with increasing dose rate. Our results also suggest that the effects in both organs were initiated in the roots, where the highest dose rates occurred, ultimately affecting photosynthesis performance and carbon assimilation. Though further detailed study of nutrient balance and ^{241}Am localisation is necessary, it is clear that radionuclide uptake and distribution is a major parameter in the global exposure effects on plant performance and health.

7.1 Introduction

One of the most important anthropogenic α-emitters in the environment is americium-241 (^{241}Am). Americium-241 is formed exclusively as a result of nuclear fission processes as a daughter nuclide of ^{241}Pu. ^{241}Pu decays through β^--mode with a half-life of 14.4 years to ^{241}Am, which in turn decays through α-emission to ^{237}Np with a half-life of 432 years. Most of the americium in the environment is a result of the atomic bomb tests' fallout (Thein, et al., 1980), though substantial amounts have been released accidentally in the past, for example in the Chernobyl accident (Ukraine) in 1986 or Windscale (UK) in 1956, mostly as ^{241}Pu. Because of the relatively recent nature of these releases and the half-lives of ^{241}Pu and ^{241}Am, environmental levels of americium are still increasing and will reach a peak around 2070-75 (DOE, 2000). Apart from the previously described releases, limited amounts of ^{241}Am are emitted annually by reprocessing plants in Sellafield (UK) and Le Hague (France) into the marine environment (EU, 2010). A key element in the assessment of the impact of ionising radiation is a correct dosimetry, which relies on the description of uptake and distribution of radionuclides within the organism studied. Though this is important for every radionuclide, it is even more so for α-emitting elements. Alpha particles are helium nuclei, which due to their large mass have a very short range inside living tissue. Nevertheless, due to their high energy (4-10 MeV), they have a high linear energy transfer (LET) and can therefore cause a large amount of ionisations over a very short distance. As this gives them a high relative biological effectiveness (RBE), a radiation weighting factor of 10 has been proposed for α-particles in non-human biota (ICRP, 2003; 2007), though there is no real consensus on this subject (Chambers et al., 2006). Whilst their short range makes them irrelevant in external exposure, they become a prime concern when taken up into the organism.

Due to its strong affinity for organic matter, transfer of ^{241}Am to plant tissue in aquatic conditions is high (Bolsunovsky et al., 2005), though the large spread on

the concentration ratio used within the ERICA tool for vascular plants (4200 ± 2950; Hosseini et al., 2008) reflects the large variation between species and experimental approaches. Studies on absorption in submerged macrophytes have shown that the nuclide migrates quickly to the plant tissue, (Bolsunovsky et al., 2005; Zotina et al., 2010), where 70-90% of the americium can be found in cellulose fraction (cell wall). The remainder is bound to the proteins and carbohydrates (Bondareva et al., 2010; Zotina et al., 2011). However, the transfer route in these studies was nearly exclusively foliar, and therefore they do not provide information on the root-to-shoot behaviour of the radionuclide. Very few hydroponic studies with ^{241}Am are available, though its overall uptake and distribution between root and shoot is expected to be similar to that of other heavy elements such as uranium or plutonium. These elements are also mostly concentrated in the roots (Lee et al., 2002; Vandenhove et al., 2006; Vanhoudt et al., 2008). Soil transfer studies report a much lower transfer, and a very low shoot:root ratio (Duffa et al., 2002; Hoyt & Adriano, 1979; Sokolik et al., 2004)

Despite the international scientific research efforts (ICRP, 2009; IUR, 2002; Larsson, 2008; UNSCEAR, 2008), there are still considerable gaps in our knowledge about biological mechanisms underlying the effects of radiation (Andersson et al., 2009; Garnier-Laplace et al., 2004). Within the recently established proposal for a strategic research agenda by the European Radioecology Alliance, a better understanding of the underlying molecular effects of radionuclide exposure has therefore been put forward as one of the main research goals (Hinton et al., 2013). The effects of ionising radiation (IR) on plant growth and physiology are diverse, ranging from growth induction to growth reduction (Holst & Nagel, 1997), depending on various factors such as exposure type, species and age. Most of these data have been obtained by γ-exposure, and very few studies have been performed on the dose-dependent effects of other types of radiation in plants (Esnault et al., 2010). At the molecular level, IR induces damage to structural and functional components of the cell, either by direct energy transfer to macromolecules such as proteins, lipids or DNA or by indirect damage including water radiolysis. Hydrolysis

produces reactive oxygen species (ROS), ultimately leading to oxidative damage to the same cellular components (Lee et al., 2009). ROS, which are also produced as a result of normal metabolism, play an important role in stress signalling and the oxidative stress response (Foyer & Noctor 2005; Mittler et al., 2002; Vranova et al., 2002). The plant cell contains several ROS scavenging pathways, which consist either of metabolites, such as ascorbate and glutathione (Noctor & Foyer, 1998), or of enzymatic reactions in which several classes of proteins such as superoxide dismutases (SOD) and catalases (CAT) remove superoxide ($O2\bullet^-$) and hydrogen peroxide (H_2O_2) respectively (Mittler et al., 2004). IR-induced DNA damage is repaired by several competing pathways, depending on the type of damage (Adams-Philips et al., 2010; Britt, 1996; Schulz et al., 2012; Waterworth et al., 2011; West et al., 2000).

In this study, we aimed to unravel the dose-dependent response of 14-day old *Arabidopsis thaliana* seedlings to chronic α-radiation exposure, by exposing them for 7 days to a wide range of environmental ^{241}Am levels in a hydroponic setup. We measured the uptake and distribution of the radionuclide in root and shoot to obtain more accurate dosimetry for each organ. In addition to growth and photosynthesis, we also aimed to characterise the plant response at the molecular level by measuring DNA damage, antioxidant metabolites and the transcriptional response of key genes in DNA repair and the oxidative stress response.

7.2 Methods

7.2.1 Plant culture and Americium-241 exposure

Prior to sowing, *Arabidopsis thaliana* (Columbia ecotype) were spread out on moist filter paper and vernalized for three days at 4°C to synchronize germination. The seeds were then sown on plugs from 1.5 mL eppendorf tubes filled with 0.6% agar. The plugs were subsequently placed in a PVC cover,

capable of holding 36 plugs, after which each cover was placed on a container filled with 1.35 L modified Hoagland solution (1mM KNO_3, 0.3 mm $Ca(NO_3)_2$, 0.2 mM $MgSO_4$, 0.1 mM $NH_4H_2PO_4$, 1.62 µM $FeSO_4$, 0.78 µM Na_2EDTA, 4.6 µM H_3BO_3, 0.9 µM $MnCl_2$, 0.032 µM $CuSO_4$, 0.055 µM H_2MoO_4, 0.077 µM $ZnSO_4.7H_2O$).

Plants were grown in a growth chamber (Binder) under a 16/8 day/night photoperiod and 22°C/16°C day/night temperatures and 65% relative humidity. Photosynthetic photon flux density was 150 µE at the leaf level (lamps here). Plants were aerated with a peristaltic pump from 7 days after sowing onwards.

After 14 days, seedlings were exposed for 4 or 7 days to 0, 50, 500, 5000 and 50000 Bq/L ^{241}Am (added as Am_2CO_3). The pH of the liquid medium was adjusted to that of the 0 Bq/L treatment prior to exposure of the plants.

7.2.2 Plant sampling and biomass

Roots and shoots were sampled after 4 and 7 days, and fresh weight determined for minimum 18 biological replicates. Half of the tissues from each treatment were snap frozen in liquid nitrogen for RNA and DNA extractions (as 50 to 100 mg samples in eppendorf tubes) and stored at -80°C until processing.

The other half was collected for dose assessment and dry weight determination and dried for 7 days at 80°C. The roots were first rinced (at 4°C) immediately after harvest to remove external Americium (2x10 min. in 1 mM $Pb(NO_3)_2$, then 1x10 min. in dH_2O).

7.2.3 Leaf Area

Leaf area was determined at regular intervals during exposure using a compact CCD digital camera (Canon). Images were analysed as in Leister et al. (1999)

using ImageJ (US National Institutes of Health, Bethesda, Maryland, US), and calibrated using centrifuge tube width as a constant scaling parameter in each image. By isolating the correct range of green values in each image, the plants could then be isolated from the background and their individual surfaces measured after transformation to a binary image.

7.2.4 Transfer and Dosimetry

Samples for transfer measurements were dry-ashed in a muffle furnace at 550 °C for 24 hours, and subsequently digested in 0.1 M HCl. Digested samples were then diluted 10x.

Two medium samples (5 mL) were also taken from each tray to check the activity concentration of each treatment. One sample from the top of the liquid without stirring, and one after thorough stirring to bring possible precipitated ^{241}Am on the bottom of the tray back into suspension. Each sample was brought to 20 mL with dH_2O after adjusting to pH 3 with 12 M HCl, and the ^{241}Am activity subsequently measured by LEGe gamma spectrometry (Canberra). Transfer factors were calculated as activity (in Bq kg dry weight^{-1} / Bq L^{-1}). Concentration ratios were calculated as on activity (in Bq) per kg fresh weight / Bq L^{-1}. Both were calculated as a ratio to the ^{241}Am activity concentration in the exposure tray before stirring, as this was considered the fraction of ^{241}Am in solution.

Internal and external root dose rates and internal shoot dose rates at each harvest point, and the corresponding absorbed doses over the exposure period, were determined by the plant dosimetry method described in Biermans et al. (2013), which uses separate dosimetry models for *Arabidopsis* root and shoot, and is based on the measured activity concentrations in the organs. Shoot dose conversion coefficient (DCC) values for each harvest point were determined by taking into account the leaf area measurements (Section 2.4). Dose rates were calculated under assumption of linear increase in tissue activity concentration during the exposure.

7.2.5 Photosynthesis measurement and pigment analysis

Immediately after harvest, four plants from each treatment were chosen at random. Their 4th leaf was then removed, and stored on wet paper in a closed petri dish in the dark.

The leaves were pre-adapted to dark conditions for at least 15 minutes and the induction curve (IC) for photosystem II (P680) was then measured using PAM Fluorometry (Dual PAM-1000; Waltz, Germany) (Schreiber et al., 2004). From these data, values for photosynthetic efficiency (φPSII), non-photochemical quenching (NPQ) and photosynthetic capacity (Fv/Fm) could be calculated. The induction curve measurement was immediately followed by a rapid light curve (RLC) measurement between 0 and 800 µE. These data were then fitted to the continuous model of Platt without photoinhibition as used in Ralph and Gademan (2005) using a Marquardt-Levenberg curve fitting algorithm in statistical software package R (R Development Core Team, 2011).

Pigments were extracted from frozen shoots by incubation in 100% N,N-dimethylformamide (DMF) overnight at 4°C under dark conditions. The pigment absorbance was measured spectrophotometrically at 480, 647 and 664 nm and pigment concentrations for chlorophyll a, chlorophyll b and carotenoids were calculated from these-absorbance values using the appropriate equations for DMF according to Wellburn (1994).

7.2.6 Base modification (8-OHdG formation)

Frozen root tissue (75-100 mg), harvested from plants irradiated for 7 days, was mechanically shredded (-80 °C; 2.5 min. at 30 Hz) with beads (MM400, Retsch), and the DNA extracted from the samples using DNeasy Plant Mini Kit

(Qiagen) following the manufacturer's instructions. DNA concentrations were measured spectrophotometrically (Nanodrop 2000, Isogen Life Sciences).

The DNA samples were then digested as described in Debiane et al. (2009). 38 µL of DNA extract was incubated for 2 minutes at 100 °C, and subsequently digested with Nuclease P1 (2µL 5U/µL; Sigma) in the presence of 3 µL 250 mM potassium acetate buffer (pH 5.4) and 3 µL 10 mM zinc sulphate. Digestion was performed at 37°C overnight, after the digests were treated for 2 hours at 37°C with 2 µL alkaline phosphatase (0.3 U/µL; Sigma) in the presence of 6 µL 0.5 M Tris-HCl buffer (pH 8.3). Base modification (8-OHdG) was determined by competitive ELISA (New 8-OHdG Check kit, Japan Institute of Aging) according to the manufacturer's instructions. The assay is based on spectrophotometric detection at 415 nm.

7.2.7 Gene Expression analysis

Frozen root and shoot tissue (50-100 mg) was homogenized in a tissue shredder (MM400, Retsch; -80 °C; 2.5 min. at 30 Hz) and the RNA extracted. RNA from shoot tissue was extracted using Ambion RNaqueous Kit (Invitrogen), and root RNA with RNeasy Plant Mini Kit (Qiagen, Venlo, Netherlands). RNA quality and integrity was checked through electrophoresis on Bioanalyzer (Agilent Technologies) and its quantity was determined with spectrophotometry at 260 nm on Nanodrop (Isogen Life Science). Genomic DNA was removed from the samples with TURBO DNA-free™ Kit (Invitrogen) according to the manufacturer's instructions. RNA was then transformed to cDNA with the High-Capacity cDNA Reverse Transcription Kit (Applied Biosystems), using equal amounts of starting material (1 µg).

Quantitative realtime-PCR was performed using SYBR Green fluorescence on a 7500 Fast Real-Time PCR system (Applied Biosystems) in a 10µL volume, containing 2.5 µL cDNA sample, 5 µL of Fast SYBR Green Master Mix (Applied Biosystems), 0.3 µL forward primer, 0.3 µL reverse primer and 1.9 µL RNase-

free water. Primes used are shown in Table 7.1. Primer efficiencies were tested with a dilution series. Gene expression data were normalized to housekeeping genes (Roots: TIP41-like, ACT2; UBC, EF1a; Shoots: At2g28390, At5g08290, ACT2) using GeNorm software according to Vandesompele et al. (2002) and presented relative to control (gene expression at 0 Bq/L) of the respective harvest point.

7.2.8 Metabolites

Ascorbate and glutathione levels were determined in the leaves and roots of *Arabidopsis thaliana* seedlings exposed for 7 days to ^{241}Am. The concentrations were determined using a spectrophotometric assay as described by Queval & Noctor (2007), which enables measurement of both oxidised and reduced forms for both components of the ascorbate-glutathione cycle.

Frozen shoot tissue (50-100 mg) was homogenized in a tissue shredder (MM400, Retsch; -80°C; 2.5 min. at 30 Hz) and extracted by addition of 800 µL 0.1M HCl.

Total glutathione concentrations (reduced form GSH + oxidised form GSSG) were measured as the capacity to reduce of 5,5-dithiobis(2-nitro-benzoic acid) (DTNB), in the presence of glutathione reductase (GR). Reactions were performed in the presence of 100 µl phosphate buffer (200 mM NaH2PO4, 10 mM EDTA (pH 7.5)), 60 µl dH2O, 10 µl 10 mM NADPH and 10 µl 12 mM DTNB. After addition of 10 µL GR, 10 µL of extract was added, after which DTNB reduction was monitored spectrophotometrically as an increase in A_{415}. To measure GSSG only, a similar measurement was performed (using 20 µL of sample) after blocking the GSH present in the sample with 2-vinylpyridine.

Total ascorbate (the sum of the oxidised (dehydroascorbate; DHA) and reduced (AsA) forms) were determined by converting the DHA present in the sample to AsA by incubation with 25 mM Dithiothreitol (DTT) and 125 mM NaH_2PO_4 (pH

7.5) for at least 15 minutes. After adjustment of the pH to 5.5, AsA and total ascorbate measurements were performed with 40 µL of extract, in the presence of 100 µl 200 mM NaH_2PO_4 (pH 5.6) and 55 µl dH_2O, by determining absorbance at 265 nm. After addition of 5 µL Ascorbate oxidase (AO), the change in A_{265} was measured until stable values were obtained.

7.2.9 Statistical Analysis

Datasets from transfer, biomass, photosynthesis, pigments, base modification and gene expression were analysed using statistical software package R (R Development Core Team, 2011).

All datasets, except those for transfer, leaf area and pigments, were analysed for each time point and tissue separately, comparing means between treatments. Assumptions of normality of the model residuals and consistency of variance were tested using a Shapiro test and a Bartlett test respectively, after which a one way-ANOVA and pairwise comparisons between means were performed using the Tukey correction. If necessary, when assumptions were not met, appropriate transformation of the data was performed using a Box Cox transformation. The assumptions were then checked again. If none of the assumptions were met, a non-parametrical Kruskal-Wallis test was performed and pairwise comparisons using the Bonferoni correction.

Transfer and leaf area datasets were analysed by time point and treatment using a two-way ANOVA and pairwise comparisons with the Tukey method. Pigment data were analysed by two-way ANOVA as described in the results (Section 7.3.6).

Gene Name	Forward Primer Sequence	Reverse Primer Sequence
At2g28390,	*AACTCTATGCAGCATTTGATCCACT*	*TGATTGCATATCTTTATCGCCATC*
At5g08290	*TTACTGTTTCGGTTGTTCTCCATTT*	*CACTGAATCATGTTCGAAGCAAGT*
ACT2	*CTTGCACCAAGCAGCATGAA*	*CCGATCCAGACACTGTACTTCCTT*
EF-1α	*TGAGCACGCTCTTCTTGCTTTCA*	*GGTGGTGGCATCCATCTTGTTACA*
TIP41-like	*GTGAAAACTGTTGGAGAGAAGCAA*	*TCAACTGGATACCCTTTCGCA*
UBC	*CTGCGACTCAGGGAATCTTCTAA*	*TTGTGCCATTGAATTGAACCC*
CKS1	CACGTCGTTCTTCCTCCTGAAG	TCCTATCGCTCGCCATTCG
DMC1	ATGAAGACGAAGATCTATTTGAGATGATT	CTTGTAGCTTTTTCACATCTCCTGC
GAR1	CTAAGATGGTTGGTGATGCAAGAGA	CGCTAAGCTCATCCAAACCCTT
KU80	CTTCTTCCAGCACAACTCCTCAA	CTACGCATCGCAGGACCTACAT
LIG4	TGATGTATCGGATATCAAGGGCA	GAATGGGACCGAGGCACG
LPP1	TCACTTTCTGATGACAATAGGGTCG	CCTCTCTGCGCCTCCTGG
MND1	GAACGAGATGGTACAATTTGCTGA	CCGACTGGTGAGCAACTTCAAT
PARP1	TGCATTGGGAGAAATACATGAGC	CCGAGCCCTTTGGTCGAG
PARP2	ATCGGAGGTGATTGATCGGTATG	AAATCATGAGGTATCACTGTGTAGAACTCT
POLG1	GAAACTGGACGCTTATCGGCTAG	CTGACGGATTTTGTACCGATCTTT
RAD51	GTCCAACAACAAGACGATGAAGAA	AACAGAAGCAATACCTGCTGCC
APX1	TGCCACAAGGATAGGTCTGG	CCTTCCTTCTCTCCGCTCAA
CAT1	AAGTGCTTCATCGGGAAGGA	CTTCAACAAAACGCTTCACGA
CAT2	AACTCCTCCATGACCGTTGGA	TCCGTTCCCTGTCGAAATTG
CAT3	TCTCCAACAACATCTCTTCCCTCA	GTGAAATTAGCAACCTTCTCGATCA
CSD1	TCCATGCAGACCCTGATGAC	CCTGGAGACCAATGATGCC
CSD2	GAGCCTTTGTGGTTCACGAG	CACACCACATGCCAATCTCC
CSD3	GTTGTTGTGCATGCGGATCC	CACATCCAACTCTCGAGCCTG
FSD1	CTCCCAATGCTGTGAATCCC	TGGTCTTCGGTTCTGGAAGTC
FSD2	TTGGAAAGGTTCAAGTCGGCT	CATTTGCAACGTCAAGTCTATTCG
FSD3	AACGGGAATCCTTTACCCGA	TGTCTCCACCACCAGGTTGC
GR1	CTCAAGTGTGGAGCAACCAAAG	ATGCGTCTGGTCACACTGC
LOX1	TTGGCTAAGGCTTTTGTCGG	GTGGCAATCACAAACGGTTC
LOX2	TTTGCTCGCCAGACACTTG	GGGATCACCATAAACGGCC
RBOHA	CATTTCGCTAGGCCAAACTG	TTCACTAACCCAGCTGCTCCA
RBOHC	TCACCAGAGACTGGCACAATAAA	GATGCTCGACCTGAATGCTC
RBOHE	GTGATGCAAGATCAACCCTGA	GCCTTGCAAAATGTGTTCTCA

Table 7.1: Primers for gene expression analysis

7.3 Results

7.3.1 Activity Concentrations of the medium

The measured activity concentrations of the ^{241}Am in solution corresponded well in order of magnitude with the desired nominal concentrations (Table 7.2). The amounts of ^{241}Am measured before and after stirring of the medium were identical (data not shown), indicating that most of the ^{241}Am was in solution.

Table 7.2: nominal and soluble activity concentrations for each ^{241}Am treatment. Values presented are mean ± SE of 4 replicates.

Activity Concentration [Bq L^{-1}]	
Nominal	In solution (after stirring)
0	0.01 ± 0.01
50	60 ± 5
500	360 ± 30
5 000	2970 ± 140
50 000	36700 ± 1100

7.3.2 Transfer

The transfer factors (based on dry weight) for ^{241}Am in the roots were significantly higher at 4 days for the 36700 Bq L^{-1} treatment compared to other treatments (Table 7.3). A similar observation could be made for the concentration ratio (based on fresh weight) (Table 7.4). Both were roughly 2-fold higher. However, at 7 days this difference has disappeared for both parameters due to a significant 2-fold decrease in transfer factor in the highest ^{241}Am treatment. For the other treatments, concentration ratios and transfer factors for the roots remained identical between harvest points.

Table 7.3: Transfer factors for *Arabidopsis thaliana* seedlings exposed for 4 and 7 days to ^{241}Am. Results present mean ± S.E. of at least 3 biological replicates. Analysis was done separately for each tissue type. Differences in lower case letters indicate significant differences in dose rate between treatments on the same harvest day ($p<0.05$). Differences in upper case letters indicate significant differences in dose rate between harvest points for a specific treatment ($p<0.05$).

		^{241}Am Transfer Factor [Bq kg^{-1} DW / Bq L^{-1}]	
		ROOTS	SHOOTS
4 DAYS	*60 Bq L^{-1}*	^{ac} 3350 ± 160 ^{A}	-
	360 Bq L^{-1}	^{a} 3000 ± 500 ^{A}	^{a} 46.4 ± 1.9 ^{A}
	2970 Bq L^{-1}	^{bc} 5530 ± 250 ^{A}	^{b} 290 ± 27 ^{A}
	36700 Bq L^{-1}	^{b} 6100 ± 1100 ^{A}	^{b} 337 ± 25 ^{A}
7 DAYS	*60 Bq L^{-1}*	^{a} 3950 ± 220 ^{A}	-
	360 Bq L^{-1}	^{a} 3700 ± 300 ^{A}	^{a} 32 ± 4 ^{A}
	2970 Bq L^{-1}	^{b} 4500 ± 500 ^{A}	^{b} 138 ± 17 ^{B}
	36700 Bq L^{-1}	^{a} 3410 ± 29 ^{B}	^{b} 199 ± 18 ^{B}

The transfer parameters of ^{241}Am from the medium to the shoots were considerably lower than those to the roots, with a shoot:root ratio between concentration ratios ranging from 0.03 to 0.12 at 4 days and between 0.3 to 0.24 at 7 days, depending on the treatment (Table 7.4).

Transfer to the shoots progressively increased with increasing environmental activity concentration, though for the 60 Bq L^{-1} exposure measurements were below the detection limit (Tables 7.3 and 7.4). For the 2970 and 36700 Bq L^{-1} exposures, the shoot transfer factors and concentration ratios declined significantly with a 2 to 2.5-fold reduction between 4 and 7 days. This indicates that though these treatments initially show a higher transfer, they also have a

much more important decline in transfer rate during exposure than that observed in the 360 Bq L^{-1} treatment.

Table 7.4: Concentration Ratios for *Arabidopsis thaliana* seedlings exposed for 4 and 7 days to ^{241}Am. Results present mean ± S.E. of at least 3 biological replicates. Analysis was done separately for each tissue type. Differences in lower case letters indicate significant differences in dose rate between treatments on the same harvest day ($p<0.05$). Differences in upper case letters indicate significant differences in dose rate between harvest points for a specific treatment ($p<0.05$).

		^{241}Am Concentration Ratio [Bq kg^{-1} FW / Bq L^{-1}]		
		ROOTS	SHOOTS	TOTAL PLANT
4 DAYS	*60 Bq L^{-1}*	^{ab} 151 ± 21 ^{A}	-	^{a} 60 ± 3 ^{A}
	360 Bq L^{-1}	^{b} 126 ± 27 ^{A}	^{a} 5 ± 0.2 ^{A}	^{a} 55 ± 9 ^{A}
	2970 Bq L^{-1}	^{ac} 250 ± 40 ^{A}	^{b} 30.7 ± 2.2 ^{A}	^{b} 119 ± 8 ^{A}
	36700 Bq L^{-1}	^{cd} 300 ± 40 ^{A}	^{b} 38 ± 3 ^{A}	^{b} 116 ± 15 ^{A}
7 DAYS	*60 Bq L^{-1}*	^{ab} 152 ± 12 ^{A}	-	^{ab} 67,4 ± 2,6 ^{A}
	360 Bq L^{-1}	^{b} 120 ± 9 ^{A}	^{a} 3.6 ± 0.6 ^{A}	^{ab} 62,1 ± 2,9 ^{A}
	2970 Bq L^{-1}	^{ac} 201 ± 25 ^{A}	^{b} 15.3 ± 1.6 ^{B}	^{a} 92 ± 7 ^{A}
	36700 Bq L^{-1}	^{b} 92 ± 8 ^{B}	^{b} 22.6 ± 1.9 ^{B}	^{bc} 56 ± 3 ^{B}

Dosimetry

Dose rates in the roots at 4 days (Table 7.5A) increased one order of magnitude for every tenfold increase in environmental activity concentration of ^{241}Am. Between 4 and 7 days, the dose rates remained constant, except in the 36700 Bq L^{-1} treatment, where it was reduced from 35 mGy h^{-1} with a factor 3 to 10.8 mGy h^{-1} due to a decline in medium-to-root transfer (Table 7.4). It has to be noted that in the roots, the external contribution to the dose rate is considered to be zero, due to the short range of α-particles. Total absorbed doses in the roots amounted to 1.7 and 3.3 Gy respectively at 4 and 7 days at the highest ^{241}Am activity concentration (Table 7.5B).

A

		^{241}Am Dose rates [µGy/h]	
		ROOTS	SHOOTS
4 DAYS	*0 Bq L^{-1}*	<0.5	<0.6
	60 Bq L^{-1}	29 ± 4	<1.0
	360 Bq L^{-1}	140 ± 30	5.66 ± 0.23
	2970 Bq L^{-1}	2400 ± 400	291 ± 21
	36700 Bq L^{-1}	35000 ± 5000	4500 ± 400
7 DAYS	*0 Bq L^{-1}*	<0.6	<1.0
	60 Bq L^{-1}	29.6 ± 2.3	<0.5
	360 Bq L^{-1}	135 ± 10	4.1 ± 0.7
	2970 Bq L^{-1}	1910 ± 240	145 ± 15
	36700 Bq L^{-1}	10800 ± 900***	2650 ± 22

B

		^{241}Am Dose [mGy]	
		ROOTS	SHOOTS
4 DAYS	*0 Bq L^{-1}*	<0.005	<0.12
	60 Bq L^{-1}	1.41 ± 0.19	<0.05
	360 Bq L^{-1}	6.9 ± 1.4	0.271 ± 0.011
	2970 Bq L^{-1}	113 ± 18	14 ± 1
	36700 Bq L^{-1}	1670 ± 240	214 ± 19
7 DAYS	*0 Bq L^{-1}*	0.03 ± 0.019	<0.24
	60 Bq L^{-1}	3.5 ± 0.3	<0.1
	360 Bq L^{-1}	16.9 ± 2	0.62 ± 0.03
	2970 Bq L^{-1}	267 ± 28	29.7 ± 1.7
	36700 Bq L^{-1}	3300 ± 300	470 ± 30

Table 7.5 Dose rates (**A**) and Total absorbed doses (**B**) for *Arabidopsis thaliana* seedlings exposed for 4 and 7 days to ^{241}Am. Results present mean ± S.E. of at least 3 biological replicates. Analysis was done separately for each tissue type. Significant differences in dose rate between harvest days are shown as * p<0.05; **p<0.01; ***p<0.001

7.3.3 Biomass and Leaf Area

No effects on shoot biomass were observed after 4 days of exposure to ^{241}Am, either on fresh weight (ANOVA , $F_{4,294}$ = 1.82, p = 0.13) or dry weight percentage (ANOVA, $F_{4,15}$ = 1.28, p = 0.32) (Table 7.6). However, root fresh weight was significantly decreased by 14 % in the highest treatment after 4 days (at 35,000 µGy h^{-1}), while root dry weight percentage showed no dose-rate dependent changes (ANOVA, $F_{4,15}$ = 1.11, p = 0.39). After 7 days, shoot dry weight percentage (ANOVA, $F_{4,15}$ = 0.47, p = 0.76) and fresh weight (ANOVA , $F_{4,319}$ = 1.81, p = 0.13) remained stable. In the roots, however, fresh weight was still decreased by 11% in the highest treatment, while root dry weight percentage showed a dose-dependent decrease, down to 52% of the control value at the highest applied concentration (Table 7.6). The relative decline in dry weight was much stronger than that in fresh weight, which indicates that the observed reduction in dry weight percentage was the result of reduced biomass production rather than a decrease in water content. No effects were observed on leaf area (data not shown).

Table 7.6: Fresh weight and dry weight percentage of roots and shoots at 4 and 7 days of exposure to ^{241}Am. Fresh weight values are the mean ± S.E. of at least 18 biological replicates. Dry weight percentages are the mean ± SE of 4 biological replicates. Significance differences between treatments and control are given for each time point and organ as * p<0.05; ** p<0.01; *** p<0.001. For associated doses and dose rates, see Table 7.5A and B.

		Fresh Weight [mg]		**% Dry Weight [%]**	
		SHOOTS	ROOTS	SHOOTS	ROOTS
4 DAYS	*0 Bq L^{-1}*	43,1 ± 0,9	19,3 ± 0,6	11,5 ± 0,5	5,0 ± 0,3
	60 Bq L^{-1}	44,8 ± 1,2	21,6 ± 0,9	11,1 ± 0,4	4,6 ± 0,7
	360 Bq L^{-1}	43 ± 1,3	21,2 ± 0,6	10,79 ± 0,10	4,1 ± 0,4
	2970 Bq L^{-1}	42,8 ± 1,0	21,8 ± 0,8	10,64 ± 0,28	4,5 ± 0,6
	36700 Bq L^{-1}	40,7 ± 1,0	16,7 ± 0,8*****	11,30 ± 0,21	5,4 ± 0,3
7 DAYS	*0 Bq L^{-1}*	90,5 ± 2,9	60,2 ± 2,5	10,9 ± 0,4	5,1 ± 0,3
	60 Bq L^{-1}	100,2 ± 2,7	61,9 ± 2,0	10,9 ± 0,4	3,9 ± 0,3*****
	360 Bq L^{-1}	97,8 ± 2,5	65,8 ± 2,4	11,2 ± 0,3	3,3 ± 0,3******
	2970 Bq L^{-1}	98,2 ± 2,3	59,9 ± 2,2	11,17 ± 0,26	4,50 ± 0,25
	36700 Bq L^{-1}	96,3 ± 2,2	53,3 ± 1,8*****	11,40 ± 0,11	2,71 ± 0,17*******

7.3.4 Photosynthesis

7.3.4.1 Maximum photosynthetic efficiency (Fv / Fm)

After 4 days, the maximum efficiency of photosynthesis, as measured by the Fv/Fm parameter, remained constant at all dose rates except at 5.66 µGy h^{-1}, where it had significantly decreased by 1% . This decrease was not biologically relevant, however (Figure 7.1). After 7 days, we observed a clear dose rate-dependent decrease in maximum efficiency, indicating increasing stress on the photosynthetic process.

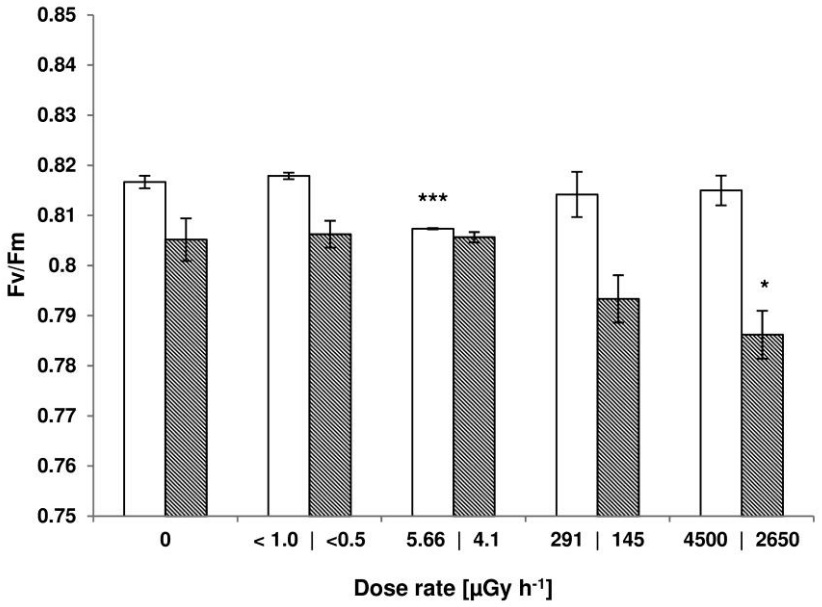

Figure 7.1: Maximum photosynthetic efficiency in shoots of *Arabidopsis thaliana* seedlings exposed for 4 days (white bars) and 7 days (grey bars) to ^{241}Am. Significance differences to control for each time point are shown as * p<0.05; ** p<0.01; *** p<0.001.

7.3.4.2 Quantum Yield and Electron Transfer Rate

Using PAM fluorometry, we measured the yields of each light pathway in photosystem II at the end of the induction curve. Figure 7.2 shows the quantum yields for each treatment after 4 and 7 days of photosynthesis (Figure 7.2C; Y_{PSII}), regulated (Figure 7.2B; Y_{NPQ}) and non-regulated (Figure 7.2A; Y_{NO}) non-photochemical quenching. Following the induction curve, we measured the response of electron transfer rate (ETR) to increasing light intensity in a rapid light curve measurement. From these curves we deduced the ETR slope under non-saturating conditions (Figure 7.3A), maximal ETR (Figure 7.3B) and the saturation point (Figure 7.3C)

After 4 days of exposure to ^{241}Am, neither Y_{PSII} (ANOVA, $F_{4,15} = 1.12$, $p = 0.38$), Y_{NPQ} (ANOVA, $F_{4,15} = 0.61$, $p = 0.66$) or Y_{NO} (ANOVA, $F_{4,15} = 0.22$, $p = 0.92$) displayed dose-rate dependent changes. After 7 days, however, there were clear effects on energy use in photosynthesis. Up to 145 µGy h^{-1}, there was a significant declining trend in regulated non-photochemical quenching (Figure 7.2 B). This reduction in buffering by regulated heat dissipation was accompanied by a corresponding increase in photosynthetic yield (Figure 7.2C). At the highest dose rate (2650 µGy h^{-1}) however, the quantum yield of photosynthesis was reduced by 4% compared to the control treatment. This was a result of significantly increased non-regulated non-photochemical quenching (Figure 7.2A) rather than controlled heat dissipation, indicating a loss of photo-protective capacity.

Electron transfer through the photosynthesis chain at 7 days also showed dose rate-dependent alterations, with an increase in saturation point Ek and ETRmax (Figure 7.3B and C) up to 145 µGy h^{-1}, followed by a significant decline at 2650 µGy h^{-1}. Both observations indicate that the improvement of photosynthetic performance with increasing dose rate shifts to a loss of photo-protection at the highest dose rate.

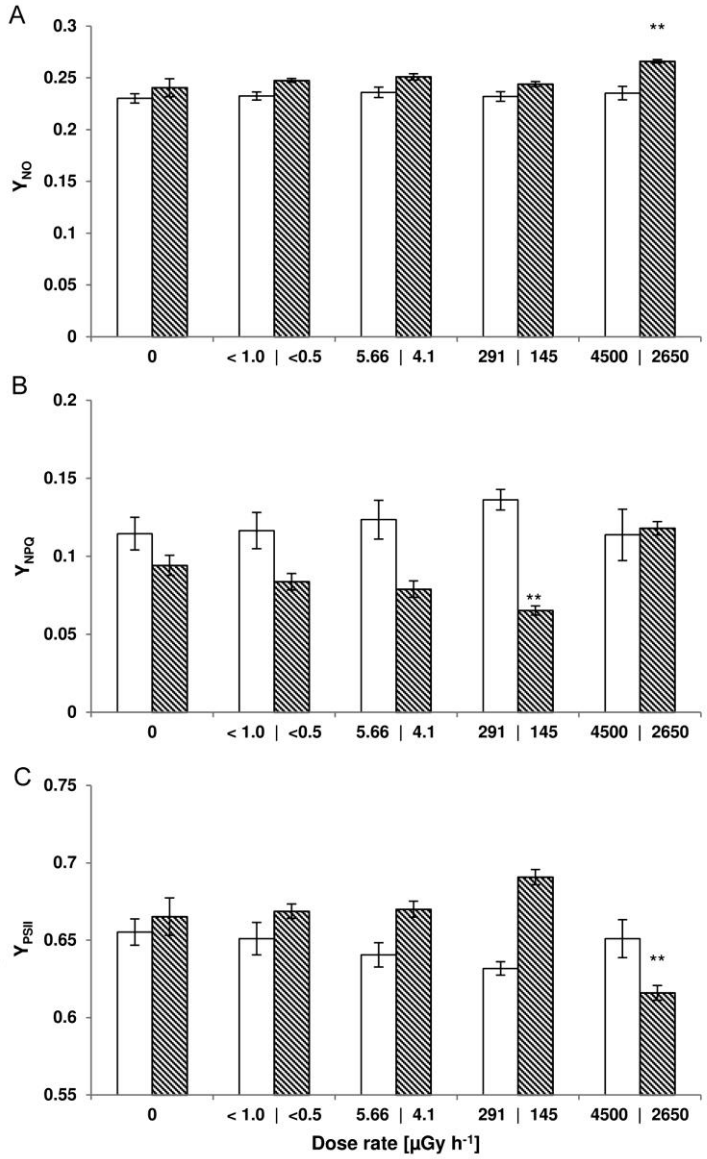

Figure 7.2: Quantum yields of non-regulated **(A)** and regulated **(B)** non-photochemical quenching and the photosynthetic **(C)** pathway of photosystem II in seedlings of A.thaliana exposed to 4 (white bars) and 7 days (grey bars) of ^{241}Am exposure. Values represented are mean ± SE of at least 3 biological replicates. Significance differences to control for each time point are shown as * p<0.05; ** p<0.01; *** p<0.001.

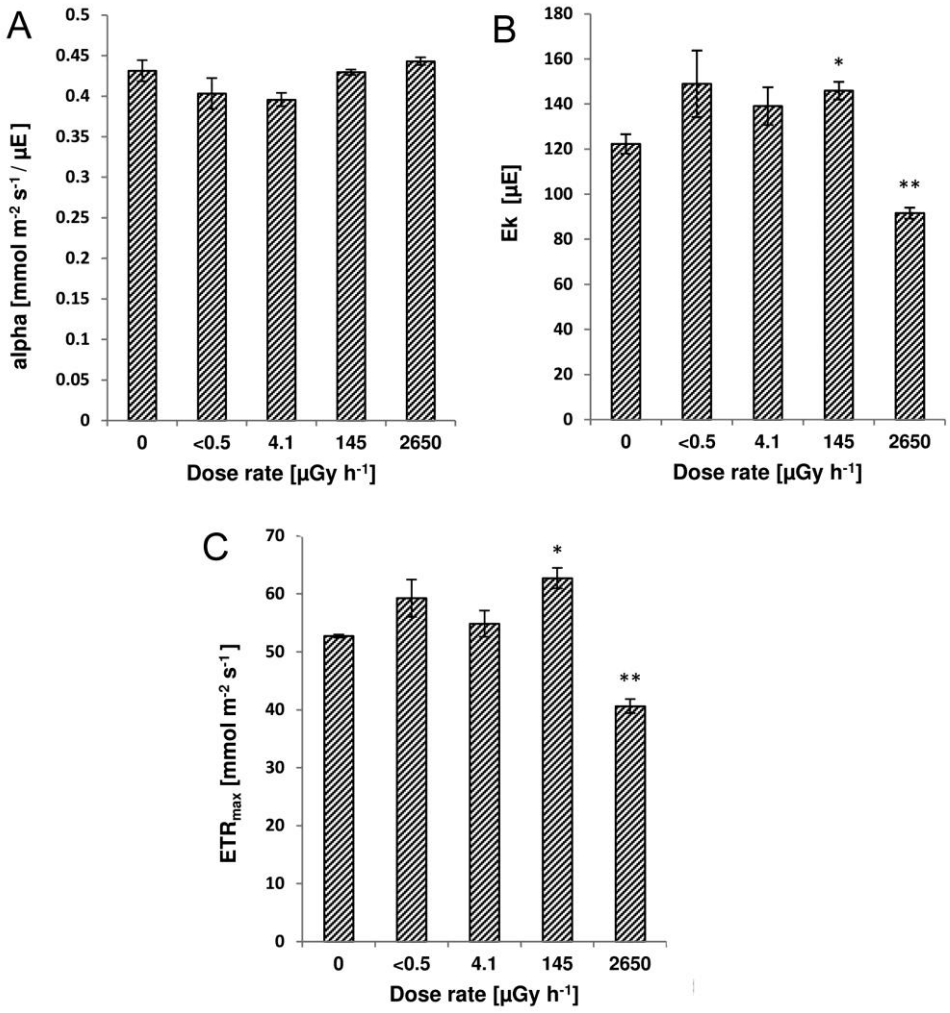

Figure 7.3: Rapid light curve parameters after 7 days ^{241}Am exposure in leaves of *Arabidopsis thaliana.* Graphs represent initial slope alpha **(A)**, the light saturation point Ek **(B)** and maximum electron transfer rate ETR_{max} **(C)**. Values represented are mean ± SE of at least 3 biological replicates. Significance levels * $p<0.05$; ** $p<0.01$; *** $p<0.001$.

7.3.5 Pigments

To assess the state of light-harvesting and light quenching compounds, we measured the pigment levels in leaves of *Arabidopsis thaliana* spectrophotometrically after extraction with DMF.

After 4 days, only chlorophyll b showed a significant change in concentration, with a slight reduction of pigment levels at 5.66 µGy h^{-1} (Table 7.7). Chlorophyll a (ANOVA, $F_{4,15} = 2.33$, $p = 0.10$) and the carotenoids (ANOVA, $F_{4,15} = 2.40$, $p = 0.10$) also showed reduced levels at that dose rate, though not significant. The a/b and chlorophyll/carotenoid ratios remained constant (Table 7.7).

At 7 days, there were no significant changes in levels of chlorophyll a (ANOVA, $F_{4,15} = 0.32$, $p = 0.86$), chlorophyll b (ANOVA, $F_{4,15} = 0.09$, $p = 0.98$) or the carotenoids (ANOVA, $F_{4,15} = 1.40$, $p = 0.28$), while both the a/b ratio and the chlorophyll/carotenoid ratio showed a significant decrease at 145 µGy h^{-1} (Table 7.7), indicating enlarged light harvesting antennae and increased photo-protection respectively. We should note that the pigment ratios increased again to control levels at 2650 µGy h^{-1}, indicating a decline of the photo-protective processes at lower dose rates.

7.3.6 DNA Damage and Repair

7.3.6.1 Base modification

Base modification by oxidative damage in the roots was measured spectrophotometrically by ELISA as the concentration of 8-OHdG in the genomic DNA. No significant changes in levels of modified base were found at either harvest point (Figure 7.4).

	Dose Rate [µGy h^{-1}]	Pigment Concentrations [µg g FW^{-1}]		
		Chl a	**Chl b**	**Carotenoids**
4 DAYS	*0 µGy h^{-1}*	0.8 ± 0.02	0.246 ± 0.004	0.1755 ± 0.0024
	< 1.0 µGy h^{-1}	0.68 ± 0.05	0.199 ± 0.016	0.15 ± 0.012
	5.66 µGy h^{-1}	0.64 ± 0.04	0.188 ± 0.015*****	0.139 ± 0.009
	291 µGy h^{-1}	0.72 ± 0.05	0.212 ± 0.017	0.15 ± 0.012
	4500 µGy h^{-1}	0.75 ± 0.02	0.226 ± 0.005	0.161 ± 0.004
7 DAYS	*0 µGy h^{-1}*	0.59 ± 0.03	0.192 ± 0.008	0.135 ± 0.006
	< 0.5 µGy h^{-1}	0.66 ± 0.03	0.203 ± 0.01	0.138 ± 0.008
	4.1 µGy h^{-1}	0.646 ± 0.022	0.198 ± 0.005	0.135 ± 0.005
	145 µGy h^{-1}	0.55 ± 0.13	0.2 ± 0.04	0.183 ± 0.027
	2650 µGy h^{-1}	0.63 ± 0.11	0.21 ± 0.04	0.157 ± 0.026

	Dose Rate [µGy h^{-1}]	**Ratio a/b**	**Ratio (a+b) / carotenoids**
4 DAYS	*0 µGy h^{-1}*	3.246 ± 0.027	5.95 ± 0.07
	< 1.0 µGy h^{-1}	3.448 ± 0.015*****	5.91 ± 0.15
	5.66 µGy h^{-1}	3.38 ± 0.05	5.91 ± 0.11
	291 µGy h^{-1}	3.39 ± 0.04	6.2 ± 0.11
	4500 µGy h^{-1}	3.29 ± 0.06	6.03 ± 0.07
7 DAYS	*0 µGy h^{-1}*	3.09 ± 0.06	5.82 ± 0.13
	< 0.5 µGy h^{-1}	3.273 ± 0.017	6.28 ± 0.07
	4.1 µGy h^{-1}	3.26 ± 0.03	6.25 ± 0.09
	145 µGy h^{-1}	2.68 ± 0.12******	3.46 ± 0.27*******
	2650 µGy h^{-1}	2.97 ± 0.06	5.34 ± 0.09

Table 7.7: Pigment concentrations and ratios in leaves of *Arabidopsis thaliana* seedlings after 4 and 7 days of exposure to ^{241}Am. Values are the mean ± S.E. of 4 biological replicates. Significance levels * $p<0.05$; ** $p<0.01$; *** $p<0.001$.

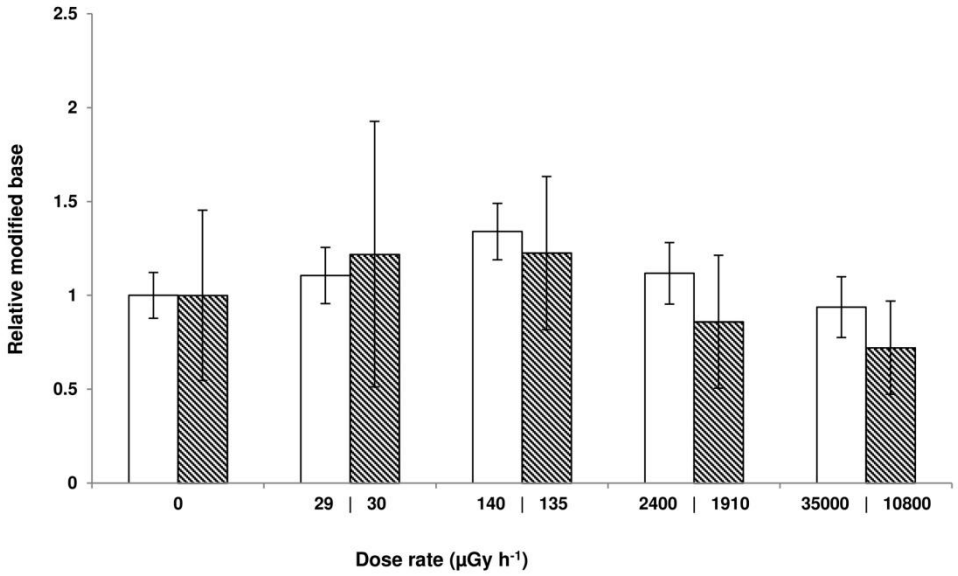

Figure 7.4: Concentration of modified base (8-OHdG) in roots of *Arabidopsis thaliana* exposed for 4 days (light bars) and 7 days (dark bars) to ^{241}Am, expressed as relative to the control treatment. Values are mean ± SE of at least 3 biological replicates.

7.3.6.2 Gene expression

We measured the expression in *Arabidopsis thaliana* seedlings of different genes involved in DNA damage and repair and the cell cycle after exposure to α-radiation from ^{241}Am for 4 and 7 days. Transcript levels are shown in Table 7.8 (Roots) and Table 7.9 (Shoots).

In the roots (Table 7.8), genes involved in the homologous recombination pathway (*RAD51 / DMC1*) were up-regulated at 4 days starting at 140 µGy h^{-1}, but showed no difference to the control treatment at 7 days. For the non-homologous end-joining pathway (NHEJ), only DNA ligase IV (*LIG4*) was differentially expressed after 7 days at 1910 µGy h^{-1}. Repair of organelle DNA

was also up-regulated starting at 140 µGy h^{-1} at 4 days, as measured by the transcript levels of Polymerase Gamma 1 (*POLG1*), but not after 7 days.
Transcript levels of PARP2 (Poly- (ADP-ribose])polymerase 2), a protein involved in the signalling response to single-stranded breaks (SSB) in DNA, were significantly increased compared to control at both time points. At 4 days, transcripts were elevated at 140 and 2400 µGy h^{-1}, whereas those at 1910 µGy h^{-1} and 10800 µGy h^{-1} were increased at 7 days of ^{241}Am exposure. *PARP1*, however, did not show dose-rate dependent expression. Among the genes involved in the cell cycle, only GAR1 was differentially expressed, with strong up-regulation at 140 µGy h^{-1} at 4 days, and above 1910 µGy h^{-1} after 7 days. *CKS1*, which is involved in cell cycle timing, showed an increasing trend in expression levels at both time points.

No changes in gene expression were found in the shoots, except for *PARP2*, which was up-regulated starting at 4.1 µGy h^{-1} at 7 days of exposure (Table 7.9).

7.3.7 Anti-oxidative response

7.3.7.1 Antioxidant Metabolites

We analysed the state of the ascorbate-glutathione scavenging pathway in roots and shoots after 7 days by spectrophotometrically measuring the concentration levels of the reduced and oxidised forms of ascorbate and glutathione. These levels also allowed for a calculation of the reduction state of each redox couple.

In the shoots, total Ascorbate levels (AsA + DHA; Figure 7.4A) remained constant at all dose rates (ANOVA, $F_{4,14} = 2.33$, $p = 0.11$) , while the redox couple shifted progressively towards the oxidised form, with significantly reduced AsA levels and increased DHA levels at 2650 µGy h^{-1} (Figure 7.4A). At this dose rate, the reduction state had decreased to 63% (Figure 7.4A; right).

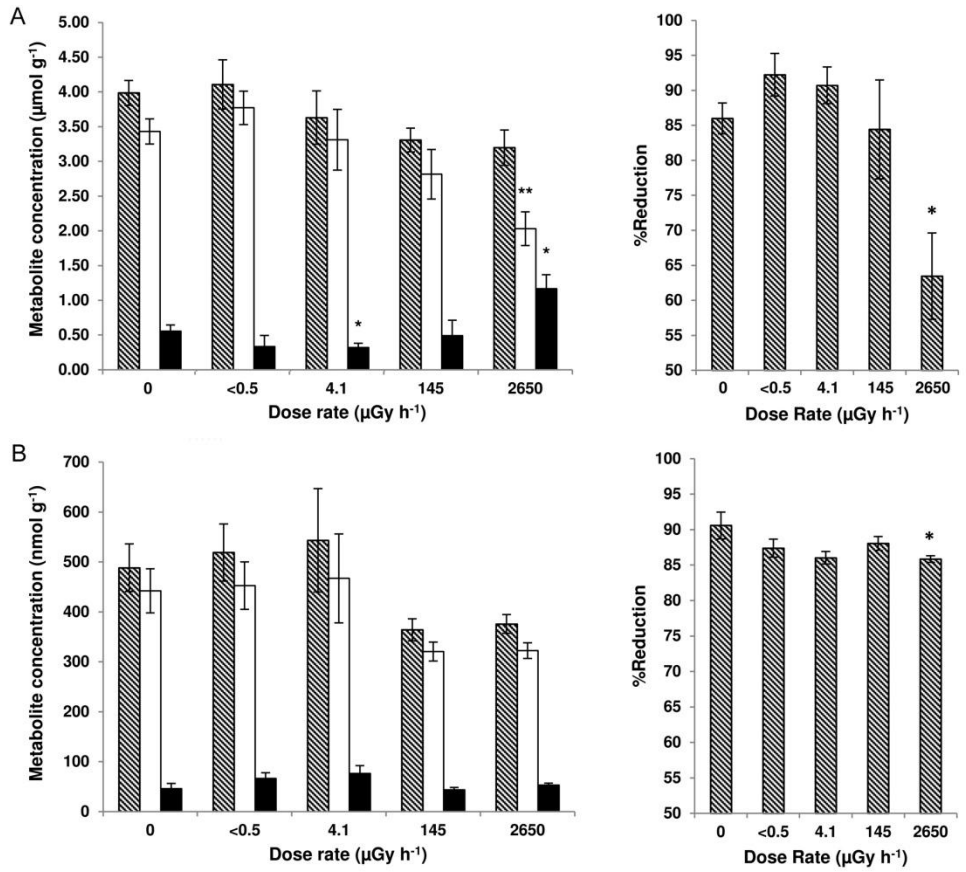

Figure 7.4: Antioxidative metabolite concentrations in *Arabidopsis* shoots exposed to ^{241}Am for 7 days. **A.** Concentrations of total ascorbate (AsA + DHA; grey bars), reduced ascorbate (white bars), dehyroascorbate (DHA; black bars) and the reduction status (right graph). **B.** Concentrations of total glutathione (GSH + GSSG; grey bars), GSH (white bars) , GSSG (black bars) and the degree of reduction (right graph). Significance levels for each metabolite compared to control are * $p<0.05$, ** $p<0.01$ *** $p<0.001$. Values are mean and SE of at least 3 biological replicates.

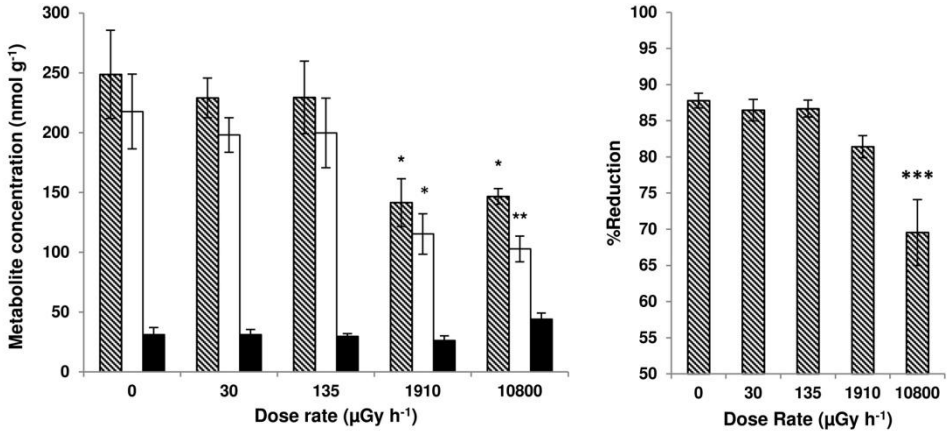

Figure 7.5: Concentrations of total glutathione (GSH + GSSG; grey bars), GSH (white bars) , GSSG (black bars) and the degree of reduction (right graph) in *Arabidopsis* roots exposed to ^{241}Am for 7 days. Significance levels for each metabolite compared to control are * $p<0.05$, ** $p<0.01$ *** $p<0.001$. Values are mean and SE of at least 3 biological replicates.

Glutathione levels remained constant at all dose rates (Figure 7.4B) for total glutathione (ANOVA, $F_{4,14} = 1.99$, $p = 0.15$), the oxidised form GSSG (ANOVA, $F_{4,14} = 1.84$, $p = 0.17$) and the reduced form GSH (ANOVA, $F_{4,14} = 2.07$, $p = 0.14$). However, as for ascorbate, the reduction state of the GSH/GSSG couple was significantly decreased by 5% at 2650 µGy h^{-1}.

Ascorbate levels in the roots could not be measured possibly because they were either too low or because stress-induced components interfered with the method. A similar observation has been made for measurements in Uranium-contaminated *Arabidopsis thaliana* roots (Eline Saenen, personal communication).

Total and reduced glutathione concentrations were found to be significantly reduced compared to control at 1910 and 10800 µGy h^{-1} (Figure 7.5; left), whilst GSSG levels remained constant (ANOVA, $F_{4,14} = 2.36$, $p = 0.10$). The

reduction state was significantly reduced by 20% at 10800 µGy h^{-1} (Figure 7.5; right).

7.3.7.2 Gene expression

Transcript levels for genes involved in oxidative stress and anti-oxidative responses are shown in Table 7.10 (Roots) and Table 7.11 (Shoots).

The root expression pattern for NADPH oxidases was limited to the highest dose rate treatment, with significantly increased *RBOHA* transcript levels at 4 days and a similar increase for *RBOHC* at 7 days (Table 7.10). Lipoxygenase 1, involved in stress signalling, was also up-regulated at 4 days for that treatment, but down-regulated after 7 days.

Superoxide CuZnSOD scavengers (cytoplasmatic *CSD1/* peroxisomal *CSD3*) and hydrogen peroxide scavengers (catalases *CAT2/CAT3*) were up-regulated at 4 days above 140 µGy h^{-1}, (Table 7.10), while after 7 days only *CSD1* and *CAT3* were significantly up-regulated at 1910 µGy h^{-1}. Changes in ascorbate peroxidase (*APX1*) and glutathione reductase (*GR1*) expression levels were only observed at 4 days, with strong up-regulation of both genes starting from 140 µGy h^{-1} (Table 7.10).

In the shoots, only NADPH oxidases showed dose-dependent differences in expression levels. After 4 days, *RBOHC* transcripts were significantly increased at 4500 µGy h^{-1}, while at 7 days *RBOHA* and *RBOHE* expression was suppressed (Table 7.11).

		0 Bq L^{-1}	**50 Bq L^{-1}**	**500 Bq L^{-1}**	**5 000 Bq L^{-1}**	**50 000 Bq L^{-1}**
	4 d	*0 µGy h^{-1}*	*29 µGy h^{-1}*	*140 µGy h^{-1}*	*2400 µGy h^{-1}*	*35000 µGy h^{-1}*
	7 d	*0 µGy h^{-1}*	*30 µGy h^{-1}*	*135 µGy h^{-1}*	*1910 µGy h^{-1}*	*10800 µGy h^{-1}*
KU80	*4 d*	1.00 ± 0.06	1.05 ± 0.05	1.16 ± 0.22	0.97 ± 0.06	0.81 ± 0.13
	7 d	1.04 ± 0.20	0.49 ± 0.03	0.43 ± 0.03	1.15 ± 0.24	1.14 ± 0.27
LIG4	*4 d*	1.00 ± 0.11	1.91 ± 0.72	4.02 ± 0.76	2.70 ± 0.64	2.13 ± 0.92
	7 d	1.64 ± 0.36	0.92 ± 0.22	1.22 ± 0.35	4.95 ± 1.34	3.62 ± 0.89
RAD51	*4 d*	1.00 ± 0.33	0.78 ± 0.42	3.96 ± 1.19	3.10 ± 0.90	4.10 ± 1.19
	7 d	2.63 ± 0.91	2.51 ± 0.80	3.86 ± 0.94	3.17 ± 1.26	1.77 ± 1.05
DMC1	*4 d*	1.00 ± 0.34	1.60 ± 0.60	2.15 ± 0.60	7.05 ± 2.53	3.70 ± 1.34
	7 d	1.96 ± 0.82	1.94 ± 0.63	1.83 ± 0.63	0.84 ± 0.28	1.26 ± 0.81
PARP1	*4 d*	1.00 ± 0.91	1.04 ± 1.08	3.10 ± 2.19	2.82 ± 1.81	2.52 ± 1.97
	7 d	1.62 ± 1.08	0.50 ± 0.34	0.42 ± 0.29	1.23 ± 0.95	0.86 ± 0.63
PARP2	*4 d*	1.00 ± 0.37	0.45 ± 0.18	2.83 ± 0.83	2.57 ± 0.70	1.25 ± 0.39
	7 d	0.52 ± 0.14	0.89 ± 0.33	0.85 ± 0.25	2.72 ± 0.86	2.43 ± 0.90
LPP1	*4 d*	1.00 ± 0.20	0.29 ± 0.05	2.81 ± 1.40	1.96 ± 0.64	1.79 ± 0.59
	7 d	5.23 ± 1.28	4.34 ± 0.91	14.9 ± 4.80	11.9 ± 5.70	9.04 ± 2.20
POLG1	*4 d*	1.00 ± 0.13	1.18 ± 0.32	4.79 ± 1.20	3.99 ± 0.74	3.46 ± 0.67
	7 d	1.77 ± 0.29	1.31 ± 0.28	1.24 ± 0.26	1.93 ± 0.43	1.65 ± 0.38
CKS1	*4 d*	1.00 ± 1.25	0.52 ± 0.53	7.39 ± 6.86	3.96 ± 3.62	3.48 ± 3.14
	7 d	1.32 ± 1.24	2.00 ± 1.90	1.32 ± 1.18	8.74 ± 8.18	6.39 ± 5.66
GAR1	*4 d*	1.00 ± 1.39	0.05 ± 0.06	7.54 ± 7.74	4.03 ± 4.03	9.25 ± 9.25
	7 d	9.82 ± 10.3	3.81 ± 3.99	3.69 ± 3.67	25.4 ± 25.8	16.8 ± 16.9

Table 7.8: Gene expression of genes involved in DNA repair and the cell cycle in the roots of *Arabidopsis thaliana* after exposure to ^{241}Am for 4 and 7 days. Data are presented relative to 0 Bq L^{-1}. Dark grey shading indicate significant up-regulation ($p<0.05$) compared to the control at that time point. Light grey shading indicates significant down-regulation ($p<0.05$). Values are mean ± SE of at least 3 biological replicates.

		0 Bq L^{-1}	**50 Bq L^{-1}**	**500 Bq L^{-1}**	**5 000 Bq L^{-1}**	**50 000 Bq L^{-1}**
	4 d	*0 µGy h^{-1}*	*<1.0 µGy h^{-1}*	*5.7 µGy h^{-1}*	*291 µGy h^{-1}*	*4500 µGy h^{-1}*
	7 d	*0 µGy h^{-1}*	*<0.5 µGy h^{-1}*	*4.1 µGy h^{-1}*	*145 µGy h^{-1}*	*2650 µGy h^{-1}*
KU80	*4 d*	1.00 ± 0.23	0.75 ± 0.16	0.69 ± 0.22	1.26 ± 0.21	0.58 ± 0.14
	7 d	0.91 ± 0.20	1.21 ± 0.23	1.42 ± 0.28	1.89 ± 0.44	2.38 ± 0.66
LIG4	*4 d*	1.00 ± 0.31	1.14 ± 0.41	0.74 ± 0.19	0.80 ± 0.19	1.40 ± 0.61
	7 d	0.68 ± 0.15	0.65 ± 0.18	0.67 ± 0.16	0.55 ± 0.16	0.77 ± 0.21
RAD51	*4 d*	1.00 ± 0.31	1.36 ± 0.45	0.75 ± 0.22	0.86 ± 0.21	0.93 ± 0.45
	7 d	0.69 ± 0.16	0.65 ± 0.18	0.67 ± 0.16	0.57 ± 0.14	0.95 ± 0.26
DMC1	*4 d*	1.00 ± 0.31	1.14 ± 0.41	0.74 ± 0.19	0.80 ± 0.19	1.40 ± 0.61
	7 d	0.68 ± 0.15	0.65 ± 0.18	0.67 ± 0.16	0.72 ± 0.22	0.9 ± 0.23
PARP1	*4 d*	1.00 ± 0.06	0.54 ± 0.16	0.62 ± 0.2	1.23 ± 0.27	0.45 ± 0.05
	7 d	0.95 ± 0.18	1.47 ± 0.15	1.60 ± 0.28	1.41 ± 0.20	1.69 ± 0.25
PARP2	*4 d*	1.00 ± 0.26	0.79 ± 0.26	0.35 ± 0.08	0.77 ± 0.22	1.46 ± 0.83
	7 d	0.39 ± 0.09	1.05 ± 0.21	1.13 ± 0.26	1.13 ± 0.24	1.47 ± 0.38
LPP1	*4 d*	1.00 ± 0.31	1.36 ± 0.45	0.74 ± 0.19	0.80 ± 0.19	1.40 ± 0.61
	7 d	0.68 ± 0.15	0.65 ± 0.18	0.67 ± 0.16	0.75 ± 0.27	0.9 ± 0.23
POLG1	*4 d*	1.00 ± 0.31	1.14 ± 0.41	0.74 ± 0.19	0.80 ± 0.21	1.40 ± 0.61
	7 d	0.69 ± 0.16	0.65 ± 0.18	0.67 ± 0.16	0.72 ± 0.22	0.90 ± 0.23
CKS1	*4 d*	1.00 ± 0.53	5.65 ± 2.14	1.21 ± 0.74	2.88 ± 1.10	1.05 ± 0.47
	7 d	1.47 ± 0.57	2.07 ± 1.09	3.68 ± 1.39	2.76 ± 1.41	3.05 ± 1.43
GAR1	*4 d*	1.00 ± 0.42	0.08 ± 0.03	0.25 ± 0.19	0.18 ± 0.06	0.91 ± 0.62
	7 d	0.19 ± 0.06	0.59 ± 0.29	0.21 ± 0.07	0.18 ± 0.09	0.69 ± 0.47

Table 7.9: Gene expression of genes involved in DNA repair and the cell cycle in the shoots of *Arabidopsis thaliana* after exposure to ^{241}Am for 4 and 7 days. Data are presented relative to 0 Bq L^{-1}. Dark grey shading indicate significant up-regulation ($p<0.05$) compared to the control at that time point. Light grey shading indicates significant down-regulation ($p<0.05$). Values are mean ± SE of at least 3 biological replicates.

		0 Bq L^{-1}	**50 Bq L^{-1}**	**500 Bq L^{-1}**	**5 000 Bq L^{-1}**	**50 000 Bq L^{-1}**
	4 d	*0 µGy h^{-1}*	*29 µGy h^{-1}*	*140 µGy h^{-1}*	*2400 µGy h^{-1}*	*35000 µGy h^{-1}*
	7 d	*0 µGy h^{-1}*	*30 µGy h^{-1}*	*135 µGy h^{-1}*	*1910 µGy h^{-1}*	*10800 µGy h^{-1}*
RBOHA	4 d	1.00 ± 0.42	1.59 ± 0.88	4.65 ± 1.58	4.45 ± 1.57	5.05 ± 1.81
	7 d	3.17 ± 1.41	1.78 ± 0.56	2.29 ± 0.71	1.76 ± 0.60	1.86 ± 0.89
RBOHC	4 d	1.00 ± 0.73	2.14 ± 1.58	7.79 ± 5.46	7.93 ± 5.44	2.57 ± 1.41
	7 d	1.00 ± 0.26	0.43 ± 0.09	1.44 ± 0.39	0.51 ± 0.29	6.66 ± 1.41
RBOHE	4 d	1.00 ± 0.64	0.54 ± 0.36	2.18 ± 1.07	2.25 ± 1.02	2.76 ± 1.33
	7 d	1.00 ± 0.40	0.34 ± 0.14	1.11 ± 0.40	0.33 ± 0.11	0.85 ± 0.40
LOX1	4 d	1.00 ± 0.69	0.57 ± 0.46	3.01 ± 1.65	2.84 ± 1.57	3.87 ± 2.02
	7 d	6.47 ± 3.68	3.95 ± 2.53	3.28 ± 1.65	2.72 ± 1.51	0.73 ± 0.42
CSD1	4 d	1.00 ± 0.05	0.49 ± 0.05	3.78 ± 0.59	3.97 ± 0.60	2.49 ± 0.41
	7 d	3.57 ± 0.76	3.01 ± 0.55	4.03 ± 0.71	15.53 ± 14.00	9.09 ± 2.58
CSD2	4 d	1.00 ± 0.30	0.95 ± 0.27	2.00 ± 0.93	2.12 ± 0.81	2.41 ± 0.63
	7 d	7.10 ± 2.11	4.72 ± 1.12	3.90 ± 1.52	8.87 ± 2.84	0.87 ± 0.19
CSD3	4 d	1.00 ± 0.50	1.40 ± 0.81	3.27 ± 1.24	3.65 ± 1.32	3.30 ± 1.42
	7 d	1.94 ± 0.83	1.21 ± 0.46	1.43 ± 0.54	1.71 ± 0.67	1.28 ± 0.71
FSD1	4 d	1.00 ± 0.03	4.27 ± 0.51	9.15 ± 2.46	7.35 ± 0.16	9.84 ± 1.97
	7 d	8.35 ± 2.05	5.04 ± 1.59	6.97 ± 1.74	10.84 ± 2.51	6.37 ± 0.65
FSD2	4 d	1.00 ± 0.99	0.30 ± 0.22	0.96 ± 0.84	0.32 ± 0.22	7.99 ± 5.96
	7 d	8.84 ± 6.48	7.67 ± 5.76	6.74 ± 4.74	13.09 ± 9.23	7.07 ± 5.38
FSD3	4 d	1.00 ± 0.50	1.25 ± 0.65	2.05 ± 0.99	1.67 ± 0.63	1.29 ± 0.54
	7 d	1.25 ± 0.57	0.83 ± 0.35	1.25 ± 0.45	1.38 ± 0.61	2.52 ± 1.80
CAT1	4 d	1.00 ± 0.70	1.27 ± 1.19	4.05 ± 2.5	2.29 ± 1.36	2.9 ± 1.81
	7 d	2.51 ± 1.69	0.70 ± 0.39	2.14 ± 1.42	1.66 ± 1.21	1.08 ± 0.65
CAT2	4 d	1.00 ± 0.54	0.77 ± 0.34	3.04 ± 1.19	6.39 ± 2.60	3.18 ± 1.22
	7 d	4.84 ± 2.09	3.24 ± 1.44	4.92 ± 1.93	5.82 ± 2.42	5.12 ± 2.78
CAT3	4 d	1.00 ± 0.41	0.53 ± 0.21	5.16 ± 1.65	6.82 ± 2.15	0.02 ± 0.02
	7 d	4.96 ± 1.46	3.59 ± 1.31	5.48 ± 1.63	15.21 ± 5.25	11.46 ± 4.03
GR1	4 d	1.00 ± 0.72	0.75 ± 0.63	6.56 ± 4.01	3.93 ± 2.41	7.67 ± 4.39
	7 d	5.16 ± 2.94	7.61 ± 4.26	6.10 ± 3.32	8.72 ± 4.80	6.15 ± 3.15
APX1	4 d	1.00 ± 0.59	1.26 ± 0.70	8.32 ± 4.66	3.66 ± 1.97	7.63 ± 3.34
	7 d	5.02 ± 2.11	2.91 ± 1.41	4.71 ± 2.30	5.20 ± 2.41	4.56 ± 2.35

Table 7.10: Gene expression of genes involved in oxidative stress in the roots of *Arabidopsis thaliana* after exposure to ^{241}Am for 4 and 7 days. Data are presented relative to 0 Bq L^{-1}. Dark grey shading indicate significant up-regulation ($p<0.05$) compared to the control at that time point. Light grey shading indicates significant down-regulation ($p<0.05$). Values are mean ± SE of at least 3 biological replicates.

		0 Bq L^{-1}	**50 Bq L^{-1}**	**500 Bq L^{-1}**	**5 000 Bq L^{-1}**	**50 000 Bq L^{-1}**
	4 d	*0 µGy h^{-1}*	*<1.0 µGy h^{-1}*	*5.7 µGy h^{-1}*	*291 µGy h^{-1}*	*4500 µGy h^{-1}*
	7 d	*0 µGy h^{-1}*	*<0.5 µGy h^{-1}*	*4.1 µGy h^{-1}*	*145 µGy h^{-1}*	*2650 µGy h^{-1}*
RBOHA	*4 d*	1.00 ± 0.40	0.80 ± 0.39	0.73 ± 0.28	0.69 ± 0.31	0.14 ± 0.06
	7 d	2.2 ± 0.65	0.82 ± 0.38	0.84 ± 0.25	1.28 ± 0.39	0.98 ± 0.48
RBOHC	*4 d*	1.00 ± 0.52	1.70 ± 0.71	0.93 ± 0.38	1.77 ± 1.13	4.17 ± 1.58
	7 d	1.63 ± 0.73	1.36 ± 0.75	1.00 ± 0.50	1.86 ± 0.92	2.01 ± 1.05
RBOHE	*4 d*	1.00 ± 0.51	1.15 ± 0.60	1.15 ± 0.75	1.55 ± 0.68	0.43 ± 0.36
	7 d	5.32 ± 1.96	1.15 ± 0.67	1.17 ± 0.48	1.76 ± 0.71	1.36 ± 0.51
LOX2	*4 d*	1.00 ± 0.93	0.34 ± 0.36	2.61 ± 2.49	1.77 ± 1.37	1.53 ± 1.41
	7 d	0.44 ± 0.32	0.37 ± 0.35	1.54 ± 1.01	2.62 ± 2.02	1.59 ± 1.05
CSD1	*4 d*	1.00 ± 0.53	1.57 ± 0.68	0.82 ± 0.38	2.52 ± 0.98	0.28 ± 0.28
	7 d	1.39 ± 0.56	2.34 ± 1.70	0.71 ± 0.34	1.49 ± 0.61	1.25 ± 0.75
CSD2	*4 d*	1.00 ± 0.28	0.89 ± 0.34	0.46 ± 0.16	0.95 ± 0.19	0.71 ± 0.20
	7 d	0.43 ± 0.10	1.01 ± 0.26	1.24 ± 0.27	0.74 ± 0.17	0.71 ± 0.21
CSD3	*4 d*	1.00 ± 0.29	1.08 ± 0.38	0.26 ± 0.14	0.98 ± 0.28	0.62 ± 0.18
	7 d	0.92 ± 0.21	1.19 ± 0.26	0.99 ± 0.20	1.13 ± 0.25	1.07 ± 0.23
FSD1	*4 d*	1.00 ± 0.05	0.68 ± 0.07	0.78 ± 0.25	1.12 ± 0.23	0.35 ± 0.10
	7 d	0.53 ± 0.16	1.26 ± 0.35	1.58 ± 0.32	0.50 ± 0.22	0.87 ± 0.10
FSD2	*4 d*	1.00 ± 0.33	1.57 ± 0.53	1.17 ± 0.38	1.18 ± 0.63	2.38 ± 0.94
	7 d	1.30 ± 0.36	0.99 ± 0.47	1.12 ± 0.49	1.14 ± 0.43	1.00 ± 0.27
FSD3	*4 d*	1.00 ± 0.12	0.45 ± 0.12	0.45 ± 0.12	0.97 ± 0.28	0.29 ± 0.06
	7 d	0.42 ± 0.09	0.83 ± 0.07	0.91 ± 0.08	1.13 ± 0.14	1.04 ± 0.23
CAT1	*4 d*	1.00 ± 0.49	1.62 ± 0.87	0.67 ± 0.38	1.24 ± 0.56	0.81 ± 0.35
	7 d	24.0 ± 16.1	1.92 ± 0.98	3.1 ± 1.14	2.08 ± 0.81	0.60 ± 0.48
CAT2	*4 d*	1.00 ± 0.56	0.78 ± 0.58	0.45 ± 0.24	0.86 ± 0.42	0.25 ± 0.20
	7 d	0.66 ± 0.29	1.06 ± 0.46	1.11 ± 0.46	0.82 ± 0.39	0.36 ± 0.24
CAT3	*4 d*	1.00 ± 0.41	0.29 ± 0.10	0.77 ± 0.49	1.19 ± 0.49	0.60 ± 0.37
	7 d	1.56 ± 0.49	2.4 ± 0.72	2.43 ± 0.77	2.44 ± 0.72	1.81 ± 0.55
GR1	*4 d*	1.00 ± 0.54	1.13 ± 0.50	0.68 ± 0.31	0.75 ± 0.33	0.37 ± 0.20
	7 d	0.94 ± 0.38	1.00 ± 0.42	0.98 ± 0.37	0.75 ± 0.30	0.37 ± 0.20
APX1	*4 d*	1.00 ± 0.16	0.67 ± 0.23	0.33 ± 0.05	0.44 ± 0.16	0.31 ± 0.14
	7 d	0.56 ± 0.07	0.51 ± 0.09	0.51 ± 0.06	0.62 ± 0.07	0.55 ± 0.07

Table 7.11: Gene expression of genes involved in oxidative stress in the shoots of *Arabidopsis thaliana* after exposure to ^{241}Am for 4 and 7 days. Data are presented relative to 0 Bq L^{-1}. Dark grey shading indicate significant up-regulation ($p<0.05$) compared to the control at that time point. Light grey shading indicates significant down-regulation ($p<0.05$).

7.4 Discussion

This study aimed to investigate the biological effects of α-radiation in seedlings of *Arabidopsis thaliana* by chronic exposure to different concentrations of ^{241}Am. To this aim, we analysed uptake and distribution of the element into roots and shoots, and measured biological responses on the morphological, physiological and molecular level.

7.4.1 ^{241}Am shows high transfer to the roots and low translocation to the leaves

Most of the data in literature on aquatic uptake of ^{241}Am have been obtained through studies on submerged macrophytes in the Yenisei river (Russia). Zotina et al. (2010) found a transfer factor between 1.1 to 2.3 x 10^4 L kg^{-1} for leaves of *Elodea canadensis*, which was comparable to the values found in their earlier studies (Bulsanovsky et al., 2005). In comparison, transfer to root dry biomass in our study was an order of magnitude lower (table 7.3). This is likely to be due to a difference in uptake route (as *Elodea* has submerged leaves, whereas the ^{241}Am in *Arabidopsis* was transferred from the roots) and a possible difference of Am bioavailability due to differences in the test medium. This large variation in transfer parameters between studies is not limited to ^{241}Am, but also exists for other (trans)uranic elements such as plutonium and uranium (Hosseini et al., 2008). Remarkably, the ^{241}Am transfer parameters found in the present study for 14-day old *Arabidopsis* roots were tenfold higher than those we obtained in a previous uptake study on 18-day old seedlings in a similar setup (Biermans et al., 2013), indicating a possible effect of age in uptake of ^{241}Am. The shoot:root pattern was comparable to that of other transuranic elements, though ^{241}Am transfer to the shoots was tenfold higher than that for plutonium (Lee et al., 2002). The uptake of ^{241}Am from the medium to the root, as well as root-to-shoot transfer initially increased with increasing medium concentration (Tables

7.2 and 7.3), though it was also apparent that root uptake (and consequently shoot transfer) decreased between 4 and 7 days of exposure, and that this reduction in uptake between harvest points became stronger with increasing medium activity concentration. This could either be the result of a change in the bioavailability of ^{241}Am, or by a disruption of uptake and transport into the tissue. The results on biomass and physiology seem to suggest the latter, though a more in-depth analysis of nutrients and ^{241}Am translocation is necessary to confirm and refine this hypothesis. Furthermore, very little is known about the uptake- and transport routes of americium in plants, which makes an analysis of potential transport and translocation impairment difficult, due to lack of mechanistic background. At some point during root transport, the element has to move to the symplast to pass the pericycle. Fractionation studies suggest a dominant association to the apoplast (Bondareva et al., 2010; Zotina et al., 2011). In summary, our data suggest that ^{241}Am is readily transported to the *Arabidopsis thaliana* roots under hydroponic conditions, and has a low root-to-shoot mobility. After 4 to 7 days of exposure, the uptake and translocation of the radionuclide showed a significant decrease, resulting in lower average dose rates in the organs.

7.4.2 α-radiation induces dose-dependent effects on biomass, redox balance and transcription of DNA repair and ROS scavenging pathways in Arabidopsis thaliana *roots.*

The dose-dependent effects of α-radiation were most clear in the roots, which up to 1910-2400 µGy h^{-1} presented a dose-dependent pattern with a strong scavenging and DNA repair response at the transcriptional level and a healthy ascorbate-glutathione cycle. In contrast, roots of seedlings exposed to the highest dose rate displayed growth reduction, loss of redox control and up-regulation oxidative burst and signalling.

One of the main morphological effects of radiation in plants described in literature is a reduction of fresh weight and growth rate (Esnault et al., 2010;

Holst & Nagel, 1997). In our study, only the plants exposed to the highest ^{241}Am levels showed reduced root growth (Table 7.6), though there was a strong decrease in the percentage of root dry weight between 4 and 7 days of exposure in all treatments. Despite these clear effects on biomass and growth in the roots, there was no indication of increased steady state levels of oxidative DNA damage due to α-radiation exposure (Figure 7.4). Nevertheless, at 4 days we found strong up-regulation of both NHEJ and HR double-strand break (DSB) repair pathways (LIG4 / RAD51 / DMC1) starting at 140 µGy h^{-1}, as well as increased transcript levels of *POLG1* (Table 7.8), suggesting that DNA damage does occur during the exposure. *POLG1* is involved in organelle DNA repair, and has previously been shown to be up-regulated under abiotic stress (Boesch et al., 2011; Parent et al., 2011) while *PARP1*, a Poly(ADP-Ribosyl)-polymerase involved in detection and repair of single-strand breaks (Chen et al., 1994), was not differentially expressed. In contrast, *PARP2*, which has a stress signalling function (Doucet-Chabeaud et al., 2001) showed transcript levels which were two-fold up-regulated in most treatments. While an early response on expression of SSB repair cannot be excluded based on our data, this transcriptional response and the absence of oxidative DNA damage do seem to agree with observations made by previous authors that α-radiation creates more DSB than SSB (Hodgekins et al., 1996). This is a direct result from the high LET compared to γ- or β- decay. When α-particles interact with DNA, they and their secondary ROS are able to cause multiple modifications and lesions in DNA on a very short distance, creating multiple local sites of complex DNA damage which result in DSB.

Steady-state oxidative DNA damage is the net result of ROS damage on one side, and DNA repair and ROS scavenging pathways on the other. If both processes counterbalance ROS production, the net result is a maintenance of the steady control levels of base modification (Figure 7.4). Plants contain several pathways to detoxify ROS before they create damage to biomolecules (Mittler et al., 2002). Superoxide dismutases (SODs) transform superoxide into hydrogen peroxide, which is subsequently transformed by catalases (CATs) in water. The

strong up-regulation of catalases (*CAT2/3*) and CuZnSODs (*CSD1/3*) at 140 and 2400 μGy h^{-1} in the roots after 4 days suggests that α-radiation from ^{241}Am induced an early transcriptional response to ROS scavenging in those treatments (Table 7.10). The response of *CAT*- and *CSD* genes was less apparent at the highest dose rate, while that treatment was characterised by strong up-regulation of ROS-producing NADPH oxidases (*RBOHA/C*) and lipoxygenase (*LOX1*), both involved in the oxidative burst and signalling (Bhattacharjee, 2005; Porta & Rocha-Sosa, 2002).

Hydrogen peroxide is also detoxified by the AsA-GSH pathway, and AsA can directly scavenge several types of ROS (Noctor & Foyer, 1998). The total root glutathione levels (GSSG + GSH) at 7 days of exposure decreased with increasing dose rate (Figure 7.5) while the amount of reduced glutathione declined, leading to a decline in redox balance. This was most clear for the highest ^{241}Am treatment, which also showed the most pronounced response on biomass and uptake. A shift of the redox pool in the roots to the oxidised form is an indication of severe oxidative stress (Blokhina et al., 2003), as it reflects the loss of control in the AsA-GSH cycle. In this context, the strong up-regulation at 4 days of two key enzymes in the cycle, ascorbate peroxidase (*APX1*) and glutathione reductase (*GR1*) (Table 7.10), might therefore represent an attempt to compensate for the declining redox balance by establishing more efficient recycling of the metabolites. It is clear from the data however that this did not suffice to maintain the balance at the two highest dose rates. Previous studies have shown an increase in capacity of these enzymes under metal stress (Cuypers, 2000; Smeets et al., 2005), though Vanhoudt et al. (2008) has noted that increased transcription does not necessary translate to a similar response on the protein level.

In summary, *Arabidopsis thaliana* roots were able to maintain redox balance in response to a week-long exposure to α-radiation up to dose rates within the order of magnitude of mGy h^{-1} by increasing transcription of DNA repair and scavenging pathways. However, at 10-fold higher dose rates, these responses

were no longer able to counterbalance ROS production, leading to a decline of redox balance.

7.4.3 α-radiation induces dose-dependent effects on redox balance and photosynthetic performance in Arabidopsis thaliana *shoots*

In the leaves, where dose rates are tenfold lower compared to the roots, a response on the transcriptional level is nearly absent at both harvest points, with only early up-regulation of *RBOHC* in the highest ^{241}Am treatment (Table 7.11) and late up-regulation of *PARP2* starting at 4.1 µGy h^{-1} (Table 7.9). Though this response might be shifted in time compared to the roots and therefore not visible at our harvest points, it is important to note that similar dose rates were able to elicit a transcriptional response in the roots. Despite the absence of a morphological or transcriptional response, there are clear indications that the shoots experience stress as well. The reduction status of both ascorbate and glutathione had significantly declined in the shoots exposed to the highest dose rate (2650 µGy h^{-1}) at the end of the 7-day exposure period. Furthermore, photosynthesis was affected after 7 days of exposure to α-radiation.

Though there were no transcriptional effects in the shoots, we did observe effects on the physiological level. Photosynthesis showed dose-dependent effects in efficiency, electron transport rate and energy use. Up until a dose rate of 145 µGy h^{-1}, Fv/Fm remained stable, while the performance of photosynthesis was improved by an increase in the photosynthetic pathway at the cost of NPQ (Figure 7.2). Above that dose rate, control decreased, leading to damage to the photosynthetic apparatus. Fv/Fm is the most widely used indicator of photosynthetic performance, though it only gives an indication about the maximum fraction of light that could potentially go the photosynthetic pathway at photosystem II and not about the performance of the chain itself (Genty et al., 1989). Therefore the other parameters, such as the distribution of energy

between different pathways and electron transfer, are needed to give additional mechanistic information.

Light energy captured by light harvesting complexes can follow three pathways: photosynthesis, controlled non-photochemical quenching as heat (NPQ), or non-controlled quenching (NO) as fluorescence (Maxwell & Johnson, 2000). The latter pathway can cause damage to the photosynthesis chain, and is therefore indirectly kept under control in healthy plants by modulating the levels of controlled quenching as heat (Adams et al., 1999). In our study, there was a clear difference between the lowest three treatments and the plants exposed to the highest ^{241}Am levels. The decrease in both the chlorophyll a/b ratio and the chlorophyll/carotenoid ratio at 145 µGy h^{-1} points towards a role of larger light harvesting antennae and increased photoprotection in this response (Demmig-Adams et al., 1995). The observed increased relative input into the photosynthesis pathway was accompanied by a higher electron transport capacity (ETR_{max}) and light saturation point (Ek) (Figure 7.3 B and C). Both these parameters give an indication of the health and functioning of the photosynthesis chain downstream. A decrease in either is an indication of damage and photoinhibition, while an increase results from a positive modulation of electron chain capacity (Ralph & Gademan, 2005; White & Critchley, 1999). By contrast, the leaves exposed at 2650 µGy h^{-1} (the 36,700 Bq L^{-1} ^{241}Am treatment) showed decreased Fv/Fm (Figure 7.1), a strong decline in ETR_{max} and Ek compared to the control treatment (Figure 7.3) and a loss of NPQ control in favour of NO which resulted in the relative decline of the photosynthetic pathway (Figure 7.2). This increase in NO reflects increased damage to light harvesting complexes and the electron transport chain.

In conclusion we can state that, despite the absence of a clear transcriptional response, the shoots showed an overall pattern of redox balance and photosynthesis control up to 145 µGy h^{-1}, and loss of control in the highest treatment.

7.4.4 The overall effects of α-radiation from ^{241}Am on Arabidopsis thaliana *are dominated by the localisation and distribution pattern of the element.*

If we want to understand the effects of ^{241}Am α-exposure to the plant as a whole, we should compare and integrate the responses in root and shoot. The similarities between the effects in root and shoot, with a controlled molecular and physiological response in the 60, 360 and 2970 Bq L^{-1} treatments and more severe physiological and morphological effects in the 36,700 Bq L^{-1} treatment, suggest that when assessing the effects of α-radiation delivered by ^{241}Am, the responses in both organs cannot be considered entirely independent from each other. Feedback between both organs is likely to modify the local effects caused by radiation in each organ separately. Reduced transport of essential nutrients from root to shoot affects photosynthesis, while carbon fixation by photosynthesis determines the carbohydrates available for root growth and biomass (Eliasson, 1968, Kirschbaum, 2011). But which process initiates the effects caused by α-radiation from ^{241}Am? The decline in root fresh weight and the DNA repair response occurs already after 4 days, while the effects on photosynthesis in the shoots are only visible 3 days later. This observation favours the hypothesis that disruption of root function and nutrient transport causes an effect on photosynthetic efficiency, which in turn affects root growth and biomass. Vanhoudt et al. (2010) previously found a modified nutrient balance in *Arabidopsis thaliana* after exposure to chronic γ-radiation. Whether our observations are a result of the local radiation exposure in the shoots or mediated by root-to-shoot signalling remains to be elucidated. Finally, we should address the apparent difference in sensitivity of the root compared to the shoot at similar dose rates of α-radiation. This is reflected in the transcriptional response, which in the roots occurs starting at 140 µGy h^{-1}, and is largely absent in the shoots at all dose rates up to 4500 µGy h^{-1}. Though very few data on localisation of ^{241}Am are available, a clue might lie in the supposed transport route and micro-distribution of the radionuclide. A constant inflow of ^{241}Am migrates from the root surface towards the vascular bundle in the centre, a route which must at least locally involve symplastic transport to pass the

pericycle. Its strong affinity for the cell wall fraction (Bondareva et al., 2010) suggests that after transport to the shoots via the xylem, the element might end up predominantly in the apoplast of the vascular elements. As α-radiation has a very short range, it is likely that a substantial part of the decay energy remains contained within the crystalline structure of the cell wall.

In conclusion, it is clear from our data that α-radiation delivered by ^{241}Am induces dose-dependent effects on the morphological, physiological and molecular level. However, due to the difference in transfer of the element between roots and shoots, there was a large resulting difference in dose rate to which the organs are exposed and in the effects resulting from this exposure. Our data also suggest that the interplay between root and shoot functions is important in the understanding of the observed effects. However, to fully understand the chain of events in *Arabidopsis thaliana* which leads from ^{241}Am α-radiation damage to the observed dose-dependent effects on uptake, transport, growth, redox status and photosynthesis, a characterisation of the evolving nutrient profile during exposure and a more accurate description of ^{241}Am behaviour within the plant are essential paths for further research.

Chapter 8:

General Discussion

8.1 Introduction

Human activity in the NORM industry and nuclear power production has led to release of radioactive material in the environment, causing increased exposure of the biosphere to ionising radiation. To allow for a robust assessment of the risks of this exposure to non-human biota, there is a need for a better understanding of the biological effects and the mechanisms involved in the response to ionising radiation stress. As primary producers and important global food source, plants have an important role in both ecology and economy. Understanding how different types of ionising radiation affect plants on the morphological, physiological and molecular level was therefore the primary objective of this study, as well as understanding the links of growth and morphology to the underlying levels. Comparing the effects between different types of radiation might provide insight into the differences and overlaps between the responses to each.

However, as dose delivery is dependent on the geometry of the organism or organ taken into consideration and the activity concentration of the radionuclide in the tissue, we first needed to establish a dosimetry model for fast growing *Arabidopsis* seedlings which takes into account both growth and radionuclide uptake. Furthermore, as previous studies observed a wide range in radiosensitivity between species and between growth stages of a single species (Esnault et al., 2010), it was essential to first obtain an insight in the age-dependent sensitivity to ionising radiation of *Arabidopsis thaliana*.

8.2 General Discussion

8.2.1 A dynamic dosimetry model for plants

We based our dosimetry model for *Arabidopsis thaliana* on the methodology which was previously adopted within several of the international risk assessment approaches for non-human biota. These approaches are based upon approximation of an organism's geometry by an ellipsoid and the subsequent calculation by Monte Carlo simulation of the fraction of the decay energy absorbed within, assuming uniform distribution of the radionuclide inside the organism. For a given radionuclide, this results in internal and external dose conversion coefficient values (DCC) which convert activity concentration into internal and external dose rates. To account for the heterogeneous uptake patterns between seedling roots and shoots as well as the differences in geometry, a separate model for each organ was made.

A method was devised to easily determine *Arabidopsis thaliana* root and shoot geometry, using root length and rosette area as main parameters. Using a static model at first (Chapter 3), the behaviour and resulting doses delivered by three radionuclides, ^{241}Am, ^{90}Sr and ^{133}Ba, representative for α-, β- and γ-radiation, were compared. It could be concluded that, while the differences in doses between roots and shoots correlate well to the uptake pattern for each radionuclide separately (Tables 3.1 and 3.1), the differences in dose delivered between radionuclides are mostly determined by the link between geometry and the behaviour of the different ionising particles. These observations are especially of importance in fast-growing seedlings, which double in size (and mass) every 36 to 48h during their exponential growth phase.

The static model was therefore expanded for the three radionuclides into a dynamic mathematical framework, adding time-dependent equations for DCC and radionuclide uptake (Chapter 4) for the first three weeks of growth. The

effect of growth on dosimetry is most apparent in the leaves, where the DCC values vary during growth due to a fast increase in rosette diameter (Figure 4.1; Tables 4.1 and 4.2). The influence of seedling growth on dose estimates for *Arabidopsis thaliana* are most visible for β-variation delivered by ^{90}Sr (Figure 4.2A-C), and to a much lesser extent for ^{133}Ba and ^{241}Am. For the roots, increase along the main growth axis does not affect external or internal dosimetry because of the very limited influence of root length on DCC (Table 4.3). Apart from the effects obtained by adding growth into the model, the addition of the equations for radionuclide uptake provide a more realistic description of the evolution of dose rate and dose throughout the exposure duration. Although we have applied this to *Arabidopsis thaliana* in particular, we postulate that any small organism which goes through fast geometrical changes is likely to present similar changes in dose absorption due to its growth. Furthermore, our methodology can be easily applied to other plant species with a rosette, or to floating species such as the macrophyte *Lemna minor*. Furthermore, inclusion of a more realistic description of uptake dynamics in a dosimetry model is essential for all organisms, regardless of their size or the radionuclide involved. Even more so in effects studies, where conservative dose and dose rate estimates are not desirable.

In addition to presenting an overall improvement compared to static dosimetry models (Figure 4.3A-C), our modified Monte Carlo methodology to calculate absorbed energy fractions dispenses with some of the technical limitations of current tools included in risk assessment models (Figure 3.1), and provides an automated tool to perform multiple DCC calculations. This ability to perform calculations for a multitude of geometrical parameters in batch opens roads to quickly explore new options in non-human biota dosimetry, such as dose rate versus size studies.

One of these options is a plant dosimetry model which bases its calculation of the DCC directly on the (logistic) growth parameters of the plant species and does not rely on the individual measurements of geometry and the subsequent

individual DCC calculations by Monte Carlo. Such a model would allow for more robust use over several different plant species, or for a more detailed dosimetric description of plant organs such as an individual leaf.

8.2.2 Age-dependent effects of ionsing radiation in Arabidopsis thaliana

A first attempt to establish a dose-response curve for β-radiation with ^{90}Sr taught us that 18-days old *Arabidopsis thaliana* seedlings did not show altered biomass or growth, despite the high uptake and subsequent dose (Chapter 3). At the physiological level, minor but inconclusive effects on photosynthesis were observed (Figure 3.2 and 3.3). As it was essential for our study to link observed morphological and physiological effects to the underlying molecular responses, we needed to assess whether a more sensitive seedling stage could be found. Seedlings of different ages (7, 10 and 14 days old) were subjected to 168 hours of 100 mGy h^{-1} external γ-radiation (Chapter 5). The effects on growth, recovery and DNA damage and repair were determined at several time points during exposure.

The results of this study show a clear transient γ-radiation exposure mediated increase in shoot biomass in plants of all ages, though the amplitude of this effect was higher in younger plants, and shifted towards growth reduction in older seedlings. However, the capacity for recovery after exposure also seemed to increase with age (Figure 5.1). At the molecular level, steady state oxidative DNA damage due to γ-irradiation in the leaves decreased with age (Figure 5.4), accompanied by a similar age-dependent decrease in transcription of the genes involved in the different single- and double-strand break DNA repair pathways such as *LIG4*, *RAD51, POLG1* and *PARP1* (Figure 5.2A-E). In addition, seedling shoots shifted from cell cycle slowdown by *CKS1* in 7-days-old plants (Figure5.3A) to suppression of *KRP2*-induced endoreduplication in 14-days old seedlings (5.3B). In this age class, we observed also indications for a role of increased lipid signalling by suppression of *LPP1* (Figure 5.3C) and increased oxidative stress signalling by *PARP2* (Figure 5.2F).

Though the data do not allow to draw clear conclusions on the mechanisms involved in the response to γ-irradiation, these are clear indications that *Arabidopsis thaliana* seedlings undergo changes in the timing and the strategy to deal with ionising radiation stress during the course of their exponential growth. Based on these data, and taking into account the practical needs for an exposure experiment, 14-days old seedlings were selected as the optimal growth stage for use in further radionuclide exposure experiments.

8.2.3 Biological effects of α- and β-radiation in Arabidopsis thaliana

To assess the effects of α- (chapter 7) and β-radiation (chapter 6), 14-days old seedlings were exposed (in hydroponics) to a range of activity concentrations of ^{241}Am (0 – 50,000 Bq L^{-1}) and ^{90}Sr (0 – 250,000 Bq L^{-1}) respectively. After 4 and 7 days of exposure, uptake, growth, biomass and photosynthesis were measured, and at these time points DNA damage and the transcriptional response of DNA repair and genes involved in oxidative stress were analysed. The status of the ascorbate- glutathione scavenging pathway and the redox state of these antioxidants was determined at the end of the exposure period. The effects of β- and α-radiation in *Arabidopsis thaliana* observed in our study are summarised in Figure 8.1 and Figure 8.2 respectively.

8.2.3.1 Effects of β-radiation

^{90}Sr is readily taken up in *Arabidopsis thaliana*, with most of the radionuclide transported to the seedlings' leaves (Table 6.4). Due to the chemical resemblance between both elements, the strontium transport most likely occurs via the calcium routes. This results in dose rates of β-radiation which are 10- to 100-fold higher in the leaves compared to the roots. Moreover, the shoots only receive internal doses with dose rates ranging from 0-12,400 μGy h^{-1}, while the

dose rate delivered to the roots (0 - 228 µGy h^{-1}) is primarily delivered by the ^{90}Sr in the surrounding liquid medium (Table 6.5).

We observed an initial increase in root fresh weight for the two highest treatments (Table 6.6), which subsequently disappeared at a later stage. Most genes involved in DNA repair, oxidative stress and ROS scavenging showed early strong down-regulation in the roots starting at dose rates as low as 1.8 µGy h^{-1} (Tables 6.9 and 6.11). At a later exposure stage, this evolved to up-regulation at the two highest dose rates of ROS producing NADPH oxidases (*RBOHC*), superoxide scavengers (*CSD1/2*) and enzymes of the ascorbate-glutathione cycle (*GR1/APX1*), as well as increased transcript levels of proteins involved in nuclear (LIG4) and organelle (*POLG1*) DSB repair and repair signalling (*PARP2*). This shift from general down-regulation to a more targeted stress response is also likely to be related to the transient nature of the increase in fresh weight we observed for both these treatments.

In the leaves, there were very little effects on biomass or photosynthesis (Figures 6.2, 6.3 and 6.4), though a transient increase in relative leaf area occurred in most ^{90}Sr treatments, with a peak at 96 h. As in the roots, β-radiation-induced transcriptional changes in the shoots were concentrated at the two highest dose rates (Table 6.8 and 6.10), with up-regulation of superoxide scavengers and DNA repair. While the latter up-regulations occurred earlier in the highest treatment than in the treatment one order of magnitude below, both treatments showed very strong early up-regulation of *LOX2*, suggesting the involvement of jasmonate signalling. The shift of ascorbate and glutathione towards their oxidised forms at a late stage (Figure 6.5) confirms that, despite the transcriptional response and the absence of effects on biomass or photosynthesis, the leaves had great difficulty in maintaining their cellular redox balance and in controlling cellular ROS levels at these dose rates. Redox imbalance can result in high levels of oxidative DNA damage (Figure 6.4) due to a reduced capacity for ROS scavenging. In this respect, the decrease of DNA damage at the highest leaf dose rate at after 7 days is puzzling, and must either

be the result of more efficient ROS scavenging, increased DNA repair or an increase in DNA content by endoreduplication. Though we found increased GSH biosynthesis (Figure 6.5A) at this dose rate, it seems to represent an attempt to save the ascorbate-glutathione cycle, and therefore unlikely to be entirely responsible for the observed decrease in DNA damage. Similarly, *CKS1* up-regulation might point towards cell cycle arrest and increased endoreduplication (Table 6.10), though conclusive evidence for the alternative explanations is lacking. Furthermore, neither of the underlying responses can explain the transient increase in leaf area (Figure 6.1).

Though the response to β-radiation for both organs seems to be confined to the two highest treatments, there is no apparent link between the effects in the roots and those in the leaves. Strikingly though, the response in the roots occurs at dose rates which do not incite any effects in the leaves. This can either point to a difference in radiosensitivity between both organs or the result of a difference in dose delivery in both organs (external in the roots, internal in the shoots).

8.2.3.2 Effects of α-radiation

Though the uptake of ^{241}Am in roots of *Arabidopsis thaliana* from a liquid medium was found to be high, transfer to the leaves was generally much lower (Tables 7.3 and 7.4), resulting in shoot activity concentrations 10- to 100-fold lower than those in the roots. Nevertheless, due to the fact that the energy of internal α-particles is completely absorbed within the tissue, internal dose rates were in the order of several mGy h^{-1} in both organs after only 4 days of ^{241}Am exposure (Table 7.5).

In the roots, these dose rates resulted in an early reduction of fresh weight at the highest dose rate. At the transcript level, we found early up-regulation of enzymes involved in the ascorbate-glutathione cycle (*APX1/GR1*), *PARP2* signalling and DSB DNA repair pathways (*LIG4*/*RAD51*) starting at 140 µGy h^{-1}.

(Tables 7.8 and 7.10), the latter reflecting the known predominance of DSBs in α-radiation damage. Similarly, steady-state oxidative DNA damage did not increase throughout exposure (Figure 7.4), indicating that DNA repair was able to keep pace with the rate of single-strand radiation damage. Up to 2,400 μGy h^{-1}, we found up-regulation of superoxide ($O_2^{\bullet-}$) CuZnSOD scavengers (*CSD1/3*) and hydrogen scavenging catalases (*CAT2/3*), while in the highest treatment (35,000 μGy h^{-1}) additionally there was an increase in lipoxygenase (*LOX1*) and ROS-producing NADPH oxidase (*RBOHA*) transcripts, suggesting the involvement of jasmonate signalling and oxidative burst. At a later exposure stage, root dry weight decreased significantly at all dose rates (Table 7.6), while root uptake and translocation to the shoots were reduced (Table 7.4), especially in the highest exposure. As a result, the overall dose rate in both organs declined (Table 7.5A). Most of the late molecular effects in the roots were found at the two highest dose rates, with loss of redox balance, reduced GSH biosynthesis (Figure 7.6), and very strong up-regulation of genes involved in cell cycle arrest (*CKS1/GAR1*; Figure 7.10). In the highest exposure, the transcripts of NADPH oxidase RBOHC and LOX1 were respectively increased and suppressed, indicating that jasmonate signalling is transient and that NADPH oxidases are involved in the response.

The early response in the leaves was limited to an increase in *RBOHC* transcripts at the highest dose rate (Table 7.11), while no effects on biomass, growth or photosynthesis could yet be observed. At a later stage, there was a positive effect up to 145 μGy h^{-1}, where photosynthesis performance was increased through controlled decrease of non-photochemical quenching in favour of Photosystem II efficiency (Figure 7.2B and C), increase of the electron transport chain capacity (Figure 7.3B and C) and increased antennae size and photoprotection (Table 7.7). In contrast, Fv/Fm (Figure 7.1) and electron transport were decreased at the highest dose rate, in addition to a loss of NPQ control and subsequent damaging uncontrolled quenching by fluorescence (Figure 7.2A). The decline in photosynthetic performance was accompanied by a severe disruption of the redox balance and loss of ascorbate-glutathione

scavenging capacity (Figure 7.5). Despite the indications of oxidative stress and damage in the shoots, there was no response at the transcript level apart from *PARP2* up-regulation (Table 7.9), suggesting that the cause of the response on photosynthesis must be found elsewhere. While it could be a result of root-to-shoot signalling, another explanation might be that early stress in the roots, and the subsequent reduction of transport of nutrients indirectly affects photosynthesis, which in turn might have a negative feedback on root biomass. However, this mechanism does not explain the absence of a transcriptional response in the leaves at dose rates that do cause a response in the roots, which might either be the result of differences in localisation of ^{241}Am, or a difference in radiosensitivity between both organs.

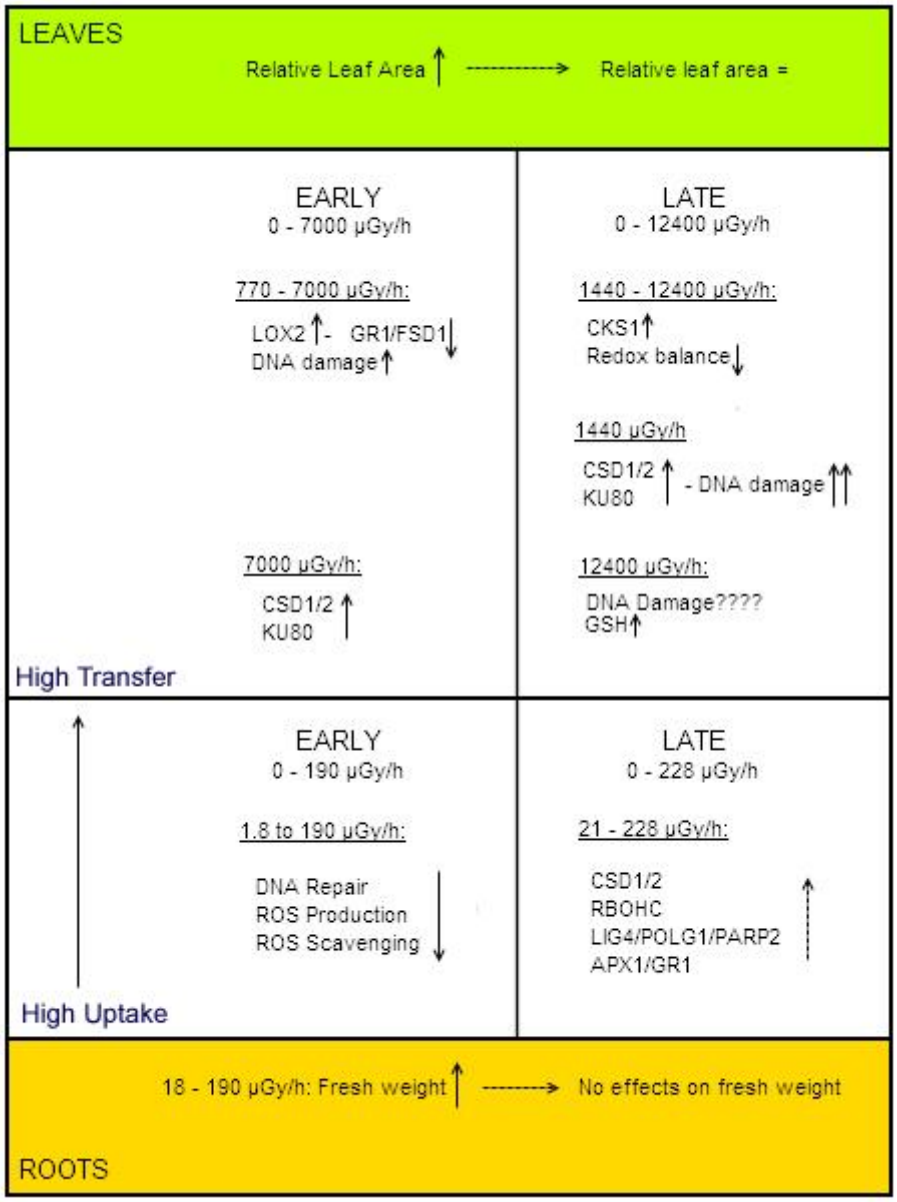

Figure 8.1: Overview of the observed early (4 days) and late (7 days) biological effects of β-radiation from ^{90}Sr in *Arabidopsis thaliana*

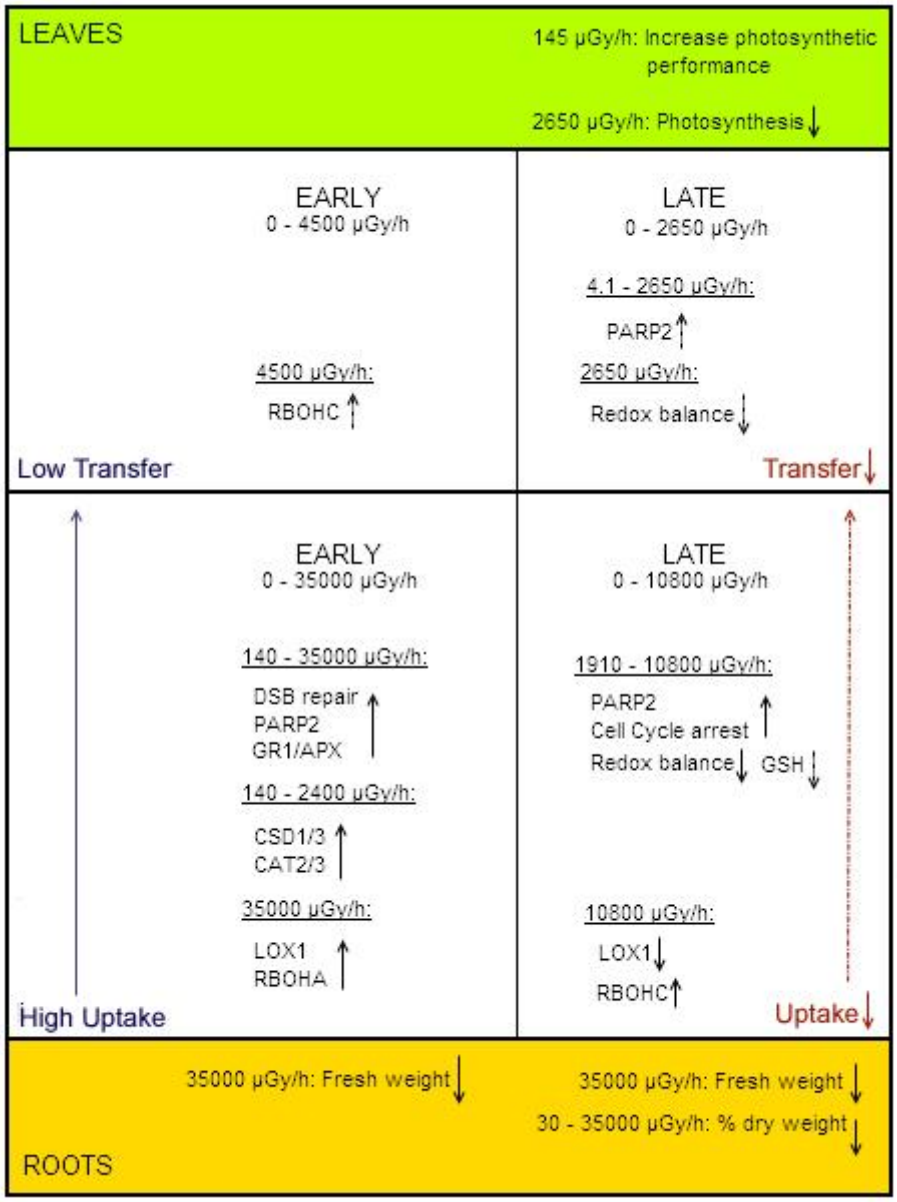

Figure 8.2: Overview of the observed early (4 days) and late (7 days) biological effects of α-radiation from ^{241}Am in *Arabidopsis thaliana*

8.2.4 Comparing radiation types.

One of the major objectives in radioecology is to understand whether different types of radiation incite different types of responses at the cellular and physiological level. In essence, whether they have different modes of action.

8.2.4.1 A common molecular response

From our data we can conclude that there are several common aspects in the responses between α- and β-radiation (Figure 8.1 and 8.2).

At the transcriptional level, both α- and β-exposure responses involve the up-regulation of (1) SOD scavenging by CuZnSOD's (CSD1/2/3), (2) nuclear and organelle DNA repair, (3) PARP2 signalling, (4) ascorbate peroxidase (APX) and glutathione reductase (GR1) and (5) NADPH oxidases (RBOHA/C) (Figure 8.3), though not necessarily at the same dose rates. Up-regulation of lipoxygenase-mediated signalling (LOX) and genes involved in the cell cycle (CKS1/GAR1) also occurs in both responses. In the case of LOX, this seems to be an early response at the highest dose rates, which is consistent with its role in stress signalling. At the level of scavenging, the imbalance in redox status of ascorbate and glutathione is observed for both radiation types at the end of the exposure.

Despite these common responses, there are also subtle differences between both responses. Most evident at the molecular level is the absence of DNA base modification in the α-exposure compared to the high levels of DNA damage during exposure to β-radiation, due to the difference in ionising behaviour between electrons. Others differences are less obvious, or demand validation, such as the differences in SOD isoforms or the (absence of) involvement of catalase scavenging.

Based upon these data, we can postulate that α- and β-radiation (and therefore most likely γ-radiation as well) rely on common molecular mechanisms of action,

with the differences between radiation types emerging from predominance of one or several interaction types (e.g. direct/indirect damage) over the others, and a subsequent difference in integrated response. (Figure 8.3).

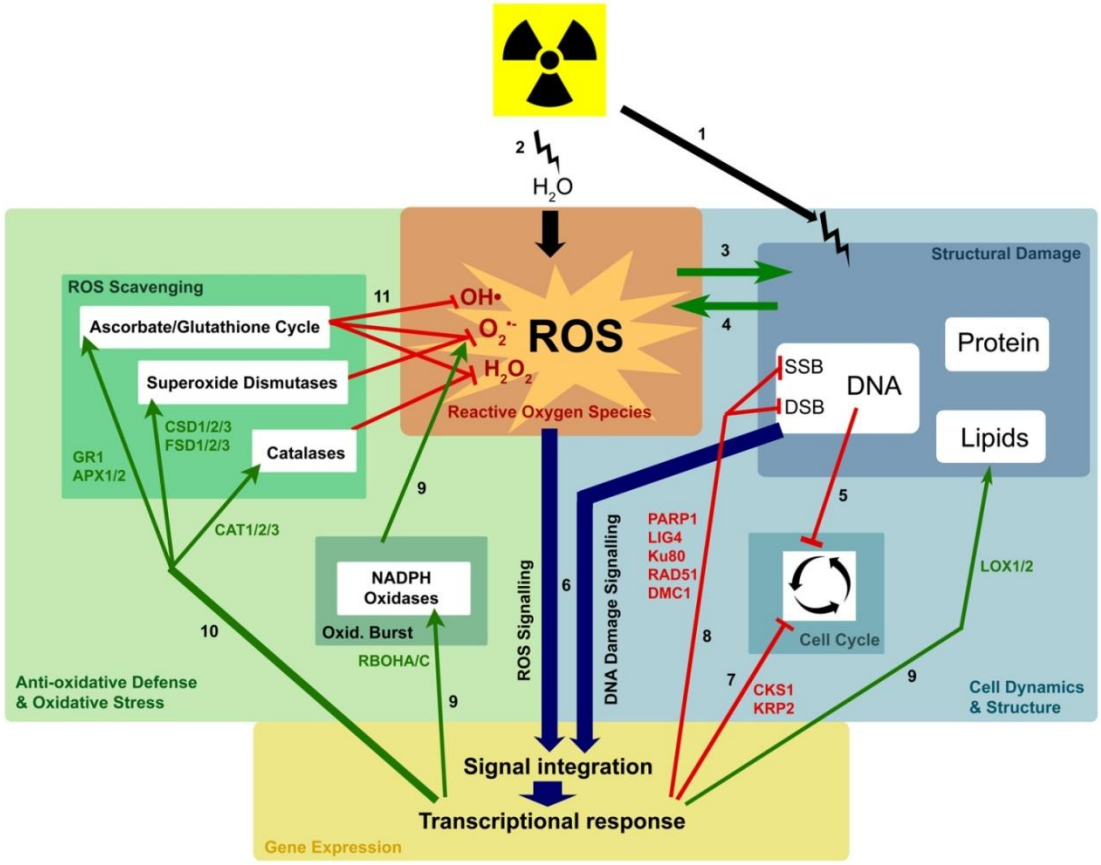
1
2
H_2O
3
4
Structural Damage
Protein
DNA
SSB
DSB
Lipids
ROS Scavenging
11
Ascorbate/Glutathione Cycle
Superoxide Dismutases
Catalases
CSD1/2/3
FSD1/2/3
GR1
APX1/2
CAT1/2/3
OH•
$O_2^{\bullet-}$
H_2O_2
ROS
Reactive Oxygen Species
9
NADPH
Oxidases
Oxid. Burst
RBOHA/C
10
ROS Signalling
6
DNA Damage Signalling
PARP1
LIG4
Ku80
RAD51
DMC1
5
8
Cell Cycle
7
CKS1
KRP2
LOX1/2
9
Anti-oxidative Defense
& Oxidative Stress
Cell Dynamics
& Structure
Signal integration
Transcriptional response
Gene Expression

Figure 8.3: General overview of the modes of action of ionising radiation and the biological response pathways at the molecular level. Arrows indicate negative (red) or positive (green) influence on the target process or molecule, or indicate a signalling response (blue).

Ionising radiation can interact with cells in two distinct ways, through **(1)** direct ionisation of structural and genetic components of the cell and through **(2)** radiolysis of water molecules. Hydrolysis results in formation of reactive oxygen species (ROS), of which superoxide (O_2•-), hydrogen peroxide (H_2O_2) and the hydroxyl radical (OH•) are the most abundant. ROS are able to **(3)** react with biomolecules, creating damage. Structural damage to proteins such as those in the mitochondrial and chloroplast electron transfer chains leads to **(4)** increased production of ROS from metabolic processes. **(5)** DNA damage, both single-strand breaks (SSB) and double-stand breaks (DSB), must be repaired before the cell cycle can progress to cell division. Both types of DNA damage slow growth by a direct signalling link to the cell cycle regulatory proteins. **(6)** Apart from their role in cellular damage, ROS are involved in cellular stress signalling. This signal likely integrates with DNA damage signalling (possibly via involvement of *PARP2*) to induce a transcriptional response. **(7)** At the level of cell cycle control, cells increase transcription of cell cycle regulating proteins such as *CKS1*, which increases the length of the cell cycle, and *KRP2*, which stimulates the transition to endoploidy. **(8)** DNA repair is increased by up-regulation of proteins involved in SSB repair (*PARP1*) and/or DSB repair (*KU80/LIG4/RAD51/DMC1*), depending on the signalled damage. **(9)** Up-regulation of lipid cleavage by lipoxygenase (*LOX*) plays a role in abscisic acid-mediated stress signalling. As ROS are important in stress signalling, cells can produce additional ROS by the action of **(9)** NADPH oxidases, which produce superoxide in the cell wall. **(10)** Cellular ROS levels are kept under control by ROS scavenging proteins and metabolites. Superoxide dismutases SODs catalyse the dismutation of superoxide to hydrogen peroxide. Only up-regulation of copper-zinc SODs (CSD1/2/3) has been observed in this study, while regulation of iron-SODs is less clear (FSD1/2/3). Hydrogen peroxide is in turn detoxified by peroxisomal catalases (CAT1/2/3) and the ascorbate-glutathione cycle. The latter consists of protein components (APX/GR1) and metabolites (Ascorbate and glutathione). Ascorbate is also responsible for direct scavenging of most types of ROS. **(11)** The balance between scavenging capacity and ROS determines the cellular redox status, and ultimately the fate of the cell.

8.2.4.2 A unified radiotoxic and ecotoxicological framework

Despite the common molecular responses, several of our observations cannot be explained purely by a common radiation response and are likely a result of radionuclide dynamics.

Radionuclides are subject to uptake, translocation and redistribution between plant organs and tissues, which renders a comparison between different radionuclides solely based upon dose and dose rate difficult. The uptake and distribution patterns of ^{90}Sr and ^{241}Am within *Arabidopsis thaliana* seedlings are completely opposite to each other, each delivering a much larger dose in one plant organ compared to the other. As the roots and leaves are functionally connected through nutrient and carbon transport, disruption of the functions of one organ has repercussions on the other. The example of ^{241}Am, where root dysfunction possibly sets in motion a response on photosynthesis, illustrates this perfectly. This also means that, while ionising radiation is the local cause of dysfunction, radionuclide distribution is the main factor which determines how physiology and growth of the plant globally evolve throughout the exposure. Furthermore, there are indications that roots and shoots do not have the same sensitivity to radiation, which is further complicating comparison.
In addition to the root-shoot distribution there is also the influence of microlocalisation. Radionuclides differ in their subcellular and in their local distribution within the organ. This is a direct result of their physical and chemical properties. Americium, for example, has a strong affinity for solid components of the cell (Bondareva et al., 2010?), and is therefore mainly associated with the cell wall fraction and to a lesser extent with proteins and lipids. Strontium on the other hand follows the route of calcium, and is mainly present in the apoplast of the vascular bundles. These locations are of importance, as the reach and attenuation of electrons and α-particles might depend on the tissue or structure they are in.

The observations above make it valid to question whether the possible differences in mode of action between the different types of radiation really

matter, if macro- and microlocalisation and the physico-chemical properties of the radionuclide have such a large influence on the biological outcomes of the exposure. Furthermore, it makes a direct comparison of radiation types to derive RBE values very difficult. Finally, it also seriously questions the concept of a dose-response curve for α- or β-radiation as such. It might instead be a more reasonable viewpoint to shift the importance to the element as such, and consider ionising radiation as part of the radionuclide's mode of action, which consists of both chemotoxic and radiotoxic components. In this way, the concepts of radioecology can be integrated more easily into a common ecotoxicological framework.

8.3 Conclusions

The aim of this study was to generate a detailed dosimetric model for *Arabidopsis thaliana*, and to unravel the biological mechanisms involved in the responses to different types of ionising radiation.

By developing a more realistic dosimetric approach for *Arabidopsis* roots and shoots which included uptake and growth dynamics, we obtained more realistic and less conservative dose estimates than with the static models which are currently available. Furthermore, our approach is able to process a large number of geometrical data in a more efficient way. This is a considerable technical and practical improvement which will allow for more and more precise calculations in a shorter time.

Chronic α-, β- and γ-radiation induce a range of pathways involved in cell cycle control, DNA damage and ROS scavenging. However, while these pathways show considerable similarities between radiation types, the timing and sensitivity of the responses differ considerably. In general, chronic radiation stress considerably alters the redox balance of the cell, which indicates that despite the relatively limited effects on growth and photosynthesis we observed, the

seedlings gradually move towards a situation in which they are less able to defend themselves against incoming ionising radiation in their cells. From our study on ^{90}Sr and ^{241}Am it became clear that ionising radiation is just one aspect in the effect of radionuclide exposure. Distribution as well as macro- and micro-localisation of the radionuclide within the plant have shown to be determining factors in the outcome of radiation exposure. Furthermore there are potential differences in organ sensitivity and density between components. Finally we have also shown that plant age is a determining factor in radiation response.

8.4 Perspectives

Within this study we developed a sound basis of a general approach onto which the effects of ionising radiation in plants can be grafted. As large amount of uncertainty remains, a more generalised holistic approach is needed to obtain an overall and integrated view of the responses. A full-scale transcriptional analysis of *Arabidopsis thaliana* seedlings under chronic α-, β- or γ-exposure is likely to reveal common and differing patterns in expression and pathway interaction between the different radiation types. Based on our data, investigation of the role of the redox balance on cell and organ death will necessitate longer exposure durations. A second objective should be to determine a way in which exposure by different radionuclides with a similar decay mode can be compared. Elements with different distribution patterns within the plant can possibly have different overall biological effects under similar doses or dose rates. This not only makes it difficult to determine parameters such as RBE based on effects data, but also adds an important confounding factor to mixture toxicity studies which would include α- or β-radiation as one of the stressors. Finally, the advances in dosimetry calculations made during this study can be used to develop a more detailed model for *Arabidopsis thaliana*, taking into account differences in radionuclide uptake and redistribution between individual leaves.

REFERENCES

ADAMS III, W.W., Demmig-Adams, B., Logan, B.A., Barker, D.H., Osmond, C.B., 1999. Rapid changes in xanthophyll cycle-dependent energy dissipation and photosystem II efficiency in two vines, *Stephania japonica* and *Smilax australis*, growing in the understorey of an open Eucalyptus forest. Plant Cell Environ. 22, 125–136.

ADAMS-PHILLIPS, L., Briggs, A.G., Bent, A.F., 2010. Disruption of poly(ADP-ribosyl)ation mechanisms alters responses of *Arabidopsis* to biotic stress. Plant Physiol. 152, 267-80.

ALSCHER, R.G., Erturk N., Heath, L.S., 2002. Role of superoxide dismutases (SODs) in controlling oxidative stress in plants. J. Exp. Bot. 53, 1331-1341.

ANDERSSON, P., Garnier-Laplace, J., Beresford, N.A., Copplestone, D., Howard, B.J., Howe, P., Oughton, D., Whitehouse, P., 2009. Protection of the environment from ionising radiation in a regulatory context (protect): proposed numerical benchmark values. J. Environ. Radioact. 100, 1100–1108.

AMIARD, S., Charbonnel, C., Allain, E., Depeiges, A., White, C.I., Gallego, M.E., 2010. Distinct roles of the ATR kinase and the Mre11-Rad50-Nbs1 complex in the maintenance of chromosomal stability in Arabidopsis. Plant Cell 22, 3020–3033.

ATSDR, 1999. Toxicological profile for uranium. U.S. Department of Health and Human Services. Public Health Service. Agency for Public Substances and Disease Registry, Atlanta.

ATSDR, 2004a. Toxicological profile for Americium. U.S. Department of Health and Human Services. Public Health Service. Agency for Public Substances and Disease Registry, Atlanta.

ATSDR, 2004b. Toxicological profile for Strontium. U.S. Department of Health and Human Services. Public Health Service. Agency for Public Substances and Disease Registry, Atlanta.

BALL, L., Accotto, G.P., Bechtold, U., Creissen, G., Funck, D., Jimenez, A., Kular, B., Leyland, N., Mejia-Carranza, J., Reynolds, H., Karpinski, S., Mullineaux, P.M., 2004. Evidence for a direct link between glutathione biosynthesis and stress defense gene expression in *Arabidopsis*. Plant Cell 16, 2448–2462.

BAUMANN, P., Benson, F. E., West, S. C., 1996. Human Rad51 protein promotes ATP-dependent homologous pairing and strand transfer reactions in vitro. Cell 87, 757-766.

BERESFORD, N.A., Barnett, C.L., Beaugelin-Seiller, K., Brown, J.E., Cheng, J-J., Copplestone, D., Gaschak, S., Hingston, J.L., Horyna, J., Hosseini, A., Howard,

B.J., Kamboj, S., Kryshev, A., Nedveckaite, T., Olyslaegers, G., Sazykina, T., Smith, J.T., Telleria, D., Vives i Batlle, J., Yankovich, T.L., Heling, R., Wood, M.D., Yu, C., 2009. Findings and recommendations from an international comparison of models and approaches for the estimation of radiological exposure to non-human biota. Radioprotection 44, 565–570.

BERGER, M.J., 1968. Energy deposition in water by photons from point isotropic sources. J. Nucl. Med. 9, 15-25.

BERGER, M.J., 1971. Distribution of absorbed dose around point sources of electrons and beta particles in water and other media. J. Nucl. Med. Suppl. 5, 5–23.

BHATTACHAREE, S., 2005. Reactive oxygen species and oxidative burst: roles in stress, senescence and signal transduction in plants. Curr. Sci. 89, 1113-1121.

BIELSKI, B.H., Arudi, R.L., Sutherland, M.W., 1983. A study of the reactivity of HO_2/O_2-with unsaturated fatty acids. J. Biol. Chem. 258, 4759-4761.

BIERMANS, G., Horemans, N., Vanhoudt, N., Vandenhove, H., Saenen, E., Ven Hees, M., Wannijn, J., Vives i Batlle, J., Cuypers, A., 2013. An organ-based approach to dose calculation in the assessment of dose-dependent biological effects of ionizing radiation in Arabidopsis thaliana. J. Environ. Radioact. *In Press.*

BLEUYARD, J.Y., Gallego, M.E., Savigny, F., White, C.I., 2005. Differing requirements for the *Arabidopsis* Rad51 paralogs in meiosis and DNA repair. Plant J. 41, 533-545.

BLOKHINA, O., Virolainen, E., Fagerstedt, K.V., 2003. Antioxidants, Oxidative Damage and Oxygen Deprivation Stress: a Review. Ann. Bot. 91, 179-194.

BOESCH, P., Weber-Lotfi, F., Ibrahim, N., Tarasenko, V., Cosset, A., Paulus, F., Lightowlers, R.N., Dietrich, A., 2011. DNA repair in organelles: Pathways, organization, regulation, relevance in disease and aging. BBA-Mol. Cell. Res. 1813, 186–200.

BOLWELL, G.P., Wojtaszek, P., 1997. Mechanism for the generation of reactive oxygen species in plant defense—a broad perspective. Physiol. Mol. Plant Pathol. 51, 347–366.

BOLWELL, G.P., Bindschedler, L.V., Blee, K.A., Butt, V.S., Davies, D.R., Gardner, S.L., Gerrish, C., Minibayeva, F., 2002. The apoplastic oxidative burst in response to biotic stress in plants: a three-component system. J. Exp. Bot. 53, 1367-76.

BOLSUNOVSKY, A., Zotina, T., Bondareva., L., Accumulation and release of 241Am by a macrophyte of the Yenisei River (*Elodea canadensis*). J. Environ. Radioact. 81, 33-46.

BONDAREVA, L., Vlasova, I., Mogilnaya, O., Bolsunovsky, A., Kalmykov, S., 2010. Microdistribution of 241Am in structures of submerged macrophyte *Elodea canadensis* growing in the Yenisei River. J. Environ. Radioact. 101, 16-21.

BOWLER, C., Van Camp, W., Van Montagu, M. & Inzé, D. 1994. Superoxide dismutase in plants. Crit. Rev. Plant Sci. 13, 199-218.

BOYES, D.C., Zayed, a M., Ascenzi, R., McCaskill, J., Hoffman, N.E., Davis, K.R., Görlach, J., 2001. Growth stage-based phenotypic analysis of *Arabidopsis*: a model for high throughput functional genomics in plants. Plant Cell 13, 1499–510.

BOYKO, A., Greer, M., Kovachuk, I., 2006a. Acute exposure to UVB has a more pronounced effect on plant genome stability than chronic exposure, Mutat. Res. 602,100-109.

BOYKO, A., Zemp, F., Filkowski, J., Kovalchuk, I. 2006b. Double-Strand Break Repair in plants is developmentally regulated. Plant Physiol. 141, 488-497.

BRITT, A.B., 1996. DNA damage and repair in plants. Annu. Rev. Plant Physiol. Plant Mol. Biol. 47, 75-100.

BRITT, A., 1999. Molecular genetics of DNA repair in higher plants. Trends Plant Sci. 4, 20-25.

BROWN, J.E., Alfonso, B., Avila, R., Beresford, N., Copplestone, D., Pröhl, G., Ulanovsky, A., 2008. The ERICA Tool. J. Environ. Radioact. 99, 1371–1383.

BOULTON, S.J., Jackson, S.P., 1996. Identification of a *Saccharomyces cerevisiae* Ku80 homologue: roles in DNA double strand break rejoining and in telomeric maintenance. Nucleic Acids Res. 24, 4639-48.

CALABRESE E.J., Baldwin, L.A., 2000. Radiation hormesis: its historical foundations as a biological hypothesis. Hum. Exp. Toxicol. 14, 41-75.

CHAMBERS, D.B., Osborne, R.V., Garva, A.L., 2006. Choosing an alpha radiation weighting factor for doses to non-human biota. J. Environ. Radioact. 87, 1-14.

CHEN, Y.M., Shall S., O'Farrell M., 1994. Poly(ADP-ribose) polymerase in plant nuclei. Eur. J. Biochem. 224, 135–142.

CHEN, M., Tan, Y.L., Ao, J., Wang, D., 2012. Effects of strontium on photosynthetic characteristics of oilseed rape seedlings. Russ. J. Plant Physl.+ 59, 772-780.

COOLS, T., De Veylder, L., 2009. DNA, stress checkpoint control and plant development. Curr. Opin. Plant Biol. 12, 23–28.

COPPLESTONE, D., Bielby S., Jones, S.R., Patton, D., Daniel, C.P., Gize, I., 2001. Impact assessment of ionising radiation on wildlife. R&D Publication 128, Environment Agency, UK and English Nature.

COPPLESTONE, D., Howard, B.J., Bréchignac, F., 2004. The ecological relevance of current approaches for environmental protection from exposure to ionising radiation. J. Environ. Radioact. 74, 31–41.

COPPLESTONE, D., Hingston, J., Real, A., 2008. The development and purpose of the FREDERICA radiation effects database. J. Environ. Radioact. 99, 1456-1463.

COUGHTREY, P.J., Thorne, M.C., 1983. Radionuclide distribution and transport in terrestrial and aquatic ecosystems, vol 1. A.A. Balkema Publishers, Amsterdam.

CULLIGAN, K.M., Robertson, C.E., Foreman, J., Doerner, P., Britt, A.B., 2006. ATR and ATM play both distinct and additive roles in response to ionizing radiation. Plant J. 48, 947–961.

CUYPERS, A., Vangronsveld, J., Clijsters, H., 2000. Biphasic effect of copper on the ascorbate-glutathione pathway in primary leaves of *Phaseolus vulgaris* seedlings during the early stages of metal assimilation. Physiol. Plant. 110, 512-517.

DALY, K., Thompson, K.H., 1975. Quantitative dose-response of growth and development in Arabidopsis thaliana exposed to chronic gamma-radiation. Int. J. Radiat. Biol. 28, 61-66.

DAT, J., Vandenabeele, S., Vranová, E., Van Montagu, M., Inzé, D., Van Breusegem, F., 2000. Dual action of the active oxygen species during plant stress responses. Cell. Mol. Life Sci. 57, 779-795.

DAVISON, A.C., Hinkley, D.V., 1997. Bootstrap methods and their application. Cambridge Series in Statistical and Probabilistic Mathematics. Cambridge University Press.

DE SCHUTTER, K., Joubès, J., Cools, T., Verkest, A., Corellou, F., Bablychuk, E., Van Der Schueren, E., Beeckman, T., Kushnir, S., Inzé, D., De Veylder, L., 2007. *Arabidopsis* WEE1 kinase controls cell cycle arrest in response to activation of the DNA integrity checkpoint. Plant Cell 19, 211–225.

DE VEYLDER, L., Beemster, G.T.S., Beeckman, T., Inzé, D., 2001a. CKS1At overexpression in Arabidopsis thaliana inhibits growth by reducing meristem size and inhibiting cell-cycle progression. Plant J. 25, 617-626.

DE VEYLDER, L., Beeckman, T., Beemster, G.T.S., Krols, L., Terras, F., Landrieu, I., Van Der Schueren, E., Maes, S., Naudts, M., Inzé, D. , 2001b. Functional analysis of cyclin-dependent kinase inhibitors of *Arabidopsis*. Plant Cell 13, 1653–1667.

DE VEYLDER, Beeckman, T., Inzé, D., 2007. The ins and outs of the plant cell cycle. Nature Rev. Mol. Cell Biol. 8, 655-665.

DEBIANE, D., Verdin, A., Durand, R., Shirali, P., Grandmougin-ferjani, A., 2009. Mycorrhization alleviates benzo[a]pyrene-induced oxidative stress in an in vitro chicory root model. Phytochemistry, 70, 1421–1427.

DEL RIO, L.A., Sandalio, L.M., Corpas, F.J., Palma, J.M., Barroso, J.B., 2006. Reactiveoxygen species and reactive nitrogen species in peroxisomes. Production, scavenging, and role in cell signaling, Plant Physiol. 141, 330-335.

DEMMIG-ADAMS, B., Adams III, W.W., Logan, B.A., Verhoeven, A.S., 1995. Xanthophyll-cycle-dependent energy dissipation and flexible photosystem II efficiency in plants acclimated to light stress. Aust. J. Plant Physiol. 22, 249–260.

DEVEAUX, Y., Alonso, B., Pierrugues, O., Godon, C., Kazmaier, M., 2000. Molecular cloning and developmental expression of AtGR1, a new growth-related *Arabidopsis* gene strongly induced by ionizing radiation. Radiat. Res. 154, 355-364.

DOE. 2000. Buried Transuranic-Contaminated Waste Information for U.S. Department of Energy Facilities. Office of Environmental Management. Washington, D.C.: DOE

DOE, 2011. Radiation Protection of the Public and the Environment. DOE Order 458.1. U.S. Department of Energy, Office of Health, Safety and Security.

DOUCET-CHABEAUD, G., Godon C., Brutesco C., de Murcia G., Kazmaier M., 2001. Ionizing radiation induces the expression of PARP-1 and PARP-2 genes in *Arabidopsis*. Mol. Genet. Genomics. 265, 954-963.

DOUTRIAUX, M.P., Couteau F., Bergounioux C.,White C.,1998. Isolation and characterization of the RAD51 and DMC1 homologs from *Arabidopsis thaliana*. Mol. Gen. Genet. 257, 283-291.

DRAZKIEWICZ, M., Skórzynska-Polit, E., Krupa, Z., 2003. Response of the ascorbate-glutathione cycle to excess copper in *Arabidopsis thaliana* (L.). Plant Sci. 164,195-202.

DUFFA, C., Renaud, P., Goutelard, F., 2002. Activities and transfers of Pu and Am in rice samples from Camargue, France. J. Radioanal. Nuc. Ch. 252, 247–248.

ELIASSON, L., 1968. Dependence of Root Growth on Photosynthesis in *Populus tremula*. Physiol. Plant. 21, 806-810.

ELSTNER, E.F., 1991. Mechanisms of oxygen activation in different compartments of plant cells. In: Pell, E.J., Steffen K.L. (eds.) Active

oxygen/oxidative stress and plant metabolism. Rockville, MD: American Society of Plant Physiologists, 13–25.

ELZHOV, T.V., Mullen, K.V., Bolker, B., 2010. minpack.lm: R interface to the Levenberg-Marquardt nonlinear least-squares algorithm found in MINPACK. R package version 1.1-5. http://CRAN.R-project.org/package=minpack.lm

ERICSSON, T., 1994. Nutrient dynamics and requirements of forest crops. New Zeal. J. For. Sci. 24, 133–168.

ESNAULT, M.-A., Legue, F., Chenal, C., 2010. Ionizing radiation: Advances in plant response. Environ. Exp. Bot. 68, 231-237.

EU, 2010. Radiation Protection 164: Radioactive effluents from nuclear power stations and nuclear fuel reprocessing sites in the European Union, 2004-08

FINCH, C.S., 1987. Acute Radiation Syndrome. JAMA 258, 664-667

FLIEDNER, T.M., Friesecke, I., Beyrer, K., 2001. (Eds.): Medical Management of Radiation Accidents--Manual on the Acute Radiation Syndrome. British Institute of Radiology, London.

FOYER, C.H., Noctor, G., 2005a. Redox homeostasis and antioxidant signaling: a metabolic interface between stress perception and physiological responses. Plant Cell 17, 1866-1875.

FOYER, C.H., Noctor, G., 2005b. Oxidant and antioxidant signaling in plants: a reevaluation of the concept of oxidative stress in a physiological context. Plant Cell Environ. 28, 1056-1071.

GALLE, P. 1997. Toxiques nucléaires. Masson, Paris.

GARCIA, V., Bruchet, H., Camescasse, D., Granier, F., Bouchez, D., Tissier, A., 2003. AtATM is essential for meiosis and the somatic response to DNA damage in plants. Plant Cell. 15, 119-32.

GARNIER-LAPLACE, J., Gilek, M., Sundell-Bergman, S., Larsson, C.M., 2004. Assessing ecological effects of radionuclides: data gaps and extrapolation issues. J. Radiol. Prot. 24, 139-155.

GARNIER-LAPLACE, J., Gilbin, R. (eds.), 2006. ERICA DELIVERABLE 5: Derivation of Predicted-No-Effect-Dose-Rate values for ecosystems (and their sub-organisational levels) exposed to radioactive substances.

GENTY, B., Briantais, J-M., Baker, N.R., 1989. The relationship between quantum yield of photosynthetic electron transport and quenching of chlorophyll fluorescence. Biochim. Biophys. Act. 990,87–92.

GILL, S.S., Tuteja, N., 2010. Reactive oxygen species and antioxidant machinery in abiotic stress tolerance in crop plants. Plant Physiol. Biochem. 48, 909-930.

GULSEN, M., Smith, A.E., Tate, D.M., 1995. A genetic algorithm approach to curve fitting. Int. J. Prod. Res. 33, 1911-1923.

HALLIWELL, B., Gutteridge, J.M., 1998. Free Radicals in Biology and Medicine. Oxford University Press, Oxford.

HALLIWELL, B., 2006. Reactive species and antioxidants. Redox biology is a fundamental theme of aerobic life. Plant Physiol. 141, 312-322.

HINTON, T.G., Garnier-Laplace, J., Vandenhove, H., Dowdall, M., Adam-Guillermin, C., Alonzo, F., Barnett, C., Beaugelin-Seiller, K., Beresford, N.A., Bradshaw, C., Brown, J., Eyrolle, F., Fevrier, L., Gariel, J.-C., Gilbin, R., Hertel-Aas, T., Horemans, N., Howard, B.J., Ikäheimonen, T., Mora, J.C., Oughton, D., Real, A., Salbu, B., Simon-Cornu, M., Steiner, M., Sweeck, L., Vives i Batlle, J., 2013. An invitation to contribute to a strategic research agenda in radioecology. J. Environ. Radioact. 115, 73–82.

HODGKINS, P.S., O'Neil, P., Stevens, D., Fairman, M.P., 1996. The severity of alpha-particle-induced DNA damage is revealed by exposure to cell-free extracts. Radiat. Res. 146,660-7.

HOLST, R.W., Nagel, D.J., 1997. Radiation effects on plants, in: Wang, W., Gorsuch, J.W., Hughes, J.S. (Eds.), Plants for Environmental Studies, CRC Press/Lewis Publishers, New York, pp. 37–79.

HOSSEINI, A., Thørring, H., Brown, J.E., Saxén, R., Ilus, E., 2008. Transfer of radionuclides in aquatic ecosystems--default concentration ratios for aquatic biota in the Erica Tool. J. Environ. radioactiv. 99,1408-29.

HOYT, G.D., Adriano, D.C., 1979. Americium-241 uptake by bahiagrass as influenced by soil type, lime, and organic matter. J. Environ. Qual.,392-396.

IAEA, 2010. Handbook of Parameter Values for the Prediction of Radionuclide Transfer in Terrestrial and Freshwater Environments. Technical Report Series 472.

ICRP, 1996. Age-dependent Doses to the Members of the Public from Intake of Radionuclides: Part 5. Compilation of Ingestion and Inhalation Dose Coefficients. ICRP Publication 72. International Commission on Radiological Protection, Pergamon Press, Oxford

ICRP, 2003. Relative Biological Effectiveness (RBE), Quality Factor (Q), and Radiation Weighting Factor (wR). ICRP Publication 92. Ann. ICRP 33 (4)

ICRP, 2007. The 2007 Recommendations of the International Commission on Radiological Protection. ICRP Publication 103, Ann. ICRP 37 (2-4).

ICRP, 2009. Environmental Protection: the Concept and Use of Reference Animals and Plants. ICRP Publication 108, Ann. ICRP 37 (4-6).

ICRU, 2011. Linear Energy Transfer. Journal of the ICRU 11.

IRSN, 2002. Fiche Radionucléide: Barium-133 et environnement.

IRSN, 2005a. Fiche Radionucléide: Americium-241 et environnement.

IRSN, 2005b. Fiche Radionucléide: Strontium-90 et environnement.

IUR, 2002. Protection of the environment: Current Status and future work. IUR Report n° 3, Osteras, Norway

JOZEFCZAK, M., Remans, T., Vangronsveld, J., Cuypers, A., 2012. Glutathione Is a Key Player in Metal-Induced Oxidative Stress Defenses. Int. J. Mol. Sci. 13, 3145-3175.

KANTER, U., Hauser., A., Michalke, B., Drälx, S., Shäffner, A.R., 2010. Caesium and strontium accumulation in shoots of *Arabidopsis thaliana*: genetic and physiological aspects. J. Exp. Bot. 61, 3995–4009.

KASHPAROV, V.A., Lundin, S.M., Zvarich, S.I., Ioshchenko, V.I., Levchuk, S.E., Khomutinin, Y.V., Maloshtan, I.M., Protsak, V.P., Pazukhin, E.M., 2003. Soil Contamination with Fuel Component of Chernobyl Radioactive Fallout. Radiochemistry+ 45, 189–200.

KAWAI, T., Inoshita, T., 1965. Effects of gamma-ray irradiation on growing rice plants: I. Irradiation of four main developmental stages. Radiat. Bot. 5, 233–255.

KILLION, D.D., Constantin, M.J., 1972. Gamma irradiation of corn plants: effects of exposure, exposure rate, and developmental stage on survival, height, and grain yield, Radiat. Bot.,159–164.

KIM, D.S., Kim, J.-B., Goh, E.J., Kim, W.-J., Kim, S.H., Seo, Y.W., Jang, C.S., Kang, S.-Y., 2011. Antioxidant response of *Arabidopsis* plants to gamma irradiation: genome-wide expression profiling of the ROS scavenging and signal transduction pathways. J. Plant Physiol. 168, 1960–1971.

KIM, J.-H., Moon, Y.R., Kim, J.-S., Oh, M.-H., Lee, J.-W., Chung, B.Y., 2007. Transcriptomic profile of *Arabidopsis* rosette leaves during the reproductive stage after exposure to ionizing radiation. Radiat. Res. 168, 267–280.

KIM, J.-H., Moon, Y. R., Lee, M.H., Kim, J.H., Wi, S.G., Park, B.-J., Kim, C.S., Chung, B.J., 2011. Photosynthetic capacity of *Arabidopsis* plants at the reproductive stage tolerates γ irradiation. J. Radiat. Res. 52, 441–449.

KIRSCHBAUM, M.U.F., Does Enhanced Photosynthesis Enhance Growth? Lessons Learned from CO2 Enrichment Studies. Plant Physiol. 155, 117-124.

KNIGHT, H., Knight, M.R., 2001. Abiotic stress signalling pathways: specificity and cross-talk. Trends Plant Sci. 6, 262–267.

KOVACZ, E., Keresztes, A., 2002. Effect of UV-B/C radiation on plant cells. Micron 33, 199-210.

KOVALCHUK, I., Molinier, J., Yao, Y., Arkhipov, A., Kovalchuk, O., 2007. Transcriptome analysis reveals fundamental differences in plant response to acute and chronic exposure to ionizing radiation. Mutat. Res. 624, 101–113.

KOVALCHUK, O., Kovalchuk, I., Titov, V., Arkhipov, A., Hohn, B., 1999. Radiation hazard caused by the Chernobyl accident in inhabited areas of Ukraine can be monitored by transgenic plants. Mutat. Res., 446, 49–55.

KOVALCHUK, O., Arkhipov, A., Barylyak, I., Karachov, I., Titov, V., Hohn, B., Kovalchuk, I., 2000. Plants experiencing chronic internal exposure to ionizing radiation exhibit higher frequency of homologous recombination than acutely irradiated plants. Mutat. Res. 449, 47–56.

KOYAMA, S., Kodama, S., Suzuki, K., Matsumoto, T., Miyazaki, T., Wanatabe, M., 1998. Radiation-induced long-lived radicals which cause mutation and transformation. Mutat. Res./Fundam. Mol. Mech. Mutagen. 421, 45–54.

KRYSHEV, I.I., Romanov, G.N., Sazykina, T.G., Isaeva, L.N., Trabalka, J.R., Blaylock, B.G., 1998. Environmental contamination and assessment of doses from radiationreleases in the southern Urals. Health Phys. 74, 687-697.

LANS, H., Marteijn, J.A., Vermeulen, W., 2012. ATP-dependent chromatin remodeling in the DNA-damage response. Epigenetics Chromatin. 5.

KURIMOTO, T., Constable, J.V.H., & Huda, A., 2010. Effects of ionizing radiation exposure on *Arabidopsis thaliana*. Health Phys., 99, 49–57.

LARSSON, C.M., 2008. An overview of the ERICA Integrated Approach to the assessment and management of environmental risks from ionising contaminants. J. Environ. Radioact. 99, 1364-1370.

LEE, J.H., Hossner, L.R., Attrep, M. Jr., Kung, K.S., 2002. Uptake and translocation of plutonium in two plant species using hydroponics. Environ Pollut. 117,61-8.

LEE, M.H., Moon, Y.R., Chung, B.Y., Kim, J.-S., Lee, K.-S., Cho, J.-Y., Kim, J.-H., 2009. Practical use of chemical probes for reactive oxygen species produced in biological systems by γ-irradiation. Radiat. Phys. Chem. 78, 323–327.

LEISTER, D., Varotto, C., Pesaresi, P., Niwergall, A., Salamini, F., 1999. Large-scale evaluation of plant growth in *Arabidopsis thalia*na by non-invasive image analysis. Plant Physiol. Bioch. 37, 671–678.

LEPICARD, S., Heling, R., Maderich, V., 2004. POSEIDON/RODOS models for radiological assessment of marine environment after accidental releases: application to coastal areas of the Baltic, Black and North Seas. J. Environ. Radioact. 72,153-161.

LUKSIENE, B., Marciulioniene, D., Gudeliene, I., Schönhofer, F., 2013. Accumulation and transfer of 137Cs and 90Sr in the plants of the forest ecosystem near the Ignalina Nuclear Power Plant. J. Environ. Radioact. 116, 1-9.

MARQUARDT, D.W., 1963. An algorithm for least-squares estimation of non-linear parameters. SIAM J. Appl. Math. 11, 431–441.

MAXWELL, K., Johnson, G. N., 2000. Chlorophyll fluorescence – a practical guide. J. Exp. Bot. 51, 659-668.

MBOULOU, M.O., Hurtgen, C., Hofkens, K., Vandecasteele, C., 1998. Vertical distributions in the Kapachi soil of the plutonium isotopes (^{238}Pu, ^{239,240}Pu, ^{241}Pu), of ^{241}Am, and of ^{243,244}Cm, eight years after the Chernobyl accident. J. Environ. Radioact. 39, 231-238.

MILLER, G., Suzuki, N., Ciftzi-Yilmaz, S., Mittler, R., 2010. Reactive oxygen species homeostasis and signalling during drought and salinity stresses. Plant Cell Environ. 33, 453–467.

MITTLER, R., 2002. Oxidative stress, antioxidants and stress tolerance. Trends Plant Sci. 7, 405-410.

MITTLER, R., Vanderauwera, S., Gollery, M., Van Breusegem, F., 2004. Reactive oxygen gene network of plants. Trends Plant Sci. 9, 490-498.

MITTLER, R., Vanderauwera, S., Suzuki, N., Miller, G., Tognetti, V.B., Vandepoele, K., Gollery, M., Shulaev, V., Van Breusegem, F., 2010. ROS signalling: the new wave? Trends Plant Sci. 16, 300-309.

MOON, Y.R., Kim, J.-H., Lee, M.H., Kim, J.-S., Chung, B.Y., 2008. Thermal Dissipation of Excess Light in Arabidopsis Leaves is Inhibited after Γ-irradiation. J. Plant Biol. 51, 52–57.

MORI, Y., Kimura S., Saotome A., Kasai N., Sakaguchi N., Uchiyama Y., Ishibashi T., Yamamoto T., Chiku H., Sakaguchi K., 2005. Plastid DNA polymerases from higher plants, Arabidopsis thaliana. Biochem. Biophys. Res. Commun. 334, 43-50.

MOU, Z., Fan, W., Dong, X., 2003. Inducers of plant systemic acquired resistance regulate NPR1 function through redox changes. Cell 113, 935–944.

MOULIN, V., Robouch, P., Vitorge, P., Allard, B. 1988. Environmental behaviour of Americium (III) in natural waters. Radiochim. acta 58/59, 179-190.

MOYEN, C., Roblin, G., 2010. Uptake and translocation of strontium in hydroponically grown maize plants, and subsequent effects on tissue ion content, growth and chlorophyll a/b ratio: comparison with Ca effects. Environ. Exp.Bot. 68, 247–257.

MUTTENAERE, C., Masset, M., 1971. Étude de la discrimination strontium-calcium chez le Haricot en fonction du rapport et des teneurs respectives en Sr et Ca de la solution nutritive. Physiol. Plant. 24, 14-17.

NEARY, G.J., Horgan, V.J., Bance, D.A., Stretch, A., 1972. Further data on DNA strand breakage by various radiation qualities. Int. J. Radiat. Biol. 22, 525-537.

NAKAMURA, Y., Ohta H., 2010. Phosphatidic acid phosphatases in seed plants. In: Munnik T. (Ed.), Lipid Signaling in Plants, Springer, Berlin, pp. 131–141.

NIKIPELOV, B.V., Romanov, G.N., Buldakov, L.A., Babaev, N.S., Kholina, Y.B., Mikerin,E.I., 1989. Accident in the southern Urals on 29 September 1957. IAEA information circular 368. Report on a radiological accident in the southern Urals on 29 September 1957, Vienna (IAEA).

NOCTOR, G., Foyer, C.H., 1998. Ascorbate and glutathione: Keeping active oxygen under control. Ann. Rev. Plant Phys. Plant Mol. Biol. 49, 249-279

NOCTOR, G., Gomez, L., Vanacker, H., Foyer, C.H., 2002. Interactions between biosynthesis, compartmentation and transport in the control of glutathione homeostasis and signalling. J. Exp. Bot. 53, 1283–1304.

NOCTOR, G., Mhamdi, A., Chaouch, S., Han, Y., Neukermans, J., Marquez-Garcia, B., Queval, G., Foyer, C.H., 2012. Glutathione in plants: An integrated overview. Plant Cell Environ. 35, 454–484.

O'BRIEN, J.A., Daudi, A., Butt, V.S., Bolwell, G.P., 2012. Reactive oxygen species and their role in plant defence and cell wall metabolism. Planta 236, 765-79.

PARENT, J.-S., Lepage, E., Brisson, N., 2011. Divergent Roles for the Two PolI-Like Organelle DNA Polymerases of *Arabidopsis*. Plant Physiol. 156, 254–262.

PIERRUGUES, O., Brutesco C., Oshiro J., Gouy M., Deveaux Y., Carman G.M., Thuriaux P., Kazmaier M. , 2001. Lipid phosphate phosphatases in *Arabidopsis*. J.Biol.Chem. 276, 20300-20308.

POOLE, R.L., 2007. The TAIR database. Methods Mol. Biol. 406, 179–212.

PORTA, H., Rocha-Sosa, M., 2002. Plant lipoxygenases. Physiological and molecular features. Plant Physiol. 130, 15-21.

POURCELOT, L., Louvat, D., Gauthier-Lafaye, F., Stille, P., 2003. Formation of radioactivity enriched soils in mountain areas. J. Environ. Radioact. 68, 215-233.

PREUSS, S.B., Britt, A.B., 2003. A DNA-damage-induced cell cycle checkpoint in *Arabidopsis*. Genetics 164, 323–334.

PROTECT, 2008. Numerical benchmarks for protecting biota against radiation in the environment: proposed levels and underlying reasoning. Protection of the Environment from Ionising Radiation in a Regulatory Context.

PSATALKI, M., Brown, J.E., Howard, B.J., in press. TRS Cs CRwo-water values for the marine environment: analysis, applications and comparisons. J. Environ. Radioactiv. In press

PUJOL, L., Sanchez-Cabeza, J.A., 2000. Natural and artificial radioactivity in surface waters of the Ebro river basin (Northeast Spain). J. Environ. Radioact. 51 ,181-210.

QUEEN, W.H., Fleming, H.W., O'Kelley, J.C., 1963. Effects on Zea Mays Seedlings of a Strontium Replacement for Calcium in Nutrient Media. Plant Physiol. 38, 410–413.

QUEVAL, G., Noctor,G., 2007. A plate reader method for the measurement of NAD, NADP, glutathione, and ascorbate in tissue extracts: Application to redox profiling during Arabidopsis rosette development. Anal. Biochem. 363,58-69.

R Development Core Team. 2011. R: A language and environment for statistical computing. R Foundation for Statistical Computing, Vienna, Austria.

RALPH, P.J., Gademann, R., 2005. Rapid light curves: A powerful tool to assess photosynthetic activity. Aquat. Bot. 82, 222–237.

REDISKE, J.H., Selders, A.A., 1953. The Absorption and Translocation of Strontium by Plants. Plant Physiol. 28, 594–605.

REMANS, T., Smeets K., Opdenakker K., Mathijsen D., Vangronsveld J., Cuypers A., 2008. Normalization of real-time RT-PCR gene expression measurements in Arabidopsis thaliana exposed to increased metal concentrations. Planta 227, 1343-1349.

ROLDAN-ARJONA, T., Ariza, R.R., 2009. Repair and tolerance of oxidative DNA damage in plants. Mutat. Res. 681, 169–179.

SAGI, M., Fluhr, R., 2006. Production of reactive oxygen species by plant NADPH oxidases. Plant Physiol. 141, 336-340.

SAHR, T., Voigt, G., Schimmack, W., Paretzke, H.G., Ernst, D., 2005. Low-level radiocaesium exposure alters gene expression in roots of Arabidopsis. New Phytol. 168, 141–148.

SAX, K.,1954. The effect of ionizing radiation on plant growth. Am. J. Bot. 42, 360-364.

SCHNEIDER, C.A., Rasband, W.S., Eliceiri, K.W., 2012. NIH Image to ImageJ: 25 years of image analysis. Nat. Methods 9, 671–675.

SCHREIBER, U., 2004. Pulse-Amplitude-Modulation (PAM) Fluorometry and Saturation Pulse Method: An Overview, in: Papageorgiou, G.C., Govindjee, G. (Eds.), Springer Netherlands, pp. 279–319.

SCHULTZ, P., Neukermans, J., Van Der Kelen, K., Mühlenbock, P., Van Breusegem, F., Noctor, G., Teige, M., Metzlaff, M., Hannah, M.A., 2012. Chemical PARP Inhibition Enhances Growth of *Arabidopsis* and Reduces Anthocyanin Accumulation and the Activation of Stress Protective Mechanisms. PLoS ONE, 7(5), e37287.

SEREGIN, I., Kozhevnikova, A., 2004. Strontium transport, distribution, and toxic effects on maize seedling growth. Russ. J. Plant Physl.+ 51, 215–221.

SINGH, S., Eapen, S., Thorat, V., Kaushik, C.P., Raj, K., D'Souza, S.F., 2008. Phytoremediation of 137-cesium and 90-strontium from solutions and low-level nuclear waste by Vetiveria zizanoides. Ecotoxicol. Environ. Saf. 69,306-11.

SKYRICZ, A., Inzé, D., 2010. More from less: Plant growth under limited water. Curr. Opin. Biotechnol. 21, 197–203.

SMEETS, K., Cuypers, A., Lambrechts, A., Semane, B., Hoet, P., Van Laere, A., Vangronsveld, J., 2005. Induction of oxidative stress and antioxidative mechanisms in *Phaseolus vulgaris* after Cd application. Plant Physiology and Biochemistry 43, 437-444.

SMEETS, K., Ruytinx, J., Belleghem, F.V., Semane, B., Lin, D., Vangronsveld, J., Cuypers, A., 2008a. Critical evaluation and statistical validation of a hydroponic culture system for *Arabidopsis thaliana*. PRism 46, 212–218.

SMEETS, K., Ruytinx, J., Semane, B., Van Belleghem, F., Remans, T., Van Sanden, S., Vangronsveld, J., Cuypers, A., 2008b. Cadmium-induced transcriptional and enzymatic alterations related to oxidative stress. Environ. Exp. Bot. 63, 1-8.

SOKOLIK, G.A., Ovsiannikova, S.V., Ivanova, T.G., Leinova, S.L., 2004. Soil – plant transfer of plutonium and americium in contaminated regions of Belarus after the Chernobyl catastrophe. Environ. Int. 30, 939–947.

SOUDEK, P., Valenová, S., Vavríková, Z., Vanek, T., 2006. (137)Cs and (90)Sr uptake by sunflower cultivated under hydroponic conditions. J. Environ. Radioact. 88, 236-50.

SPARROW, A.H., Miksche, J.P., 1961. Correlation of nuclear volume and DNA content with higher plant tolerance to chronic radiation. Science 134, 282-283.

SU, Y., Maruthi Sridhar, B.B., Han, F.X., Diehl, S.V., Monts, D.L., 2007. Effect of Bioaccumulation of Cs and Sr Natural Isotopes on Foliar Structure and Plant

Spectral Reflectance of Indian Mustard (Brassica Juncea). Water Air Soil Pollut. 180, 65-74.

THEIN, M., Ballestra, S., Yamato, A., Fukai, R., 1980. Delivery of transuranic elements by rain to the Mediterranean. Geochim. Cosmochim. Act. 44, 1091–1097.

TORRES, M.A, Dangl, J.L., 2005. Functions of the respiratory burst oxidase in biotic interactions, abiotic stress and development. Curr. Opin. Plant Biol. 8,397–403

TRIANTAPHYLIDES, C., Krischke, M., Hoeberichts, F.A., Ksas, B., Gresser, G., Havaux, M., Van Breusegem, F., Mueller, M.J., 2008. Singlet oxygen is the major reactive oxygen species involved in photooxidative damage to plants. Plant Physiol. 148, 960-968.

TURNER, J.E., 2005. Interaction of ionizing radiation with matter. Health Phys. 88, 520-544.

UNSCEAR, 1996. Sources and effects of ionizing radiation. Scientific Annex: Effects of Radiation on the Environment. United Nations Scientific Committee on the Effects of Atomic Radiation Report to the General Assembly, Vienna

UNSCEAR, 2000. Report to the general assembly: sources and effects of ionizing radiation. United Nations Scientific Committee on the Effects of Atomic Radiation, Vienna.

UNSCEAR, 2008. Report to the general assembly: sources and effects of ionizing radiation. United Nations Scientific Committee on the Effects of Atomic Radiation, Vienna.

URBAN, P., Mignotte, C., Kazmaier, M., Delorme, F., and Pompon, D., 1997. Cloning, yeast expression, and characterization of the coupling of two distantly related Arabidopsis thaliana NADPH-cytochrome P450 reductases with P450 CYP73A5. J. Biol. Chem. 272, 19176–19186.

VANDENHOVE, H., 2002. European sites contaminated by residues from the ore-extracting and -processing industries. International Congress Series 1225, 307-315.

VAN DER STRICHT, E., Kirchmann (Eds.) 2001. Radioecology: radioactivity & ecosystems, International Union of Radioecology, Liège, Belgium.

VAN VOLKENBURGH, E., 1999. Leaf expansion – an integrating plant behaviour. Plant Cell Environ. 22, 1463-1473.

VERKEST, A., Manes, C.L., Vercruysse, S., Maes, S., Van Der Schueren, E., Beeckman, T., Genschik, P., Kuiper, M., Inzé, D., De Veylder, L., 2005. The cyclin-dependent kinase inhibitor KRP2 controls the onset of the

endoreduplication cycle during Arabidopsis leaf development through inhibition of mitotic CDKA;1 kinase complexes. Plant Cell. 17,1723-36.

VON FIRCKS, Y., Rosén, K., Sennerby-Forsse, L., 2002. Uptake and distribution of 137Cs and 90Sr in Salix viminalis plants. J. Environ. Radioact. 63, 1-14.

VAN SCHOOTEN, B., Testerink C., Munnik T., 2006. Signalling diacylglycerol pyrophosphate, a new phosphatidic acid metabolite. Biochim Biophys Acta. 1761,151-9.

VANDENHOVE, H., Cuypers, A., Van Hees, M., Koppen, G. & Wannijn, J., 2006. Oxidative stress reactions induced in beans (Phaseolus vulgaris) following exposure to uranium. Plant Physiol. Biochem. 44, 795-805.

VANDENHOVE, H., Vanhoudt, N., Cuypers, A., van Hees, M., Wannijn, J., Horemans, N., 2010. Life-cycle chronic gamma exposure of *Arabidopsis thaliana* induces growth effects but no discernable effects on oxidative stress pathways. Plant Physiol. Biochem. 48, 778-86.

VANDESOMPELE, J., De Preter K., Pattyn F., Poppe B., Van Roy N., De Paepe A., Speleman F., 2002. Accurate normalization of real-time quantitative RT-PCR data by geometric averaging of multiple internal control genes. Genome Biology 3, research 0034.

VANHOUDT, N., Vandenhove, H., Horemans, N., Wannijn,J., Van Hees, M., Vangronsveld, J., Cuypers, A., 2010. The combined effect of uranium and gamma radiation on biological responses and oxidative stress induced in Arabidopsis thaliana. J. Environ. Radioact. 101, 923-930.

VANHOUDT, N., Vandenhove, H., Horemans, N., Martinez Bello, D., Van Hees, M., Wannijn, J., Carleer, R., Vangronsveld, J., Cuypers, A., 2011. Uranium Induced Effects on Development and Mineral Nutrition of Arabidopsis thaliana. J. Plant Nutr. 34, 1940–1956.

VANHOUDT, N., Vandenhove, H., Real, A., Bradshaw, C., Stark, K., 2012. A review of multiple stressor studies that include ionising radiation. Environ. Pollut. 168, 177-92.

VERKEST, A., Manes, C.L., Vercruysse, S., Maes, S., Van Der Schueren, E., Beeckman, T., Genschik, P., Kuiper, M., Inzé, D., De Veylder, L., 2005. The cyclin-dependent kinase inhibitor KRP2 controls the onset of the endoreduplication cycle during *Arabidopsis* leaf development through inhibition of mitotic CDKA;1 kinase complexes. Plant Cell 17,1723-36.

VIVES I BATLLE, J., Jones, S.R., Gómez-Ros, J.M., 2004. A method for calculation of dose per unit concentration values for aquatic biota. J. Radiol. Prot. 24, 13–34.

VIVES I BATLLE, J., Wilson, R.C., Watts, S.J., Jones, S.R., McDonald, P., Vives-Lynch, S., 2008. Dynamic model for the assessment of radiological exposure to marine biota. J. Environ. Radioact. 99,1711-1730.

VIVES I BATLLE, J., 2011. Impact of nuclear accidents on marine biota. Integrated Environ. Assess. Manag. 7, 365–367.

VRANOVA, E., Inzé, D., Van Breusegem, F., 2002. Signal transduction during oxidative stress. J Exp Bot 53: 1227–1236.

WANG, J.-J., Wang, C.-J., Huang, C.-C., Lin, Y.-M., 1998. Transfer factors of 90Sr and 137Cs from paddy soil to the rice plant in Taiwan. J. Environ. Radioact. 39, 23-34.

WATERWORTH, W.M., Drury, G.E., Bray, C.M., West, C.E., 2011. Repairing breaks in the plant genome: the importance of keeping it together. New Phytol. 192, 805–822.

WELLBURN, A.R., 1994. The spectral determination of chlorophylls a and b, as well as total carotenoids, using various solvents with spectrophotometers of different resolution. Plant Physiol. 144, 307–313.

WEST, C.E., Waterworth, W.M. Jiang, Q., Bray, C.M. 2000. Arabidopsis DNA ligase IV is induced by gamma-irradiation and interacts with an *Arabidopsis* homologue of the double strand break repair protein XRCC4. Plant J. 24, 67-78.

WHITE, A.J., Critchley, C., 1999. Rapid light curves: a new fluorescence method to assess the state of the photosynthetic apparatus. Photosynth. Res. 59,63–72.

WHITE, PJ., 2001. The pathways of calcium movement to the xylem. J. Exp. Bot. 52, 891–899.

WI, S.G., Chung, B.Y., Kim, J.S., Kim, J.H., Baek, M.H., Lee, J.W., Kim, Y.S., 2007. Effects of gamma irradiation on morphological changes and biological responses in plants. Micron 38, 553–564.

WILLEKENS, H., Inzé, D., Van Montagu, M., van Camp, W., 1995. Catalases in plants. Mol. Breed. 1, 207-228.

ZAKA, R., Chenal, C., Misset, M.T., 2004. Effects of low doses of short-term gamma irradiation on growth and development through two generations of Pisum sativum. Sci. Total Environ. 320, 121-129.

ZOTINA, T.A., Bolsunovsky, A.Y., Bondareva, L.G., 2010. Accumulation of (241)Am by suspended matter, diatoms and aquatic weeds of the Yenisei River. J. Environ. Radioact. 101,148-52.

ZOTINA, T.A., Kalacheva, G.S., Bolsunovsky, A.Y., 2011. Biochemical fractionation and cellular distribution of americium and plutonium in the biomass of freshwater macrophytes. Journal of Radioanalytical and Nuclear Chemistry 290, 447-451.